Information-theoretic measures of atomic and molecular systems

TESIS DOCTORAL

por

Sheila López Rosa

Departamento de Física Atómica, Molecular y Nuclear

Universidad de Granada

28 Junio 2010

Editor: Editorial de la Universidad de Granada
Autor: Sheila López Rosa
D.L.: GR 3528-2010
ISBN: 978-84-693-5202-1

Tesis doctoral dirigida por:

Dr. Juan Carlos Angulo Ibáñez

Dr. Jesús Sánchez-Dehesa

D. Juan Carlos Angulo Ibáñez, Doctor en Física y Profesor Titular del Departamento de Física Atómica, Molecular y Nuclear de la Facultad de Ciencias de la Universidad de Granada.

D. Jesús Sánchez-Dehesa Moreno-Cid, Doctor en Física, Doctor en Matemáticas y Catedrático del Departamento de Física Atómica, Molecular y Nuclear de la Facultad de Ciencias de la Universidad de Granada.

MANIFIESTAN:

Que la presente Memoria titulada "Information-theoretic measures of atomic and molecular systems", presentada por Sheila López Rosa para optar al Grado de Doctora en Física, ha sido realizada bajo nuestra dirección en el Departamento de Física Atómica, Molecular y Nuclear de la Universidad de Granada y el Instituto Carlos I de Física Teórica y Computacional de la Universidad de Granada.

Granada, 20 de Mayo de 2010

Fdo.: Juan Carlos Angulo Ibáñez

Fdo.: Jesús Sánchez-Dehesa Moreno-Cid.

Memoria presentada por Sheila López Rosa para optar al Grado de Doctora en Física por la Universidad de Granada.

Fdo.: Sheila López Rosa

Título de Doctor con Mención Europea

Con el fin de obtener la Mención Europea en el Título de Doctor, se han cumplido, en lo que atañe a esta Tesis Doctoral y a su Defensa, los siguientes requisitos:

1. La tesis está redactada en inglés con una introducción en español.
2. Al menos uno de los miembros del tribunal provienen de una universidad europea no española.
3. Una parte de la defensa se ha realizado en inglés.
4. Una parte de esta Tesis Doctoral se ha realizado en Alemania, en el Max-Planck-Institut für Quantenoptik de Garching.

A mis padres, a mi hermano,

y sobre todo a Manolo....

Agradecimientos

Escribir los agradecimientos nunca es fácil, hay mucha gente que ha influido en mí durante estos cuatro años y me ha hecho estar donde estoy ahora, ahí van...

En primer lugar quisiera agradecer a mis directores de tesis su confianza en mí durante estos años. A Jesús, por darme la oportunidad de empezar en este mundo, por haberme enseñado que, al final, con paciencia y tesón, todo acaba yendo hacia delante; gracias por tener esa confianza que en algunos momentos a mí me ha faltado. A Juan Carlos, por tu dedicación durante este tiempo, por guiarme con tus consejos y sugerencias en este camino que es el de escribir una tesis. En definitiva, gracias a los dos por estos años de trabajo; sin duda, sin vuestra ayuda esta tesis no se hubiera escrito.

A Rosario, Pablo, Rafa..., y al resto de los miembros del grupo, gracias porque siempre habéis estado dispuestos a ayudarme cuando lo he necesitado. Y especialmente a Juan Antolín, cuya colaboración en este trabajo ha sido esencial, gracias por tu dedicación y entusiasmo.

A Rodolfo, gracias por darme la oportunidad de realizar una estancia México, porque aprendí mucho durante el tiempo que estuve allí. Gracias por tu ayuda durante esos meses, no sólo en el ámbito profesional, porque entre todos (no olvido a tu familia y a Araceli, Diana, María, Annik,...) hicisteis que México fuera mi casa durante tres meses; gracias de corazón.

Quisiera manifestar también mi agradecimiento por la financiación recibida del Ministerio de Educación y Ciencia por la beca FPU, así como por las ayudas de los proyectos FIS2008-02380 del MICINN y de los proyectos de excelencia FQM-1735, FQM-2445 y FQM-4643 así como del FQM-207 de la Junta de Andalucía, que es lo que me ha permitido llevar a cabo mi labor, asistir a congresos y realizar estancias de investigación.

A mis compañeros de fatiga Jorge, Lidia, Antonio, Jesús, Paqui, Alex, Rosa, Pablo, Raquel (físicos o no) por compartir conmigo tantos buenos momentos durante la carrera y durante estos años de doctorado, por tantas noches de fiesta, de cervezas, de juegos, de series y películas frikis. Habéis hecho que estos cuatro años hayan pasado como si fueran simplemente unos pocos meses, porque aunque a partir de ahora la vida nos lleve por caminos diferentes, siempre guardaré estos momentos en mi memoria a la espera de poder volver a repetirlos, ¡mil gracias!

A Dani por todo lo anterior y porque no todo el mundo tiene la suerte de que sean sus amigos quienes se conviertan en sus compañeros de trabajo, yo sí la tengo (y por cierto....no ganabais siempre...ahí queda dicho). A Bea, por todo lo anterior y más, por ser mi compañera de carrera y luego de trabajo, pero sobre todo mi amiga, porque en esto de la investigación hemos "crecido" juntas, alegrándonos por los éxitos de la otra y

sirviéndonos como apoyo en los momentos de flaqueza. Ya me he acostumbrado...pero se hace raro venir al despacho y que no estés sentada en la mesa de enfrente...

A Olmo, Elvira, Victor, Alex, Luis y Adri, por tantos buenos momentos pasados y por todos los que nos quedan por pasar, por esas fiestas, ¿cuándo hacemos una para celebrar esto?, por esos viajes...., porque empezasteis siendo lo amigos de mi novio y pasásteis a ser los míos propios, ¡y no sabéis lo que me alegro de ello!

A mis sorianas con las que a pesar de llevar ya casi doce años en Granada, sigo manteniendo esa amistad que empezamos de niñas, y que espero seguir disfrutando durante muchísimos años más. Y especialmente a Esther, que se ha convertido en la otra "soriana-semi-granaina", porque a pesar de que no podamos vernos mucho, sabemos que siempre podemos contar la una con la otra.

A Arantxa y Raquel, mis niñas, qué deciros que no sepáis ya, gracias por vuestro apoyo incondicional, vuestros consejos, vuestros ánimos en momentos de flaqueza, siempre puedo contar con vosotras, siempre estáis cuando os necesito, simplemente gracias por ser mucho más que mis amigas y por estar conmigo en los buenos y en los malos momentos, porque sé que por mucho tiempo que pase siempre estaréis ahí, no me cabe duda.

A mi familia, abuelos, tíos, primos, cuñada,.... porque aunque no puedo nombraros a todos aquí, os llevo siempre presentes, que aunque las distancias no nos permitan vernos todo lo que nos gustaría me alegra saber que estáis ahí, porque tengo una familia maravillosa.

A mis padres, creo que en este caso sobran los motivos.... gracias por apoyarme siempre, por animarme a hacer lo que yo quisiera, por respetar todas mis decisiones, buenas o malas. Gracias por estar siempre conmigo, porque sin todo lo que me habéis dado y enseñado no me hubiera convertido en la persona que soy ahora. Y a mi hermano, gracias por ser como eres, una persona muy diferente a mí que me hace ver muchas veces las cosas desde otras perspectivas, creo que no podría haberme tocado un hermano mejor. Gracias a los tres porque sé que siempre podré contar con vosotros.

Y sobre todo a Manolo, porque sin tu apoyo el camino hasta aquí hubiera sido sin duda muchísimo más duro, por aguantarme los momentos de estrés, por animarme cuando me venía abajo diciendome que puedo con todo esto y con mucho más, por hacerme reir con esas ocurrencias que sólo tú tienes y que son parte de lo que te hace ser tan especial, por quererme y dejarme que te quiera.... simplemente gracias por estar aquí conmigo.

Contents

Foreword

This Thesis is a contribution to the debate on the implications of the information theory of quantum systems for the description of numerous quantum phenomena of the electronic structure. It contains several applications of the basic concepts, techniques and relations of the information theory to selected problems of atomic and molecular structure and chemical reactivity. Such treatment gives rise to the information-entropic representation of the atomic and molecular states, which complements the familiar energy-representation of the density-functional and wave-function-based theories. The most important role in this treatment is played by the concepts of information, complexity and divergence.

The Thesis is structured in three Parts and two Appendices. Each part is composed by four Chapters, which are deeply self-contained with their own Introduction and Conclusions. They correspond to one (Chapters 3 and 8 and App. A), two (Chapters 4, 6, 10, 11) and three (Chapters 2, 7, 12) scientific publications.

In the following we briefly outline the contents of the Thesis. A more detailed introduction and motivation can be found at the beginning of the respective parts and chapters.

Part I, which is entitled "Entropic functionals of some selected quantum systems", is devoted to the study of some physical and chemical systems and processes in terms of different information-theoretic measures. This Part starts with the presentation and discussion of the concept of "information" in Chapter 1, where some of the information measures that will be used throughout this Thesis are defined (i.e. the standard deviation, the Shannon, Rényi and Tsallis entropies, the Fisher information as well as the entropic moments), their properties and distinctive characteristics are pointed out. Then, in Chapter 2, we carry out the analytical determination of the single information-theoretic measures and their associated uncertainty relations for multidimensional hydrogenic systems. The spreading properties of the ground and excited states of d-dimensional hydrogenic systems by means of these information measures are investigated in terms of their quantum numbers. Emphasis on the circular and Rydberg states is made. In Chapter 3, the Fisher information is used to study a one- and a two-step simple chemical reactions; namely, a typical nucleophilic substitution reaction and the radical abstraction

reaction involving a free radical (atomic hydrogen) as an intermediate reactive, respectively. We will show that this measure seems to be very useful in order to analyze the course of the chemical reaction because, due to its local character, the Fisher information is able to detect the relevant points in the reaction path (such as transition state or bond breaking/forming regions) which are not so clear from the energy profile. Finally, in Chapter 4, the multidimensional extremization problems of the Shannon, Tsallis and Fisher information measures subject to a radial expectation value as main constraint are analyzed and applied to all ground-state neutral atoms from Hydrogen to Lawrencium. In addition, the existence conditions for the d-dimensional Maximum Entropy problem problem are found, which extends a number of results previously encountered by various authors for the one-dimensional case.

Part II, which is called "Complexity measures of atomic and molecular systems", is devoted to the study of the complexity. Although there is no general agreement about what complexity is, there exist various technical notions of this quantity which have been shown to be very useful for the quantum mechanical interpretation of numerous physical and chemical phenomena of atomic and molecular systems. This Part begins in Chapter 5 with a discussion of the concept of complexity and its description by means of three product-like measures of complexity (the LMC shape, the Fisher-Shannon and the Cramér-Rao complexities) and their generalizations: the Shape-Rényi and the Fisher-Rényi complexities. Then, in Chapter 6, we explore the analytical properties of these measures as well as the associated uncertainty-like inequalities. Moreover, the generalized complexities defined in the previous chapter are employed in order to analyze atomic electron densities. In Chapter 7, we study both analytically and numerically the Fisher-Shannon and LMC shape complexities of the multidimensional hydrogenic systems, emphasizing the realistic hydrogenic atoms in position space. In addition we study the relativistic effects of Klein-Gordon type in the aforementioned measures of complexity. Finally, in Chapter 8, we perform a numerical study of the complexity measures and the information planes of some molecular systems, finding interesting trends in the behaviour of molecular complexities when these quantities are interpreted according to the molecular structure and composition, reactivity, etc.

Part III, entitled "Divergence measures of atomic systems and processes", is devoted to the study of the divergence measures. In the previous Parts I and II we have focused in the quantification of the information features of a given systems and their connection with its physical or chemical properties. In this Part we will analyze the similarity or dissimilarity between two or more systems in terms of the divergence measures. We start with the elucidation of the concept of divergence and other related information-theoretic indices in Chapter 9, giving the definition of the measures that will be used in this Part, i.e, the quadratic distance, the quantum similarity index as well as Jensen-like and Fisher divergences. Then, in Chapter 10, we study the dissimilarity or divergence between neutrals and/or ions throughout the Periodic Table by using the Jensen-Shannon and

Fisher divergence. These quantities are found to show the complex organization and the shell-filling patterns throughout the Periodic Table. In Chapter 11 we propose an extension of the Jensen-Shannon divergence by means of the use of the Shannon entropy generalizations, i.e., the Rényi and Tsallis entropies, from which the Jensen-Rényi and the Jensen-Tsallis divergences, respectively, are defined. Application of these measures to the study of the dissimilarity among neutral atoms are also carried out. Finally, in Chapter 12 we present other applications of the divergence measures. We start analyzing the interelectronic repulsion by means of the computation of the divergence between atomic densities with the Hartree-Fock and Bare-Coulomb-Field models. Then, we use the generalization of the Jensen-like divergences for a set of distributions in order to provide a very useful tool for quantifying the information content of a composite system with respect to that of their constituents.

Prefacio

En esta Tesis se utiliza la teoría de información en la descripción cuántica de numerosos fenómenos relacionados con la estructura electrónica de sistemas atómicos y moleculares. Contiene varias aplicaciones de los conceptos básicos, técnicas y relaciones de la teoría de información a varios problemas relacionados con la estructura atómica y molecular y la reactividad química. Este tratamiento proporciona una representación teórico-informacional de los estados atómicos y moleculares, que complementa a la representación energética proporcionada por las teorías basadas en la función de onda y los métodos funcionales de la densidad.

La Tesis está dividida en tres partes y dos apéndices. Cada parte está compuesta por cuatro capítulos, que son autocontenidos en gran medida, con su propia introducción y conclusiones. Cada capítulo corresponde a una (Capítulos 3, 8, y Apéndice A), dos (Capítulos 4, 6, 10, 11) o tres (Capítulos 2, 7, 12) publicaciones científicas.

A continuación se hace una breve descripción de los contenidos de la Tesis. Una introducción más detallada junto con la motivación del trabajo puede encontrarse al inicio de cada una de las partes.

La Parte I, titulada "Funcionales entrópicos de sistemas cuánticos", está dedicada al estudio de varios sistemas físicos multidimensionales y reacciones químicas, en términos de medidas teórico-informacionales. Esta parte comienza con la presentación y discussión del significado del concepto de información en el Capítulo 1, donde se definen las medidas de información y de dispersión que se usarán durante el resto de la tesis (desviación estándar, entropías de Shannon, Rényi y Tsallis, información de Fisher, momentos entrópicos de la densidad), así como sus propiedades más relevantes. A continuación, en el Capítulo 2 se lleva a cabo un estudio analítico de las medidas de información, así como de las relaciones de incertidumbre, de los sistemas hidrogenóides multidimensionals. Se obtienen las propiedades de esparcimiento del estado fundamental y de los estados excitados de los sistemas hidrogenoides d-dimensionales en términos de los números cuánticos que caracterizan el estado, haciendo especial hincapié en los estados circulares y en los estados Rydberg. En el Capítulo 3 se utiliza la información de Fisher para describir dos reacciones químicas sencillas: una reacción de sustitución

nucleofílica y una reacción de abstración (con un átomo de hidrógeno como radical libre). Se mostrará que esta medida de información parece ser muy útil a la hora de analizar el curso de una reacción química, ya que, debido a su marcado carácter local, la información de Fisher es capaz de detectar puntos relevantes del camino de reacción (como puede ser el estado de transición o las regiones de rotura/formación de enlaces) que se pierden en el perfil energético. Para finalizar, en el Capítulo 4, se analizan los problemas de extremización de las entropías de Shannon y Tsallis así como de la información de Fisher en sistemas multidimensionales cuando las ligaduras del mismo vienen dadas por valores esperados radiales, aplicando los resultados al estado fundamental de los sistemas atómicos de la Tabla Periódica. Además se obtienen las condiciones de existencia de las densidades que maximizan la entropía de Shannon (problema maxEnt) en d dimensiones, extendiendo los resultados obtenidos previamente por varios autores para el caso unidimensional.

La segunda parte de la Tesis, Parte II, "Medidas de complejidad de sistemas atómicos y moleculares", está dedicada al estudio de la complejidad. Aunque hasta ahora no hay un acuerdo generalizado acerca del significado del término complejidad, existen evidencias que han mostrado su utilidad para la interpretación desde el punto de vista cuántico de numerosos fenómenos físicos y químicos en sistemas atómicos y moleculares. Esta parte comienza con el Capítulo 5 donde se trata de clarificar el concepto de complejidad y se definen las medidas de la misma que se usarán en los estudios posteriores (las complejidades LMC, Fisher-Shannon y Cramér-Rao), así como sus generalizaciones en términos de la entropía de Rényi (las complejidades Shape-Rényi y Fisher-Rényi). Posteriormente, en el Capítulo 6, se obtienen una serie de propiedades analíticas y relaciones de incertidumbre que verifican las complejidades anteriormente descritas. Además, se usarán las complejidades generalizadas para analizar las densidades de sistemas atómicos tanto en el espacio de configuración (espacio de posiciones) como en su espacio conjugado (espacio de momentos). En el Capítulo 7 se estudia de forma analítica y numérica las complejidades de forma LMC y de Fisher-Shannon en sistemas hidrogenoides d-dimensionales haciendo especial hincapié en el átomo de Hidrógeno ($d = 3$) en su espacio de configuración. En este mismo capítulo se estudiarán los efectos relativistas de tipo Klein-Gordon en las medidas de complejidad previamente estudiadas en los sistemas hidrogenoides. Finalmente, en el Capítulo 8 se realiza un estudio numérico de diferentes complejidades y planos de información en una serie de sistemas moleculares, encontrando tendencias relevantes en el comportamiento dichas medidas en comparación con la estructura molecular, su composición, su reactividad, etc.

La última parte, Parte III, se titula "Medidas de divergencia de sistemas y procesos atómicos". En las dos partes anteriores de este trabajo nos hemos centrado en la cuantificación de las propiedades teórico-informacionales de los sistemas, relacionándolas con sus propiedades físicas y químicas. En esta parte analizaremos la similitudes y diferencias

entre dos o más sistemas en terminos de diferentes medidas de divergencia. Empezaremos con la definición del concepto de divergencia en el Capítulo 9, proporcionando la definición de las diferentes medidas que se usarán durante esta parte, como son la distancia cuadrática, el índice de similitud cuántica, así como las divergencias de tipo Jensen y la divergencia de Fisher. En el Capítulo 10 estudiamos las similitudes y diferencias entre átomos neutros y/o iones a lo largo de la Tabla Periódica a través del cálculo numérico de las divergencias de Jensen-Shannon y de Fisher. Se ha encontrado que estas medidas muestran la compleja organización y los patrones del proceso de llenado de capas en la Tabla Periódica. En el Capítulo 11 proponemos una serie de extensiones de la divergencia de Jensen-Shannon basada en las generalizaciones de la entropía de Shannon, a saber, las entropías de Rényi y de Tsallis, definiendo entonces las divergencias de Jensen-Rényi y Jensen-Tsallis respectivamente y aplicándolas al estudio de las similitudes y diferencias entre átomos neutros. Por último, en el Capítulo 12, presentamos otras posibles aplicaciones de las medidas de divergencia utilizadas en los capítulos previos. Primero, analizamos la repulsión interelectrónica a través del cálculo de las medidas de divergencia entre las densidades atómicas proporcionadas por el modelo Hartree-Fock y el modelo de campo Coulombiano desnudo. Tras esto, utilizamos la generalización de las divergencias de tipo Jensen para el estudio de las similitidues entre un conjunto de tres o más densidades con el fin de proporcionar una herramienta útil para cuantificar el contenido teórico-informacional de un sistema compuesto por varias partes frente al proporcionado por cada uno de sus componentes.

Author's publications

Publications upon which this Thesis is based (the numbers in brackets at the end of each reference indicate the Chapters and Appendices where they have been used):

J.S. Dehesa, S. López-Rosa, B. Olmos and R.J. Yáñez, *Information measures of hydrogenic systems, Laguerre polynomials and spherical harmonics.* Journal of Computational and Applied Mathematics 179 (2005) 185. [Ch. 2]

J.S. Dehesa, S. López-Rosa, B. Olmos and R.J. Yáñez, *The Fisher information of D-dimensional hydrogenic systems in position and momentum spaces.* Journal of Mathematical Physics 47 (2006) 052104. [Ch. 2]

J.S. Dehesa, S. López-Rosa and R.J. Yáñez, *Information-theoretic measures of hyperspherical harmonics.* Journal of Mathematical Physics 48 (2007) 043503. [App. A]

S. López-Rosa, J.C. Angulo, J.S. Dehesa and R.J. Yáñez, *Existence conditions and spreading properties of extreme entropy D-dimensional distributions.* Physica A 387 (2008) 2243 [Ch. 4]

S. López-Rosa, J.C. Angulo and J.S. Dehesa, *Spreading measures of information-extremizer distributions: applications to atomic one-particle densities in position and momentum spaces.* European Physical Journal D 51 (2009) 321. [Ch. 4]

S. López-Rosa, J.C. Angulo and J. Antolín, *Rigorous properties and uncertainty-like relationships on complexity measures: Application to atomic systems.* Physica A 388 (2009) 2081. [Ch. 6]

J. Antolín, J.C. Angulo and S. López-Rosa, *Fisher and Jensen-Shannon divergences: quantitative comparisons among distributions. Application to position and momentum atomic densities.* Journal of Chemical Physics 130 (2009) 074110. [Ch. 10]

S. López-Rosa, D. Manzano and J.S. Dehesa, *Complexity of D-dimensional hydrogenic systems in position and momentum spaces.* Physica A 388 (2009) 3273. [Ch. 7]

J.S. Dehesa, S. López-Rosa and D. Manzano, *Configuration complexities of hydrogenic atoms.* European Physical Journal D 55 (2009) 539. [Ch. 7]

S. López-Rosa, J. Antolín, J.C. Angulo and R.O. Esquivel, *Divergence analysis of atomic ionization processes and isoelectronic series.* Physical Review A 80 (2009) 012505(1-9). [Ch. 10]

J. Antolín, J.C. Angulo and S. López-Rosa, *Rényi complexities and information planes: atomic structure in conjugated spaces.* Chemical Physics Letters 474 (2009) 233. [Ch. 6]

J.S. Dehesa, S. López-Rosa, A. Martínez-Finkelshtein and R.J. Yáñez, *Information theory of D-dimensional hydrogenic systems. Application to circular and Rydberg states.* International Jounal of Quantum Chemistry 110 (2010) 1529. [Ch. 2]

J.C. Angulo, S. López-Rosa and J. Antolín, *Effect of the interelectronic repulsion on the information content of position and momentum atomic densities.* International Journal of Quantum Chemistry 110 (2010) 1738. [Ch. 12]

J.C. Angulo, J. Antolín, S. López-Rosa and R.O. Esquivel, *Jensen-Shannon Divergence in conjugated spaces: entropy excess of atomic systems and sets with respect to their constituents.* Physica A 389 (2010) 899. [Ch. 12]

S. López-Rosa, R.O. Esquivel, J.C. Angulo, J. Antolín, J.S. Dehesa and N. Flores-Gallegos, *Fisher information study in position and momentum spaces for elementary chemical reactions.* Journal of Chemical Theory and Computation 6 (2010) 145. [Ch. 3]

R.O. Esquivel, N. Flores-Gallegos, J.S. Dehesa, J.C. Angulo, J. Antolín, S. López-Rosa and K.D. Sen, *Phenomenological description of a three center insertion reaction: An information-theoretic study.* Journal of Physical Chemistry A 114 (2010) 1906.

J.C. Angulo, J. Antolín, S. López-Rosa and R.O. Esquivel, *Jensen-Tsallis divergence and atomic dissimilarity for position and momentum space electron densities.* Journal of Chemical Physics 132 (2010) 044105(1-7). Selected by Virtual Journal of Quantum Information, issue 2 (February 2010). [Ch. 11]

R.O. Esquivel, J.C. Angulo, J. Antolín, J.S. Dehesa, S. López-Rosa and N. Flores-Gallegos, *Analysis of complexity measures and information planes of selected molecules in position and momentum spaces.* Physical Chemistry Chemical Physics (2010). DOI 10.1039/b927055h. [Ch. 8]

D. Manzano, S. López-Rosa and J.S. Dehesa, *Complexity analysis of Klein-Gordon single particle systems.* Europhysics Letterss (2010). Accepted. [Ch. 7]

* * * *

S. López-Rosa, D. Manzano and J.S. Dehesa, *Multidimensional hydrogenic complexities*. Mathematical Physics and Field Theory: Julio Abad, in Memoriam. Editors: M. Asorey et al. Prensas Universitarias de Zaragoza, (2009). See also arXiv:0907.0570.

J.S. Dehesa, S. López-Rosa, A. Martínez-Finkelshtein and R.J. Yáñez, *Asymptotics of orthogonal-polynomial functionals and Shannon information entropy of Rydberg atoms*. Special issue devoted to the Proceedings of the International Workshop of ECMI (European Consorcium for Mathematics in Industry) 2008, held at University College, London, 30 June-4 July 2008. En A. D. Fitt et al (editors), Progress in Industrial Mathematics (Springer, Berlin, 2010)

J.C. Angulo, S. López-Rosa, J. Antolín and R.O. Esquivel. *Generalized Jensen divergence analysis of atomic electron densities in conjugated spaces*. International Journal of Quantum Chemistry (2010). Special issue devoted to the Proceedings of the "14th International Workshop on Quantum Systems in Chemistry and Physics (QSCP-XIV)", held at El Escorial, Madrid, 13-19 September 2009. Accepted [Chs. 11 and 12]

J.S. Dehesa, S. López-Rosa and D. Manzano, *Entropy and complexity analyses of D-dimensional quantum systems*. Chapter of the book: "Statistical Complexities: Applications in Electronic Structures", edited by K.D. Sen. Springer, Berlín, 2010.

Part I

Entropic functionals of some selected quantum systems

Introduction

The Information Theory was developed by Claude E. Shannon in 1940s to find fundamental limits on signal processing operations such as compressing data as well as on reliably storing and communicating data. He applied the word "information", only in a descriptive sense, to the output of an information source within the framework of telecommunications. Shannon further developed works of Hartley [1] and Nyquist [2], who introduced fundamental ideas related to the transmission of information in the context of the telegraph as a communication system during the ninety twenties. In fact, the word information was already used in 1925 by Fisher [3] in a qualitatively different way within the theory of statistical inference.

Information Theory arises as a branch of applied mathematics and electrical engineering involving the quantification of information. Since its beginning, it has found applications in many other areas, including statistical inference [4, 5], natural language processing [6], cryptography [7], networks [8], neurobiology [9], cognitive psychology [10], model selection in ecology [11], atomic and molecular physics [12–14], quantum computing [15] and different forms of data analysis, among others. In fact, during the last seventy years, scientists have created a bulk of information theories: Shannon's statistical [16, 17], information theory, Fisher's [3], philosophy [18] semantic [19], dynamic [20] and economical [21] information theories, among others.

The concept of information is currently playing an increasing role in Physics, following the rapid growth of the information theory of the quantum physics, which is on the basis of the fields of quantum information and quantum computation (see e.g. Ref. [15]). These are new and exciting fields of physics whose interests concern primarily with the foundations and conceptual status of quantum mechanics but, as well, with a deeper insight of the physico-chemical interpretation of numerous classical and quantum phenomena ranging from atomic and molecular physics and chemistry to cosmology, cryptography, condensed matter and, of course, statistical mechanics. Concentration on the possible ways of using the distinctively quantum-mechanical properties of systems for the purposes of carrying and processing information has led to a considerable deepening of our understanding of quantum theory. This is best illustrated with the phenomena of uncertainty and entanglement.

Moreover, there is a feeling that the advent of the information theory of quantum systems heralds a new way of doing physics and supports the view that information should play a more central role in our picture of the world. In its extreme form, the thought is that information is perhaps the fundamental category from which all else flows, and that the new task of Physics is to describe how this information evolves, manifests itself and can be manipulated [22]. It seems natural to believe that the information theory of quantum systems has much to say about the physical and chemical properties of atoms and molecules, since the measurement problem is in many ways the central interpretative problem in the quantum description of these systems and that measurement is a transfer of information, an attempt to gain knowledge.

In this sense, it is crucial to distinguish between the everyday notion and the technical notions of information (information-theoretic measures) provided by information theory such as those derived from the work of Shannon, Rényi, Tsallis, Fisher, von Neumann, Kullback and Leibler, Wehrl, Maasen and Uffink, among others. Information, we might say, is what is provided when somebody is informed about something; then, the everyday notion of information is closely associated to the concepts of knowledge, language and meaning.

The technical notions of information are, by contrast, specified by use of a purely mathematical and physical vocabulary. A technical notion of information might be concerned with describing correlations and the statistical features of signals, as in communication theory with the Shannon concept, or it might be concerned with statistical inference (e.g., Fisher, Kullback and Leibler). Other technical notions of information have been introduced to capture certain abstract notions of structure and organization such as complexity and divergence (see Parts II and III of this Thesis) or functional role [23]. Generally, there is no *a priori* preferred technical notion of information, information-theoretic measure, in physical applications and its specific choice appears to be purpose-dependent. The development of their properties and applications of the diverse technical notions of information has been done by a large number of people: Majernik (see e.g., [24–27]), Frieden, Nalewajski, Sen, A. Plastino, A.R. Plastino, Dehesa, Esquivel, Angulo, Antolin, Romera, Petz (see e.g., [28–30]), Massen, Nalewajski, Vignat, Zozor, Bercher, Bilaynicki-Birula, Geerlings, Harremoës, Nagy, López-Ruíz, Panos, etc.

Throughout this Thesis, we will apply the concept of information based on the statistical information theory (in the Shannon sense) to study a great variety of quantum phenomena encountered in different physical and chemical systems. In this context, *Information is the removed uncertainty.* Quantum Mechanics is a probabilistic theory, i.e., the theory does not in general predict exactly what will happen in a physical experiment, but it specifies only the probability of possible outcomes. With each experiment we may associate a characteristic degree of predictability, or an amount of uncertainty. This degree of predictability is high when the probability distribution is concentrated and it is low when the distribution is roughly uniform. Information theory provides us

with different measures which quantify this uncertainty [31], e.g. Shannon [32], Rényi [33] and Tsallis [34] entropies or Fisher information [3], among others (for further details about their definition and meanings see Chapter 1).

Let us remark that the extremization techniques of these information-theoretic measures are very useful constructive methods which objectively estimate the unknown distribution when only incomplete data are available. Jaynes was the first one who showed that the maximum Shannon entropy hypothesis provides a method for constructing the whole of the conventional or extensive statistical thermodynamics [4, 5, 35]. More recently, the maximization of the Tsallis entropy has been shown to be the basis of the modern non-extensive statistical mechanics [36]. On the other hand, the minimization of the Fisher information (or the closely related extremization physical information of Frieden [37]) gives rise to a differential equation and hence to multiple solutions specified by appropriate boundary conditions. As claimed by Frieden, only the Fisher information is able to provide the fundamental wave equations and the conservation laws of natural systems at small and large scales by means of a single unifying principle, that of extreme physical information (EPI), which is related to the theory of measurement. Indeed, from EPI he derived Maxwell's equations, the Einstein field equations, the Klein-Gordon and Dirac equations, various laws of statistial physics, and even a few previously undiscovered laws governing nearly incompressible turbulent fluid flows. Moreover, Nalewajski [38, 39] has recently derived from this principle the well-known Kohn-Sham equation of the Density Functional Theory (DFT) and has explored the entropic principles of Daudel's loge theory [40, 41] of the molecular electronic structure [42].

This first part of the Thesis contains two applications of the Information Theory to some atomic systems (emphasizing the hydrogenic systems with standard and non-standard dimensionalities) and chemical reactions. It is composed of four chapters. In Chapter 1, the standard deviation and the main single information-theoretic measures used throughout this work are defined (i.e., Shannon, Rényi and Tsallis entropies, Fisher information and entropic moments), and their distinctive characteristics and uncertainty relations are pointed out. Then, in Chapter 2 these measures and their uncertainty relations are analytically studied in both ground and excited states of the d-dimensional hydrogenic systems, emphasizing the circular and Rydberg cases for which numerous experimental results are being provided at present. In Chapter 3, the Fisher information is used to study a one-step and a two-step elementary chemical reactions; namely, a typical nucleophilic substitution reaction and the simplest radical abstraction reaction involving a free radical (atomic hydrogen) as an intermediate reactive, respectively. Finally, in Chapter 4, the multidimensional extremization problems of the Shannon, Tsallis and Fisher information measures subject to radial expectation values as main constraints are analyzed and applied to all ground-state neutral atoms with nuclear charge $Z = 1 - 103$. In addition, the existence conditions for the d-dimensional maxEnt problem are found,

what extends a number of results previously encountered by various authors [43] for the one-dimensional case.

Chapter 1

Information-theoretic measures: Concepts and definitions

The physical and chemical properties of atoms and molecules strongly depend on the spread of the probability density which characterizes their allowed quantum-mechanical states. This spread can be differently grasped and complementary quantified by various information-theoretic measures beyond the celebrated standard deviation or its square, the variance.

The determination of these information-theoretic quantities is a main goal of the information theory of the finite quantum systems, which is the strongest support of the modern information and computation [15]. Moreover, these measures and the related notions of uncertainty, randomness, disorder and localization are basic ingredients encountered to play a relevant role for the identification and description of numerous quantum phenomena in physical systems and chemical processes. This was initially pointed out by Bialynicki-Birula and Mycielski [44], Gadre, Parr and Sears et al [45–49], Levine [50] and the members of the Granada [12, 51–53] and Kingston [14, 54, 55] groups, who make profit of ideas and methods of Fisher [3], Frieden [37], Jaynes [4, 5, 35, 56, 57], Rényi [58], Shannon [16], Tsallis [34], Stam [59] and Kolmogorov [60], among others, previously developed in statistics, statistical mechanics, communication theory and classical information theory.

In this Chapter we consider the single information-theoretic measures used throughout this work which complementarily describe the spreading of a probability distribution all over its domain of definition beyond the celebrated standard deviation (or its square, the variance), giving their definitions and interpretations. It is divided into three parts. First, in Section 1.1, we consider the measures of global character which quantify the total extent of the probability density in various ways according to their different analytic structure; namely, they are described by means of power (entropic moments, Rényi and Tsallis) and logarithmic (Shannon) functionals of the density. Then, in Section 1.2, the

Fisher information is discussed. This is a qualitatively different quantity because it is a functional of the gradient of the probability density, so being very sensitive to the point-wise analytic behaviour of the density; it is a measure of local character in this sense. A brieg comparisong among these measures is carried out in Section 1.3. Finally, in Section 1.4, some uncertainty relations corresponding to the information measures defined in this chapter are given.

1.1 Global measures

Let us here briefly discuss the main spatial delocalization or spreading quantities of global character which are often used as quantum uncertainty measures; namely, the standard deviation, the entropic moments and the single information-theoretic measures of Shannon, Rényi and Tsallis types. As well, we will briefly survey the uncertainty relations associated to these measures in quantum systems of any dimensionality. It is worth emphasizing that we do not attempt to define an information content of the physical system as a whole, but rather we wish to set an appropriate measure of uncertainty and information for concrete pure states of a quantum system.

Standard deviation

For a random variable X with N possible values $\{X_i\}_{i=1}^N$ with probabilities $\{p_i\}_{i=1}^N$, the uncertainty in the result of a measurement is given by the *standard deviation* $\sigma = \Delta x$ which is defined by the square root of the *variance*:

$$V[X] \equiv \left\langle X^2 \right\rangle - \langle X \rangle^2 , \tag{1.1}$$

where $\langle X \rangle$ is the mean value defined as

$$\langle X \rangle = \sum_{i=1}^{N} p_i X_i . \tag{1.2}$$

and similarly for $\left\langle X^2 \right\rangle$ in terms of X_i^2.

We can see that the variance is defined in terms of a sum for all possible values multiplied by its probabilities; so it does not depend on the order one takes these values. This is related to its global character.

The variance can be straightforwardly generalized to continuous variables. Indeed for a continuous variabes we have a probability density $\rho(x)$ with $x \in [a, b]$, the variance is

$$V\left[\rho\right] = \left\langle x^2 \right\rangle - \langle x \rangle^2 , \tag{1.3}$$

where the mean value of a function $f(x)$ is given by

$$\langle f(x)\rangle = \int_a^b f(x)\rho(x)dx. \tag{1.4}$$

The standard deviation $\Delta x = \sqrt{V}$ gives a good quantification of the spreading of the probability density around its centroid. It is a measure of the separation of the region(s) of concentration from a particular point of the distribution (the mean value), rather than a measure of the extent to which the distribution is in fact concentrated. Moreover, this quantity is a direct measure of spreading in the sense of having the same units as the random variable, and has the virtues of being invariant under translations and reflections, scaling linearly with x ($\Delta y = a\Delta x$ for $y = ax$), and vanishing in the limit that the random variable has some definite value. So, the standard deviation vanishes for a Dirac delta distribution and its value is increasing when one goes away from it. In the Gaussian case, the standard deviation is closely related to the width-at-half-height of the density. These observations have supported the use of the standard deviation as a measure of uncertainty all over the years. Nowadays, this use is strongly questioned because it is inappropriate and, moreover, it is arbitrary in the sense that it is not based on an axiomatics. Concerning to the former, the standard deviation is a good estimation of the uncertainty for Gaussian and quasigaussian distributions, but in other cases it is not so good; let us consider, e.g., the sine-squared and the Cauchy distribution given by

$$p(x) = \frac{1}{\pi}\left(\frac{\sin x}{x}\right)^2 \tag{1.5}$$

and

$$p(x,\alpha) = \frac{\alpha}{\pi(x-a)^2+\alpha^2}, \tag{1.6}$$

respectively, where the standard deviation diverges for all possible non-negative values of the parameter α in spite of the fact that this density becomes arbitrarily concentrated as $\alpha \to 0$, i.e., that $p(x)$ tends towards the Dirac delta distribution when $\alpha > 0$. Actually, the standard deviation is neither a natural nor a generally adequate measure of quantum uncertainty and the Heisenberg, or better, Kennard-Weyl-Heisenberg inequality [61], $\Delta x\Delta p \geq 1/2$, though mathematically correct, is not always an appropriate expression of the uncertainty principle. The reason for this inadequacy arises because the standard deviation gives an ever increasing weight to the tails of a distribution. Indeed, because of this strong tail dependence of the standard deviation, a probability distribution may approach a Dirac delta function while its standard deviation remains arbitrarily large. Thus, a very slight contribution to the probability density, provided that is located very far from the mean value, may cause the standard deviation to blow up. This dependence is not relevant when the tails fall off exponentially, as it occurs for a Gaussian distribution, but for quantum-mechanical probability distributions the standard deviation generally does not express what one intuitively interprets as the width

of the distribution [62]. Following Hilgevoord, an adequate measure of the width is the length of the smallest interval on which the main part of the distribution is placed. It is worth to mention that there exist exact uncertainty relations which hold for this kind of width as was first obtained by Landau and Pollak [63] in 1961 and later on by other authors using information-theoretic quantities, expressing the intuitive content of the uncertainty principle.

This definition can be extended to an arbitrary number d of dimensions in a straightforward manner. Indeed, for a d-dimensional probability density, $\rho(\vec{r})$, defined on the domain $\Delta \subseteq \Re^d$, the variance is

$$V[\rho] \equiv \left\langle r^2 \right\rangle - \langle r \rangle^2 , \tag{1.7}$$

where $r = |\vec{r}|$ and the expectation value of a function $f(\vec{r})$ is given by

$$\langle f(\vec{r}) \rangle = \int_\Delta f(\vec{r}) \rho(\vec{r}) d\vec{r}. \tag{1.8}$$

Shannon entropy

One of the most relevant concepts in this Thesis, the Shannon entropy, finds its roots in the context of communication theory. In the nineteen forties Claude Elwood Shannon proposed a set of reasonable assumptions that should satisfy a candidate for being an appropriate measure of average uncertainty contained in the probability distribution for a finite set of observational events; i.e. the outcomes of a measurement or a detection of a signal in a communication channel. For a random variable X with N possible values, $\{X_i\}_{i=1}^N$, described by the probability distribution $\{p_i\}_{i=1}^N$, these conditions are:

- The uncertainty must be a continuous and symmetric function of $\{p_i\}_{i=1}^N$, i.e., small variations of the probabilities should cause only small changes of the uncertainty.
- When all probabilities are equal, $p_1 = p_2 = \cdots = p_N = \frac{1}{N}$, the uncertainty measure should reach its maximum value, being also an increasing function of N, i.e., in the equiprobability situation, the higher number of possibilities (N) for the random variable X, the higher the uncertainty is.
- The uncertainty associated to $\{p_i\}_{i=1}^N$ should be equal than the uncertainty associated to $\{p_i\}_{i=1}^M$ if $p_{N+1} = p_{N+2} = \cdots = p_M = 0$, i.e., adding an arbitrary set of possible values with null probability to the variable X keeps the uncertainty of the measure.

Shannon showed [16, 32] that these assumptions are only satisfied by the expression

$$H[X] \equiv -k \sum_{i=1}^{N} p_i \ln p_i, \tag{1.9}$$

in which $p_i \ln p_i = 0$ for $p_i = 0$ and with k being an arbitrary positive constant, choosing in what follows the value $k = 1$ for the sake of simplicity. This definition can be naturally generalized to a continuous probability density $p(x)$, $x \in \Delta \subseteq \Re$, as proposed by Shannon himself, in the form

$$H[X] = -\int_{\Delta} p(x) \ln p(x) dx, \tag{1.10}$$

where it is assumed that $p(x) \ln p(x) = 0$ for those values x for which $p(x) = 0$. This concept is often known as *differential entropy*. The values of this quantity for an extensive list of continuous probability densities are gathered in Ref. [64]. Later on, this notion was axiomatically obtained by Hatori [65] in a similar way as in the discrete version. It can also be deduced by discretizing the continuous distribution by means of the partition of the supporting interval Δ in subintervals, considering the discrete entropy and then taking its limit when the width of the subintervals tends to zero, though one has to renormalize the final result as explained in section 9.3 of Ref. [64]. The extension to multidimensional probability distribution $\rho(\vec{r})$ given as

$$S\left[\rho\right] = -\int_{\Delta} \rho(\vec{r}) \ln \rho(\vec{r}) d\vec{r}, \tag{1.11}$$

where $\Delta \subseteq \Re^d$, is straightforward.

Shannon introduced the name *entropy* for these expressions, referring to them also as a measures for information and uncertainty. Notions of entropy, information and uncertainty are intertwined and cannot be sharply differentiated. In normal parlance the terms "information" and "uncertainty" are considered as opposites of each other, rather than synonyms. By contrast, entropy is introduced by Shannon as the uncertainty on the outcome of an experiment based on a given probability distribution. Then, it is a measure of ignorance or lack of information concerning the outcome of the experiment, since the uncertainty appears, of course, because this probability distribution does not enable us to predict exactly what the actual outcome will be; so, the terms entropy and uncertainty are synonymous to some extent. On the other hand, the uncertainty is, of course, removed when the experiment is performed and the actual outcome becomes known. This shows that another way of thinking about the Shannon entropy is as a measure of the amount of information that we expect to gain on performing a probabilistic experiment. Thus, when the information is small (i.e., when one cannot almost predict the outcome of an experiment from the given probability distribution), the information gained by the performance of the experiment is also small. Summarizing, the Shannon entropy is a measure of the uncertainty of a probability distribution as well as a measure of information. Normally, the growth of uncertainty is identified with an increase of the entropy, which in turn is interpreted as an information loss.

Although the differential entropy has a number of properties which are quite different from those of its discrete counterpart (e.g., it may take negative values), the differential entropy is actually very useful. In fact, it retains enough properties of its discrete

analogue, such as the Schur concavity [66] (i.e., it is non decreasing under a doubly stochastic transformation) and it provides a lower bound for the standard deviation σ of all probability densities, given by

$$H[\rho] \leq \ln \sigma \sqrt{2\pi e}, \tag{1.12}$$

with equality holding for Gaussian distributions. This result is quite useful for the study of quantum-mechanical uncertainty relations. Moreover, let us also mention that the potential negativity does not pose any trouble in practice because it is always true that the lesser uncertainty, the lesser the entropy is; the only point now is that the more concentrated is the probability density (the lesser uncertainty), the entropy more approaches towards minus infinity. To avoid this trouble and to guaranty that the uncertainty is non-negative, it is more convenient to use the *exponential entropy* defined as

$$L\left[\rho\right] \equiv e^{S[\rho]}, \tag{1.13}$$

as a measure of uncertainty. Notice, in addition, that this exponential entropy has the same dimensions as the standard deviation and its transformation under the coordinate change $x \rightarrow y = ax$ takes a more natural form than the differential entropy.

Rényi entropy

The Shannon entropy is distinguished by several unique properties, as already mentioned, but it is often convenient to introduce the generalized Rényi entropy which is parametrized by a continuous parameter $\alpha > 0$. They are defined as

$$R^{(\alpha)}[X] \equiv \frac{1}{1-\alpha} \ln \left(\sum_{i=1}^{N} p_i^{\alpha} \right), \tag{1.14}$$

for a discrete probability distribution $\{p_i; i = 1, ., N\}$, which consists of non-negative numbers summing to unity. Rényi called this quantity the measure of information of order α associated with the probability distribution $\{p_i; i = 1, ., N\}$.

The continuous version is given by

$$R^{(\alpha)}\left[\rho\right] = \frac{1}{1-\alpha} \ln \int_{\Delta} \rho^{\alpha}(\vec{r}) d\vec{r}, \tag{1.15}$$

where $\rho(\vec{r})$ is a probability density defined over the domain $\Delta \subseteq \Re^d$. The Rényi measures of information may be also viewed as measures of uncertainty since after all the uncertainty is the missing of information as previously discussed.

The allowed range of values for the characteristic parameter α of the Rényi entropy in the continuous case is determined by the convergence conditions on the integral in the

definition, being imposed by the short- and long-range behaviours of the distribution $\rho(\vec{r})$. Apart from the necessary (but not sufficient) condition $\alpha > 0$ for the finiteness of $R^{(\alpha)}$, the particular value $\alpha = 1$ appears as a limiting case, because both the numerator and the denominator in Eq. (1.15) vanish, the limit giving rise to

$$R^{(1)}[\rho] = S[\rho] = -\int_{\Delta} \rho(\vec{r}) \ln \rho(\vec{r}) d\vec{r}, \tag{1.16}$$

that is, the Rényi entropy of order 1 is the Shannon entropy S; so that, the Rényi entropy $R^{(\alpha)}$ represents an extension or generalization of the Shannon entropy. Often particular Rényi entropies with parameter other than one have relevant applications by their own as recently discussed [67–69]. See also Ref. [67] for a survey of their basic properties.

This measure has been applied in biology, medicine, genetics, lingüistics, electrical engineering, computer science and economics. Moreover, the Rényi entropy has been widely used in quantum physics, such as in the analysis of quantum entanglement [70, 71], quantum communications [72], atomic ionization properties [73], quantum revivals [74] and localization properties [75], among others.

Tsallis entropy

The Rényi method to generalize the Shannon entropy is by far not the only one as it is extensively described in the monograph of Kapur [76] and Arndt [31]. Havrda and Charvat [77] in 1967 and Tsallis [34] in 1988 introduced the following generalized measure [78]:

$$T^{(\alpha)}[X] \equiv \frac{1}{\alpha - 1} \left(1 - \sum_{i=1}^{N} p_i^{\alpha} \right), \tag{1.17}$$

which is usually referred as *Tsallis entropy* for discrete probability distributions. This quantity has also been extended to the continuous variable $\vec{r} \in \Delta \subseteq \Re^d$ as follows:

$$T^{(\alpha)}[\rho] = \frac{1}{\alpha - 1} \left(1 - \int_{\Delta} \rho(\vec{r})^{\alpha} d\vec{r} \right). \tag{1.18}$$

where $\rho(\vec{r})$ is a probability density defined over the domain $\Delta \subseteq \Re^d$. Remark that the Tsallis expression may be seen as a linearization of the Renyi expression. For an exhaustive review of the basic properties and physical applications of this quantity, see the recent monograph of Tsallis [36].

As in the case of the Rényi entropy, the limit $\alpha \to 1$ provides the Shannon entropy, $T^{(1)}[\rho] = S[\rho]$. The same comments regarding the convergence conditions for the Rényi entropy apply also for the Tsallis one.

In contrast to the Rényi entropy, it has been shown that by a suitable definition of average values, namely $\langle A \rangle_T = \int A(x) \rho^{\alpha}(x) dx$, this information-theoretic measure has

important variational properties of the type associated with the usual Shannon entropy for extensive systems. In particular, it is always a concave function of the density for $\alpha > 1$ (and convex for $\alpha < 1$), whereas the Rényi entropy does not. Hence, the Tsallis maximizing distributions, under some specific constraints, are uniquely defined for $\alpha > 0$. For instance, when the constraint is that the distribution is finitely supported, then the Tsallis maximizing distribution is uniform. More interestingly, for any dimension $d \geq 1$, the Tsallis maximizing distribution with a given covariance matrix has a multidimensional Student-t form if $d/(d+2) < \alpha < 1$ [79]. This result generalizes the well-known property that Shannon entropy is maximized for the normal distribution. On the other hand, while the Shannon entropy is additive (i.e., for a system composed of any two probabilistically independent subsystems, the Shannon entropy of the sum is equal to the sum of the entropies), the Tsallis entropy violates this property and, therefore, it is non-additive. The Tsallis entropies are in fact pseudoadditive (i.e. $T^{(\alpha)}[\rho_1 \otimes \rho_2] = T^{(\alpha)}[\rho_1] + T^{(\alpha)}[\rho_2] + (1-\alpha)T^{(\alpha)}[\rho_1]\,T^{(\alpha)}[\rho_2]$). Moreover, in thermodynamical terms, while the Boltzmann-Gibbs-Shannon entropy was specifically designed to be applicable to extensive systems, the Tsallis entropy extends it to the nonextensive systems. Let us bring here that the entropy of a system or a subsystem is said to be *extensive* if, for a large number N of its elements (probabilistically independent or not), the entropy is (asymptotically) proportional to N; otherwise, it is nonextensive. Let us also point out that the second order Tsallis entropy, i.e.

$$T^{(2)}[\rho] = 1 - \omega^{(2)}[\rho] = 1 - \int_{\Delta} [\rho(\vec{r})]^2 \, d\vec{r} \tag{1.19}$$

is the simplest entropy, providing a good alternative to the Shannon entropy in many cases. In fact, it is more than that; it refers directly to the experimental results of mutually complementary measurements, so opposite to the Shannon entropy which is applicable when the measurements exhibit a preexisting symmetry [80]. It is called linear or linearized entropy [81], having been used not only as an impurity measure of the quantum state but also as measure of decoherence, entanglement, complexity and mixedness of three-dimensional quantum systems.

Entropic moments

The Shannon, Rényi and Tsallis entropies are measures of uncertainty of a probability distribution as well as measures of information. A measure of uncertainty is a quantitative measure of the lack of concentration of a probability distribution; this is called an uncertainty because it quantifies our uncertainty about what the outcome of an experiment completely described by the probability distribution in question will be. Uffink [66] provided an axiomatic derivation of measures of uncertainty, deriving a class of quantities whose key property is Schur concavity; for details see [15, 82, 83]. These expressions

are essentially the so-called *frequency or entropic moments* of the (d-dimensional) probability density, defined by

$$\omega^{(\alpha)}[\rho] \equiv \int_{\Delta} \rho^{\alpha}(\vec{r}) d\vec{r}, \tag{1.20}$$

with $\vec{r} \in \Delta \subseteq \Re^d$. It is straightforward to see that the Rényi, Tsallis and Shannon entropies can be easily derived from these quantities. In fact the entropic moments were early considered by mathematicians [84, 85] and statisticians [86, 87], but its usefulness in finite quantum systems was discovered much later, especially with the advent of the Density Tunctional Theory [88, 89]. Let us only point out that they describe, save for a proportionality factor, the atomic Thomas-Fermi and the Dirac exchange energy when α is equal to 5/3 and 4/3, respectively; see Ref. [90] for further physico-mathematical details and connections with other density functionals.

The power α of the distribution in Eq. (1.20), allows to enhance or diminish, by increasing or decreasing its value, the contribution of the integrand over different regions to the whole integral and, consequently, to the frequency moments and the Rényi, $R^{(\alpha)}$, and Tsallis, $T^{(\alpha)}$, entropies. Higher values of α make the function $\rho^{\alpha}(\vec{r})$ to concentrate around the local maxima of the distribution, while the lower values have the effect of smoothing that function over its whole domain. It is in that sense that the parameter α provide us with a powerful tool in order to get information on the structure of the distribution by means of the Rényi and Tsallis entropies.

A relevant particular case of the frequency moments corresponds to $\alpha = 2$, from which arises the definition of *disequilibrium* D as the second-order frequency moment $\omega^{(2)}$, namely

$$D[\rho] \equiv \omega^{(2)}[\rho] = \int_{\Delta} \rho^{2}(\vec{r}) d\vec{r}, \tag{1.21}$$

which is a well-known descriptor of the level of departure from uniformity of the distribution [83, 91].

1.2 Local measures: Fisher information

The quantities defined in the previous section have a global character, i.e., they are very little sensitive to strong changes on the distribution over a small-sized region. So, it appears useful to have at our disposal measures that could be able to detect these local changes of the density in order to better describe the system in an information-theoretical way.

Let us keep in mind that the term information, as it is used here following Shannon concept, refers to information about the outcome of an experiment, governed by a given probability distribution. This is to be contrasted with the technical notion of information concerned with statistical inference, the so-called *parametric Fisher information* [3],

which was introduced by Ronald A. Fisher, a British biostatistician who was among the first one to develop and employ in genetics and eugenics methods such as maximum likelihood, the analysis of variance and the design of experiments. The parametric Fisher information refers to the information about an unknown parameter in the probability distribution estimated from observed outcomes.

Let us suppose that we want to estimate a parameter θ doing N measures in an experiment. These data, $\vec{y} \equiv \{y_i\}_{i=1}^N$, obey $y_i = \theta + x_i$ where $\vec{x} \equiv \{x_i\}_{i=1}^N$ are added noise values. The noise $\vec{x}$ is assumed to be intrinsic to the parameter θ under measurement (θ has a definite but unknown value). This system is specified by a conditional probability law $p_\theta(\vec{y}|\theta) = p(y_1, y_2, \cdots, y_N|\theta)$ and $\hat{\theta}(\vec{y}|\theta)$ is, on average, a better estimate of θ as compared to any of the data observables, $\hat{\theta}(\vec{y}) = \theta$. In this case, we can define the Fisher information as

$$I \equiv \int \left[\frac{\partial \ln p_\theta(\vec{y})|\theta}{\partial\theta}\right]^2 p_\theta(\vec{y}|\theta)d\vec{y}, \tag{1.22}$$

which fulfils the consequence of the Cauchy-Schwartz inequality known as the Cramér-Rao inequality [64]

$$\sigma^2 \times I \geq 1, \tag{1.23}$$

where σ^2 is the mean-square error given by

$$\sigma^2 = \int \left[\hat{\theta}(\vec{y}) - \theta\right]^2 p_\theta(\vec{y})d\vec{y}. \tag{1.24}$$

Then, the parametric Fisher information measures the ability to estimate a parameter, that is, it gives the minimum error in estimating θ from the given probability density $p(\vec{y}\,|\theta\,)$

In the particular case of $N = 1$, $p_\theta(\vec{y}|\theta) = p(y|\theta)$ and the fluctuations x are invariant to the size of θ, $p_\theta(y|\theta) = p_x(y - \theta)$ with $x = y - \theta$ (i.e. shift invariance); one has

$$I = \int \left[\frac{\partial \ln p(x)}{\partial x}\right]^2 p(x)dx, \tag{1.25}$$

which is the so-called *(translationally-invariant) Fisher information*. This quantity measures the gradient content of the probability distribution which describes the system; so, it reflects the irregularities of the density and then, it is a measure of systems disorder.

The one-dimensional Fisher information can be generalized for d-dimensional densities $\rho(\vec{r})$, with $\vec{r} \in \Delta \subseteq \Re^d$, in the following way:

$$I\,[\rho] = \int_\Delta \left|\vec{\nabla}_d \ln \rho(\vec{r})\right|^2 \rho(\vec{r})d\vec{r} = \int_\Delta \frac{\left|\vec{\nabla}_d \rho(\vec{r})\right|^2}{\rho(\vec{r})}d\vec{r}, \tag{1.26}$$

where $\vec{\nabla}_d$ is the d-dimensional gradient operator given by

$$\vec{\nabla}_d = \frac{\partial}{\partial r}\hat{r} + \frac{1}{r}\sum_{i=1}^{d-2}\frac{1}{\prod_{k=1}^{i-1}\sin\theta_k}\frac{\partial}{\partial\theta_i}\hat{\theta}_i + \frac{1}{r\prod_{i=1}^{d-2}\sin\theta_i}\frac{\partial}{\partial\varphi}\hat{\varphi}, \tag{1.27}$$

where the symbol $\hat{a}$ denotes the unit vector associated to the corresponding coordinate.

This formula defines a convex and isotropic functional. Moreover, being the scalar product of two vectors, it is independent of the reference frame [92]. The Frieden monograph [37] presents the most detailed discussion of the basic properties of the Fisher information, gleaned from branches of physics as diverse as classical and fluid mechanics, electro- and thermodynamics, quantum theory and general relativity, in which this notion appears. Moreover, Frieden compares Fisher information with the Shannon, Boltzmann and Kullback-Leibler definitions of entropy, which likewise represent attempts to identify scalar measures of information. The comparison is most easily made with the Shannon entropy. In contrast to the Shannon entropy, which measures the spread of the probability distribution and it is a global quantity because of its logarithmic-functional form, the Fisher information measures the narrowness of the distribution and it has a property of locality because of its gradient-functional form.

Let us finally remark that the Shannon entropy and Fisher information are the basic variables of two extremization procedures: the maximum entropy method [93] and the principle of extreme physical information [37], respectively, as it will be shown in Chapter 4. Moreover, both measures (i) are closely related to fundamental and/or experimentally measurable quantities of finite electronic and nucleonic systems [45, 51, 52, 93–95], (ii) they have been used to identify the most distinctive nonlinear phenomena (avoided crossings) encountered in atomic and molecular spectra under external fields [96, 97], and (iii) they are the cornerstones of two alternative formulations of the classical thermodynamics [57, 98].

This concept was firstly introduced for one-dimensional random variables in statistical estimation [3] but nowadays it is playing an increasing role in numerous fields [37], in particular, for many-electron systems, partially because of its formal resemblance with kinetic [37, 45, 94, 99, 100] and Weiszäcker [52, 101] energies. The Fisher information, contrary to the Rényi, Shannon and Tsallis entropies, is a local measure of spreading of the density $\rho(\vec{r})$ because it is a gradient functional of $\rho(\vec{r})$. The higher this quantity is, the more localized is the density, the smaller is the uncertainty and the higher is the accuracy in estimating the localization of the particle. However, it has an intrinsic connection with Shannon entropy via the de Bruijn inequality [64, 102] as well as a simple connection with the precision (variance $V[\rho]$) of the experiments by means of the celebrated Cramér-Rao inequality [64, 102, 103]

$$I[\rho] \times V[\rho] \geq d^2, \tag{1.28}$$

The notion of Fisher information has been shown to be very fertile to identify, characterize and interpret numerous phenomena and processes in atomic and molecular physics such as e.g., correlation properties in atoms, spectral avoided crossings of atoms in external fields [97], the periodicity and shell structure in the Periodic Table of chemical elements [104] and the transition state and other stationary points in chemical reactions [105] (see Chapter 3). Moreover, it has been used for the variational characterization of quantum equations of motion [37] as well as to rederive the classical thermodynamics without requiring the usual concept of Boltzmann's entropy [106]. As well, Fisher information has been shown to be a versatile tool to describe the evolution laws of physical systems [37, 107], to accurately describe the behaviour of dynamic systems and to characterize the complex signals generated by these systems [108]. Later on, this observation has been used to characterize the dynamics of electroencephalographic (EEG) [109] and earthquake-related geoelectrical [110] signals.

1.3 Comparison among information measures

The purpose of this section is to mutually compare some of the global and local spreading measures mentioned above. Let us start highlighting the differences between some global spreading measures (variance, disequilibrium and Shannon entropy) and a local quantity such as the Fisher information by calculating them in two simple, but illustrative, probability distributions given by the exponential density $f(x)$ of the form e^{-ax} and a similar density modified by a small sinusoidal perturbation, $g(x)$, given by $e^{-ax} + \epsilon \quad sin^2 nx$

They are depicted in Figure 1.1, where we notice that both density functions have a similar global shape. The results are gathered in Table 1.1. Therein, we observe that not only the standard deviation, but also the disequilibrium and the Shannon entropy, have very similar values for the two functions; this is mainly due to the fact that all these measures have a global character because they quantify the probability density as a whole; this is because of their analytical structure in terms of the density which has a powerlike (variance, disequilibrium; see Eqs. (1.7) and (1.21), respectively) and logarithmic (Shannon entropy; see Eq. (1.10)) form.

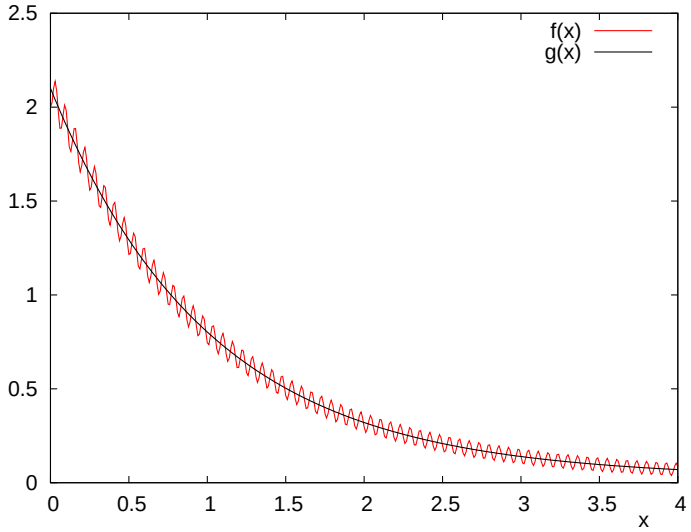

FIGURE 1.1: Representation of $f(x) \sim e^{-ax}$ and $g(x) \sim e^{-ax} + \epsilon sin^2 nx$.

Function	Shannon entropy	Variance	Disequilibrium	Fisher information
$f(x)$	1.3485	0.07962	0.2690	9.3×10^{-1}
$g(x)$	1.3476	0.07966	0.2695	3.7×10^{3}

TABLE 1.1: Information-theoretic measures of $f(x)$ and $g(x)$

By contrast the Fisher information have very different numerical values for these two functions, being much higher for $g(x)$ than for $f(x)$. As we can see in the figure, this is due to the highly oscillatory behaviour for large n which $g(x)$ possesses. The Fisher information has a gradient functional form, what makes this measure very sensitive to strong local changes (as in the present example) of the distribution.

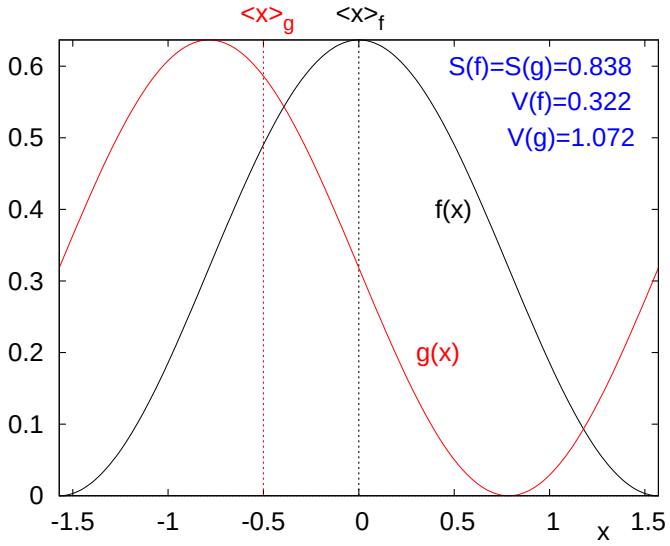

FIGURE 1.2: Representation of $f(x) = \frac{2}{\pi}\cos^2(x)$ and $g(x) = \frac{2}{\pi}\cos^2\left(x + \frac{\pi}{4}\right)$.

Secondly, let us now choose another couple of probability densities where one can disentangle between the roles of the Shannon entropy and the variance more appropriately.

We have taken two finitely supported density functions on the interval $x \in [-\pi/2, \pi/2]$, namely the cosine function $f(x) = \frac{2}{\pi}\cos^2(x)$, and the shifted cosine function given by $g(x) = \frac{2}{\pi}\cos^2\left(x + \frac{\pi}{4}\right)$ which are represented in Figure 1.2. Therein, we observe that both functions have the same Shannon entropy, but in this case the variances differ. As we mentioned before in Section 1.1, the variance measures the spread of the distribution with respect to its centroid (depicted in the figure); so, depending on the position of this centroid, $\langle x \rangle$, the variance has different values for each distribution. Let us remark that the Fisher information for both functions have the same values, as also occurs with the disequilibrium

1.4 Uncertainty relations

In this Section we shall give the uncertainty relations corresponding to the power, logarithmic and entropic moments together with those associated to the Rényi, Shannon and Tsallis entropies and the Fisher information of general d-dimensional quantum systems. These relations are different mathematical formulations of the quantum-mechanical uncertainty principle which describes a characteristic feature of quantum mechanics and states the limitations to perform measurements on a system without disturbing it. Moreover, since the two canonically conjugate observables involved in the uncertainty relations here considered -position and momentum- do not conmute, both observables cannot be precisely determined in any quantum state of the system.

The d-dimensional position-momentum Heisenberg-like uncertainty relation is known [111] to have the form

$$\left\langle r^{d/\alpha} \right\rangle^{\alpha} \left\langle p^{d/\beta} \right\rangle^{\beta} \geq \alpha^{\alpha}\beta^{\beta} \frac{\Gamma^2\left(1+\frac{d}{2}\right)}{\Gamma\left(1+\alpha\right)\Gamma\left(1+\beta\right)} e^{d-\alpha-\beta}; \qquad \alpha, \beta > 0, \tag{1.29}$$

obtained by using information-theoretic methods. For $\alpha = \beta = d/2$, this expression simplifies to the familiar d-dimensional form of Heisenberg inequality

$$\left\langle r^2 \right\rangle \left\langle p^2 \right\rangle \geq \frac{d^2}{4}, \tag{1.30}$$

which shows that the more accurately the position is known, the less accurately is the momentum determined, and vice-versa. For completeness let us quote here that Eq. (1.29) for $d = 3$ can be cast in the form

$$\langle r^{\alpha} \rangle^{1/\alpha} \left\langle p^{\beta} \right\rangle^{1/\beta} \geq \left(\frac{\pi\alpha\beta}{16\Gamma\left(\frac{3}{\alpha}\right)\Gamma\left(\frac{3}{\beta}\right)} \right)^{1/3} \left(\frac{3}{\alpha}\right)^{\frac{1}{\alpha}} \left(\frac{3}{\beta}\right)^{\frac{1}{\beta}} e^{1-\frac{1}{\alpha}-\frac{1}{\beta}}; \;\; \alpha, \beta > 0, \tag{1.31}$$

which for the specially interesting case $a = b > 0$ takes the form

$$\langle r^\alpha \rangle \langle p^\alpha \rangle \geq \left\{ \left(\frac{27\pi}{16\alpha\Gamma\left(\frac{3}{\alpha}\right)} \right)^{\frac{1}{3}} \left(\frac{\alpha e}{3} \right)^{1-\frac{2}{\alpha}} \right\}^{\alpha}, \qquad \alpha > 0, \tag{1.32}$$

Note that for $a = 2$ this inequality reduces to Eq. (1.30) with $d = 3$. For alternative forms of these two inequalities in terms of variances or even in terms of moments around a point other than the origin, see Eqs. (2.9) and next ones of Ref. [112].

A generalization of the (power-moments-based) Heisenberg-like uncertainty relation was obtained by Rajagopal [113] by use of the entropic moments in position and momentum spaces. He extended to d dimensions and improve the one-dimensional results of Maassen-Uffink [82], obtaining the following entropic-moment-based uncertainty relation (see also [114, 115]):

$$\left\{ \omega^{(\alpha+1)}\left[\rho\right] \right\}^{-\frac{1}{\alpha}} \times \left\{ \omega^{(\beta+1)}\left[\gamma\right] \right\}^{-\frac{1}{\beta}} \geq \left[\frac{\pi(1+2\alpha)^{1+\frac{1}{2\alpha}}}{1+\alpha} \right]^{d}, \tag{1.33}$$

which is valid for $\alpha \geq -\frac{1}{2}$ and $\beta = -\frac{\alpha}{1+2\alpha}$. For $\alpha = \beta = 0$ it reduces to the (Shannon-entropy-based) entropic uncertainty relation

$$S\left[\rho\right] + S\left[\gamma\right] \geq d\left(1 + \ln \pi\right), \tag{1.34}$$

first derived by Hirschman [116] and later improved independently by Beckner [117] and Bialynicki-Birula and Mycielski [44]. This expression indicates that the total uncertainty in position and momentum cannot be decreased beyond the value given by Eq. (1.34). The entropic uncertainty relation can be recast into the form

$$J\left[\rho\right] \times J\left[\gamma\right] \geq \frac{1}{4}, \tag{1.35}$$

where the position Shannon entropic power is defined by

$$J\left[\rho\right] \equiv \frac{1}{2\pi e} e^{\frac{2}{d}S[\rho]}, \tag{1.36}$$

and similarly for the momentum Shannon entropy power $J\left[\gamma\right]$. Let us point out here that the Shannon-entropy sum $S[\rho] + S[\gamma]$ has shown its usefulness for numerous physical issues (e.g., to study the correlation energy of atomic systems [118]), having been postulated a new entropy maximization principle based in it by Gadre [93]. This author and his collaborators [119] have numerically shown some interesting properties of this entropy sum for atoms in a Hartree-Fock framework; in particular, it has a minimum value for the ground state which is scale invariant while the individual entropies are not.

The expressions (1.18) and (1.33) have allowed Rajagopal [113] to obtain the Tsallis-entropy-based uncertainty relation as

$$\left\{1+(1-p)T^{(p)}[\rho]\right\}^{-\frac{1}{2p}} \times \left\{1+(1-q)T^{(q)}[\gamma]\right\}^{\frac{1}{2q}} \geq \left(\frac{q}{\pi}\right)^{\frac{d}{4q}} \left(\frac{p}{\pi}\right)^{-\frac{d}{4p}}, \tag{1.37}$$

with $\frac{1}{p}+\frac{1}{q}=2$. Finally, let us quote here the Rényi-entropy-based uncertainty relation found by Bialynicky-Birula [120] and independently by Zozor and Vignat [121]. They obtained it in the one-dimensional case as

$$R^{(\alpha-1)}[\rho]+R^{(\beta-1)}[\gamma] \geq -\frac{1}{2(1-\alpha)}\ln\frac{\alpha}{\pi}-\frac{1}{2(1-\beta)}\ln\frac{\beta}{\pi}, \tag{1.38}$$

for $\alpha>\beta$. The extension to d dimensions has been recently found by Zozor et al [122].

Finally, let us discuss the uncertainty relations which involve the Fisher informations. Since the nineteen fifties [59] the Stam inequalities are known:

$$I[\rho] \leq 4\left\langle p^2\right\rangle; \qquad I[\gamma] \leq 4\left\langle r^2\right\rangle, \tag{1.39}$$

which link the position (momentum) Fisher information and the momentum (position) radial expectation value $\left\langle p^2\right\rangle$ (respectively $\left\langle r^2\right\rangle$). See also Ref. [104] for its generalization to finite many-electron systems. Recently, the Fisher-information-based uncertainty relation has been found [123] to be

$$I[\rho] \times I[\gamma] \geq 4d^2, \tag{1.40}$$

which is valid not only for one-dimensional [124] but also for d-dimensional [125] real-valued wavefunctions.

Chapter 2

Information-theoretic study of d-dimensional hydrogenic systems

The hydrogenic system (i.e. a negatively-charged particle moving around a positively-charged core which electromagnetically binds it in its orbit), with standard ($d = 3$) and non-standard dimensionalities, plays a central role in d-dimensional Quantum Physics and Chemistry [126]. It includes not only a large variety of three-dimensional physical systems (e.g., hydrogenic atoms and ions, exotic atoms, antimatter atoms, Rydberg atoms,) but also a number of nanoobjects so much useful in semiconductor nanostructures (e.g., quantum wells, wires and dots) [127, 128] and quantum computation (e.g., qubits) [129, 130]. Its deeper knowledge is basic not only to gain full a insight into the intimate structure of matter but also for numerous phenomena of quantum cosmology [131], nanotechnology [127, 128] (e.g., for low dimensional semiconductor nanostructures such as quantum wells, wires and dots), quantum computation [130, 132] (e.g., one- and two-dimensional hydrogenic atoms which have been proposed as qubits), d-dimensional physics [126, 133–138] and quantum field theory [137, 139–141]. Let us also remark that the existence of hydrogenic systems with non-standard dimensionalities has been proved for $d < 3$ [128] and suggested for $d > 3$ [133]. We should also highlight the use of d-dimensional hydrogenic wavefunctions as complete orthonormal sets for many-body problems [142, 143] in both position and momentum spaces, explicitly for three-body Coulomb systems (e.g. the hydrogen molecular ion and the helium atom); generalizations are indeed possible in momentum-space orbitals as well as attending to their role as Sturmians in configuration spaces.

Since the early days of Quantum Mechanics the hydrogenic system has played a central role, mainly because its Schrödinger equation can be solved analytically. Although numerous known results about the macroscopic and spectroscopic properties of this system are scattered in the literature, the exact expressions for the radial expectation values of their quantum-mechanical states in position [144] and momentum [145, 146] spaces

have not been obtained until very recently. Moreover, tremendous advances [147–150] have been witnessed since the seventies up to now in understanding the spectroscopic properties of three-dimensional Rydberg hydrogenic atoms (i.e., hydrogenlike atoms in states with high principal quantum number). In particular, the production of Rydberg atoms in circular states (i.e., states with angular quantum numbers $l = |m_l| = n - 1$) by using electron excitation and the creation of localized electron wavepackets by means of weak static electric fields has provided an experimental basis for numerous fascinating investigations on fundamentals of Quantum Mechanics.

The information theory of d-dimensional hydrogenic systems includes the description of their macroscopic and spectroscopic properties by means of information-theoretical techniques. Here we investigate the spatial extension or spreading of the electronic position and momentum probability densities of a d-dimensional atom far beyond the variance, by means of the power and logarithmic moments and the information-theoretic measures of global and local character; namely, the Shannon entropy

$$S_r\left[\rho\right] = -\int \rho\left(\vec{r}\right) \ln \rho\left(\vec{r}\right) d\vec{r}, \tag{2.1}$$

and the Fisher information

$$I_r\left[\rho\right] = \int \frac{\left|\vec{\nabla}_d \rho(\vec{r})\right|^2}{\rho(\vec{r})} d\vec{r}, \tag{2.2}$$

respectively, for the position space density $\rho(\vec{r})$. The symbol $\vec{\nabla}_d$ denotes the d-dimensional gradient operator given by Eq. (1.27). The same quantities are defined similarly for the momentum density $\gamma(\vec{p})$.

The structure of this chapter is the following. First, in Section 2.1 we solve the Schrödinger equation in order to obtain the probability densities in position and momentum spaces which describe hydrogenic systems. Then, in Section 2.2 we analyze various theoretical tools which quantify the multidimensional spreading of d-dimensional hydrogenic system in position and momentum spaces, including diverse expectation values (such as the power and logarithmic moments), global information measures (the variance and the Shannon entropy) and the Fisher information which has the property of locality. In Section 2.3, we discuss the associated uncertainty relationships in the light of the improvement recently discovered for central potentials [125]. Section 2.4 is devoted to the explicit calculation of the spreading measures of d-dimensional circular states. In Section 2.5, we obtain the Heisenberg, Shannon and Fisher spreading measures of Rydberg atoms in d dimensions. Finally, in Section 2.6, some conclusions are given.

2.1 Probability distributions of hydrogenic systems

In this section we fix the notation and we describe in hyperspherical polar coordinates the wave functions of the d-dimensional hydrogenic orbitals (i.e., the solutions of the nonrelativistic, time-independent Schrödinger equation in d dimensions describing the quantum mechanics for the motion of an electron in the Coulomb field of a nucleus with charge $+Ze$, where e refers to the absolute value of the electron charge) in the configuration (or position) and momentum spaces, as well as the associated probability densities. In what follows, atomic units will be used (i.e. $m = e = \hbar = a_0 = 1$, m and $a_0 = \frac{\hbar^2}{me^2}$ being the electron mass and Borh radius, respectively)

2.1.1 Position orbitals

Let us consider an electron moving under the action of the d-dimensional ($d \geqslant 2$) Coulomb potential $V(\vec{r}) = -\dfrac{Z}{r}$, where $\vec{r} = (r, \theta_1, \theta_2, ..., \theta_{d-2}, \varphi)$ denotes the electronic vector position in polar coordinates with the nucleus (located) at the origin, and Z is the nuclear charge. The electronic probability density of the stationary states for the d-dimensional hydrogenic system is given by $\rho(\vec{r}) = |\Psi(\vec{r})|^2$, where the wavefunction $\Psi(\vec{r})$ is the physical solution of the time-independet Schrödinger equation

$$\left(-\frac{1}{2}\vec{\nabla}_d^2 - \frac{Z}{r}\right)\Psi(\vec{r}) = E\Psi(\vec{r})\,. \tag{2.3}$$

with E being the total energy of the system.

Besides, the vector position is written $\vec{r} = (r, \theta_1, \theta_2, ..., \theta_{d-1} \equiv \varphi)$ in polar coordinates and the d-dimensional gradient operator is given by Eq. (1.27).

It is known [129] that the energies belonging to the discrete spectrum are

$$E = -\frac{Z^2}{2\eta^2}, \qquad \eta = n + \frac{d-3}{2}; \quad n = 1, 2, 3, ..., \tag{2.4}$$

and the associated wavefunction can be expressed as

$$\Psi_{n,l,\{\mu\}}(\vec{r}) = R_{n,l}(r)\mathcal{Y}_{l,\{\mu\}}(\Omega_{d-1}), \tag{2.5}$$

where $(l, \{\mu\}) \equiv (l \equiv \mu_1, \mu_2, ..., \mu_{d-1})$ denote the hyperquantum numbers associated to the angular variables $\Omega_{d-1} \equiv (\theta_1, \theta_2, ..., \theta_{d-1})$, which may take all values consistent with the inequalities $l \equiv \mu_1 \geq \mu_2 \geq ... \geq |\mu_{d-1}| \equiv |m| \geq 0$. The radial wavefunction is given

by

$$R_{n,l}(r) = N_{n,l}\left[\frac{\omega_{2L+1}(\tilde{r})}{\tilde{r}^{d-2}}\right]^{1/2}\mathcal{L}^{2L+1}_{\eta-L-1}(\tilde{r}) \tag{2.6}$$
$$= \left(\frac{\lambda^{-d}}{2\eta}\right)^{1/2}\left[\frac{\omega_{2L+1}(\tilde{r})}{\tilde{r}^{d-2}}\right]^{1/2}\tilde{\mathcal{L}}^{2L+1}_{\eta-L-1}(\tilde{r}),$$

where the "grand orbital angular momentum quantum number" L and the adimensional parameter $\tilde{r}$ are

$$L = l + \frac{d-3}{2}, \quad l = 0, 1, 2, \ldots \tag{2.7}$$
$$\tilde{r} = \frac{r}{\lambda}, \qquad \lambda = \frac{\eta}{2Z}. \tag{2.8}$$

The normalization constant is given by

$$N_{n,l} = \lambda^{-d/2}\left\{\frac{(\eta-L-1)!}{2\eta\,[(\eta+L)!]}\right\}^{1/2}, \tag{2.9}$$

in such a way that $\int \left|\Psi_{n,l,\{\mu\}}(\vec{r})\right|^2 d\vec{r} = 1$

The symbols $\mathcal{L}^{\alpha}_{m}(x)$ and $\tilde{\mathcal{L}}^{\alpha}_{m}(x)$ denote the orthogonal and orthonormal, respectively, Laguerre polynomials with respect to the weight $\omega_{\alpha}(x) = x^{\alpha}e^{-x}$ on the interval $[0,\infty)$, so that

$$\tilde{\mathcal{L}}^{\alpha}_{m}(x) = \left(\frac{m!}{\Gamma(m+\alpha+1)}\right)^{1/2}\mathcal{L}^{\alpha}_{m}(x). \tag{2.10}$$

The angular part of the wavefunction is given by the hyperspherical harmonics $\mathcal{Y}_{l,\{\mu\}}(\Omega_{d-1})$, which have the following expression [151–153]:

$$\mathcal{Y}_{l,\{\mu\}}(\Omega_{d-1}) = A_{l,\{\mu\}}e^{im\varphi}\prod_{j=1}^{d-2}C^{\alpha_j+\mu_{j+1}}_{\mu_j-\mu_{j+1}}(\cos\theta_j)(\sin\theta_j)^{\mu_{j+1}}$$
$$= \frac{1}{\sqrt{2\pi}}e^{im\varphi}\prod_{j=1}^{d-2}\tilde{C}^{\alpha_j+\mu_{j+1}}_{\mu_j-\mu_{j+1}}(\cos\theta_j)\,(\sin\theta_j)^{\mu_{j+1}}\,, \tag{2.11}$$

with $\alpha_j = (d-j-1)/2$, and the normalization constant is

$$\left|A_{l,\{\mu\}}\right|^2 = \frac{1}{2\pi}\prod_{j=1}^{d-2}\frac{(\alpha_j+\mu_j)(\mu_j-\mu_{j+1})!\,[\Gamma(\alpha_j+\mu_{j+1})]^2}{\pi 2^{1-2\alpha_j-2\mu_{j+1}}\Gamma(2\alpha_j+\mu_j+\mu_{j+1})}$$
$$\equiv \frac{1}{2\pi}\prod_{j=1}^{d-2}A^{(j)}_{\mu_j,\mu_{j+1}}. \tag{2.12}$$

The symbols $C^{\alpha}_{m}(x)$ and $\tilde{C}^{\alpha}_{m}(x)$ denote, respectively, the orthogonal and orthonormal Gegenbauer polynomials with respect to the weight funciont $\omega^{*}_{\alpha}(x) = (1-x^2)^{\alpha-\frac{1}{2}}$ on

the interval $[-1,+1]$, so that

$$\tilde{C}_m^{\alpha}(x) = \left(\frac{m!(m+\alpha)\Gamma^2(\alpha)}{\pi 2^{1-2\alpha}\Gamma(2\alpha+m)}\right)^{1/2} C_m^{\alpha}(x). \tag{2.13}$$

Then, the electronic probability density of d-dimensional hydrogenic systems in configuration space is

$$\rho(\vec{r}) = \left|\Psi_{n,l,\{\mu\}}(\vec{r})\right|^2 = R_{n,l}^2(r)\left|\mathcal{Y}_{l,\{\mu\}}(\Omega_{d-1})\right|^2. \tag{2.14}$$

It is worth noticing that this expression simplifies as

$$\rho(\vec{r})(ns) = \frac{2^{2d-1}Z^d\Gamma\left(\frac{d}{2}\right)}{\pi^{\frac{d}{2}}(2n+d-3)^{d+1}}e^{-\frac{r}{\lambda}}\left|\tilde{\mathcal{L}}_{n-1}^{d-2}\left(\frac{r}{\lambda}\right)\right|^2, \tag{2.15}$$

for the linear or ns-states (i.e. when $\mu_i = 0,\ \forall\ i = 1,\ldots,d-1$), and

$$\rho(\vec{r})(g.s.) = \left(\frac{2Z}{d-1}\right)^d \frac{1}{\pi^{\frac{d-1}{2}}\Gamma\left(\frac{d+1}{2}\right)}e^{-\frac{4Z}{d-1}r}, \tag{2.16}$$

for the ground state (i.e. $n=1$, $l=0$).

2.1.2 Momentum orbitals

On the other hand, the probability density in momentum spaces $\gamma(\vec{p})$ is obtained by squaring the d-dimensional Fourier transform of the configuration eigenfunction, i.e., the momentum wavefunction [151, 153]

$$\tilde{\Psi}_{n,l,\{\mu\}}(\vec{p}) = \mathcal{M}_{n,l}(p)\mathcal{Y}_{l\{\mu\}}(\Omega_{d-1}), \tag{2.17}$$

where the radial momentum wavefunction is

$$\begin{aligned}\mathcal{M}_{n.l}(p) &= K_{n,l}\frac{(\eta\tilde{p})^l}{(1+\eta^2\tilde{p}^2)^{L+2}}C_{\eta-L-1}^{L+1}\left(\frac{1-\eta^2\tilde{p}^2}{1+\eta^2\tilde{p}^2}\right)\\ &= \left(\frac{\eta}{Z}\right)^{d/2}(1+y)^{3/2}\left(\frac{1+y}{1-y}\right)^{\frac{d-2}{4}}\sqrt{\omega_{L+1}^*(y)}\tilde{C}_{\eta-L-1}^{L+1}(y).\end{aligned} \tag{2.18}$$

The normalization constant is given by

$$K_{n,l} = Z^{-d/2}2^{2L+3}\left(\frac{(\eta-L-1)!}{2\pi(\eta+L)!}\right)^{1/2}\Gamma(L+1)\,\eta^{\frac{d+1}{2}}, \tag{2.19}$$

and $y \equiv (1-\eta^2\tilde{p}^2)/(1+\eta^2\tilde{p}^2)$.

Then, the momentum probability density is

$$\gamma(\vec{p}) = \left|\tilde{\Psi}_{n,l,\{\mu\}}\left(\vec{p}\right)\right|^2 = \mathcal{M}^2_{n,l}(p)\left[\mathcal{Y}_{l\{\mu\}}(\Omega_{d-1})\right]^2, \tag{2.20}$$

which normalization as $\int \gamma(\vec{p})d\vec{p} = 1$ arises from the value of the constant given by Eq. (2.19).

It is worth noting that this expression simplifies as

$$\gamma(\vec{p})(ns) = \frac{(2n+d-3)^d \Gamma\left(\frac{d}{2}\right)}{8\pi^{\frac{d}{2}} Z^d}\left[\tilde{C}^{\frac{d-1}{2}}_{n-1}\left(\frac{1-\eta^2\tilde{p}^2}{1+\eta^2\tilde{p}^2}\right)\right]^2, \tag{2.21}$$

for the ns-states, and

$$\gamma(\vec{p})(g.s.) = \frac{(d-1)^d \Gamma\left(\frac{d+1}{2}\right)}{Z^d \pi^{\frac{d+1}{2}}} \frac{1}{\left(1+\frac{(d-1)^2}{4}\tilde{p}^2\right)^{d+1}}, \tag{2.22}$$

for the ground state.

Finally, let us mention here that alternative (but equivalent) expressions for the position and momentum wavefunctions of the d-dimensional hydrogenic atom have been published elsewhere [134, 135], and that for the particular case $d = 3$ the expressions (2.14) and (2.20) reduce to the well-known position and momentum probability densities of the three-dimensional hydrogenic atom [145, 154–157].

2.2 Information-theoretic measures of hydrogenic systems

In this section we will obtain (i) some expectation values such as power moments and logarithmic expectation values, and (ii) some information measures, i.e. the Shannon entropy and the Fisher information, for the d-dimensional hydrogenic systems in both position and momentum spaces

2.2.1 Power moments and logarithmic expectation values

As we have noticed in the previous chapter (Section 1.1), the most common and familiar way to quantify the spreading of the probability density in position space, $\rho(\vec{r})$, is the standard desviation $\triangle r$, whose square is the variance

$$V[\rho] = \left\langle r^2 \right\rangle - \langle r \rangle^2, \tag{2.23}$$

where $\langle r^\alpha \rangle$, $\alpha \ \epsilon \ \Re$, denotes the radial expectation value of order α, given by

$$\begin{aligned}\langle r^\alpha \rangle &\equiv \int r^\alpha \rho(\vec{r}) d\vec{r} = \int_0^\infty r^{\alpha+d-1} R_{nl}^2(r)\, dr \\ &= \frac{1}{2\eta}\left(\frac{\eta}{2Z}\right)^\alpha \int_0^\infty \omega_{2L+1}(\tilde{r}) \left[\tilde{\mathcal{L}}_{n_r}^{(2L+1)}(\tilde{r})\right]^2 \tilde{r}^{\alpha+1} d\tilde{r},\end{aligned} \tag{2.24}$$

with the radial hyperquantum numbers $n_r \equiv \eta - L - 1 = n - l - 1$ and $2L+1 = 2l+d-2$. This expression is valid for any $\alpha > -2L-3$, constraint which arises from the convergence of the integral at the lower boundary. In the second equality we have taken into account the solid-angle element

$$d\vec{r} = r^{d-1} dr d\Omega_{d-1}, \qquad d\Omega_{d-1} = \left(\prod_{j=1}^{d-2} \sin^{2\alpha_j}\theta_j d\theta_j\right) d\varphi, \tag{2.25}$$

with $\alpha_j = (d-j-1)/2$, and the orthonormalization relations of the hyperspherical harmonics $\mathcal{Y}_{l,\{\mu_j\}}(\Omega_{d-1})$ [153]. The quantities $\langle r^\alpha \rangle$ have been shown to have the following expressions [144]:

$$\left(\frac{2Z}{\eta}\right)^\alpha \langle r^\alpha \rangle = \frac{\Gamma(2L+\alpha+3)}{2\eta\Gamma(2L+2)} {}_3F_2\left(\begin{matrix} -\eta+L+1, & -\alpha-1, & \alpha+2 \\ 2L+2, & 1 & \end{matrix}\middle| 1\right) \tag{2.26}$$

$$\begin{aligned}&= \frac{1}{2n+d-3}\frac{(n-l-1)!}{(n+l+d-3)!} \\ &\quad \times \sum_{i=0}^{n-l-1} \binom{\alpha+1}{n-l-i-1}^2 \frac{\Gamma(\alpha+2l+d+i)}{i!},\end{aligned} \tag{2.27}$$

where $2L+\alpha+3 = 2l+d+\alpha > 0$. Moreover these quantities satisfy the recursion relation [158]

$$\frac{Z}{\eta^2}\left\langle r^{s-1}\right\rangle = \frac{2s-1}{s}\left\langle r^{s-2}\right\rangle - \frac{1}{Z}\frac{s-1}{4s}\left[(2L+1)^2 - (s-1)^2\right]\left\langle r^{s-3}\right\rangle, \tag{2.28}$$

for $s > -2L$. From Eqs. (2.26), (2.27) or (2.28) one obtains [158] that

$$\langle r \rangle = \frac{1}{2Z}\left[3\eta^2 - L(L+1)\right], \tag{2.29}$$

$$\left\langle r^2 \right\rangle = \frac{\eta^2}{2Z^2}\left[5\eta^2 - 3L(L+1) + 1\right], \tag{2.30}$$

so that the variance (2.23) has the value

$$V[\rho] = \frac{\eta^2(\eta^2+2) - L^2(L+1)^2}{4Z^2}. \tag{2.31}$$

It is worth noticing that for $d = 3$ this expression reduces to the known expression for the variance of a hydrogenlike atom [145, 156, 157]

$$V\left[\rho\right](d=3) = \frac{1}{4Z^2}\left[n^2(n^2+2) - l^2(l+1)^2\right]. \tag{2.32}$$

In momentum space we can operate similarly to quantify the spreading of the corresponding probability density $\gamma(\vec{p})$ by means of the radial expectation values $\langle p^\alpha \rangle$, given by

$$\begin{aligned}\langle p^\alpha \rangle &:= \int p^\alpha \gamma(\vec{p}) d\vec{p} = \int_0^\infty p^{\alpha+d-1} \mathcal{M}_{nl}^2(p)\, dp \\ &= \left(\frac{Z}{\eta}\right)^\alpha \int_{-1}^{1} \omega_\nu^*(y) \left[\tilde{C}_k^\nu(y)\right]^2 (1-y)^{\frac{\alpha}{2}} (1+y)^{1-\frac{\alpha}{2}}\, dy,\end{aligned} \tag{2.33}$$

where we have used $\nu \equiv L+1 = l + \frac{d-1}{2}$ and $k = n-l-1$ for mathematical convenience. It is knwon [146] that

$$\begin{aligned}\langle p^\alpha \rangle = &\frac{2^{1-2\nu} Z^\alpha \sqrt{\pi}}{k!\, \eta^{\alpha-1}} \frac{\Gamma\left(k+2\nu\right)\Gamma\left(\nu+\frac{\alpha+1}{2}\right)\Gamma\left(\nu+\frac{3-\alpha}{2}\right)}{\Gamma^2\left(\nu+\frac{1}{2}\right)\Gamma\left(\nu+1\right)\Gamma\left(\nu+\frac{3}{2}\right)} \\ &\times {}_5F_4\left(\left.\begin{matrix} -k, & k+2\nu, & \nu, & \nu+\frac{\alpha+1}{2}, & \nu+\frac{3-\alpha}{2} \\ & 2\nu, & \nu+\frac{1}{2}, & \nu+1, & \nu+\frac{3}{2} \end{matrix}\right| 1\right),\end{aligned} \tag{2.34}$$

valid for $\alpha \in (-2l-d, 2l+d+2)$. Let us remark that this expression for $\langle p^\alpha \rangle$ is a single sum (as Eq. (2.27) for $\langle r^\alpha \rangle$), since it involves a terminating and Saalschutzian (or balanced) ${}_5F_4(1)$ hypergeometric function. It can be easily shown that $\langle p^0 \rangle = 1$ and that

$$\langle p^2 \rangle = \frac{Z^2}{\eta^2}; \qquad \langle p^4 \rangle = \frac{Z^4}{\eta^4} \frac{8\eta - 3(2L+1)}{2L+1}. \tag{2.35}$$

Moreover, algebraic manipulation of the hypergeometric function involved in Eq. (2.34) allows one to find the reflection formula

$$\left(\frac{\eta}{Z}\right)^{2-\alpha} \langle p^{2-\alpha} \rangle = \left(\frac{\eta}{Z}\right)^\alpha \langle p^\alpha \rangle, \tag{2.36}$$

which is not trivial for $\alpha \neq 1$. The use of this formula allows to find additionally the momentum expectation value

$$\langle p^{-2} \rangle = \frac{\eta^2}{Z^2} \frac{8\eta - 3(2L+1)}{2L+1}. \tag{2.37}$$

For the ground state ($n = 1$ and $l = 0$ or, equivalently, $\nu = \frac{d-1}{2}$ and $k = 0$), the momentum expectation values (2.34) simplify as

$$\langle p^\alpha \rangle_{g.s.} = \left(\frac{2Z}{d-1}\right)^\alpha \frac{2\Gamma\left(\frac{d-\alpha}{2}+1\right)\Gamma\left(\frac{d+\alpha}{2}\right)}{d\Gamma^2\left(\frac{d}{2}\right)}; \qquad -d < \alpha < d+2 \tag{2.38}$$

so that

$$\langle p \rangle_{g.s.} = \frac{4Z}{d(d-1)} \frac{\Gamma^2\left(\frac{d+1}{2}\right)}{\Gamma^2\left(\frac{d}{2}\right)}, \qquad \langle p^2 \rangle_{g.s.} = \left(\frac{2Z}{d-1}\right)^2, \tag{2.39}$$

and the variance becomes

$$V\left[\gamma\right](g.s.) = \left(\frac{2Z}{d-1}\right)^2 \left[1 - \frac{4}{d^2}\left(\frac{\Gamma\left(\frac{d+1}{2}\right)}{\Gamma\left(\frac{d}{2}\right)}\right)^4\right]. \tag{2.40}$$

Moreover, from Eq. (2.38), the ground-state momentum expectation values of hydrogenic atoms and ions ($d = 3$) have the values

$$\langle p^\alpha \rangle_{g.s.}(d=3) = \frac{8Z^\alpha \Gamma\left(\frac{5-\alpha}{2}\right)\Gamma\left(\frac{3+\alpha}{2}\right)}{3\pi}, \tag{2.41}$$

so that

$$\langle p \rangle_{g.s.}(d=3) = \frac{8Z}{3\pi}, \qquad \langle p^2 \rangle_{g.s.}(d=3) = Z^2, \tag{2.42}$$

and the variance being consequently

$$V\left[\gamma\right](g.s.;\ d=3) = \left(1 - \frac{64}{9\pi^2}\right) Z^2. \tag{2.43}$$

Not trivially, we have obtained in the large dimensionality limit the following behaviour:

$$\langle r^\alpha \rangle = \left(\frac{d^2}{4Z}\right)^\alpha \left(1 + \frac{\alpha(\alpha+1)}{2d} + O\left(d^{-2}\right)\right), \tag{2.44}$$

for the position power moments [159], and

$$\langle p^\alpha \rangle = \left(\frac{Z}{\eta}\right)^\alpha \left(1 + \frac{\alpha(\alpha-2)(2n-2l-1)}{2d} + O\left(d^{-2}\right)\right), \tag{2.45}$$

for the momentum ones of an arbitrary hydrogenic state for given hyperquantum numbers $(n, l, \{\mu\})$.

An alternative manner to quantify the spreading of a d-dimensional hydrogenlike atom in the two conjugated spaces is provided by the position and momentum logarithmic expectation values, which are given by

$$\langle \ln r \rangle = \int (\ln r)\, \rho(\vec{r})\, d\vec{r}, \tag{2.46}$$

and

$$\langle \ln p \rangle = \int (\ln p)\, \gamma(\vec{p})\, d\vec{p}, \tag{2.47}$$

respectively. Often these quantities are spreading measures more appropiate than the variance, because they weight the different regions of the density all over the integration domain in a more balance way.

Taking into account the algebraic properties of the Laguerre and Gegenbauer polynomials it is possible to find the following values for these measures [146]:

$$\begin{aligned}\langle \ln r \rangle &= \ln \eta + \frac{2\eta - 2L - 1}{2\eta} + \psi(\eta + L + 1) - \ln 2 - \ln Z \\ &= \ln\left(n + \frac{d-3}{2}\right) + \frac{2n - 2l - 1}{2n + d - 3} + \psi(n + l + d - 2) - \ln 2 - \ln Z, \end{aligned} \tag{2.48}$$

where $\psi(x) = \frac{\Gamma'(x)}{\Gamma(x)}$ is the digamma function, and

$$\begin{aligned}\langle \ln p \rangle &= -\ln \eta + \frac{2\eta(2L+1)}{4\eta^2 - 1} - 1 + \ln Z \\ &= -\ln\left(n + \frac{d-3}{2}\right) + \frac{(2n + d - 3)(2l + d - 2)}{(2n + d - 3)^2 - 1} - 1 + \ln Z \end{aligned} \tag{2.49}$$

Notice that for the ground state ($n = 1$, $l = 0$) the logarithmic expectation values are

$$\langle \ln r \rangle_{g.s.} = \ln(d-1) - 2\ln 2 + \psi(d) - \ln Z, \tag{2.50}$$

and

$$\langle \ln p \rangle_{g.s.} = -\ln(d-1) + \ln 2 - \frac{1}{d} + \ln Z. \tag{2.51}$$

On the other hand the logarithmic expectation values for a generic state (n, l, m) of three-dimensional hydrogenlike atoms are

$$\langle \ln r \rangle (d = 3) = \ln n + \frac{2n - 2l - 1}{2n} + \psi(n + l + 1) - \ln(2Z), \tag{2.52}$$

$$\langle \ln p \rangle (d = 3) = -\ln n + \frac{2n(2l+1)}{4n^2 - 1} - 1 + \ln Z, \tag{2.53}$$

in the position and momentum spaces, respectively.

2.2.2 The Shannon entropy

Let us now deal with the analytical expresion of the Shannon entropy of d-dimensional hydrogenic systems. In doing so, the decomposition of the densities as a product of a radial and an angular factor will be essential.

Position space

The global or bulk extent of the position probability density for d-dimensional hydrogenic atoms is best measured by the Shannon entropy $S[\rho]$ given by Eq. (2.1). From Eqs.

(2.1) and (2.5) one has for the state $(n, l, \{\mu\})$ that

$$S[\rho] = S[R_{n,l}] + S\left[\mathcal{Y}_{l,\{\mu\}}\right], \tag{2.54}$$

where

$$S[R_{n,l}] \equiv -\int_0^\infty r^{d-1} R_{n,l}^2(r) \ln R_{n,l}^2(r) dr, \tag{2.55}$$

is the radial Shannon entropy, and

$$S\left[\mathcal{Y}_{l,\{\mu\}}\right] \equiv -\int_{S_{d-1}} \left|\mathcal{Y}_{l,\{\mu\}}(\Omega_{d-1})\right|^2 \ln \left|\mathcal{Y}_{l,\{\mu\}}(\Omega_{d-1})\right|^2 d\Omega_{d-1}, \tag{2.56}$$

is the angular Shannon entropy. It is worth noticing that the radial entropy does not depend on the magnetic quantum numbers nor the angular entropy on the principal quantum number because of the spherical symmetry of the Coulomb potential. Employing Eqs. (2.6) and (2.55), the radial entropy has been shown [53, 160, 161] to have the expression

$$S[R_{n,l}] = A_0(n,l,d) + \frac{(\eta - L - 1)!}{2\eta(\eta + L)!} E_1\left(\mathcal{L}_{\eta-L-1}^{2L+1}\right) - d \ln Z \tag{2.57}$$

$$= A_1(n,l,d) + \frac{1}{2\eta} E_1\left(\tilde{\mathcal{L}}_{\eta-L-1}^{2L+1}\right) - d \ln Z, \tag{2.58}$$

where the terms $A_i(n,l,d)$, $i = 0, 1$ have the values

$$A_0(n,l,d) = -\ln\left[\frac{2^{d-1}(\eta - L - 1)!}{\eta^{d+1}(\eta + L)!}\right] + \frac{3\eta^2 - L(L+1)}{\eta} - 2l\left[\frac{2\eta - 2L - 1}{2\eta} + \psi(\eta + L + 1)\right], \tag{2.59}$$

and

$$A_1(n,l,d) = A_0(n,l,d) + \ln\left[\frac{(\eta - L - 1)!}{(\eta + L)!}\right]. \tag{2.60}$$

The symbol $E_1(y_n)$ denotes the entropic integral

$$E_1(y_n) \equiv -\int_0^\infty x \omega_{2L+1}^*(x) y_n^2(x) \ln y_n^2(x) dx, \tag{2.61}$$

so that $E_1(\mathcal{L})$ and $E_1(\tilde{\mathcal{L}})$ are the entropic integrals corresponding to the orthogonal and orthonormal Laguerre polynomials, respectively. Let us point out that for circular states $(l = m = n - 1)$, the radial entropy, given by Eq. (2.57), reduces as

$$S[R_{n,n-1}] = A_0(n, l = n-1, d) - d \ln Z$$
$$= -\ln\left[\frac{2^{d-1}}{\eta^{d+1}(2\eta - 1)!}\right] - 2(n-1)\left[\frac{1}{2\eta} + \psi(2\eta)\right] + 2\eta + 1 - d \ln Z. \tag{2.62}$$

Then, the radial entropy for the ground state ($n = 1, l = 0$) turns out to be

$$S\left[R_{1,0}\right] = d - \ln \frac{2^{2d}}{(d-1)^{d+1}(d-2)!} - d \ln Z, \tag{2.63}$$

so that for $d = 3$ one has that

$$S\left[R_{1,0}\right](d=3) = 3 - 2\ln 2 - 3\ln Z. \tag{2.64}$$

On the other hand, taking into account Eqs. (2.11), (2.12) and (2.56) the angular entropy $S(\mathcal{Y})$ can be expressed [162] for $d \geq 2$ as

$$S\left[\mathcal{Y}_{l,\{\mu\}}\right] = B_0(l, \{\mu\}, d) + \sum_{j=1}^{d-2} A^j_{l,\{\mu\}} E\left(C^{\alpha_j+\mu_{j+1}}_{\mu_j-\mu_{j+1}}\right) \tag{2.65}$$

$$= B_1(l, \{\mu\}, d) + \sum_{j=1}^{d-2} E\left(\tilde{C}^{\alpha_j+\mu_{j+1}}_{\mu_j-\mu_{j+1}}\right), \tag{2.66}$$

where the terms $B_i(l, \{\mu\}, d)$, $i = 0$ and 1, have the values

$$B_0(l, \{\mu\}, d) := B_1(l, \{\mu\}, d) - \sum_{j=1}^{d-2} \ln A^j_{l,\{\mu\}}, \tag{2.67}$$

and

$$B_1(l, \{\mu\}, d) = \ln 2\pi - 2\sum_{j=1}^{d-2} \mu_{j+1} \left[\psi(2\alpha_j + \mu_j + \mu_{j+1}\right.$$
$$\left. -\psi(\alpha_j + \mu_j) - \ln 2 - \frac{1}{2(\alpha_j + \mu_j)}\right], \tag{2.68}$$

and the symbol $E(y_n)$ denotes the Shannon entropy of the polynomial $y_n(x)$ defined by

$$E(y_n) = -\int \omega^*_\lambda(x) y_n^2(x) \ln y_n^2(x) dx, \tag{2.69}$$

so that $E(C_n^{(\lambda)})$ and $E(\tilde{C}_n^{(\lambda)})$ are the entropies corresponding to the orthogonal and orthonormal Gegenbauer polynomials with respect to the weight function $\omega^*_\lambda(x) = (1-x^2)^{\lambda-1/2}$. The explicit values for the angular entropy $S\left[\mathcal{Y}\right]$ given by Eqs. (2.65) or (2.66) for any multi-index $(l, \{\mu\})$ are not known because the calculation of the Shannon entropy for the Gegenbauer polynomials is a formidable analytical task, not yet accomplished except for some particular cases despite numerous recent efforts. Nevertheless, an algorithm has been recently proposed which determines very efficiently the numerical values of the angular entropy [163]. From the analytical standpoint let us remark a few cases. For $d = 2$ the sum involved in Eq. (2.65) is empty, so that the angular entropy $S(\mathcal{Y}) = \ln 2\pi$. For $d \geq 3$ we can calculate explicitly this quantity whenever either

$\mu_j - \mu_{j+1} = 0$ and 1, or $\alpha_j + \mu_{j+1} = 0, 1$ and 2 for every j within the range $1 \leq j \leq d-2$; so, for the states $(l, \{l\})$ the degree of the involved Gegenbauer polynomial is zero and its entropy vanishes, giving rise to the angular entropy

$$\begin{aligned} S\left[\mathcal{Y}_{l,\{l\}}\right] &= B_0(l, \{l\}, d) \\ &= \ln\left[\frac{2^{2l(d-2)+1}\pi^{d/2} l!}{\Gamma\left(l + \frac{d}{2}\right)}\right] \\ &\quad - 2l \sum_{j=1}^{d-2} \left[\psi(2\alpha_j + 2l) - \psi(\alpha_j + l) - \frac{1}{2(\alpha_j + l)}\right]. \end{aligned} \tag{2.70}$$

In particular, for the ns states (i.e., $l = 0$) the angular entropy is given by

$$S\left[\mathcal{Y}_{0,\{0\}}\right] = \ln \frac{2\pi^{d/2}}{\Gamma\left(\frac{d}{2}\right)}, \tag{2.71}$$

which is the maximum value for the angular entropy (for further details see Appendix A). It is worth noticing that the last two expressions simplify for three-dimensional systems as follows:

$$S\left[Y_{l,l}\right](d=3) = \ln\left[\frac{2^{2l+1}\pi^{3/2} l!}{\Gamma\left(l + \frac{3}{2}\right)}\right] - 2l\left[\psi(2l+1) - \psi\left(l + \frac{1}{2}\right) - \frac{1}{2l+1}\right], \tag{2.72}$$

and

$$S\left[\mathcal{Y}_{0,0}\right](d=3) = \ln(4\pi). \tag{2.73}$$

Finally, let us combine the expressions (2.54), (2.58) and (2.66). We obtain that the total position Shannon entropy has the value

$$S[\rho] = A_1(n, l, d) + \frac{1}{2\eta} E_1\left(\tilde{\mathcal{L}}^{2L+1}_{\eta-L-1}\right) + S\left[\mathcal{Y}_{l,\{\mu\}}\right] - d \ln Z \tag{2.74}$$

$$= A_1(n, l, d) + B_1(l, \{\mu\}, d) + \frac{1}{2\eta} E_1\left(\tilde{\mathcal{L}}^{2L+1}_{\eta-L-1}\right) + \sum_{j=1}^{d-2} E\left(\tilde{C}^{\alpha_j+\mu_{j+1}}_{\mu_j-\mu_{j+1}}\right) - d \ln Z. \tag{2.75}$$

Although the involved entropic integrals of orthonormal Laguerre and Gegenbauer polynomials can be numerically computed quite accurately [163], their analytical determination is not yet possible except for very special cases. In particular, for the ground state one obtains

$$S[\rho]\,(g.s.) = \ln\left[\frac{(d-1)^d}{2^d} \pi^{\frac{d-1}{2}} \Gamma\left(\frac{d+1}{2}\right)\right] + d - d \ln Z, \tag{2.76}$$

for the position Shannon entropy.

Momentum space

A similar procedure for the momentum probability density $\gamma(\vec{p})$ given by Eq. (2.20) allows one to find the global multidimensional extent in momentum space of the hydrogenlike state $(n, l, \{\mu\})$ by means of the momentum Shannon entropy

$$S[\gamma] = -\int \gamma(\vec{p}) \ln \gamma(\vec{p}) d\vec{p} = S[\mathcal{M}_{n,l}] + S\left[\mathcal{Y}_{l,\{\mu\}}\right], \tag{2.77}$$

according to Eq. (2.17), where the angular part $S(\mathcal{Y})$ is the entropy of hyperspherical harmonics previously discussed, and the radial part is given by

$$S[\mathcal{M}_{n,l}] = -\int_0^\infty p^{d-1} \mathcal{M}_{n,l}^2(p) \ln \mathcal{M}_{n,l}^2(p) dp. \tag{2.78}$$

Taking into account the functionals of Gegenbauer polynomials given by Theorems 3 and 4 of Ref. [146], we find the following expression for the momentum radial entropy:

$$S[\mathcal{M}_{n,l}] = F_0(n,l,d) + d \ln Z + \frac{2^{2L+1}\eta(\eta-L-1)!\Gamma^2(L+1)}{\pi(\eta+L)!} E\left(C_{\eta-L-1}^{(L+1)}\right) \tag{2.79}$$

$$= F_1(n,l,d) + E\left(\tilde{C}_{\eta-L-1}^{(L+1)}\right) + d \ln Z, \tag{2.80}$$

with

$$F_0(n,l,d) = F_1(n,l,d) - \ln\left(\frac{2^{2L+1}\eta(\eta-L-1)!\Gamma^2(L+1)}{\pi(\eta+L)!}\right), \tag{2.81}$$

and

$$F_1(n,l,d) = -\ln\frac{\eta^d}{2^{2L+4}} - (2L+4)\left[\psi(\eta+L+1) - \psi(\eta)\right] + \frac{L+2}{\eta} - (d+1)\left[1 - \frac{2\eta(2L+1)}{4\eta^2-1}\right]. \tag{2.82}$$

The symbols $E(C_m^{(\lambda)})$ and $E(\tilde{C}_m^{(\lambda)})$ denote, as defined by Eq. (2.69), the Shannon entropy of the orthogonal and orthonormal Gegenbauer polynomials, respectively.

Finally, we gather the relations (2.77), (2.80) and (2.66) to find the following expression for the total momentum Shannon entropy:

$$S[\gamma] = F_1(n,l,d) + E\left(\tilde{C}_{\eta-L-1}^{L+1}\right) + S\left[\mathcal{Y}_{l,\{\mu\}}\right] + d \ln Z \tag{2.83}$$

$$= F_1(n,l,d) + B_1(l,\{\mu\},d) + E\left(\tilde{C}_{\eta-L-1}^{L+1}\right) + \sum_{j=1}^{d-2} E\left(\tilde{C}_{\mu_j-\mu_{j+1}}^{\alpha_j+\mu_{j+1}}\right) + d \ln Z. \tag{2.84}$$

The entropy of the orthonormal Gegenbauer polynomial can be numerically computed by use of the highly efficient algorithm of Buyarov et al [163]; however, its analytical calculation has not yet been done except for a few cases. In particular, it can be

analytically determined for $n-l-1=0$ and 1. So, for circular states (i.e. for $l=n-1$) one finds from Eq. (2.79) that

$$S\left[\mathcal{M}_{n,n-1}\right] = 1+\frac{1}{\eta}-\frac{d+1}{2\eta+1}-\ln\frac{\eta^d\Gamma\left(\eta+1\right)}{\sqrt{\pi}2^{2\eta+1}\Gamma\left(\eta+1/2\right)} - 2\left(\eta+1\right)\left[\psi(2\eta)-\psi(\eta)\right]+d\ln Z. \tag{2.85}$$

Then, for the ground state (i.e. when $n=1$, $l=0$) the radial entropy is

$$S\left[\mathcal{M}_{1,0}\right] = \frac{d+1}{d(d+1)}-\ln\frac{(d-1)^d\Gamma\left(\frac{d-1}{2}\right)}{\sqrt{\pi}2^{2d+1}\Gamma\left(d/2\right)}-(d+3) - (d+1)\left[\psi(d-1)-\psi\left(\frac{d-1}{2}\right)\right]+d\ln Z. \tag{2.86}$$

Therefore, according to Eqs. (2.71) and (2.86), we find the value

$$\begin{aligned} S\left[\gamma\right](g.s.) &= S\left[\mathcal{M}_{1,0}\right]+S\left[\mathcal{Y}_{0,\{0\}}\right] \\ &= \ln\frac{2^{2d+1}\pi^{\frac{d+1}{2}}}{(d-1)^d\Gamma\left(\frac{d+1}{2}\right)}+d\ln Z+\frac{d+1}{d(d-1)}-(d+1)\left[\psi(d-1)-\psi\left(\frac{d-1}{2}\right)\right], \end{aligned} \tag{2.87}$$

for the total momentum Shannon entropy of the ground state.

2.2.3 The Fisher information

Let us now analytically determine the Fisher information for the d-dimensional hydrogenic systems in both position and momentum spaces.

Position space

Contrary to the spreading measures of the position probability density $\rho(\vec{r})$ discussed previously, the Fisher information $I\left[\rho\right]$ given by Eq. (2.2) is a functional of the gradient of $\rho(\vec{r})$. This quantity can be also expressed as

$$I\left[\rho\right] = 4\int_{\Re^d}\left|\vec{\nabla}_d\Psi_{n,l,\{\mu\}}(r,\theta_1,\theta_2,...,\theta_{d-2},0)\right|^2 d\vec{r}. \tag{2.88}$$

From Eqs. (2.2) and (1.27), one has [151] that

$$I\left[\rho\right] = I\left[R_{n,l}\right]+\left\langle r^{-2}\right\rangle I\left[\mathcal{Y}_{l,\{\mu\}}\right], \tag{2.89}$$

where the radial part is given by

$$I\left[R_{n,l}\right] = 4\int_0^\infty \left[\frac{d}{dr}R_{nl}(r)\right]^2 r^{d-1}dr$$
$$= \frac{4Z^2}{\eta^3}\left\{\eta - \frac{2}{2L+1}\left[L(L+1) - \frac{1}{4}(d-1)(d-3)\right]\right\}. \tag{2.90}$$

Here we have used Eq. (2.6) for the second equality. The angular part is

$$I\left[\mathcal{Y}_{l,\{\mu\}}\right] = 4\sum_{i=1}^{d-2}\int_{\Omega_{d-1}}\left[\frac{1}{\prod_{k=1}^{i-1}\sin\theta_k}\frac{\partial}{\partial\theta_i}\mathcal{Y}_{l,\{\mu\}}(\theta_1,...,\theta_{d-2},0)\right]^2 d\Omega_{d-1}$$
$$= 4L(L+1) - (d-1)(d-3) - 2\left|m\right|(2L+1). \tag{2.91}$$

Then, according to Eqs. (2.89)-(2.91) and taking into account that

$$\left\langle r^{-2}\right\rangle = \frac{2Z^2}{\eta^3}\frac{1}{2L+1}, \tag{2.92}$$

one has the following expression for the position Fisher information of the d-dimensional hydrogenlike system [151]:

$$I\left[\rho\right] = \frac{4Z^2}{\eta^3}\left[\eta - \left|m\right|\right], \qquad d \geq 2. \tag{2.93}$$

Let us point out, for completeness, that this expression can be alternatively obtained by means of the expression for the position Fisher information of a particle moving in a general central potential [152]

$$I\left[\rho\right] = 4\left\langle p^2\right\rangle - 2\left|m\right|(2l+d-2)\left\langle r^{-2}\right\rangle, \tag{2.94}$$

together with the Coulomb values of $\left\langle p^2\right\rangle$ and $\left\langle r^{-2}\right\rangle$ given by Eqs. (2.35) and (2.92), respectively.

Moreover, from Eq. (2.93) we have the values

$$I\left[\rho\right](ns) = \left(\frac{2Z}{\eta}\right)^2, \qquad I\left[\rho\right](g.s.) = \left(\frac{4Z}{d-1}\right)^2, \tag{2.95}$$

for the position Fisher information of the ns and ground states, respectively.

Momentum space

Operating similarly as before, one finds that the Fisher information of the momentum probability density $\gamma(\vec{p})$ can be expressed as

$$I[\gamma] = I[\mathcal{M}_{n,l}] + \langle p^{-2} \rangle I\left[\mathcal{Y}_{l,\{\mu\}}\right], \tag{2.96}$$

where the radial part is given [151] by

$$\begin{aligned} I[\mathcal{M}_{n,l}] &= 4\int_0^\infty \left[\frac{d}{dp}\mathcal{M}_{nl}(p)\right]^2 p^{d-1}dp \\ &= \frac{\eta^2}{Z^2}\left\{2(5\eta^2 - 3L(L+1)+1) + \frac{1}{2L+1}(2L-d+3)(2L+d-1)(6L-8\eta+3)\right\}, \end{aligned} \tag{2.97}$$

and the angular part $I\left[\mathcal{Y}_{l,\{\mu\}}\right]$ has been already expressed by Eq. (2.91). Then taking into account Eqs. (2.37), (2.91), (2.96) and (2.97) one has the following value for the momentum Fisher information:

$$I[\gamma] = 2\frac{\eta^2}{Z^2}\left[5\eta^2 - 3L(L+1) - |m|(8\eta - 6L - 3) + 1\right]; \qquad d \geq 2. \tag{2.98}$$

Here again this value can be alternatively obtained by the conjugate relation of Eq. (2.94), namely

$$I[\gamma] = 4\langle r^2 \rangle - 2|m|(2l+d-2)\langle p^{-2} \rangle, \tag{2.99}$$

together with the expressions (2.30) and (2.37), respectively.

For completeness, let us write down that, according to Eq. (2.98), we have the values

$$I[\gamma](ns) = \frac{\eta^2}{Z^2}\left[10\eta^2 - \frac{3}{2}(d-3)(d-1) + 2\right], \tag{2.100}$$

and

$$I[\gamma](g.s.) = \frac{d(d+1)(d-1)^2}{4Z^2}, \tag{2.101}$$

for the position Fisher information of ns and ground states, respectively.

Cramér-Rao products

The combination of the expectation values $\langle r^2 \rangle$ and $\langle p^2 \rangle$, given by Eqs. (2.30) and (2.35), with the Fisher informations $I[\rho]$ and $I[\gamma]$ given by Eqs. (2.93) and (2.98), respectively, has allowed us to find the Cramér-Rao products

$$\langle r^2 \rangle I[\rho] = \frac{2}{\eta}\left[5\eta^2 - 3L(L+1) + 1\right][\eta - |m|] \tag{2.102}$$

and

$$\left\langle p^2 \right\rangle I\left[\gamma\right] = 2\left[5\eta^2 - 3L(L+1) - |m|\left(8\eta - 6L - 3\right) + 1\right] \tag{2.103}$$

in position and momentum spaces respectively. We notice that (i) neither Cramér-Rao produtcs depend on the nuclear charge Z, and (ii) these two products satisfy the following Cramér-Rao inequalities for single-particle systems moving in a d-dimensional central potential:

$$\left\langle r^2 \right\rangle I\left[\rho\right] \geqslant 4\left(1 - \frac{2\left|m\right|}{2L+1}\right)\left(L + \frac{3}{2}\right)^2 \tag{2.104}$$

$$\left\langle p^2 \right\rangle I\left[\gamma\right] \geqslant 4\left(1 - \frac{2\left|m\right|}{2L+1}\right)\left(L + \frac{3}{2}\right)^2 \tag{2.105}$$

recently found [125].

2.3 Uncertainty relationships

In this section we discuss the uncertainty relations associated to the spreading measures of the d-dimensional hydrogenic systems obtained in the previous section. We begin with the determination of the Heisenberg-like relation and later we calculate the three uncertainty relations (the logarithmic, the Shannon entropy-based and the Fisher-information-based relations), which are more adequate and precise mathematical expressions of the uncertainty principle. The corresponding expressions are given, emphasizing their explicit values for ns-states. Let us advance saying that they do not depend on the nuclear charge Z, what is in accordance with the general result of Sen and Katriel for homogeneus potential

2.3.1 Heisenberg-like uncertainty products

From the explicit expressions of the radial expectation values $\left\langle r^2 \right\rangle$ and $\left\langle p^2 \right\rangle$ given by Eqs. (2.30) and (2.35), respectively, one has the Heisenberg-like uncertainty product

$$\begin{aligned}\left\langle r^2 \right\rangle \left\langle p^2 \right\rangle &= \frac{1}{2}\left[5\eta^2 - 3L(L+1) + 1\right] \\ &= \frac{d^2}{4}\left\{1 + \frac{1}{d}(10n - 6l - 9) + \frac{1}{d^2}\left[10n(n-3) - 6l(l-2) + 20\right]\right\},\end{aligned} \tag{2.106}$$

valid for any hydrogenic atom in d dimensions.

It is interesting to remark here that this expression fulfils not only the Heisenberg-like uncertainty inequality

$$\left\langle r^2 \right\rangle \left\langle p^2 \right\rangle \geq \frac{d^2}{4}, \tag{2.107}$$

valid for any d-dimensional quantum system, but also the recently obtained Heisenberg-like :uncertainty relation for central potentials [164] given by

$$\left\langle r^2 \right\rangle \left\langle p^2 \right\rangle \geqslant \left(L + \frac{3}{2} \right)^2 . \tag{2.108}$$

Moreover, the product (2.106) reduces as

$$\left\langle r^2 \right\rangle \left\langle p^2 \right\rangle (ns) = \frac{1}{4} \left[10n^2 + (d-3)(10n + d - 6) + 2 \right], \tag{2.109}$$

for the ns states, and

$$\left\langle r^2 \right\rangle \left\langle p^2 \right\rangle (g.s.) = \frac{1}{4}(d^2 + d), \tag{2.110}$$

for the ground state.

To find the Heisenberg uncertainty relation in the appropriate canonically conjugate radial coordinates, we have to consider not the momentum operator $\vec{p}$ but the radial momentum operator [165]

$$p_r = -i\hbar \frac{1}{r^{\frac{d-1}{2}}} \frac{\partial}{\partial r} r^{\frac{d-1}{2}} = -i\hbar \left(\frac{\partial}{\partial r} + \frac{d-1}{2r} \right), \tag{2.111}$$

which is manifestly Hermitian. Then, it happens that

$$p_r^2 = \vec{p}^2 - \frac{L(L+1)}{r^2}. \tag{2.112}$$

So, one has the expectation values $\langle p_r \rangle = 0$, and

$$\left\langle p_r^2 \right\rangle = \left\langle \vec{p}^{\,2} \right\rangle - L(L+1) \left\langle r^{-2} \right\rangle = \frac{Z^2}{\eta^2} \left[1 - \frac{2}{\eta} \frac{L(L+1)}{2L+1} \right]. \tag{2.113}$$

Then, the radial momentum standard deviation $\triangle p_r$ becomes

$$\triangle p_r = \sqrt{\left\langle p_r^2 \right\rangle - \left\langle p_r \right\rangle^2} = \frac{Z}{\eta} \left[1 - \frac{2}{\eta} \frac{L(L+1)}{2L+1} \right]^{1/2}, \tag{2.114}$$

which, together with the radial position standard deviation (see Eq. (2.31)) provides

$$\triangle r = \sqrt{\left\langle r^2 \right\rangle - \left\langle r \right\rangle^2} = \sqrt{V\left[\rho\right]} = \frac{1}{2Z} \left[\eta^2(\eta^2 + 2) - L^2(L+1)^2 \right]^{1/2}, \tag{2.115}$$

which allows us to obtain the Heisenberg uncertainty product

$$\triangle r \triangle p_r = \frac{1}{2\eta} \left\{ \frac{\left[\eta^2(\eta^2+2) - L^2(L+1)^2 \right] \left[\eta(2L+1) - 2L(L+1) \right]}{\eta(2L+1)} \right\}^{1/2}. \tag{2.116}$$

It is worth noticing that for $d = 3$ this uncertainty product simplifies as

$$(\triangle r \triangle p_r)\,(d=3) = \frac{1}{2n}\left\{\frac{\left[n^2(n^2+2) - l^2(l+1)^2\right]\left[n(2l+1) - 2l(l+1)\right]}{n(2l+1)}\right\}^{1/2}, \tag{2.117}$$

which has been previously found by Hey [157].

2.3.2 Logarithmic uncertainty relation

The logarithmic expectation values for a general hydrogenic state $(n, l, \{\mu\})$ in d-dimensional position and momentum spaces are given by Eqs. (2.48) and (2.49), respectively. So that the logarithmic sum becomes

$$\begin{aligned}\langle \ln r\rangle + \langle \ln p\rangle &= \frac{2\eta - 2L - 1}{2\eta} + \frac{2\eta(2L+1)}{4\eta^2 - 1} - \ln 2 - 1 + \psi(\eta + L + 1) \\ &= \frac{2n - 2l - 1}{2n + d - 3} + \frac{(2n+d-3)(2l+d-2)}{(2n+d-3)^2 - 1} - \ln 2 - 1 + \psi(n + l + d - 2),\end{aligned} \tag{2.118}$$

where we can observe that the sum of logarithmic expectation values does not depend on the nuclear charge Z of the hydrogenic system.

It is worth noticing that for the ns-states this expression reduces to

$$(\langle \ln r\rangle + \langle \ln p\rangle)\,(ns) = \frac{2n-1}{(2n+d-3)} + \frac{(2n+d-3)(d-2)}{(2n+d-3)^2 - 1} - \ln 2 - 1 + \psi(n + d - 2), \tag{2.119}$$

and for the ground state one has that

$$(\langle \ln r\rangle + \langle \ln p\rangle)\,(g.s.) = -\frac{1}{d} - \ln 2 + \psi(d). \tag{2.120}$$

It is straightforward to check that the last three expressions fulfils the Beckner logarithmic uncertainty relation

$$\langle \ln r\rangle + \langle \ln p\rangle \geq \psi\left(\frac{d}{4}\right) + \ln 2, \tag{2.121}$$

valid for any d-dimensional single-particle system moving in an arbitrary central potential [117].

2.3.3 Shannon-entropy-based (or entropic) uncertainty relation

To obtain the entropic uncertainty sum for a hydrogenic system in d dimensions, let us combine the position and momentum Shannon entropies given by Eqs. (2.74) and

(2.83), respectively, so that

$$S\left[\rho\right]+S\left[\gamma\right]=A_1(n,l,d)+F_1(n,l,d)+\frac{1}{2\eta}E_1\left(\tilde{\mathcal{L}}^{2L+1}_{\eta-L-1}\right)+E\left(\tilde{\mathcal{C}}^{L+1}_{\eta-L-1}\right)+2S\left[\mathcal{Y}_{l,\{\mu\}}\right]. \tag{2.122}$$

Or, alternatively, Eqs. (2.75) and (2.84), where the angular entropy is partially developed (see Eq. (2.66)), allow us to obtain

$$\begin{aligned}S\left[\rho\right]+S\left[\gamma\right]=&A_1(n,l,d)+F_1(n,l,d)+2B_1(l,\{\mu\},d)\\&+\frac{1}{2\eta}E_1\left(\tilde{\mathcal{L}}^{2L+1}_{\eta-L-1}\right)+E\left(\tilde{\mathcal{C}}^{L+1}_{\eta-L-1}\right)+2\sum_{j=1}^{d-2}E\left(\tilde{C}^{\alpha_j+\mu_{j+1}}_{\mu_j-\mu_{j+1}}\right),\end{aligned} \tag{2.123}$$

where the terms A_1, B_1 and F_1 are explicitly given by Eqs. (2.60), (2.68) and (2.82), respectively. The entropic integrals $E_1\left(\tilde{\mathcal{L}}^{\alpha}_{m}\right)$ and $E\left(\tilde{C}^{\alpha}_{m}\right)$ for orthonormal Laguerre and Gegenbauer polynomials have been defined in Eqs. (2.61) and (2.69), respectively.

In going beyond for the analytical study, we need the exact expressions for the entropic integrals, what constitutes a very difficult task which has nor yet been done except in a few particular cases, such as e.g. the linear ($\mu_i=0$, $\forall i=1,\ldots,d-1$), nearly circular ($\mu_i=n-1$, $\forall i=1,\ldots,d-1$) and Rydberg (large n) states. Finally, let us also mention that the entropic sum (2.123) for the ground state drastically reduces to

$$(S\left[\rho\right]+S\left[\gamma\right])(g.s.)=\ln\left(\frac{4^{d+1}\pi^d}{d}\right)+\frac{2}{d-1}+\frac{d^2-1}{d}-(d-1)\left[\psi(d-1)-\psi\left(\frac{d-1}{2}\right)\right],$$

which certainly fulfils the entropic uncertainty relation found by Bialynicki-Birula and Mycielski [44]

$$(S\left[\rho\right]+S\left[\gamma\right])\geq d\left(1+\ln\pi\right), \tag{2.124}$$

valid for general quantum systems.

2.3.4 Fisher-information-based uncertainty relation

Since the explicit expressions for the position and momentum Fisher information of a hydrogenic state $(n,l,\{\mu\})$ are given by Eqs. (2.93) and (2.98), respectively, we can determined the value of the Fisher uncertainty product as

$$I\left[\rho\right]\times I\left[\gamma\right]=\frac{8}{\eta}(\eta-|m|)\left[5\eta^2-3L(L+1)-|m|\left(8\eta-6L-3\right)+1\right], \tag{2.125}$$

valid for $d \geq 2$. It is observed that for the states $(n, 0, 0, \ldots, 0)$ or ns-states, the Fisher product becomes

$$I[\rho] \times I[\gamma](ns) = 8\left[5\eta^2 - \frac{3}{4}(d-1)(d-3) + 1\right] = 2\left[5(2n+d-3)^2 - 3(d-1)(d-3) + 4\right], \quad (2.126)$$

so that for the ground state ($n = 1$) its value is

$$(I[\rho] \times I[\gamma])_{g.s.} = 4d(d+1), \quad (2.127)$$

which fulfils the corresponding uncertainty relation for d-dimensional single-particle systems with central potentials

$$I[\rho] \times I[\gamma] \geq 16\left(1 - \frac{2|m|}{2L+1}\right)^2 \left(L + \frac{3}{2}\right)^2, \quad (2.128)$$

recently found [125, 152, 164].

2.4 Circular states in d-dimensional hydrogenic systems

A circular state is a single-electron state of highest hyperangular momenta allowed within a given electronic manifold; i.e. a state with hyperangular momentum quantum numbers $\mu_1 = \mu_2 = \cdots = \mu_{d-1} = n - 1$ The electronic probability density, $\rho_{\text{circ}}(\vec{r})$, of such d-dimensional states is, according to Eqs. (2.5) and (2.14),

$$\rho_{\text{circ}}(\vec{r}) = \frac{2^{d+2-2n} Z^d}{\pi^{\frac{d-1}{2}}(2n+d-3)^d \Gamma(n)\Gamma\left(n+\frac{d-1}{2}\right)} \times e^{-\frac{r}{\lambda}} \left(\frac{r}{\lambda}\right)^{2n-2} \prod_{j=1}^{d-2} (\sin\theta_j)^{2n-2}, \quad (2.129)$$

in position space and, according to Eqs. (2.18)-(2.20),

$$\gamma_{\text{circ}}(\vec{p}) = \frac{2^{2n-2}(2n+d-3)^d \Gamma\left(n+\frac{d-1}{2}\right)}{Z^d \pi^{\frac{d+1}{2}} \Gamma(n)} \frac{(\eta p/Z)^{2n-2}}{(1+\frac{\eta^2 p^2}{Z^2})^{2n+d-1}} \prod_{j=1}^{d-2} (\sin\theta_j)^{2n-2}, \quad (2.130)$$

in momentum space. The purpose of this section is to give the explicit expressions for the main spreading measures of the position and momentum electronic probability clouds of these states, as well as their associated uncertainty relations, directly in terms of the principal quantum number n, the space dimensionality and the strength Z of the Coulombian force.

Let us begin with the power moments. According to Eqs. (2.26) or (2.27) we have the values

$$\langle r^\alpha \rangle = \left(\frac{2n+d-3}{4Z}\right)^\alpha \frac{\Gamma(2n+d-2+\alpha)}{\Gamma(2n+d-2)}; \qquad \alpha > -2n-d+2, \quad (2.131)$$

for the position power moments; and, according to Eq. (2.34), the values

$$\langle p^{\alpha}\rangle = \left(\frac{2Z}{2n+d-3}\right)^{\alpha} \frac{\Gamma\left(n+\frac{d+\alpha-2}{2}\right)\Gamma\left(n+\frac{d-\alpha}{2}\right)}{\left(n+\frac{d-2}{2}\right)\Gamma^2\left(n+\frac{d-2}{2}\right)}, \tag{2.132}$$

for the momentum power moments taking into account the constraint $-2n-d+2 < \alpha < 2n+d$. So that the generalized Heisenberg-like product becomes

$$\langle r^{\alpha}\rangle \langle p^{\alpha}\rangle = \frac{\Gamma(2n+d-2+\alpha)\Gamma\left(n+\frac{d-2+\alpha}{2}\right)\Gamma\left(n+\frac{d-\alpha}{2}\right)}{2^{\alpha}\left(n+\frac{d-2}{2}\right)\Gamma^2\left(n+\frac{d-2}{2}\right)\Gamma(2n+d-2)}, \tag{2.133}$$

for $-2n-d+2 < \alpha < 2n+d$; then, for $\alpha = 2$ we have the Heisenberg-like uncertainty product

$$\left\langle r^2\right\rangle \left\langle p^2\right\rangle = \frac{1}{4}(2n+d-1)(2n+d-2) \tag{2.134}$$

and the radial Heisenberg uncertainty product

$$\triangle r \triangle p_r = \frac{1}{2}\sqrt{\frac{2n+d-2}{2n+d-4}}, \tag{2.135}$$

where the expression (2.116) has been taken into account.

On the other hand, from Eqs. (2.48) and (2.49), we find the values

$$\langle \ln r\rangle = \ln(2n+d-3) + \psi(2n+d-3) + \frac{1}{2n+d-3} - 2\ln 2 - \ln Z, \tag{2.136}$$

and

$$\langle \ln p\rangle = -\ln(2n+d-3) - \frac{1}{2n+d-2} + \ln 2 + \ln Z, \tag{2.137}$$

for the logarithmic expectation values in position and momentum spaces, respectively. Then, the logarithmic uncertainty sum is equal to

$$\langle \ln r\rangle + \langle \ln p\rangle = \psi(2n+d-3) + \frac{1}{(2n+d-2)(2n+d-3)} - \ln 2, \tag{2.138}$$

and, as for an arbitray (n,l,m) state, it does not depend on the nuclear charge Z.

To find the Shannon entropies of d-dimensional circular states we start from Eqs. (2.75) and (2.84) for their corresponding expressions in position and momentum spaces, respectively. Since $\eta - L - 1 = 0$ and $\mu_j - \mu_{j+1} = 0$, $\forall j = 1,\ldots,d-1$, the involved Laguerre and Gegenbauer polynomials are of degree zero, so that the corresponding entropic integrals vanish; and one has

$$S[\rho] = A_0(n, n-1, d) + B_0(n-1, \{n-1\}, d) - d\ln Z, \tag{2.139}$$

and

$$S[\gamma] = F_0(n, n-1, d) + B_0(n-1, \{n-1\}, d) + d\ln Z, \tag{2.140}$$

Now, taking into account the expressions (2.59), (2.67) and (2.81) for the terms A_0, B_0 and F_0, respectively, we finally obtain the values

$$S[\rho] = 2n + d - 2 - (n-1)\left[\psi(n) + \psi\left(n + \frac{d-1}{2}\right)\right] - d\ln 2 + \ln\left[(2n+d-3)^d \pi^{\frac{d-1}{2}} \Gamma(n)\Gamma\left(n + \frac{d-1}{2}\right)\right] - d\ln Z, \tag{2.141}$$

for the position Shannon entropy, and

$$S[\gamma] = -1 + \ln\left[\frac{2^{d+1}\pi^{\frac{d+1}{2}}\Gamma(n)}{(2n+d-3)^d \Gamma\left(n + \frac{d-1}{2}\right)}\right] - (n-1)\psi(n) - \frac{d+1}{2}\psi\left(n + \frac{d}{2}\right) + (2n+d-1)\psi\left(n + \frac{d+1}{2}\right) + d\ln Z, \tag{2.142}$$

for the momentum Shannon entropy. Then, the Shannon uncertainty sum is equal to

$$S[\rho] + S[\gamma] = 2n + d - 2 + \ln\left(2\pi^d \Gamma^2(n)\right) - 2(n-1)\psi(n) + \frac{d+1}{2}\left[\psi\left(n + \frac{d-1}{2}\right) - \psi\left(n + \frac{d}{2}\right)\right]. \tag{2.143}$$

Let us now consider the hydrogenic circular states of Rydberg type (i.e., with large n and l). In this case the previous expressions allow us to find the values

$$S_{\text{Rydberg}}[\rho] = \frac{3d+1}{2}\ln n + \frac{d-1}{2} + \ln\left(2\pi^{\frac{d+1}{2}}\right) + \frac{9d^2 - 24d - 5}{12n} - d\ln Z + O\left(\frac{1}{n^2}\right), \tag{2.144}$$

for the position entropy,

$$S_{\text{Rydberg}}[\gamma] = -(3d-1)\ln n + \frac{d-1}{2} + \ln\left(2\pi^{\frac{d+1}{2}}\right) - \frac{3d^2 - 7d + 2}{4n} + d\ln Z + O\left(\frac{1}{n^2}\right), \tag{2.145}$$

for the momentum entropy, and

$$(S_{\text{Rydberg}}[\rho] + S_{\text{Rydberg}}[\gamma]) = -\ln n + (d-1) - \frac{3d+4}{12n} + \ln\left(4\pi^{d+1}\right) + O\left(\frac{1}{n^2}\right), \tag{2.146}$$

for the net Shannon entropy.

Finally, let us calculate the position and momentum Fisher information of the circular states. From Eqs. (2.93) and (2.98), one has the values

$$I[\rho] = \frac{2(d-1)Z^2}{\eta^3} = \frac{16(d-1)Z^2}{(2n+d-3)^3}, \tag{2.147}$$

for the position Fisher information, and

$$I\left[\gamma\right]=\frac{(2n+d-3)^{2}}{4Z^{2}}\left[(2n+d)(d-1)+2\right], \tag{2.148}$$

for the momentum one. So that we obtain the expressions

$$I\left[\rho\right]\times I\left[\gamma\right]=\frac{4(d-1)}{2n+d-3}\left[(2n+d)(d-1)+2\right], \tag{2.149}$$

for the Fisher-information-based uncertainty product, and

$$\left\langle r^{2}\right\rangle I\left[\rho\right]=\frac{(d-1)(2n+d-1)(2n+d-2)}{(2n+d-3)}, \tag{2.150}$$

$$\left\langle p^{2}\right\rangle I\left[\gamma\right]=(2n+d)(d-1)+2, \tag{2.151}$$

for the Cramér-Rao products in position and momentum spaces, respectively.

2.5 Spreading measures of d-dimensional Rydberg states

In this section we investigate the spatial extension or multidimensional spreading of Rydberg hydrogenic states (i.e. states where the electron has a large principal quantum number n, so being highly excited), in both position and momentum spaces with standard and non-standard dimensionalities, by means of the following measures: power moments, variances, logarithmic expectation values, Shannon entropy and Fisher information. We show that all these measures can be expressed in closed form in terms of the principal quantum number η (and the grand angular momentum quantum number L in those cases where L is also large) and the space dimensionality d. This requires the knowledge of the asymptotics of orthogonal polynomials involved in the general expressions for the spreading measures of the d-dimensional hydrogenic systems shown in the Section 2.2.

Let us begin with the position power moments given by Eqs. (2.24)-(2.30) for any d-dimensional hydrogenic system. The use of Eq. (2.24) and the Laguerre asymptotics of Szegö [166] given by

$$\left[\mathcal{L}_{m}^{(\alpha)}(x)\right]^{2}\omega_{\alpha}(x)=\frac{1}{\pi}\frac{1}{\sqrt{x}}m^{\alpha-\frac{1}{2}}\cos^{2}\left(2\sqrt{mx}-\frac{\alpha\pi}{2}-\frac{\pi}{4},\right)+o(m^{\alpha-1}), \tag{2.152}$$

allows one to obtain [167] that the position power moments of Rydberg systems are

$$\left(\frac{Z}{\eta^{2}}\right)^{\alpha}\left\langle r^{\alpha}\right\rangle=\frac{2^{\alpha+1}}{\sqrt{\pi}}\frac{\Gamma\left(\alpha+\frac{3}{2}\right)}{\Gamma(\alpha+2)}+o(1);\qquad\alpha>-\frac{3}{2}, \tag{2.153}$$

for large n and (l,d) fixed. Recently, Aptekarev et al [159] have done a detailed study of these expectation values for arbitrary α except for $\alpha=\dfrac{3}{2}$.

On the other hand, and in order to find the momentum power moments of Rydberg systems we start from the expression (2.33) for a general hydrogenic system. Since the Gegenbauer weight $\omega_\nu^*(t) = (1-t^2)^{\nu-\frac{1}{2}}$ belongs to the Szegö class, i.e. $\omega_\nu^* \in L^2([-1,+1])$, and

$$\int_{-1}^{+1} h_0 \ln \omega_\nu^*(t) > -\infty, \qquad \text{with} \quad h_0 = \frac{1}{\pi}\frac{1}{\sqrt{1-t^2}}, \tag{2.154}$$

we have (Ref. [166], Th. 12.1.4) that

$$\tilde{C}_k^\nu(t) = \sqrt{2}\left[\frac{h_0(t)}{\omega_\nu^*(t)}\right]\cos\left[n\theta + \delta(\theta)\right] + o(1), \tag{2.155}$$

uniformly on $[-1,+1]$ with $\theta \in [0,\pi]$ and $t = \cos\theta$. Then, Eq. (2.33) transforms into

$$\left(\frac{\eta}{Z}\right)^\beta \left\langle p^\beta \right\rangle = \frac{2}{\pi}\int_{-1}^{+1}(1-t)^{\frac{\beta-1}{2}}(1+t)^{\frac{1-\beta}{2}}\cos^2\left[n\theta+\delta(\theta)\right]dt + o(1). \tag{2.156}$$

Now, taking into account the Lemma 2.1 of Aptekarev et al in Ref. [168] one has that

$$\begin{aligned}\left(\frac{\eta}{Z}\right)^\beta \left\langle p^\beta \right\rangle &= \frac{2}{\pi^2}\int_0^\pi \cos^2\theta d\theta \int_{-1}^{+1}(1-t)^{\frac{\beta-1}{2}}(1+t)^{\frac{1-\beta}{2}}dt + o(1) \\ &= \frac{2}{\pi}B\left(\frac{3-\beta}{2},\frac{1+\beta}{2}\right) + o(1); \qquad -1<\beta<3,\end{aligned} \tag{2.157}$$

for large n and fixed (l,d). Here the symbol $B(a,b) = \Gamma(a)\Gamma(b)/\Gamma(a+b)$ denotes the beta function. Recently, this result has been obtained [159] by means of the powerful methods of the modern approximation theory relative to the asymptotics of the varying orthogonal Laguerre and Gegenbauer polynomials.

The multiplication of expressions (2.153) and (2.157) gives rise to the generalized Heisenberg-like uncertainty product

$$\left\langle r^\alpha \right\rangle \left\langle p^\beta \right\rangle = \frac{2^{\alpha+2}}{\pi\sqrt{\pi}}\frac{\Gamma\left(\alpha+\frac{3}{2}\right)\Gamma\left(\frac{3-\beta}{2}\right)\Gamma\left(\frac{1+\beta}{2}\right)}{\Gamma(\alpha+2)}\frac{\eta^{2\alpha-\beta}}{Z^{\alpha-\beta}} + o\left(\eta^{2\alpha-\beta}\right), \tag{2.158}$$

for large η values and $\alpha > -\frac{3}{2}$, $-1 < \beta < 3$. It is worth noticing that this expression fulfils the general uncertainty relation $\left\langle r^\alpha \right\rangle \left\langle p^\beta \right\rangle \geqslant f(\alpha,\beta,d)$ found by Angulo [12]. Moreover, for $\alpha = \beta$ one has the uncertainty product

$$\left\langle r^\alpha \right\rangle \left\langle p^\alpha \right\rangle = \frac{2^{\alpha+2}}{\pi\sqrt{\pi}}\frac{\Gamma\left(\alpha+\frac{3}{2}\right)\Gamma\left(\frac{3-\alpha}{2}\right)\Gamma\left(\frac{1+\alpha}{2}\right)}{\Gamma(\alpha+2)}\eta^\alpha + o\left(\eta^\alpha\right), \tag{2.159}$$

valid for $-1 < \alpha < 3$. Notice that (i) this product includes and generalizes the Heisenberg uncertainty product given by Eq. (2.106) for the particular case $\alpha = 2$, and (ii) this result can be extended to other values of α by using the rigorous results of Aptekarev et al [159].

Let us now find the logarithmic expectation values of the Rydberg d-dimensional hydrogenic states. Taking into account that $\psi(x) \sim \ln x + \frac{1}{2x}$ for large x, from Eq. (2.48) one has that

$$\langle \ln r \rangle = 2 \ln \eta + 1 - \ln 2 - \ln Z + O(\eta^{-2}) \tag{2.160}$$

for the position logarithmic expectation value, and from Eq. (2.49) we obtain that

$$\langle \ln p \rangle = - \ln \eta - 1 + \frac{L + \frac{1}{2}}{\eta} + \ln Z + O(\eta^{-2}), \tag{2.161}$$

for the momentum logarithmic expectation value, provided of course that l and d are finite and n large. Then, the uncertainty logarithmic sum for the Rydberg states behaves as

$$\langle \ln r \rangle + \langle \ln p \rangle = \ln \eta - \ln 2 + \frac{L + \frac{1}{2}}{\eta} + O(\eta^{-2}) \tag{2.162}$$

which corresponds to the large-n limit of Eq. (2.118)

To obtain the values of the position Shannon entropy of a d-dimensional Rydberg state we need, according to Eq. (2.74), to know the asymptotic behavior of the entropic integral for the orthonormal Laguerre polynomials $E_1\left(\tilde{\mathcal{L}}^{2L+1}_{\eta-L-1}\right)$ for large n and fixed (l, d); this implies large η and fixed L. For this purpose we use the following formula [169]:

$$\begin{aligned} E_1(\tilde{\mathcal{L}}^{\alpha}_m) &\equiv - \int_0^{\infty} x \omega_{\alpha}(x) \left[\tilde{\mathcal{L}}^{\alpha}_m(x)\right]^2 \ln \left[\tilde{\mathcal{L}}^{\alpha}_m(x)\right]^2 dx \\ &= -6m^2 + (2\alpha + 1) m \ln m + \ln(2\pi) - 2\alpha - 4 + o(m), \end{aligned} \tag{2.163}$$

for the orthonormal Laguerre polynomials $\tilde{\mathcal{L}}^{\alpha}_m(x)$ for fixed real $\alpha > -1$ and $m \to \infty$. Then, from Eqs. (2.74) and (2.163), we get the value

$$S[\rho] = 2d \ln n + (2 - d) \ln 2 + \ln \pi + d - 3 - d \ln Z + S\left(\mathcal{Y}_{l,\{\mu\}}\right) + o(1) \tag{2.164}$$

for the position Shannon entropy of the Rydberg d-dimensional hydrogenic state characterized by the large principal quantum number n and the hyperquantum numbers $(l, \{\mu\})$.

In a similar way we have calculated the momentum Shannon entropy of a d-dimensional hydrogenic state by means of Eq. (2.83) provided that one is able to determine the asymptotics of the entropy of the involved Gegenbauer polynomials, $E\left(\tilde{\mathcal{C}}^{L+1}_{\eta-L-1}\right)$, for large n and fixed (l, d); this implies large η and fixed L. This is a non-trivial task in the field of orthogonal polynomials, which can be solved by means of the following

asymptotic formula [168, 170, 171]:

$$E(\tilde{\mathcal{C}}_m^{\alpha}) \equiv -\int_{-1}^{+1} \omega_{\alpha}^{*}(x) \left[\tilde{\mathcal{C}}_m^{\alpha}(x)\right]^2 \ln\left[\tilde{\mathcal{C}}_m^{\alpha}(x)\right]^2 dx$$
$$= \ln\pi + (1-2\alpha)\ln 2 - 1 + o(1), \tag{2.165}$$

for the Gegenbauer polynomials $\tilde{\mathcal{C}}_{\eta-L-1}^{L+1}(x)$ which are orthonormal with respect to the weight $\omega_{\alpha}^{*}(x) = (1-x^2)^{\alpha-\frac{1}{2}}$ for fixed α and large m. Then, according to Eqs. (2.83) and (2.165) one has the expression

$$S[\gamma] = -d\ln n + (d+2)\ln 2 + \ln\pi - d - 2 + d\ln Z + S\left(\mathcal{Y}_{l,\{\mu\}}\right) + o(1) \tag{2.166}$$

for the momentum Shannon entropy of the Rydberg d-dimensional hydrogenic state characterized by the large principal quantum number n and the hyperquantum numbers $\{l \equiv \mu_1, \mu_2, \ldots, \mu_{d-1}\}$.

The combination of Eqs. (2.164) and (2.166) allows one to compute the entropic sum

$$S[\rho] + S[\gamma] = d\ln n + 4\ln 2 + 2\ln\pi - 5 + 2S\left(\mathcal{Y}_{l,\{\mu\}}\right) + o(1), \tag{2.167}$$

for Rydberg states (large n, and fixed $l, \{\mu\}$). Let us remind that the angular entropy $S\left[\mathcal{Y}_{l,\{\mu\}}\right]$, which appears in the basic expressions (2.164), (2.166) and (2.167), can be numerically evaluated by the highly efficient algorithm of Buyarov et al [163] and analytically calculated in some specific cases. In particular, for (ns)-Rydberg states one has that

$$S[\rho](ns) = 2d\ln n + (2-d)\ln 2 + 2\ln\pi + d - 3 + o(1), \tag{2.168}$$

and

$$S[\gamma](ns) = -d\ln n + (d+3)\ln 2 + 2\ln\pi - d - 2 + o(1), \tag{2.169}$$

so that the entropic sum becomes

$$(S[\rho] + S[\gamma])(ns) = d\ln n + 6\ln 2 + 4\ln\pi - 5 + o(1), \tag{2.170}$$

which certainly fulfils the general Shannon-entropy-based (or entropic) uncertainty relation [44] given by Eq. (2.124).

Here let us determine the explicit expressions for the position and momentum Fisher information of a Rydberg d-dimensional hydrogenic state with large n and fixed angular hyperquantum numbers $(l, \{\mu\})$. They can be obtained from Eqs. (2.93) and (2.98), respectively, by making η large and taking into account that L and μ_{d-1} are fixed. We find that

$$I[\rho] = \left(\frac{2Z}{\eta}\right)^2 + O\left(\frac{1}{\eta^3}\right), \tag{2.171}$$

and

$$I\left[\gamma\right] = \frac{2}{Z^2}\eta^3(5\eta - 8\mu_{d-1}) = \frac{10}{Z^2}\eta^4 + O\left(\eta^3\right), \tag{2.172}$$

for such position and momentum quantities, respectively. So that the Fisher-information-based uncertainty product becomes

$$I\left[\rho\right] \times I\left[\gamma\right] = 40\eta^2 + O(\eta) = 10(2n + d - 3)^2 + O(n), \tag{2.173}$$

which is in accordance with the expression (2.125) for large n values.

2.6 Conclusions

In this chapter, the spatial extension of the d-dimensional hydrogenic states has been quantitatively estimated by means of various spreading quantities of global (variance, power moments, logarithmic expectation values, Shannon entropy) and local (Fisher information) character.

We have investigated the spreading properties of the d-dimensional hydrogenic systems in both position and momentum spaces far beyond the statistical variance and power moments, by means of the logarithmic expectation values and some information-theoretic measures (Shannon entropy, Fisher information) of the corresponding quantum probability densities for both ground and excited states.

We have begun gathering the fundamental algebraic properties of the d-dimensional hydrogenic wavefunctions, their radial expectation values in the direct and reciprocal spaces, and the present knowledge of their information-theoretic measures, which are widely scattered and incompletely solved in the literature. Then we critically discuss and apply them to various physical situations; particularly to circular and Rydberg states, whose selective creation by means of tunable dye lasers is providing an experimental basis for fascinating investigations of fundamental Quantum Mechanics which are being performed in various laboratories.

Chapter 3

Fisher information of some elementary chemical reactions

Theoretical studies of potential-energy surfaces, a subject of increasing interest, have been performed at various levels of sophistication in an attempt to understand the stereochemical course of chemical reactions [172]. Particular interest has been focussed on extracting information about the stationary points of the energy surface. In the Born-Oppenheimer framework, (i) minima on the d-dimensional potential energy surface for the nuclei can be identified with the classical picture of equilibrium structures of molecules, and (ii) saddle points can be related to transition states (TSs) and reaction rates. Since the formulation of TS theory [173, 174] a great effort has been devoted to develop models in order to characterize the TSs. This theory is assumed to govern the height of a chemical reaction barrier, so that any insight into the nature of the TS is likely to provide deeper understanding of the chemical reactivity. Computational quantum chemistry has sidestepped the inherent problems by managing rigorous mathematical definitions of critical points on a potential-energy hypersurface, and hence assigning them to equilibrium complexes or TSs. Within this approach, minima and saddle points have been fully characterized through the first and second derivatives of the energy (gradient and Hessian) over the nuclei positions [175–185]

Despite the fact that minima, maxima and saddle points are useful mathematical features of the energy surface to reaction-path following [175], it has been difficult to attribute too much chemical or physical meaning to these critical points [186]. Whereas the reaction rate and the reaction barrier are chemical concepts which have been rigorously defined and experimentally studied since the early days of the transition state theory [173, 174], the structure of the TS remains as a quest of physical organic chemistry. Understanding the TS is a fundamental goal of chemical reactivity theories which implies the knowledge of the chemical events that take place in order to better understand the kinetics and the

dynamics of a reaction. On the other hand, a variety of density descriptors have been employed to study chemical reactions [173, 187, 188].

In connection with the above, there are a number of studies in the literature which have employed density descriptors to study either the TS structure or to follow the course of the chemical reaction path. For instance, Shi and Boyd performed a systematic analysis of model S_N2 reactions in order to study the TS charge distribution in connection with the Hammond-Leffler postulate [189]. Bader et al developed a theory of reactivity based solely on the properties of the charge density by employing the properties of the Laplacian of the density, so as to align the local charge concentrations with regions of charge depletion of the reactants by mixing in the lowest-energy excited state of the combined system to produce a relaxed charge distribution corresponding to the transition density [190]. By studying the time evolution of a bimolecular exchange reaction Balakrishnan et al showed that information-theoretic entropies in dual or phase space rised to a maximum in a dynamical study [191]. Following the course of two elementary S_N2 reactions, Ho et al showed that information-theoretic measures were able to reveal geometrical changes of the density which were not diplayed by the energy profile although the transition state was not apparent from the study [192]. In an attempt to build a density-based theory of chemical reactivity, Knoerr et al [193] reported correlations between features of the quantum-mechanically determined charge density and the energy-based measures of Shaik and collaborators to describe the charge transfer, stability, and charge localization accompanying a S_N2 reaction [194]. Moreover, Tachibana [195] was able to visualize the formation of a chemical bond in selected model reactions by using the kinetic energy density $n_T(\vec{r})$ to identify the intrinsic shape of the reactants, the TS and the reaction products along the course of the intrinsic reaction coordinate (IRC). The reaction force of a system's potential energy along the reaction coordinate has been employed to characterize changes in the structural and/or electronic properties in chemical reactions [196–199]. However, to the best of our knowledge, none of them have been able to conceptually describe the reaction mechanism of elementary reactions in a simple and direct fashion.

In recent years, there has been an increasing interest in applying information-theory (IT) measures to the electronic structure of atoms and molecules [51, 93, 95, 200–210]; however, it has not been clearly assessed whether information-theoretic measures are good descriptors for characterizing chemical reactions parameters, that is, the stationary points of the IRC path (the TS and the equilibrium geometries of the complexes species) and the bond breaking/forming regions. Recently, significant advances have been achieved with information-theoretic analyses which allow a phenomenological description of the course of two elementary chemical reactions by revealing important chemical regions that are not present in the energy profile, such as the ones in which bond forming and bond breaking occur [211]. Furthermore, the synchronous reaction mechanism of a S_N2 type chemical reaction and the nonsynchronous mechanistic behaviour of

the simplest abstraction reaction were predicted by use of the Shannon entropy [212].

In this Chapter, we contribute to this field, using information measures in order to describe the course of two elementary chemical reactions by detecting the transition state and the stationary points unfolding the bond-forming and bond-breaking regions which are not revealed in the energy profile. We have centered our attention in the abstraction reaction and nucleophilic substitution reaction.

The central quantity under study is the Fisher information

$$I = \int \frac{\left|\vec{\nabla}\rho(\vec{r})\right|^2}{\rho(\vec{r})} d\vec{r}. \tag{3.1}$$

We have analyzed both position (I_r) and momentum (I_p) spaces chatacterized by $\rho(\vec{r})$ and $\gamma(\vec{p})$, the normalized-to-unity electron densities in the position and momentum spaces, respectively. The total electron density of a molecule, in the independent particle approximation, consists of a sum of contributions from electrons in occupied orbitals. Thus, in momentum space, the contribution from an electron in a molecular orbital $\varphi_i(\vec{p})$ to the total electron density is given by $|\varphi_i(\vec{p})|^2$. The orbitals $\varphi_i(\vec{p})$ are related by Fourier transforms to the corresponding orbitals in position space $\phi_i(\vec{r})$. Standard procedures for the Fourier transformation of position space orbitals generated by ab-initio methods have been described [213]. The orbitals employed in ab-initio methods are linear combinations of atomic basis functions and since analytic expressions are known for the Fourier transforms of such basis fuctions [214], the transformations of the total molecular electronic wavefunction from position to momentum space is computationally straightforward [215].

In recent studies, the utility of employing other chemical descriptors in order to interpret information-theoretic measures has been assessed . In this study, we find interesting to use the molecular electrostatic potential (MEP), the hardness, geometrical parameters, dipole moment and vibrational frequencies.

The MEP represents the molecular potential energy of a proton at a particular location near a molecule [216] say at nucleus A. Then the electrostatic potential, V_A, is given by

$$V_A = \left(\frac{\partial E^{molecule}}{\partial Z_A}\right)_{N,Z_{B\neq A}} = \sum_{B\neq A} \frac{Z_B}{|R_B - R_A|} - \int \frac{\rho(\vec{r})d\vec{r}}{|\vec{r} - R_A|'}, \tag{3.2}$$

where $\rho(\vec{r})$ is the molecular electron density and Z_A is the charge on nucleus A, located at R_A. Generally speaking, negative electrostatic potential corresponds to an attraction of the proton by the concentrated electron density in the molecules from lone pairs, pi-bonds, etc. (colored in shades of red in contour diagrams). Positive electrostatic potential corresponds to a repulsion of the proton by the atomic nuclei in regions with

a low electron density and the nuclear charge being incompletely shielded (colored in shades of blue in contour diagrams).

We have also evaluated some reactivity parameters that may be useful to analyze the chemical reactivity of the processes. Parr and Pearson proposed a quantitative definition of hardness (η) within conceptual DFT [101, 217]:

$$\eta = \frac{1}{2S} = \frac{1}{2}\left(\frac{\partial \mu}{\partial N}\right)_{v(\vec{r})}, \qquad \text{where} \qquad \mu = \left(\frac{\partial E}{\partial N}\right)_{v(\vec{r})}, \tag{3.3}$$

is the electronic chemical potential of an N electron system in the presence of an external potential $v(\vec{r})$, E is the total energy and "S" is called the softness. Using finite difference approximation, Eq. (3.3) becomes

$$\eta = \frac{1}{2S} = \left(E_{N+1} - 2E_N + E_{N-1}\right)/2 = \left(I - A\right)/2, \tag{3.4}$$

where E_N, E_{N-1} and E_{N+1} are the energies of the neutral, cationic and anionic systems; and I and A, are the ionization potential (IP) and electron affinity (EA), respectively. Applying Koopmans' theorem [218, 219], Eq. (3.3) can be written as

$$\eta = \frac{1}{2S} \equiv \frac{\epsilon_{LUMO} - \epsilon_{HOMO}}{2}, \tag{3.5}$$

where ϵ denotes the frontier molecular orbital energies. In general terms, hardness and softness are good descriptors of chemical reactivity; the former measures the global stability of the molecule (larger values of η means less reactive molecules), whereas the S index quantifies the polarizability of the molecule [220–223]. Thus soft molecules are more polarizable and possess predisposition to acquire additional electronic charge [224]. The chemical hardness η is a central quantity for use in the study of reactivity and stability, through the hard and soft acids and bases principle [225–227]. A comprehensive review on hardness has been recently published by Ayers [228].

The electronic structure calculations in this study were carried out with the Gaussian 03 suite of programs [229]. Reported TS geometrical parameters for the abstraction and the S_N2 exchange reaction were employed. Calculations for the IRC were performed at the MP2 (UMP2 for the abstraction reaction) level of theory with at least 35 points for each one of the directions (forward/reverse) of the IRC. Next, a high level of theory and a well-balanced basis set (diffuse and polarized orbitals) were chosen for determinig all of the porperties for the chemical structures corresponding to the IRC. Thus, the QCSID(T) method was employed in addition to the 6-311++G** basis set, unless otherwise stated. The hardness and softness chemical parameters were calculated by use of Eqs. (3.4) and (3.5) and the standard hybrid B3LYP (UB3LYP for the abstraction reaction) functional [229]. Molecular frequencies corresponding to the normal modes of vibration depend on the roots of the eigenvalues of the Hessian (its matrix elements are associated with force constants) at the nuclei positions of the stationary points. We have

found illustrative to calculate these values for the normal mode associated with the TS (possessing one imaginary frequency or negative force constant) which were determined analytically for all points of the IRC path at the MP2 (UMP2 for the abstraction reaction) level of theory. The molecular Fisher informations in position and momentum spaces for the IRC were obtained in this study by employing the necessary software along with $3D$ numerical integration routines [230, 231] and the DGRID suite of programs [215]. The bond breaking/forming regions along with electrophilic/nucleophilic atomic regions were calculated through the MEP by use of MOLDEN [232]. Atomic units are employed throughout the study except for the dipole moment (Debye), vibration frequencies (cm^{-1}) and geometrical parameters (Angstroms).

3.1 Abstraction reaction

The reaction $H + H_2 \rightarrow H_2 + H$ is the simplest radical abstraction reaction involving a free radical (atomic hydrogen) as a reactive intermediate. This kind of reaction involves at least two steps (S_N1 reaction type): in the first step a new radical (atomic hydrogen in this case) is created by homolysis and in the second one the new radical recombines with another radical species. Such homolytic bond cleavage occurs when the bond involved is not polar and there is no electrophile or nucleophile at hand to promote heterolytic patterns. When the bond is made, the product has a lower energy than the reactants and consequently it follows that breaking the bond requires energy.

For this reaction, the IRC was obtained at the UMP2/6-311G level of theory, and 72 points evenly distributed between the forward and reverse directions of the IRC were obtained. A relative tolerance of 1.0×10^{-5} was set for the numerical integrations [230, 231].

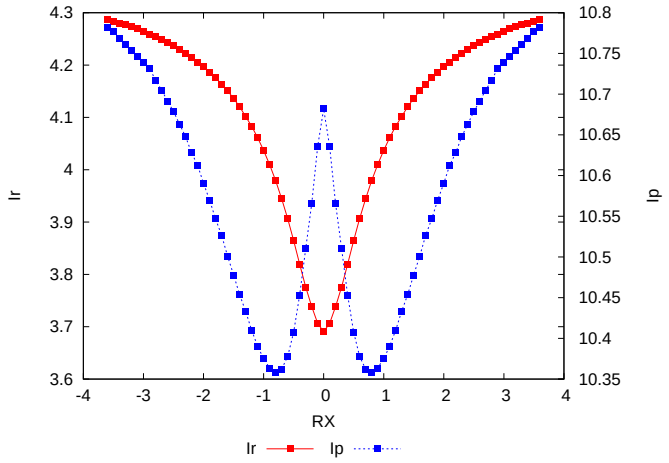

FIGURE 3.1: Fisher information in position (red line) and momentum (blue line) spaces for the IRC of $H_a^{\bullet} + H_2 \rightarrow H_2 + H_a^{\bullet}$.

In Figure 3.1 the Fisher information in both position and momentum spaces are depicted. At a first glance, we observe that both quantities behave in a similar way toward the reactive complexes ($H_a^{\bullet} \ldots H - H$ and $H - H \ldots H_b^{\bullet}$) and tend to decrease toward the TS region, but with a very important difference that we analyze below. It is worth mentioning that according to a previous study [211], we have insight into the structural features of the distributions in both spaces, i.e., concernig the spreading (localization/delocalization) of the densities. However, the behavior of the densities about their local changes (uniformity/irregularity) can only be provided by a local measure such as the Fisher information.

Both position and momentum Fisher information measures possess more structure at the vicinity of the TS as it may be observed from Figure 3.1. It is worthy to remark that this phenomenon is not present in the energy profile. By closer inspection, we note that the Fisher information I_r possesses a global minima at the TS, whereas the momentum one, I_p, possesses a local maxima and two local minimum at the vicinity of the TS (approximately $R_X \simeq 0.9$). This is interesting on chemical grounds since the structure observed for the Fisher information in momentum space at the vicinity of the TS can be associated with a process of bond breaking/forming (depending on the reaction direction) followed by stabilization of the structure at the TS [211].

The chemical picture proceeds in this way: as the intermediate radical ($H_a^{\bullet}$) approaches the molecule at the TS region, the molecular density exerts important changes so as to undergo the homolysis. This represents a physical situation where the density in position space gets localized in preparation for the bond rupture, which in turn results in a local increase of the kinetic energy. This provides explanation for the well-known fact that bond breaking requires energy. Next, the bond is formed and as a consequence, the TS structure shows lower kinetic energy than the reactant/product complex (H_a or H_b). Interestingly, from an information-theoretic point of view all of the above happens: both I_r and I_p decrease as the radical intermediate approaches the molecule at the TS region, which means that the gradient of the density distributions (in both spaces) becomes smaller, i.e., these densities are less irregular and more uniform. For the position space the Fisher information reaches a minimum at the TS, i.e., at this point the position space density is the most uniform and delocalized (structurally less distorted) among all other structures at the vicinity of the TS. In momentum space, the Fisher information shows minima at the vicinity of the TS ($R_X \simeq |0.9|$) corresponding to a delocalized and uniform momentum density. It is worth noting that it is at these minima where the processes of bond breaking/forming occur [211]. At the TS, the Fisher information, I_p, is maximum corresponding with the least uniform and the highest localized momentum density with respect to the structures in its neighborhood. It is interesting to mention that minima of the Fisher information in momentum space coincide with the BCER (Bond Cleavage Energy Reservoir) defined in Ref. [211] and hence they might be characterized by the Fisher measure in momentum space.

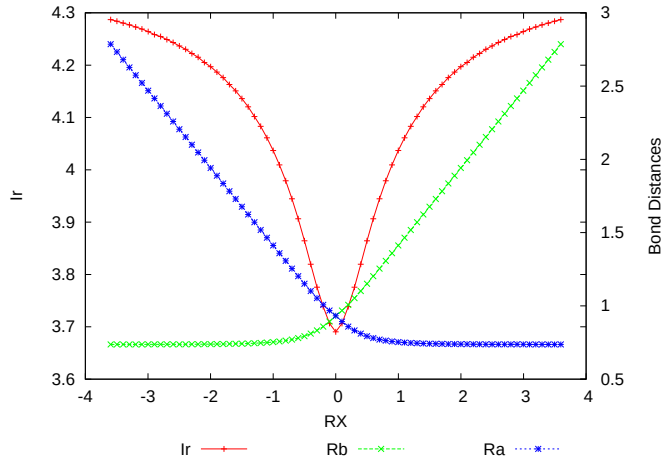

FIGURE 3.2: Fisher information in momentum space (red line) and the bond distances $R_a \equiv R(H_a - H)$ (blue line for the entering hydrogen) and $R_b \equiv R(H - H_b)$ (green line for the leaving hydrogen) for the IRC of $H_a^{\bullet} + H_2 \rightarrow H_2 + H_b^{\bullet}$.

To better understand the shape of the Fisher information, in Figure 3.2, the bond distances between the entering/leaving hydrogen radicals and the central hydrogen atom are plotted. This clearly shows that at the vicinity of the TS a bond breaking/forming chemical situation is occurring since the $R_b \equiv R(H - H_b)$ is elongating at the right side of the TS and the $R_a \equiv R(H_a - H)$ is stretching at the left side of the TS. It is worth noting that the chemical process does not happen in a synchronous manner, i.e., the homolytic bond breaking occurs first and then the molecule stabilizes by forming the TS structure which is clearly observed in the Figure 3.2,. As the incoming radical approaches the molecule, the bond breaks. Since the Fisher information represents the gradient of a probability distribution, it is natural to associate this to the change in the corresponding density. Therefore, from Figure 3.2, one can see that as the incoming hydrogen approaches, the bond enlarges in the region where the Fisher information in momentum space increases more rapidly. In contrast, the Fisher information in position space is not describing the bond breakink/forming process.

Next, we would like to test the non-polar bond pattern characteristic of homolytic bond-breaking reactions which should be reflected through the dipole moment of the molecules at the IRC. This is indeed observed in Figure 3.3, where these values along with the ones of the momentum Fisher information are depicted for comparison purposes. At the TS the dipole moment is zero, and the same behavior is observed as the process tends to the reactants/products in the IRC, reflecting the non-polar behavior of the molecule in these regions. However, it is also interesting to observe, from this property, how the molecular densities get distorted, reaching maximal values at the vicinity of the TS. In contrast, the behavior of the momentum Fisher information is totally opposite: this quantity decreases (increases) when the dipole moment increases (decreases), being minimum (maximum) approximately at the same points where the dipole moment reaches its

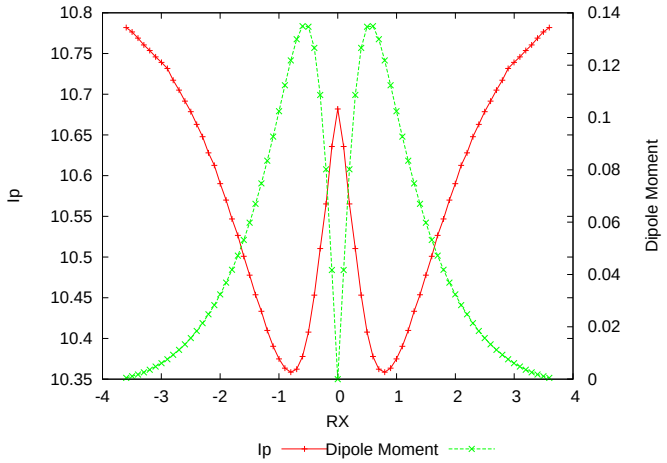

FIGURE 3.3: Fisher information in momentum space (red line) and the dipole moment values (green line) for the IRC of $H_a^{\bullet} + H_2 \rightarrow H_2 + H_b^{\bullet}$.

maximum (minimum) value. It means that in the regions where the molecule has a non-polar behavior, the momentum electronic density has a higher gradient content corresponding to a high irregular and localized density.

In Figure 3.4 the eigenvalues of the Hessian for the normal mode associated with the TS along the IRC of the reaction are depicted along with the momentum Fisher information values. The Hessian values represent the transition vector "frequencies" which show maxima at the vicinity of the TS and a minimal value at the TS. Several features are worthy mentioning the TS corresponds indeed to a saddle point, maxima at the Hessian correspond to high kinetic energy values (largest "frequencies" for the energy cleavage reservoirs correspond to the BCER [211]). In contrast, at the TS, the Hessian reaches a minimum value; this means that in this point the kinetic energy is the lowest one (minimal molecular frequency) [211] and, as we can see, it corresponds to a maximal Fisher information in momentum space. So it seems viable that I_p resembles the behavior of the TS vector. In connection with the Fisher information also depicted in Figure 3.4, it is interesting to note that in the transition state region (where the frequencies become imaginary [196–199, 211]) the Fisher information exerts its largest change as a gradient of the distribution in momentum space.

There are several density descriptors used in chemistry to determine the reactivity behavior such as the hardness and softness (see the previous Section). In Figure 3.5 we have plotted the values for the hardness along with the Fisher information in momentum space for comparison purposes. From a DFT conceptual point of view we may interpret Figure 3.5 as that chemical structures at the maximal hardness (minimal softness) values possess low polarizability and hence are less prone to acquire additional charge (less reactive). These regions correspond with minimal Fisher information regions in momentum space associated to a highly uniform momentum density. According to considerations discussed above, these structures are found at the defined (in a previous work

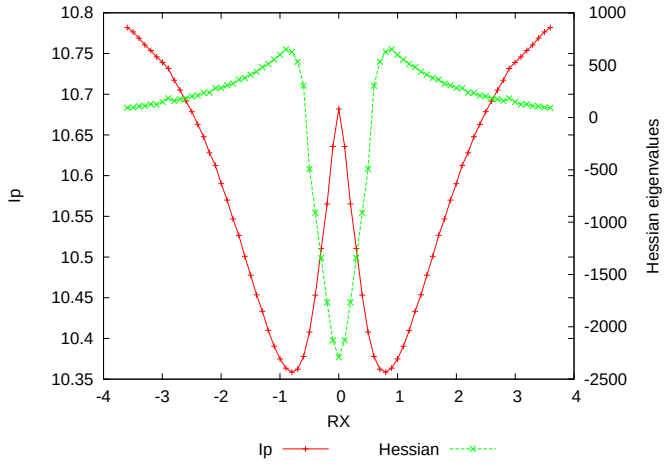

FIGURE 3.4: Fisher information in momentum space (red line) and the eigenvalues of the Hessian (green line) for the IRC of $H_a^{\bullet} + H_2 \rightarrow H_2 + H_b^{\bullet}$. It should be noted that negative values actually correspond with imaginary numbers (roots of negative force constants) so that the negative sign only represents a flag.

[211]) BCER regions, i.e., they are maximally distorted, with highly delocalized momentum densities (maximal dipole moment values, see Figure 3.3). In contrast, hardness values are minimal at the reactant complexes regions which correspond with localized momentum densities [211] with null dipole moments hence they are more prone to react (more reactive). At the TS, a local minimum for the hardness may be observed, then it is locally more reactive and leaning to acquire charge because its dipole moment is null.

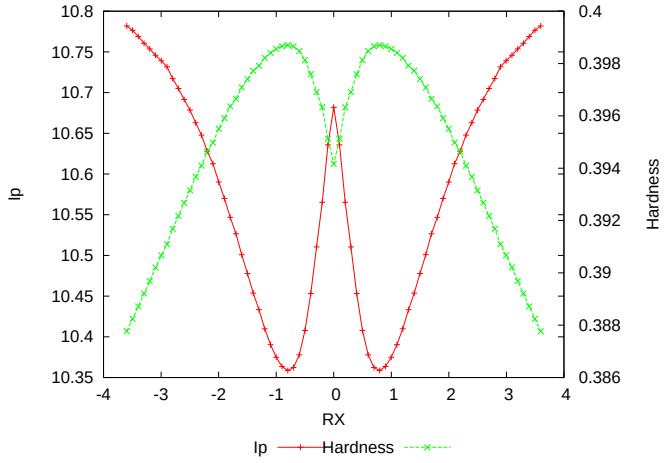

FIGURE 3.5: Fisher information in momentum space (red line) and the hardness values (green line) for the IRC of $H_a^{\bullet} + H_2 \rightarrow H_2 + H_b^{\bullet}$.

From the point of view of Fisher information the TS represents a more irregular distribution. It is interesting to note that the I_r in Figure 3.1 can only be associated with the hardness at the TS (Figure 3.5), in that more reactive structures correspond to the most uniform density in position space.

3.2 Nucleophilic substitution reaction

In this Section, we analyze a typical nucleophilic substitution (S_N2) reaction whose chemical process involves only one step in contrast with the abstraction reaction studied before which involves two steps. In the anionic form, the S_N2 mechanism can be depicted as

$$Y^- + RX \rightarrow RY + X^- \tag{3.6}$$

which is characterized by being kinetically of second order (first order in each of the reactants: the nucleophile Y^- and the substrate R_X, where X^- is the nucleofuge or leaving atom). For identity S_N2 reactions $X = Y$. It was postulated that the observed second order kinetics is the result of passage through the well-known Walden inversion transition state where the nucleophile displaces the nucleofuge (leaving group) from the backside in a single concerted reaction step.

The $H_a^- + CH_4 \rightarrow CH_4 + H_b^-$ represents the typical identity S_N2 reaction and we proceed with the calculations as follows: since diffuse functions are important to adequately represent anionic species [189], we have performed calculations for the IRC at the MP2/6-311++G** level of theory, generating 93 points evenly distributed between the forward and reverse directions of the IRC. A relative tolerance of 1.0×10^{-5} was set for the numerical integrations unless otherwise be stated [230, 231].

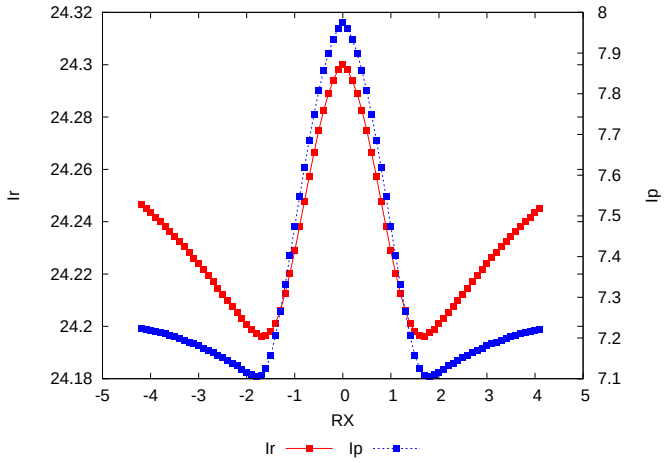

FIGURE 3.6: Fisher information in position (red line) and momentum (blue line) spaces for the IRC of $H_a^- + CH_4 \rightarrow CH_4 + H_b^-$.

Displaying both Fisher informations, I_r and I_p in the same picture, Figure 3.6, we can observe that they show a similar structure, both possessing a maximum at the TS and minimal values at its vicinity. This behavior is significantly different than the abstraction reaction analyzed before in which the position Fisher information shows the opposite behavior as compared with the momentum Fisher information at the TS region.

From a previous study [211] with Shannon entropies, a delocalized position density and a localized momentum density in the TS region were found, i.e., corresponding with a chemically relaxed structure (structurally less distorted with low kinetic energy and null dipole moment, see below). In contrast, the reactive complexes toward reactants/products show more localized densities with less delocalized momentum densities, i.e., the chemical structures at these regions are structurally distorted and posses more kinetic energy as compared to the TS. In the vicinity of the TS, at around $R_X \simeq |1.7|$, critical points for these measures are observed; they correspond to ionic complexes that characterize position densities which are highly localized and with highly delocalized momentum densities and high kinetic energies. At a first glance, it seems likely these regions correspond with BCER where bond breaking may start occurring.

One of the main differences of the S_N2 reaction with respect to the abstraction one is that for the former the course of the reaction occurs by an heterolytic rupture with an exchange of charge, whereas for the latter the mechanism is homolytic, i.e., a spin coupling process occurs. In this reaction, as the incoming hydrogen approaches the molecule it transfers charge, through the carbon bonding, to the leaving hydrogen so as to reach an equally charged distribution among the incoming/leaving hydrogens. As this process evolves, the gradient of the distribution involved in the position Fisher information I_r increases so as to reach a maximum at the TS.

To further support the charge transfer process mentioned above we can witness the heterolytic bond/breaking process through the contour values of the MEP at several stages of the S_N2 reaction in the plane of the $[H_a \cdots C \cdots H_b]^-$ atoms. We may observe from Figure 3.7(a) the initial step of the bond breaking process for the leaving hydrogen (nucleofuge) at $R_X = -1.5$ (forward direction), by noting that this particular atom is losing bonding charge as it leaves (in the region where the potential is positive). This is in contrast with the entering hydrogen which possesses the nucleophilic power of an hydride ion (in the region where the potential is negative).

It is also interesting to note that the remaining attached hydrogen atoms possess the expected electrophilic nature of the molecular bonding environment although its "philic" nature barely changes. In Figure 3.7(b) at $R_X = -0.9$ in the forward direction of the reaction, the $C - H_b$ bond cleavage is about to complete as the H_b atom has lost bonding charge (maximum electrophilic power) and the nucleophilic hydrogen is about to form a new bond by losing charge (nucleophilic power). In Figure 3.7(c) we have depicted the MEP at the TS where we can observe the point where the gradient of the position density reaches its maximum because the charge becames equalized according to Figure 3.6.

In order to analyze in more detail this reaction, we find instructive to plot the distances between the nucleophilic hydrogen (H_a) and the leaving hydrogen (H_b) in Figure 3.8. Distances show the stretching/elongating features associated with the bond

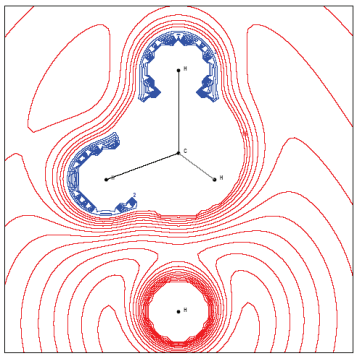

(a) At $R_X = -1.5$

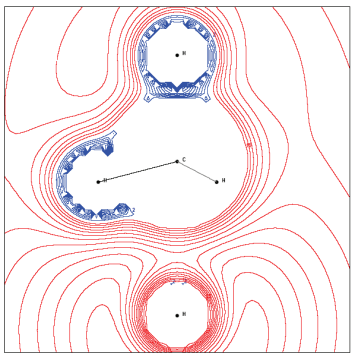

(b) At $R_X = -0.9$

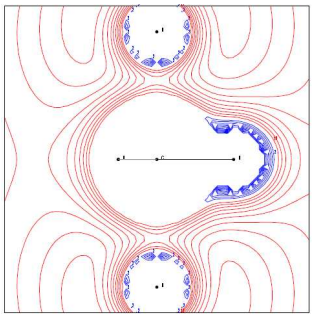

(c) At the transition state

FIGURE 3.7: The MEP contour lines in the plane of $[H_a \cdots C \cdots H_b]^-$ (H_a stands for the nucleophilic atom and H_b is the nucleofuge, on bottom and top, respectively) showing nucleophilic regions (blue contour lines) and electrophilic regions (red contour lines) at several reaction coordinates for the S_N2 reaction at (a) $R_X \equiv -1.5$, (b) $R_X \equiv -0.9$ and (c) at the TS.

forming/breaking situation that we have anticipated before. In contrast with the previously analyzed abstraction reaction, the S_N2 reaction occurs in a concerted and synchronous manner, i.e., the bond breaking/forming occurs at unison. An interesting feature which might be observed from Figure 3.8 is that whereas the elongation of the carbon-nucleofuge bond (R_b) changes its curvature significantly at $R_X \simeq -1.7$ (forward direction of the reaction) the stretching of the nucleophile-carbon bond does it in a smooth way, due to the repulsive forces that the ionic molecule exerts as the nucleophile approaches, which provokes the breaking of the carbon-nucleofuge to happen as the molecule starts liberating its kinetic energy. In this sense is that the reaction occurs in a concerted manner, i.e., the bond-breaking/dissipating-energy processes occurring simultaneously. It is interesting to note that minima for the momentum Fisher information coincide with the bond breaking/forming regions and that the change in the curvature of the bond distances marks the region where the gradient of the density in momentum space starts increasing.

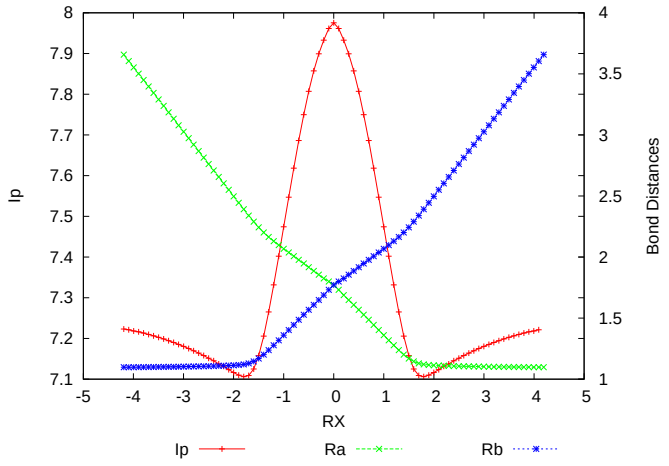

FIGURE 3.8: Fisher information in momentum space (red line) and the bond distances $R_a \equiv R(H_a - C)$ (green line, where H_a stands for the nucleophile) and $R_b \equiv R(C - H_b)$ (blue line, where H_b stands for the nucleofuge) for the IRC of $H_a^- + CH_4 \rightarrow CH_4 + H_b^-$.

In Figure 3.9 we have plotted the internal angle between $H_a^- \cdots C - H$ along with the Fisher information in momentum space for comparison purposes. Thus, the internal angle shows clearly that the molecule starts exerting the so called "inversion of configuration" at around $R_X \simeq -1.7$, where the nucleophile starts displacing the nucleofuge from the backside of the molecule in a single concerted reaction step. This starts occurring at the BCER regions [211]. We may observe from the figure that I_p possesses two minimum values that coincides with the inflexion points of the angle so marking the regions where the inversion of configuration occurs, i.e., the region where the gradient increases and the momentum density distribution becomes less irregular.

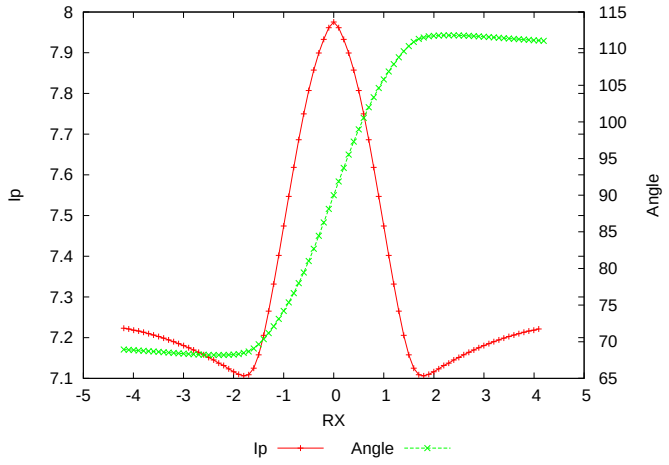

FIGURE 3.9: Fisher information in momentum space (red line) and the internal angle $H_a^- \cdots C - H$ (green line, where H_a stands for the nucleophile and H stands for any hydrogen attached to the methyl molecule) in degrees for the IRC of $H_a^- + CH_4 \rightarrow CH_4 + H_b^-$.

The S_N2 reaction is a good probe to test the polar bond pattern characteristic of heterolytic bond-breaking (with residual ionic attraction because of the ionic nature of the products) which should be reflected through the dipole moment of the molecules at the IRC. This is indeed observed in Figure 3.10, where these values along with those of the Fisher momentum information are depicted for comparison purposes.

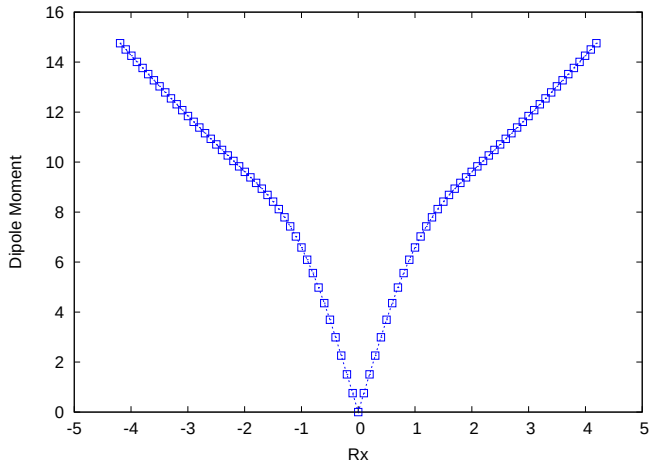

FIGURE 3.10: Dipole moment for the IRC of $H_a^- + CH_4 \rightarrow CH_4 + H_b^-$.

At the TS the dipole moment is zero, showing the non polar character of the TS structure with both nucleophile/nucleofuge atoms repelling each other evenly through its carbon bonding. As the ionic complexes approach the reactants/products regions the dipole moment increases monotonically, reflecting the polar bonding character of these ionic molecules with a significant change of curvature at the TS vicinity at around $R_X \simeq |1.0|$ (a change of curvature was already noted for Fisher information in momentum space at the same region). In going from reactants to products it is evident that the inversion of the dipole moment values reflects clearly the inversion of configuration of the molecule (this reaction starts and ends with a tetrahedral sp^3 carbon in the methyl molecule passing through a trigonal bipyramid at the TS), which is an inherent feature of S_N2 reactions. At these regions the gradient increases up to a maximum at the TS.

We found illustrative to include the hardness values of the IRC in the analysis, which is depicted in Figure 3.11. We can observe that the hardness shows largest values towards the reactant/product regions and minima at the TS, where the Fisher information in momentum space gets a maximum value. The TS corresponds with a metastable structure with a lowest hardness (largest softness), i.e., it is the most polarizable structure as compared to the rest at the IRC and hence it is the most reactive one. Also, it may be observed that the reactive complexes toward the reactant/product regions possess the largest hardness (lowest softness), corresponding to highly stable molecules which are less prone to acquire additional charge. In the vicinity of the TS we find "hardness bassins" at the BCER that we interpret as to chemically metastable and energetically

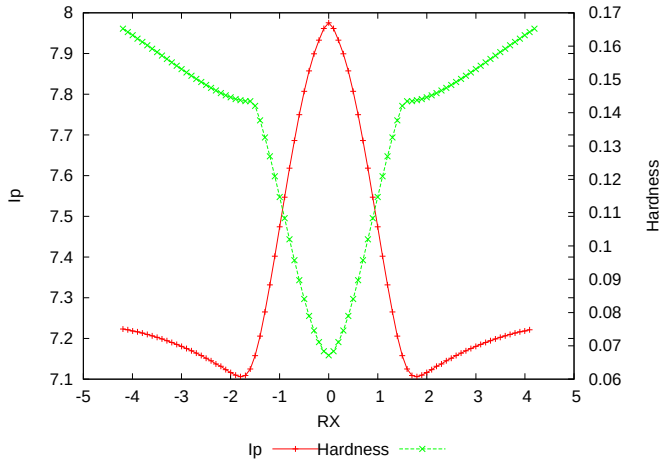

FIGURE 3.11: Fisher information in momentum space (red line) and the hardness values (green line) for the IRC of $H_a^- + CH_4 \rightarrow CH_4 + H_b^-$.

reactive regions. We note from Figure 3.11 that the momentum Fisher information reflects the behavior above described as an increment of the gradient.

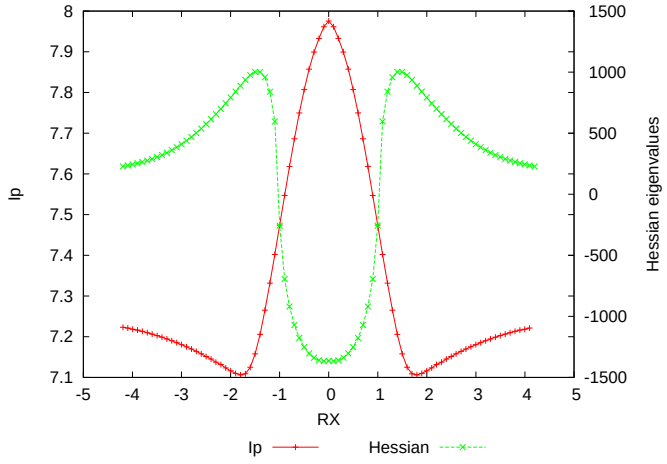

FIGURE 3.12: Fisher entropy in momentum space (red line) and the Hessian eigenvalues (green line) for the IRC of $H_a^- + CH_4 \rightarrow CH_4 + H_b^-$. It should be noted that negative values actually correspond with imaginary numbers (roots of negative force constants) so that the negative sign only represents a flag.

The eigenvalues of the Hessian for the normal mode associated with the TS along the IRC of the reaction are depicted in Figure 3.12 along with the Fisher information values in momentum space. As it may be observed from this figure, the Hessian values show maxima at the BCER and reach their minimal values at the TS. The former are associated with high kinetic energy values (high vibrational frequencies) which seem to coincide with the minimal values in the momentum Fisher information profile. The TS at the saddle point is associated with a low kinetic energy structure at the minimal molecular frequency value of the Hessian profile and with a maximum value of the

Fisher information in momentum space which corresponds to a density with the highest gradient content (very localized density). It is important to mention that the region where the frequencies become imaginary a transient of continuum has been established by Zewail and Polanyi [233] for the transition region and this is clearly reflected by the zone where the gradient increases in momentum space and, consequently, the associated Fisher information increases too.

3.3 Conclusions

In this Chapter we have shown the usefulness of the information-theoretic measures of the Fisher type to characterize elementary chemical reactions. In a previous work [211], the Shannon entropy of elementary chemical reactions was studied as a global measure that quantifies the localization/delocalization of the density; however, the behavior of the densities regarding their local changes (uniformity/irregularity) can only be provided by a local measure such as the Fisher information. We have verified that the local character of Fisher information indeed provokes an enhanced sensitivity to changes on the position and momentum densities along the chemical reaction paths. One of the manifestations of the local changes exerted by the densities is due to the charge transfer process which is directly reflected in the heterolitic behaviour of the S_N2 reaction, in contrast with the abstraction reaction whose mechanim is homolitic, i.e., the Fisher information is capable of differentiating between both types of mechanims because of its local character.

The TS structure, at least for the reactions studied in this work, was clearly predicted by Fisher information in both spaces whereas the stationary points that delimit the TS region are predicted by the momentum Fisher information solely. Besides, through the chemical probes we were capable to observe the basic chemical phenomena of bond breaking/forming showing that the Fisher information measures are highly sensitive in detecting these chemical events, mainly in momentum space.

According to Fisher information in position space, it is possible to detect differences in the mechanism for both reactions in that for the S_N2 the measure is able to witness the charge exchange process where the Fisher information is maximum at the TS.

It remains to be studied whether the overall behavior of the abstraction reaction as compared with the exchange S_N2 reactions represents a manner of studying reaction mechanisms by means of the Fisher information measures. We are aware of the fact that more chemical probes are necessary in order to pose more general statements.

Chapter 4

Entropic extremization problems: Applications to atomic systems

The extremization methods of entropic information measures provide us with powerful tools to estimate the probability distributions of random variables from the knowledge of partial information on these variables. They supply very useful constructive methods which objectively estimate the unknown distribution when only incomplete data is available. The least biased or minimally prejudiced estimate of the distribution consistent with the available data is that which extremizes the information-theoretic measure characteristic of each method.

The maximum entropy technique (maxEnt) [4, 5, 35, 56] associated to the Shannon entropy

$$S\left[\rho\right] = -\int \rho(\vec{r}) \ln \rho(\vec{r}) d\vec{r}. \tag{4.1}$$

which is the basis of the conventional or extensive statistical mechanics [57], is the most popular one; however, it does not always lead to an appropiate solution of the extremization problem.

At present, the extremum Fisher information (exfinf) method, based on such a quantity, namely

$$I\left[\rho\right] = \int \frac{\left|\vec{\nabla}_d \rho(\vec{r})\right|^2}{\rho(\vec{r})} d\vec{r}, \tag{4.2}$$

for a d-dimensional distribution, was considered [37] in order to provide the fundamental wave equations and/or the conservation laws of numerous natural systems at small and large scales.

The maximization of the Tsallis entropy (maxTent) [34, 234, 235]

$$T^{(q)}\left[\rho\right] = \frac{1}{q-1}\left(1 - \int \rho(\vec{r})^q d\vec{r}\right). \tag{4.3}$$

has been recently encountered to be the basis of the modern non-extensive statistical mechanics [236]. The use of these information measures and their extremization is a subject of much current interest in density functional methods of multi-electronic systems [52, 95, 237].

Then, the knowledge of the existence conditions for these extremization problems and the spreading properties of the associated extremum information measures is a two-folded problem of scientific relevance in physical science. Although the analytical expression of the extremum information distributions subject to some moment equality or inequality constraints is, at times, known (mostly for the maxEnt case), there are still numerous open questions about their existence conditions in spite of the efforts of many authors [51, 57, 238–249]. On the other hand, there has not been a systematical investigation into the spreading properties of these distributions. This situation is a serious lack not only from a conceptual standpoint but also because of its effects for a great deal of problems and phenomena in science, finances or engineering [244, 250, 251]. For a recent exhaustive review of the maxEnt problem until 2004 see Ref. [241].

Here we consider d-dimensional probability distributions, mainly because of two reasons: (i) numerous phenomena of physical systems in our three-dimensional world can be better explained via quantum-mechanical probability distributions with non-standard dimensionalities (e.g., quantum dots, quantum wells, quantum wires, ...) [126, 127], and (ii) it is commonly believed at present that the best way to explain the unification of all forces of physics is via the idea of higher dimensionalities [252].

The extremum information method associated to a generic information-theoretic measure

$$Q \equiv \int \rho(\vec{r}) F[\rho(\vec{r})] d\vec{r}, \tag{4.4}$$

consists of the extremization of Q subject to the constraints of normalization to unity, i.e.

$$\int \rho(\vec{r}) d\vec{r} = 1 \tag{4.5}$$

as well as

$$\int \rho(\vec{r}) f_i(\vec{r}) d\vec{r} = a_i; \qquad i = 1, 2, ..., n, \tag{4.6}$$

where each $f_i(\vec{r})$ is a given function of $\vec{r}$ with $f_0(\vec{r}) \equiv 1$. Using the method of Lagrange multipliers, one considers the functional

$$Q^* = Q + \sum_{i=0}^{n} \lambda_i \left[\int f_i(\vec{r}) \rho(\vec{r}) d\vec{r} - a_i \right], \tag{4.7}$$

where λ_i are the $n+1$ Lagrange multipliers, and sets its variation to zero so that

$$\delta Q^* = \int \left\{ \frac{\delta F\left[\rho(\vec{r})\right]}{\delta \rho(\vec{r}} + \sum_{i=0}^{n} \lambda_i f_i(\vec{r}) \right\} \delta \rho(\vec{r}) d\vec{r} = 0, \tag{4.8}$$

This equation yields the density $\rho(\vec{r})$ in terms of the multipliers λ_i determined from the $n+1$ equations given by Eqs. (4.5) and (4.6), giving rise to the extremum information probability density.

The maxEnt problem has a unique solution [239] which maximizes the Shannon entropy, whenever it exists, for the given set of expectation values $\{a_i\} = \{a_0 = 1, a_1, ..., a_n\}$. In contrast with this situation, the exfinf problems can have multiple solutions. Then, the question is which solution should be chosen. It has been argued that the solution with no nodes (the ground-state solution) leading to the lowest Fisher information is the equilibrium one, so laying the foundations of the conventional or equilibrium thermodynamics based on the concept of Fisher information. The choice of linear superpositions of this ground state with excited state solutions leads us to non-equilibrium thermodynamics [253].

The maxEnt problem under different moment constraints (i.e., those where all $f_i(\vec{r})$ are integer power of $r = |\vec{r}|$) has been discussed in numerous places for several scientific situations; see, e.g., Refs. [244, 246, 247, 249, 254–256]. For the analysis of the exfinf and maxTent problems we refer to Refs. [37, 52, 242] and [234, 235, 245], respectively. See also Ref. [241] for more detailed information. There are two kinds of exfinf problems in current use: minimum Fisher information (minInf) [37, 242, 257–259] and extreme physical information (EPI) [37, 260]. Nevertheless we do not distinguish between these two treatments for our present purposes. Let us only point out that the probability distribution which minimizes the Fisher information will be "as non-informative as possible" while still satisfying the constraints [260].

These four information-theoretic problems, although similar at a first sight, are markedly different in their world views and applicability in Physics [261, 262]. Contrary to the EPI method, which does not depend upon arbitrary subjective choices, the maxEnt, minInf and maxTent problems require the choice of arbitrary or subjectively defined inputs.

This chapter has three parts which correspond to the d-dimensional maxEnt (Section 4.1), minInf (Section 4.2) and maxTent (Section 4.2), problems. Each part begins with the determination of the distribution which extremizes the associated information-theoretic measure (namely, Shannon, Fisher or Tsallis, respectively) under some given constraints, and then the spread of the resulting extremum density is investigated by means of its information-theoretic measures given by Eqs. (4.1)-(4.3) other than that extremized, and, additionally, its variance

$$V = \left\langle r^2 \right\rangle - \left\langle r \right\rangle^2 \tag{4.9}$$

with $\langle r^m \rangle = \int r^m \rho(\vec{r}) d\vec{r}$.

For the maxEnt problem, the condition for the existence of the probability distribution which maximizes the Shannon entropy is given for the d-dimensional case in subsection

4.1.1. Then, in Section 4.4, we center our attention on the many-electron systems, studying the spreading measures obtained in the previous sections when the constraints of these extremization problems are atomic radial expectation values (in both position and momentum spaces), as well as analyzing the relationship between their values and relevant physical properties of those systems. Finally, in Section 4.5 some conclusions are given.

4.1 The maxEnt problem

Following the method described before, the d-dimensional density $\rho_S(\vec{r})$ which maximizes the Shannon entropy (4.1) with the known constraints $a_i = \langle f_i(\vec{r})\rangle$ $(i = 0, 1, \cdots, m)$ is

$$\rho_S(\vec{r}) = \exp\left\{-\lambda_0 - \sum_{i=1}^{m} \lambda_i f_i(\vec{r})\right\}. \tag{4.10}$$

For this general problem, the existence conditions for $\rho_S(\vec{r})$ are still unknown. Then we shall restrict ourselves to some specific cases where such conditions are known; namely, when the constraints are just one or two radial expectation values $\langle r^\alpha\rangle$ in addition to the normalization to unity constraint.

A.- d-dimensional case with a given expectation value $\langle \mathbf{r}^\alpha\rangle$

In this case the density which maximizes the Shannon entropy $S[\rho]$ is given by

$$\rho_S(\vec{r}) = \exp\left\{-\lambda_0 - \lambda_1 r^\alpha\right\}, \tag{4.11}$$

where the Lagrange multipliers have, according to Eqs. (4.5)-(4.6), the values

$$\lambda_0 = \ln\left[\frac{2\pi^{\frac{d}{2}}\Gamma\left(\frac{d}{\alpha}\right)}{\alpha\,\Gamma\left(\frac{d}{2}\right)}\right] + \frac{d}{\alpha}\ln\left[\frac{\alpha}{d}\,\langle r^\alpha\rangle\right], \tag{4.12}$$

$$\lambda_1 = \frac{d}{\alpha\,\langle r^\alpha\rangle}, \tag{4.13}$$

for any $\alpha > 0$ as impossed by the finiteness of the norm.

Moreover, from Eqs. (4.1) and (4.11), the corresponding value for the maximum entropy is

$$S_{max}[\rho_S] = A_0(\alpha, d) + \frac{d}{\alpha}\ln\langle r^\alpha\rangle, \tag{4.14}$$

with

$$A_0(\alpha, d) = \frac{d}{\alpha} + \ln\left[\frac{2\pi^{\frac{d}{2}}}{\alpha}\left(\frac{\alpha}{d}\right)^{\frac{d}{\alpha}}\frac{\Gamma\left(\frac{d}{\alpha}\right)}{\Gamma\left(\frac{d}{2}\right)}\right]. \tag{4.15}$$

And, according to Eqs. (4.2), (4.3) and (4.9), we have determined the values

$$V\left[\rho_S\right] = A_1(\alpha, d)\left\langle r^{\alpha}\right\rangle^{\frac{2}{\alpha}}, \tag{4.16}$$

for the variance,

$$I\left[\rho_S\right] = A_2(\alpha, d)\left\langle r^{\alpha}\right\rangle^{-\frac{2}{\alpha}}, \tag{4.17}$$

for the Fisher information, and

$$T^{(q)}\left[\rho_S\right] = \frac{1}{q-1}\left\{1 - q^{-\frac{D}{\alpha}}\left[A_3(\alpha, d)\right]^{q-1}\left\langle r^{\alpha}\right\rangle^{\frac{d}{\alpha}(1-q)}\right\} \tag{4.18}$$

for the Tsallis entropy of the maximizer entropy $\rho_S(\vec{r})$, respectively. The coefficients A_i $(i = 1, 2, 3)$ are functions of the parameters α and d as follows:

$$A_1(\alpha, d) = \left(\frac{d}{\alpha}\right)^{-\frac{2}{\alpha}}\left\{\frac{\Gamma\left(\frac{d+2}{\alpha}\right)}{\Gamma\left(\frac{d}{\alpha}\right)} - \left(\frac{\Gamma\left(\frac{d+1}{\alpha}\right)}{\Gamma\left(\frac{d}{\alpha}\right)}\right)^2\right\}, \tag{4.19}$$

$$A_2(\alpha, d) = \alpha^2\left(\frac{d}{\alpha}\right)^{\frac{2}{\alpha}}\frac{\Gamma\left(\frac{d-2}{\alpha}+2\right)}{\Gamma\left(\frac{d}{\alpha}\right)}, \tag{4.20}$$

$$A_3(\alpha, d) = \frac{\alpha}{2}\left(\frac{d}{\alpha}\right)^{\frac{d}{\alpha}}\frac{\Gamma\left(\frac{d}{2}\right)}{\pi^{\frac{d}{2}}\Gamma\left(\frac{d}{\alpha}\right)}, \tag{4.21}$$

which drastically simplify for specific values of α and/or d.

In Figures 4.1 and 4.2 we have plotted the four spreading measures (Shannon, variance, Fisher and Tsallis $T^{(q)}$, with $q = 0.9$ for illustration) calculated according to Eqs. (4.14)-(4.21) in order to analyze the dependence on the expectation order α and the dimensionality d of the masure under consideration, respectively. In doing so, the position density of the d-dimensional Hydrogen atom in its ground state has been considered. From Figure 4.1 we observe that, for the three dimensional case, (i) the three global measures (Shannon, variance and Tsallis) have an increasing behaviour with α, contrary to the decreasing monotonic behaviour of the local Fisher measure, (ii) the Tsallis entropy $T^{(0.9)}$ increases faster than the Shannon entropy, and both of them are systematically bigger than the Fisher information as α is increasing; the latter behaviour is not fulfilled by the variance, and (iii) for a given order α, $T^{(0.9)} > S_{max} > I$ always, $I > V$ for $\alpha < 24$ and $I < V$ for $\alpha > 24$.

From Figure 4.2 we realize that for fixed $\alpha = 2$, (i) the three global spreading measures increase, displaying a convex parabolic form in term of the dimensionality d, (ii) the local Fisher measure has a decreasing convex form, and (iii) for a given dimensionality, it occurs that $T^{(0.9)} > S_{max} > V$.

On the other hand, the algebraic manipulation of Eqs. (4.14)-(4.21) leads to the following mutual relations among the spreading measures under consideration. We

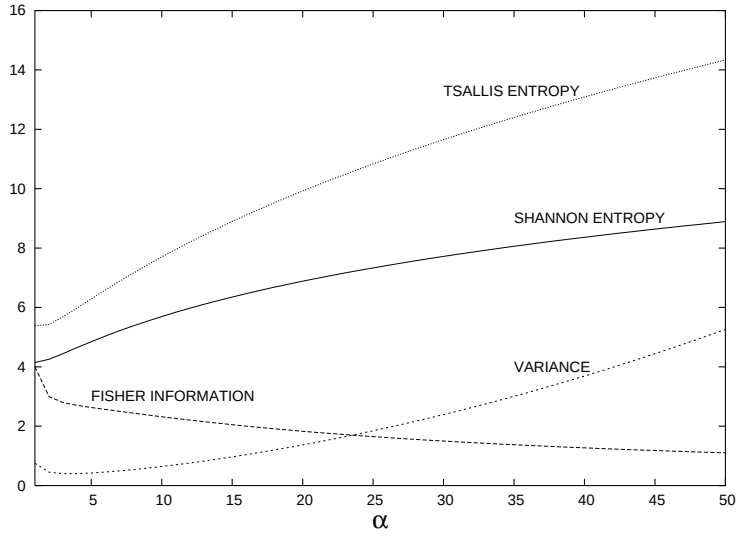

FIGURE 4.1: Variance, Fisher information and Shannon and Tsallis (with $q = 0.9$) entropies for the maxEnt problem with the constraint $\langle r^\alpha \rangle$ as functions of the expectation order α in the three-dimensional case. Atomic units are used.

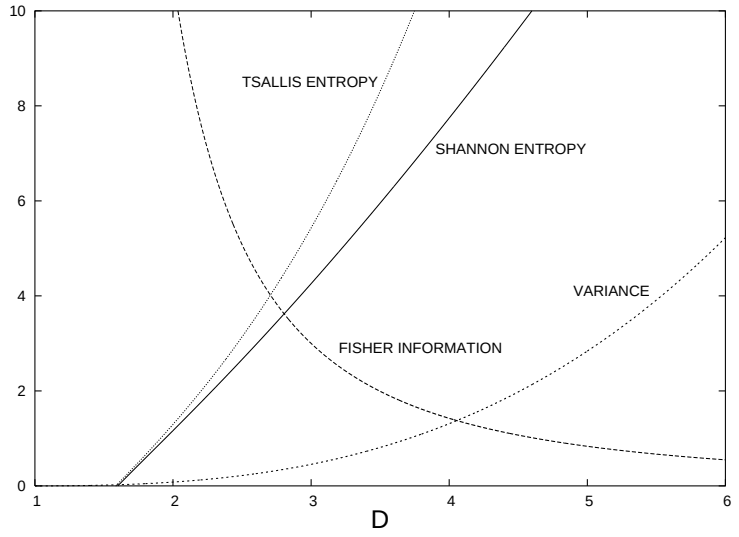

FIGURE 4.2: Variance, Fisher information and Shannon and Tsallis (with $q = 0.9$) entropies for the maxEnt problem as functions of the dimension d constrained by the radial expectation value $\langle r^2 \rangle$. Atomic units are used.

find that

$$I\left[\rho_S\right] = \frac{A_1(\alpha, d) A_2(\alpha, d)}{V\left[\rho_S\right]}, \tag{4.22}$$

$$S_{max}\left[\rho_S\right] = F_1(\alpha, d) + \frac{d}{2} \ln V\left[\rho_S\right] = F_2(\alpha, d) - \frac{d}{2} \ln I\left[\rho_S\right], \tag{4.23}$$

and

$$S_{max}\left[\rho_S\right] = F_3(\alpha, q, d) + \frac{1}{1-q} \ln \left[1 + (1-q) T^{(q)}\left[\rho_S\right]\right], \tag{4.24}$$

where F_i $(i = 1, 2, 3)$ are simple relations of the coefficients A_i given by the expressions (4.19)-(4.21). The mutual relationships (4.22)-(4.24) among the four spreading measures drastically simplify when the dimensionality d and/or the other two involved parameters α and q are appropriately chosen.

B.- One-dimensional case with given $\langle \mathbf{x} \rangle$ and $\langle \mathbf{x^2} \rangle$

Let us now consider the maxEnt problem with constraints $\left\{\left\langle x^0 \right\rangle = 1, \langle x \rangle, \left\langle x^2 \right\rangle\right\}$ for one-dimensional distribution $(d = 1)$.

In this case the maximizer density becomes

$$\rho_S(x) = \exp\left\{-\lambda_0 - \lambda_1 x - \lambda_2 x^2\right\}. \tag{4.25}$$

Here the existence conditions are known to be given by the inequalities (4.35) and (4.37), as we discusse in the next subsection. Moreover, operating similarly as previously we obtain that the maximum value of the Shannon entropy is a logarithmic function of the variance,

$$S_{max}\left[\rho_S\right] = \ln\sqrt{2\pi e} + \ln\left(\left\langle x^2 \right\rangle - \langle x \rangle^2\right) = \ln\sqrt{2\pi e} + \ln V[\rho_S] \tag{4.26}$$

and the Fisher information I is exactly equal to the reciprocal of variance, so that

$$S_{max}\left[\rho_S\right] = \ln\sqrt{2\pi e} - \ln I\left[\rho_S\right]. \tag{4.27}$$

Moreover, the Tsallis entropy of the maximizer density can be also explicitly expressed as

$$T^{(q)}\left[\rho_S\right] = \frac{(2\pi)^{\frac{1-q}{2}}}{(1-q)\sqrt{q}}\left(\left\langle x^2 \right\rangle - \langle x \rangle^2\right)^{\frac{1-q}{2}}, \tag{4.28}$$

so that the following relation with the maximum Shannon entropy is fulfilled:

$$S_{max}\left[\rho_S\right] = \frac{1}{2}\left(1 - \ln 2\pi\right) + \frac{1}{1-q}\ln q + \frac{2}{1-q}\ln\left[1 + (1-q)T^{(q)}\left[\rho_S\right]\right]. \tag{4.29}$$

4.1.1 Existence conditions for the maxEnt problem

In this subsection we consider the reduced d-dimensional maxEnt problem, where one tries to approximate an absolutely continuous distribution $\rho(\vec{r})$ in $\Re^d$ from a finite number of radial expectation values

$$\langle r^m \rangle = \int r^m \rho(\vec{r}) d\vec{r}; \quad m = 0, 1, 2, ..., n, \tag{4.30}$$

where $\vec{r} = (r, \theta_1, \theta_2, ..., \theta_{d-1})$ describes the d-dimensional vector $\vec{r}$ in hyperspherical coordinates so that the hyperradius varies as $0 \leq r < \infty$, and the angles, $0 \leq \theta_j < \pi$ for

$1 \leq j < d-2$ and $0 \leq \theta_{d-1} < 2\pi$. The volume element $d\vec{r}$ is

$$d\vec{r} = r^{d-1} dr d\Omega_d; \qquad d\Omega_d = \left(\prod_{j=1}^{d-2} (\sin\theta_j)^{2\alpha_j} d\theta_j \right) d\theta_{d-1}, \tag{4.31}$$

with $\alpha_j = \frac{d-j-1}{2}$. For the special case $d = 1$, remark that $r = x \in [0, \infty)$.

The application of the general considerations explained before to the Shannon entropy provides that the maxEnt problem has a maximum entropy distribution whose density function is given by

$$\rho_S(r) = \exp\left(-\sum_{i=0}^{n} \lambda_i r^i \right), \tag{4.32}$$

where the Lagrange multipliers λ_i, $i = 0, 1, ..., n$, are chosen to fulfil the conditions

$$\int_0^\infty r^m exp\left(-\sum_{i=0}^{n} \lambda_i r^i \right) r^{D-1} dr = \langle r^m \rangle; \quad m = 0, 1, ..., n \tag{4.33}$$

where Ω_d is the generalized solid angle

$$\Omega_d \equiv \int d\Omega_d = \frac{2\pi^{d/2}}{\Gamma\left(\frac{d}{2}\right)}, \tag{4.34}$$

so that $\Omega_1 = 2$, $\Omega_2 = 2\pi$ and $\Omega_3 = 4\pi$. For the case $n = 2$ (i.e. for given $\langle r \rangle$ and $\langle r^2 \rangle$) the determination of the associated Stieltjes problem [263] and the solvability of the integral relations (4.33) of the corresponding maxEnt problem [239, 240, 264] require the involved radial expectation values to satisfy the inequalities

$$< r >^2 \leq < r^2 > \leq \frac{d+1}{d} < r >^2 \tag{4.35}$$

The lower bound to $< r^2 >$ is a straightforward consequence of the non-negativity of the Hankel determinant

$$\begin{vmatrix} < r^0 > & < r > \\ < r > & < r^2 > \end{vmatrix} \geq 0$$

corresponding to the involved Stieltjes moment problem. Alternatively, the same result can be found by use of the Hölder inequality. The upper bound to $< r^2 >$ is obtained by means of the existence condition of the aforementioned maxEnt problem which, according to Einbu's theorem [239, 241] or the Junk-Tagliani results [240, 264], is given by

$$\mu_{d+1} \leq \frac{d+1}{d} \Omega_d \mu_d^2, \tag{4.36}$$

where the moments $\mu_{d+\alpha-1}$ are

$$\mu_{d+\alpha-1} = \frac{1}{\Omega_d} < r^\alpha >; \qquad \alpha > -d \tag{4.37}$$

In the application of the same procedure to the radial expectation values

$\{< r^0 >= 1, < r^\alpha >, < r^\beta >\}$,

i.e. to the moments $\{\mu_{d-1},\ \mu_{d+\alpha-1},\ \mu_{d+\beta-1}\}$, we have found the following inequalities:

$$< r^\alpha >^{\frac{\beta}{\alpha}} \leq < r^\beta > \leq\ f(d,\alpha,\beta) < r^\alpha >^{\frac{\beta}{\alpha}}, \tag{4.38}$$

with arbitrary $\beta > \alpha > 1 - d$ (if $\alpha < 0$, then $\frac{\beta}{\alpha}$ must be integer), and the constant

$$f(d,\alpha,\beta) \equiv \left(\frac{\alpha}{d}\right)^{\frac{\beta}{\alpha}} \frac{\Gamma\left(\frac{\beta+d}{\alpha}\right)}{\Gamma\left(\frac{d}{\alpha}\right)} \tag{4.39}$$

It is worth noticing out that Eqs. (4.38)-(4.39) boil down to Eq. (4.35), and moreover when $d = 1$ the last expression contains the Dowson-Wragg condition [43] for the max-Ent problem associated to the univariate probability distributions when the first two moments are given.

The following desirable step forward is to find the existence conditions for the d-dimensional maxEnt distributions subject to the radial expectation values
$\left\{< r^0 >= 1, < r^\alpha >, < r^\beta >, < r^\gamma >;\quad \gamma > \beta > \alpha\right\}$
or equivalently the moments $\{\mu_{d-1},\ \mu_{d+\alpha-1},\ \mu_{d+\beta-1},\ \mu_{d+\gamma-1};\quad \gamma > \beta > \alpha > 0\}$. This would extend the celebrated Kociszewski [238] criteria for the existence of maximum entropy Stieltjes univariate ($d = 1$) distributions having prescribed the first three moments besides the normalization; that is, for given $\{\mu_0,\ \mu_1,\ \mu_2,\ \mu_3\}$. For completeness let us mention here that methodologies to obtain the desired existence inequalities for the four d-dimensional radial expectation values could be possible d-dimensional extensions of the Einbu theorems [239] or the Milano-Trento-Caracas maxEnt approach [243, 265, 266] for the fractional lacunary Stieltjes moment problem.

4.2 The minInf problem

As compared to the previous variational problem, the minimization of Fisher information under some given constraints presents different characteristics from the conceptual and mathematical points of view. As its own name indicates, now the aim is to find a minimizer information distribution instead of a maximizer one. The reason is the kind of functional to extremize, namely the Fisher information which, contrary to the convex functionals $S[\rho]$ and $T^{(q)}[\rho]$ (Shannon and Tsallis entropies, the last one will be analyzed below), is a concave one.

Also the local character of $I[\rho]$, opposite to the global one of S and $T^{(q)}$, justifies the replacement of a maximization by a minimization problem. The fact that the gradient of

the distribution appears in the definition of $I[\rho]$ makes its minimum values to be reached for highly spread distributions, according to the concept of least-biased functions.

In this case, the general method described before shows that the d-dimensional density $\rho_I(\vec{r})$ which minimizes the Fisher information, Eq. (4.2) with the known constraints $a_i = \langle f_i(\vec{r})\rangle$ fulfils the differential equation

$$\left[\frac{\vec{\nabla}_d \rho_I(\vec{r})}{\rho_I(\vec{r})}\right]^2 + 2\vec{\nabla}_d \left[\frac{\vec{\nabla}_D \rho_I(\vec{r})}{\rho_I(\vec{r})}\right] + \lambda_0 + \sum_{k=1}^{m} \lambda_k f_k(\vec{r}) = 0, \tag{4.40}$$

where $\vec{\nabla}_d$ denotes the d-dimensional gradient operator. The case $d = 3$ has already been treated in detail (see Ref. [52]). For the sake of simplicity and transparency purposes we have restricted ourselves to a concrete and fundamental three-dimensional case: the unique constraint $a_1 = \left\langle r^{-1}\right\rangle$, besides the normalization to unity. Then, the density $\rho_I(\vec{r})$ is given by [52]

$$\rho_I(\vec{r}) = \pi^{-1}\left\langle r^{-1}\right\rangle^3 \exp\left(-2\left\langle r^{-1}\right\rangle r\right), \tag{4.41}$$

which corresponds to the minimal Fisher information

$$I_{min}[\rho_I] = 4\left\langle r^{-1}\right\rangle^2 \tag{4.42}$$

Moreover, this minimizer density $\rho_I(\vec{r})$ has the following values of other information measures:

$$V[\rho_I] = \frac{3}{4\left\langle r^{-1}\right\rangle^2}, \tag{4.43}$$

and

$$S[\rho_I] = 3 + \ln\pi - 3\ln\left\langle r^{-1}\right\rangle, \tag{4.44}$$

for the variance and the Shannon entropy, and

$$T^{(q)}[\rho_I] = \frac{1}{q-1}\left[1 - \frac{\pi^{1-q}}{q^3}\left\langle r^{-1}\right\rangle^{3(q-1)}\right]; \qquad q > 0, \quad q \neq 1 \tag{4.45}$$

for the Tsallis entropy. So that, they are mutually related by

$$I_{min}[\rho_I] = \frac{3}{V[\rho_I]} = 4\pi^{\frac{2}{3}} e^2 \exp\left(-\frac{2}{3}S[\rho_I]\right), \tag{4.46}$$

and

$$I_{min}[\rho_I] = 4\pi^{\frac{2}{3}} q^{\frac{2}{q-1}}\left[1 + (1-q)T^{(q)}[\rho_I]\right]^{\frac{2}{3(q-1)}}, \qquad q > 0, q \neq 1 \tag{4.47}$$

so that for $q = 2$ one has that $T^{(2)}[\rho_I] = 1 - \dfrac{I_{min}[\rho_I]}{64\pi}$.

Similar analyses can be done for other concrete cases, such as $(a_0, a_1) = (1, \left\langle r^2\right\rangle)$ and $(a_0, a_1, a_2) = (1, \left\langle r^{-1}\right\rangle, \left\langle r^2\right\rangle)$, $(1, \left\langle r^{-2}\right\rangle, \left\langle r^2\right\rangle)$, where the minimizer densities are known

to exist [52]. We should point out, however, that for the general case above mentioned neither the solution of Eq. (4.40) nor its existence conditions are known except for some specific constraints. Unfortunately, this is even true for the particular cases where the constraints are one or various radial expectation values of generic order. The search of existence conditions for the minInf problem just mentioned is an important yet open task, which lies beyond the scope of this work since it involves high-brow questions of partial differential equations as in Eq. (4.40). On the other hand it is worthy to mention here the Frieden's [37, 258, 259] Lagrangian formalism for the minInf problem and the Luo's application of the maxEnt and minInf problems [262].

4.3 The maxTent problem

The maximizer density $\rho_T(\vec{r})$ of the three-dimensional maxTent problem given by Eqs.(4.3)-(4.8) with constraints $(a_0, a_1) = (1, \langle r^\alpha \rangle)$ depends on the value of q (the order of the Tsallis entropy) and α. There are three different cases:

- If $q > 1$ and $\alpha > 0$, the maximum entropy density has a finite support $r \in [0, a]$, vanishing out from the sphere of radius a centered at the origin.
- If $0 < q < 1$ and $\alpha > \frac{3(1-q)}{q}$, the maximum entropy density has as domain the whole three-dimensional space.
- If $q > 1$ and $-\frac{3(q-1)}{q} < \alpha < 0$, the maximum entropy density does not vanish only within the unbounded interval $r \in [a, \infty)$.

For the first case, the extreme probability density is

$$\rho_T(r) = C \left(\frac{1}{q}(a^\alpha - r^\alpha) \right)^{\frac{1}{q-1}}, \tag{4.48}$$

for $r \leq a$ and zero in other case, according to the general extremization method shown in the iintroduction of this chapter. The constants C and a are functions of the Lagrange multipliers; they have the following expressions:

$$a = \left(\frac{3(q-1) + q\alpha}{3(q-1)} \langle r^\alpha \rangle \right)^{\frac{1}{\alpha}}, \tag{4.49}$$

$$C = \frac{q^{\frac{1}{q-1}} \alpha}{4\pi B\left(\frac{3}{\alpha}, \frac{q}{q-1}\right)} \left(\frac{3(q-1) + q\alpha}{3(q-1)} \langle r^\alpha \rangle \right)^{-\frac{3}{\alpha} - \frac{1}{q-1}}, \tag{4.50}$$

where $B(\alpha, \beta) = \frac{\Gamma(\alpha)\Gamma(\beta)}{\Gamma(\alpha+\beta)}$ is the beta function.

This density has information measures with the following values:

$$T_{max}^{(q)}\left[\rho_T\right] = \frac{1}{q-1}\left[1 - C_0(\alpha,q)\langle r^\alpha\rangle^{-\frac{3(q-1)}{\alpha}}\right], \tag{4.51}$$

for the maximal Tsallis entropy,

$$S\left[\rho_T\right] = C_1(\alpha,q) + \frac{3}{\alpha}\ln\langle r^\alpha\rangle, \tag{4.52}$$

$$V\left[\rho_T\right] = C_2(\alpha,q)\langle r^\alpha\rangle^{\frac{2}{\alpha}}, \tag{4.53}$$

for the Shannnon entropy and the variance, and

$$I\left[\rho_T\right] = C_3(\alpha,q)\langle r^\alpha\rangle^{-\frac{2}{\alpha}}; \qquad 1 < q < 2, \tag{4.54}$$

for the Fisher information. The coefficients $C_i(\alpha,q)$, $i = 0, 1, 2$ and 3, have the following expressions:

$$C_0(\alpha,q) = \frac{q^q\alpha^{2q-1}[3(q-1)]^{\frac{3(q-1)}{\alpha}}}{\left[4\pi B\left(\frac{3}{\alpha},\frac{2q-1}{q-1}\right)\right]^{q-1}}\left(3(q-1)+q\alpha\right)^{-\frac{3(q-1)+q\alpha}{\alpha}}, \tag{4.55}$$

$$\begin{aligned} C_1(\alpha,q) = {} & \frac{1}{q-1}\left[\psi\left(\frac{q}{q-1}+\frac{3}{\alpha}\right) - \psi\left(\frac{q}{q-1}\right)\right] - \ln\left(\frac{\alpha}{4\pi B\left(\frac{3}{\alpha},\frac{q}{q-1}\right)}\right) \\ & + \frac{3}{\alpha}\ln\left(\frac{3(q-1)+\alpha q}{3(q-1)}\right), \end{aligned} \tag{4.56}$$

$$\begin{aligned} C_2(\alpha,q) = {} & \left(\frac{3(q-1)+q\alpha}{3(q-1)}\right)^{\frac{2}{\alpha}} \frac{\Gamma\left(\frac{q}{q-1}+\frac{3}{\alpha}\right)}{\Gamma\left(\frac{3}{\alpha}\right)} \\ & \times\left[\frac{\Gamma\left(\frac{5}{\alpha}\right)}{\Gamma\left(\frac{5}{\alpha}+\frac{q}{q-1}\right)} - \frac{\Gamma^2\left(\frac{4}{\alpha}\right)\Gamma\left(\frac{q}{q-1}+\frac{3}{\alpha}\right)}{\Gamma\left(\frac{3}{\alpha}\right)\Gamma^2\left(\frac{5}{\alpha}+\frac{q}{q-1}\right)}\right], \end{aligned} \tag{4.57}$$

$$C_3(\alpha,q) = \frac{\alpha^2}{(q-1)^2}\left(\frac{3(q-1)+q\alpha}{3(q-1)}\right)^{-\frac{2}{\alpha}} \frac{B\left(\frac{1}{\alpha}+2,\frac{1}{q-1}-1\right)}{B\left(\frac{3}{\alpha},\frac{q}{q-1}\right)}, \tag{4.58}$$

where $\psi(x) = \frac{\Gamma'(x)}{\Gamma(x)}$ is the digamma function.

Contrary to the previous entropy extremization problems where the extremizer density has an exponential form, now we have found the power law given by Eq. (4.48) as already pointed out by different authors [234–236, 248]. To gain insight into this powerlike maximizer density of the Tsallis entropy we have plotted in Figures 4.3 and 4.4 the curves of the four spreading measures mentioned above against the expectation order

α and the non-extensivity parameter q, respectively. From Figure 4.3 we notice that $I > T_{max}^{(q)}$ (with $q = 1.7$) for any expectation value, having the maximum Tsallis entropy a widely extended convex shape. From Figure 4.4, corresponding to $\alpha = 3$, we find that the Fisher information (i) monotonically increases as q increases and (ii) $S > T_{max}^{(q)} > V$ for all values of the non-extensivity parameter. Besides, Fisher information crosses both Tsallis and Shannon measures at a critical q around 1.15 and 1.45 respectively.

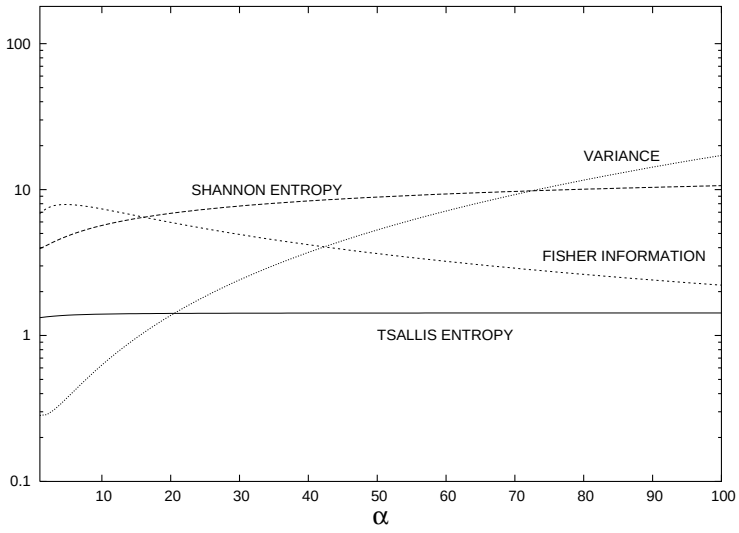

FIGURE 4.3: Variance, Fisher information and Shannon and Tsallis (with order $q = 1.7$) entropies in the three-dimensional maxTent problem with constraint $\langle r^{\alpha} \rangle$, as functions of the expectation order α in the three-dimensional case ($d = 3$). Atomic units are used.

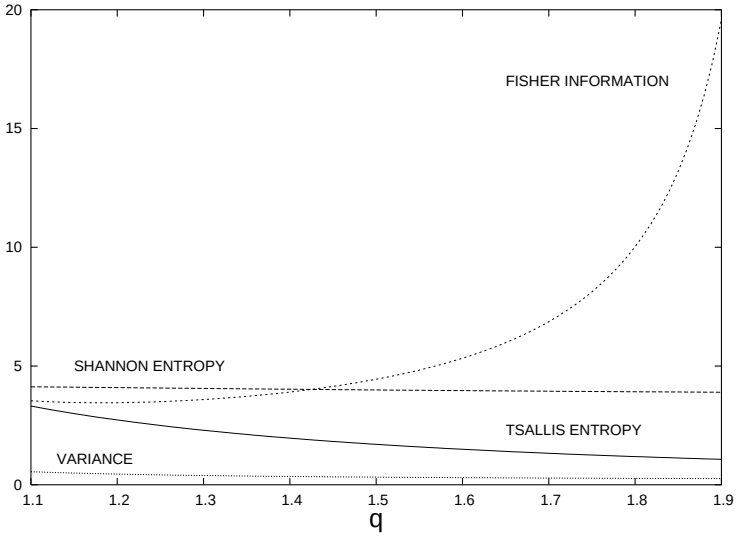

FIGURE 4.4: Variance, Fisher information and Shannon and Tsallis (with order $q = 2$) entropies in the three-dimensional maxTent problem as functions of the non-extensivity parameter q constrained by the radial expectation value $\langle r^3 \rangle$. Atomic units are used.

Similar analyses can be done for the two remainig cases. Finally, for completeness, let us also mention the recent work of Brody, Buckley and Constantinou [251, 267, 268] where they maximize the monodimensional Rényi entropy

$$R^{(q)}\left[\rho\right] := \frac{1}{q-1} \ln \int_0^\infty \left[\rho(x)\right]^q dx, \tag{4.59}$$

under the constraints $(a_0, a_1) = (1, \langle x^\alpha \rangle)$, $\alpha > 0$. They show that the solution of this one-dimensional problem has also the powerlike form of the type (4.48), what should not be surprising since the Rényi and Tsallis entropies are mutually related by

$$R^{(q)}(\rho) = \frac{1}{q-1} \ln \left[1 - (1-q) T^{(q)}\left[\rho\right]\right], \tag{4.60}$$

so that maximizing $R^{(q)}\left[\rho\right]$ is tantamount to maximizing $T^{(q)}\left[\rho\right]$.

4.4 Application to atomic systems

The measures described in previous sections are defined in the present one (whenever being possible) for normalized-to-one distributions $\rho(\vec{r})$ defined over the three-dimensional space $\Re^3$. Consequently, the vector $\vec{r}$ consists of 3 components, which can be expresses equivalently in cartesian of spherical coordinates, namely $\vec{r} = (x, y, z) = (r, \theta, \phi)$, where $r = |\vec{r}|$.

In principle, it is not guaranteed that those information measures be well-defined for any arbitrary distribution, because their definition requieres the involved integral to be convergent and, for the Fisher information, the distribution to be differentiable. For illustration, the definition of the variance $V\left[\rho\right]$, Eq. (4.9), requires appropriate short- and long-range behaviors of the distribution for the involved first- and second-order radial expectation values to be finite, namely $r^4\rho(r) \to 0$ as $r \to 0$ and $r^5\rho(r) \to 0$ as $r \to \infty$. Similar requirements need also to be verified in the Tsallis entropy case (determined by the considered value of the $T^{(q)}\left[\rho\right]$ parameter), Eq. (4.3), as well as the aforementioned differentiability over the whole domain when considering Fisher information $I\left[\rho\right]$, Eq. (4.2). Nevertheless, all these convergence and differentiability conditions are verified by the atomic distributions analyzed in the present work.

One of the basic ingredients in the study of many-fermion systems (e.g. atoms, molecules) is the one-particle density $\rho(\vec{r})$ on the three-dimensional space, as revealed by the well-known Density Functional Theory (DFT). Such a density describes the distribution of the electron cloud around each position $\vec{r}$ in $\Re^3$, and it plays the main role within the DFT for describing many different properties of the system, such as kinetic, exchange and correlation energies, among others [101].

Altough the position distribution $\rho(\vec{r})$ is the basic element of the DFT, it is very usual to deal additionally with the corresponding distribution in the so-called conjugated space. This is the case in which the $\vec{r}$-space distribution of a N-particle system is defined from an initial wavefunction $\Psi(\vec{r},\vec{r}_2,\ldots,\vec{r}_N)$ by integrating $|\Psi|^2$ on all variables except $\vec{r}$, so giving rise to $\rho(\vec{r})$. If one considers the $3N$-dimensional Fourier transform $\tilde{\Psi}(\vec{p},\vec{p}_2,...,\vec{p}_N)$ to build up the associated distribution in momentum space $\gamma(\vec{p})$ (preserving normalization), many properties and characteristics of both densities $\rho(\vec{r})$ and $\gamma(\vec{p})$ are well-known to be strongly related. As mentioned above, this is the case, for instance, of the one-particle densities for many-particle systems (e.g. atoms, molecules). Similarly as $\rho(\vec{r})$ (position space density, in what follows) provides the electronic charge density around each location $\vec{r}$, the momentum space density $\gamma(\vec{p})$ quantifies the linear momentum distribution around the momentum vector $\vec{p}$.

It is worthy to point out that, for atomic systems at their ground state in the absence of external fields, it is sufficient to deal with the spherically averaged densities $\rho(r)=\frac{1}{4\pi}\int\rho(\vec{r})d\Omega$ and $\gamma(r)=\frac{1}{4\pi}\int\gamma(\vec{p})d\Omega$ for a complete description, the independent variable (r or p) ranging over the non-negative real line $[0,\infty)$ (we use them troughtout this Thesis unless stated otherwise).

Some radial expectation values (in both spaces) are specially relevant for atomic systems from a physical point of view. It is well known, for instance, that $\langle r^{-1}\rangle$ is essentially the electron-nucleus attraction energy, $\langle r^2\rangle$ is related to the diamagnetic susceptibility, $\langle p^{-1}\rangle$ is twice the height of the peak of the Compton profile, and $\langle p^2\rangle$ is twice the kinetic energy and $\langle p^4\rangle$ its relativistic correction. So, those physically relevant and/or experimentally accessible quantities provide also information on the spreading measures of the system.

The main aim in the present section is the study, for ground-state neutral atoms throughout the Periodic Table with nuclear charge $Z=1-103$, of the information-theoretic measures S, $T^{(q)}$, I and V for the extremizer distributions (i.e. the solutions of the maxEnt, maxTent and minInf problems), constrained by normalization and an α-order expectation value, in both position and momentum spaces. For carrying out the numerical calculations, the accurate Near-Hartree-Fock wavefunctions of Koga et al [269] will be employed. Such a study will be done by analyzing the dependence of the measures on both the nuclear charge Z and the constraint order α for each conjugated space. The associated radial expectation values are defined for $\alpha>-3$ in position space and within the range $-3<\alpha<5$ in the momentum one, due to the rigorously known short- and long-range behaviors of the densities. Concerning the information measures, all of them are finite-valued for these systems (taking into account the differentiability of the densities at any point as well as the aforementioned behaviors at zero and infinity), with the only constraint $q>3/8$ in momentum space as a consequence (in order to the integral appearing in the definition of $T^{(q)}$ to be convergent) of the long-range behavior of the one-particle density $\gamma(p)$ as p^{-8} [270].

For completeness, the existence conditions for the two-moment (α, β)-maxEnt problem obtained in subsection 4.1.1 will be also checked for these systems by means of their radial expectation values obtained within the aforementioned Near-Hartree-Fock framework.

The maxTent atomic problem

Although the Tsallis entropy constitutes an extension or generalization of the Shannon entropy in the sense that $T^{(1)}[\rho] = S[\rho]$, the maximizer distribution of both entropies (Eqs. (4.11) and (4.48) for S and $T^{(q)}$ respectively) are significantly different.

This is the reason for being so interesting to carry out, for the spreading measures associated with both the maxTent and the maxEnt problems, a similar study concerning the dependence on the nuclear charge Z and the constraint order α of the corresponding information measures, in both conjugated spaces. For illustration, the $q = 1.7$ value of Tsallis parameter will be considered in order to perform the numerical calculations, but similar conclusions are derived from the results obtained considering other values. Additionally, when dealing with a fixed constraint order α, most comments are also valid independently of its value.

In Figure 4.5, variance, Fisher information and Shannon and Tsallis entropies of the maxTent distributions are displayed (employing some scaling factors in order to better compare among themselves) for the ground-state neutral atoms with nuclear charge $Z = 1-103$ in position (Fig. 4.5(a)) and momentum (Fig. 4.5(b)) spaces, with constraint order $\alpha = 1$. Some comments are in order:

1. A first comparison between Figs. 4.5(a) and 4.5(b) reveals the very apparent structural differences according to the space we deal with. There appears a very rich piecewise structure on curves corresponding to information measures in position space (Figure 4.5(a)), while much softer shapes are displayed in momentum space (Figure 4.5(b)). Focussing our attention upon position space, the spatial relationship among the atoms is checked for the location of extrema and for the process of atomic shell-filling. In this sense, different periods throughout the Periodic Table are represented by apparent pieces of the curves. Within each period, all global measures decrease (in overall) when adding an electron while, on the other hand, the local Fisher information increases.

   Moreover, other structural properties, such as the anomalous shell-filling, are also revealed by the additional peaks associated with the corresponding elements. This is the case, for instance of systems with $Z = 24, 29$ (3d valence subshell), $Z = 41 - 42, 44 - 47$ (4d valence subshell) and $Z = 78, 79$ (5d valence subshell).

2. As mentioned before, the Fisher functional is a local measure of information, contrary to the variance and Shannon and Tsallis entropies, which are quantities of

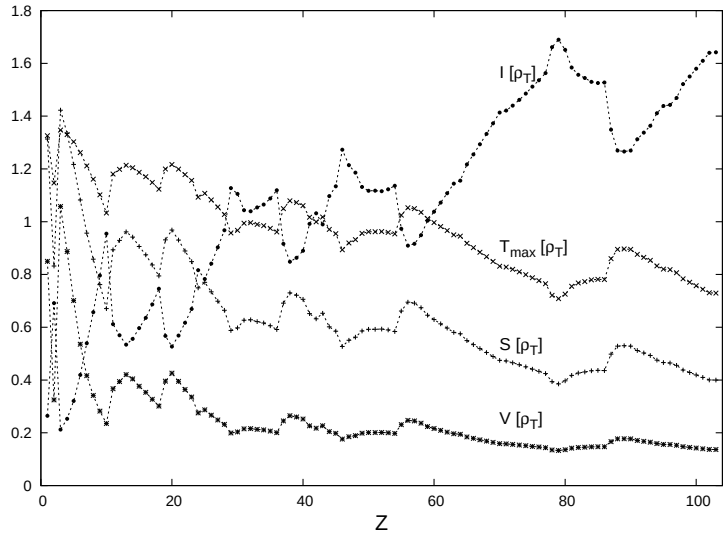

(a) position space

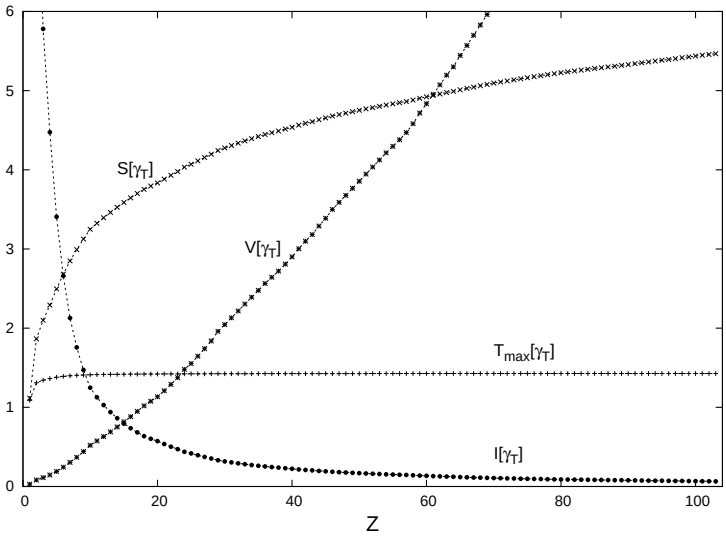

(b) momentum space

FIGURE 4.5: Variance, Fisher information and Shannon and Tsallis entropies of the maxTent (maximum Tsallis entropy) solution for $q = 1.7$ with radial constraint order $\alpha = 1$ in (a) position ($3\times V\left[\rho_T\right]$, $I\left[\rho_T\right]/26$, $S\left[\rho_T\right]/3$ and $T_{max}^{(1.7)}\left[\rho_T\right]$), and (b) momentum ($V\left[\gamma_T\right]/3$, $I\left[\gamma_T\right]$, $S\left[\gamma_T\right]/2$ and $T_{max}^{(1.7)}\left[\gamma_T\right]$) spaces, for all ground-state neutral atoms with nuclear charge $Z = 1 - 103$. Atomic units are used.

global character. This fact is clearly appreciated in Figure 4.5(a), where local maxima of the global measures appear at the same position as local minima of the local measure, and conversely (e.g. maxima of global measures occur, with very few exceptions, for noble gases, namely closed-shell systems). Such a behavior indicates that a higher spreading of the distribution raises the global measures but decreases the local one, as should be expected according to the meaning and the definitions of the different information quantities.

3. A similar comment can also be done by analyzing Figure 4.5(b) (momentum space),

now in terms of monotonicity properties instead of location of extrema. In this sense, it is worthy to remark that curves corresponding to global measures are monotonically increasing as well as concave in what concerns the dependence on the nuclear charge Z, while the behavior in the Fisher case is just the opposite one, namely it decreases with Z displaying a convex shape.

It is also interesting to consider the dependence of the information measures on the order α of the chosen constraint, as illustrated in Figure 4.6 for the Shannon entropy $S[\rho_T]$ of the Tsallis extremized distribution in position space with $q = 1.7$, again for $Z = 1 - 103$. As clearly observed, the quantity $S[\rho_T]$ provided by the particular values $\alpha = 1, 2, 3, 4$ behaves in a similar fashion independently of the constraint order, differing among themselves only (roughly) by a scaling factor. According to the global character of Shannon entropy and its relation with the Tsallis one, most comments concerning location of extrema and its interpretation in terms of periodicity and shell structure, as well as the relevant structural differences between the position and the momentum space studies, are quite similar to those provided when discussing the Figure 4.5, being also valid for any α.

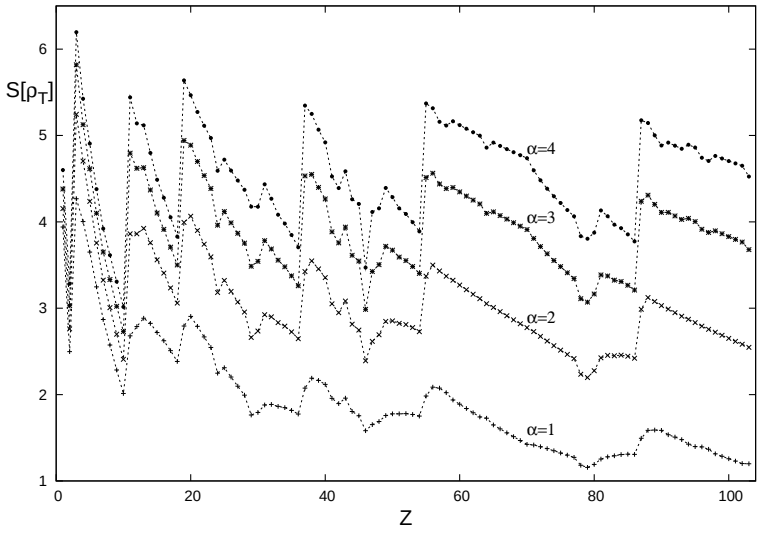

FIGURE 4.6: Shannon entropy ($S[\rho_T]$) of the maxTent solutions with $q = 1$ in position space with radial constraint orders $\alpha = 1, 2, 3, 4$, for all ground-state neutral atoms with nuclear charge $Z = 1 - 103$. Atomic units are used.

The maxEnt atomic problem

After the similar interpretation of the Z dependence for both the maxTent and the maxEnt problems, let us now analyze in more detail the dependence of the measures associated with the maxEnt distribution on the constraint order α in both conjugated spaces by considering, for illustration, the maximal Shannon entropy in position space

($S_{max}[\rho_S]$) and Fisher information in momentum space ($I[\gamma_S]$), that is, a global and a local measure. Nevertheless, additional comments will be also done concerning other quantities in both spaces, apart from those displayed in the figure. Specially interesting is the different behavior displayed by these quantities (the other global measures behaves in a similar way as the Shannon entropy) attending to the space we are dealing with, not only in what concerns the level of structure but also in the way the global measures appear ordered.

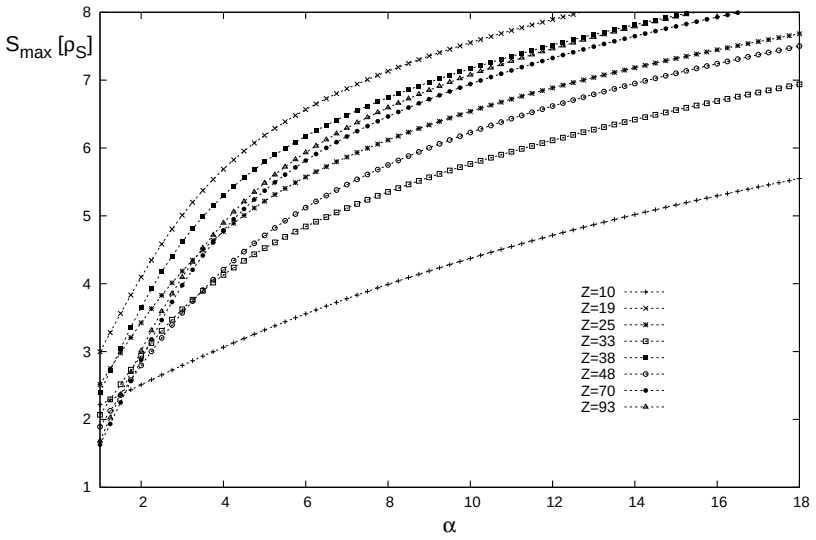

(a) Shannon entropy in position space

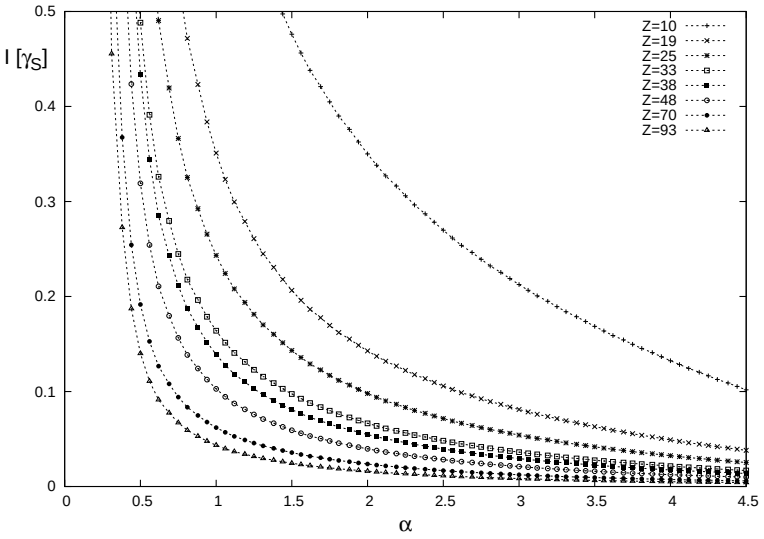

(b) Fisher information momentum space

FIGURE 4.7: (a) Shannon entropy in position space ($S_{max}[\rho_S]$), and (b) Fisher information in momentum space ($I[\gamma_S]$), of the maxEnt solution with the radial constraint $\langle r^\alpha \rangle$ as a funtion of α, for ground-state neutral atoms with nuclear charge $Z = 10, 19, 25, 33, 38, 48, 70, 83$. Atomic units are used.

For illustration, a comparison of these quantities as functions of α is carried out for different ground-state atomic systems ($Z = 10, 19, 25, 33, 38, 48, 70, 83$) in Figure 4.7.

The selection of those systems is not arbitrary, but instead made in order to include a variety of valence subshells and occupation numbers. It is worthy to remark that (i) the position space Shannon entropy $S_{max}\left[\rho_S\right]$ monotonically increases while the momentum space Fisher information $I\left[\gamma_S\right]$ monotonically decreases for all systems considered (the same applies for any other Z values), and (ii) both quantities also differ on higher order monotonicity properties, namely the position space Shannon entropy $S_{max}\left[\rho_S\right]$ is a concave function of α, the Fisher information $I\left[\gamma_S\right]$ (momentum space) being convex. Concerning other information measures in the two conjugated spaces, let us also point out that, except for very small values of α, (i) the three global measures here considered (variance and Shannon and Tsallis entropies) monotonically increase in the two conjugated spaces, the local one (Fisher information) being monotonically decreasing in both them, and (ii) the four measures in momentum space, as well as the variance and the Fisher information in position space, display convex shapes, while Shannon and Tsallis entropies in position space are (in overall) concave functions of the constraint order α.

Another relevant difference between Figures 4.7(a) and 4.7(b) concerns ordering of curves (from above to below) attending to the space considered. While in momentum space they are ordered according to the nuclear charge Z, ordering in position space is governed by the electronic configuration of the valence subshell. The same comment is also valid for all other information measures considered in this section.

Finally, and for completeness, let us mention that we have checked the existence conditions of maxEnt solutions (provided in subsection 4.1.1) when adding a second radial constraint (i.e. with $M = 2$ in Eq. (4.11)). In doing so, we have considered radial expectation values of integer-order α within the range -2 to 4. The analysis carried out reveals that they are not verified by any system neither in position nor in momentum space, independently of the pair of constraints considered. Consequently, there does not exist maxEnt solution under those conditions for atomic charge and momentum densities, at least for the atomic systems here considered.

The minInf atomic problem

As disscused in Section 4.2, the only case for which an analytical solution of minInf problem has been obtained is that corresponding to a unique constraint (apart from normalization) of order $\alpha = -1$. Nevertheless, for our present purposes (namely the application of the minInf information measures to the study of atomic systems), such an order is specially relevant and meaningful from a physical point of view in both position and momentum spaces, because the associated constraints in conjugated spaces, namely $\langle r^{-1}\rangle$ and $\langle p^{-1}\rangle$ are proportional to the electron-nucleus attraction energy and to the height of the peak of the Compton profile, respectively.

The analysis of the information measures associated with the minimizer distributions is carried out below according to their dependence on the nuclear charge Z for both position and momentum spaces, as displayed in Figure 4.8 (employing some scaling factors in Figure 4.8(a) for a better comparison of the position spaces quantities). For illustration, the value $q = 0.9$ has been chosen for the characteristic parameter of the Tsallis entropy $T^{(q)}$.

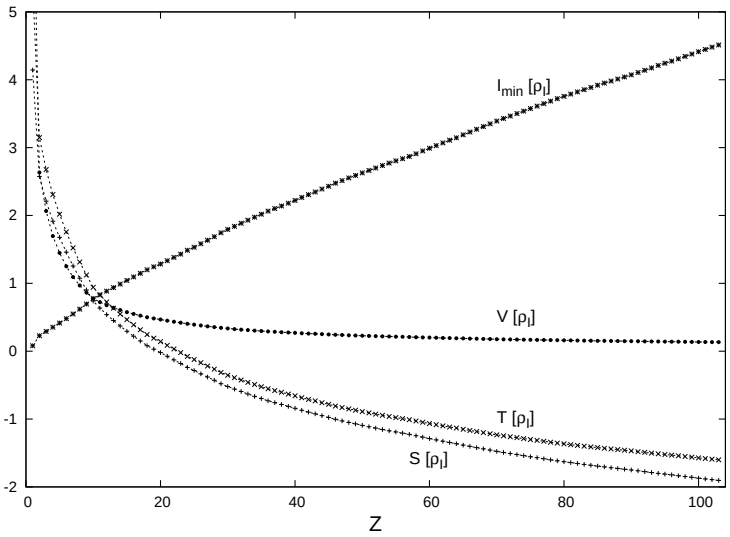

(a) position space

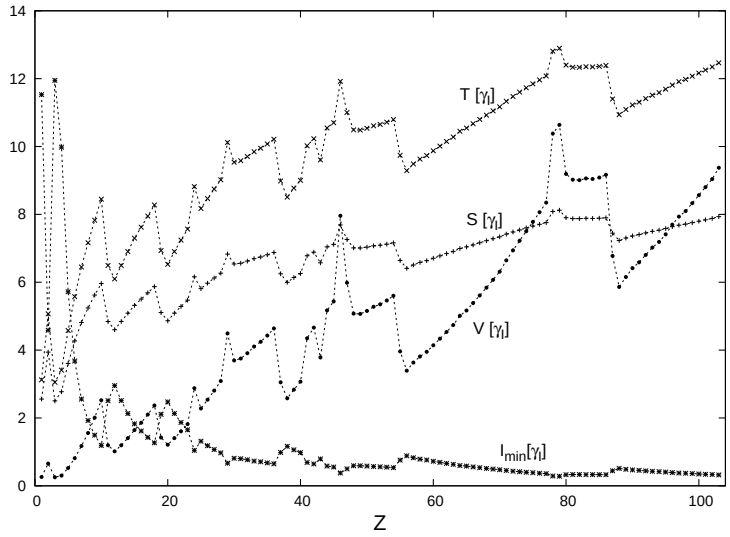

(b) momentum space

FIGURE 4.8: Variance, Fisher information and Shannon and Tsallis entropies of the minInf (minimum Fisher information) solution with radial constraint order $\alpha = -1$ in (a) position ($10 \times V[\rho_I]$, $I_{min}[\rho_I]/50$, $S[\rho_I]$ and $T^{(0.9)}[\rho_I]$), and (b) momentum ($V[\gamma_I]$, $I_{min}[\gamma_I]$, $S[\gamma_I]$ and $T^{(0.9)}[\gamma_I]$) spaces, for all ground-state neutral atoms with nuclear charge $Z = 1 - 103$. Atomic units are used.

As in the preceding maximization problems, the different structures displayed in a given space by all the information measures of the minimized Fisher information distribution are clearly revealed. However, the most remarkable point is that momentum space is

now the one where the curves display a higher level of structure, again with a high number of local extrema whose location is determined by the shell-filling process and displaying periodicity patterns.

The shell-structure properties of atomic systems are mainly characterized by the valence orbital, usually the outermost subshell. The aforementioned results on all extremization problems allow one to conclude that the information-theoretic apport of the valence orbital to the global measures is much more significant in position space, while Fisher information appears to be more sensitive to valence contribution in momentum space.

Summarizing, it has been clearly revealed the complementary usefulness of global and local information measures, as well as their values in both conjugated spaces (position and momentum), in order to get a complete description of the information content of the atomic systems, as well as its interpretation in terms of relevant physical properties and their main structural characteristics.

4.5 Conclusions

A problem of extremum information asserts that one should choose as the least biased (minimally prejudiced or maximally unpresumptive) probability distribution that which extremizes the involved information-theoretic measure subject to some known constraints on the system. We have outlined the procedures for maximizing the Shannon (Section 4.1) and Tsallis (Section 4.3) entropies and a method for minimizing the Fisher information (Section 4.2) in scenarios with standard and non-standard dimensionalities under various constraints of moment or radial expectation type. These three information-theoretic measures are logarithmic (Shannon), powerlike (Tsallis) and gradient (Fisher) functionals of the probability density; so, whilst the former two have a global character as also the variance has, the latter has a property of locality. It is worth noticing that the resulting Shannon maximizer and Fisher minimizer densities have an exponential form, in contrast with the Tsallis maximizer density which follows a power law.

We have investigated the spreading properties of the extremizer density associated to the three extremum information problems mentioned above (i.e., maxEnt, minInf and maxTent). The mutual functional relations and the explicit expressions of the variance, the extremized entropy and the other two information-theoretic measures of the extremizer density have been obtained in terms of the moment constraints and the dimensionality of the system under consideration. Moreover, the d-dimensional maxEnt and maxTent problems with the constraints $(a_0, a_1) = (1, \langle r^\alpha \rangle)$ have been numerically examined. It is found, in particular, that for the maximum entropy density the gobal measures increase with the expectation order α, while the Fisher information decreases. All the measures considered have a convex parabolic dependence on the dimensionality.

The existence condition for the d-dimensional maxEnt problem with the constraints $(a_0, a_1, a_2) = (1, \langle r^\alpha \rangle, \langle r^\beta \rangle)$ for $1 - d < \alpha < \beta$ and $\beta > 0$, is also obtained in subsection 4.1.1, extending to d dimensions and to arbitrary radial expectation values with non-necessarily consecutive orders the one-dimensional results of Dowson-Wragg for the two-lower-order moment constraints [43].

Then, in Section 4.4, we have analyzed the mutual dependence among the one-constraint solutions of the extremization problems and the values of their information-theoretic measures for three-dimensional physical systems, namely neutral atoms throughtout the whole Periodic Table. The behavior in terms of the nuclear charge Z and the constraint order α has been studied in both conjugated spaces, displaying in some cases the shell-structure patterns (including anomalous shell-filling) according to the global or local character of the involved spreading measure. The characteristic atomic periodicity appears strongly related to the location of maxima and minima in the information curves. In this sense, it is worthy to remark that, while the information measures of the minInf solution are much more sensitive to valence orbital occupation number for the momentum space density $\gamma(\vec{p})$, the same is true for the maxEnt and maxTent ones but in the conjugate space, i.e. for the charge density $\rho(\vec{r})$. Other properties, such as ordering among the measures, monotonicity (strict or piecewise) and convexity on the Z and α variables have been considered. Additionally, for the maxEnt case it has been checked that, in the present Hartree-Fock framework, the existence conditions for the two-constraint problem, which has been determined analytically in Section 4.1.1, do not hold for any neutral atom neither in position nor in momentum space, at least for integer-order constraints.

Part II

Complexity measures of atomic and molecular systems

Introduction

In the Webster dictionary [271], the word "complexity" has the following definition: *the quality or state of being complex*, where something "complex" is a whole made up of involved or interrelated parts. Reading this definition, it might be confuse what complexity does really mean and how can be quantitatively determined. Our intuition tells us that a completely ordered system (e.g. a perfect cristal), which possesses a very high internal structure, as well as a totally disordered one (e.g. an isolated ideal gas), are not complex systems. Between these two extreme cases, we find many others in which order and disorder are involved simultaneously.

Classical science, as exemplified by Newtonian mechanics, is essentially reductionist: it reduces all complex phenomena to their simplest components, and tries to describe these components in a complete, objective and deterministic manner [272]. The philosophy of complexity asserts that, in general, this method is impossible to realize: complex systems, such as organisms or societies, have properties that cannot be reduced to the mere properties of their parts. At the best, we can find certain statistical regularities in their quantitative features, or understand their qualitative behavior through models.

In the ninetine sixties, the Kolmogorov complexity concept was introduced (also called descriptive complexity, algorithmic complexity or algorithmic entropy) [60]. This quantity measures, for a finite binary string of characters, the length of the shortest computer program that can generate such a string. Despite its usefulness, the Kolmogorov complexity does not capture the intuitive notion of complexity appropriately because, for a random string, this quantity reaches a very large value (infinite in the limiting case). This is the reason for considering Kolmogorov complexity as a measure of randomness instead of as a measure of the internal structure.

There exist numerous definitions for the complexity concept other than Kolmogorov's one, depending on the field we are dealing with. Indeed, we can find in the literature, several works where different definitions and classifications of complexity have been proposed [273–278]. In particular, Rescher (see Ref. [277], p. 10) classified the complexity in different categories depending on the way that we want to quantify the complexity of a given system:

- Formulaic complexity: Descriptive (length of account that must be given to provide an adequate description of the system), algorithmic (the length of the system instructions) [60] and computational (the time required to solve a problem) [279] complexities.
- Compositional complexity: Constitutional (number of parts or components) and taxonomical (numbers of different kinds of components in the physical configurations of the system) [280] complexities.
- Structural complexity: Organizational (number of different ways of arranging components in different modes of interrelationship) and hierarchical (organizational disaggregation into subsystems) complexities.
- Functional complexity: Operational (variety of modes of operation) and nomic (degree of elaboration of the laws which govern a phenomena) complexities.

All of these categories of complexity have been employed in recent decades in the physical [91, 281], chemical [282, 283] and biological [284, 285] sciences as well as in engineering [279], mathematics [286], economics [287] and sociology [288], among other areas.

Thus, the term "complexity" possesses many different meanings and adjectives (algorithmic, geometrical, computational, stochastic, effective, statistical or structural) and it has been used in numerous fields: dynamical systems, disordered systems, spatial patterns, languages, multielectronic systems, cellular automata, neural networks, self-organization, DNA analysis or social sciences, among others [208, 283, 289, 290]. So, qualitatively speaking, the notion of complexity is nowadays frequently used, but yet poorly defined. It tries to encompass a great variety of scientific and technological methods of natural and artificial systems. Gell-Mann [291] has coined the name *plectics* to refer to the science of complexity, keeping in mind that the word complexity is made from the Latin roots: com (meaning *together*) and plectere (meaning *to plait*). An important feature of complexity has to do with the fact that both very ordered and very disordered systems are, in the sense of plectics, considered to be simple, not complex, as we have mentioned before.

Attending to its so many and different applications, we note that the concept of complexity is closely related to that of "understanding", in the sense that the latter is based upon the accuracy of model descriptions of the system obtained by using a condensed information about it. Hence, the complexity measures how easily modelling a system may be. In this sense, fundamental concepts such as uncertainty or randomness are frequently employed in the definitions of complexity although some other concepts such as clustering, order, localization or organization might be also important for characterizing the complexity of systems and processes.

Let us stress this idea by considering two exponential functions $f(x) = ae^{-ax}$ and $g(x) = be^{-bx}$. Then, we wonder *what function is more complex than the other?*. Well, both of them

are exponential functions which only depends on one paremeter and hence, they have the same complexity. Nevertheless, if we consider the function $f(x) + g(x)$, or any other linear combination of $f(x)$ and $g(x)$, which depends on two parameters, it must be more complex than the two single functions because it is more difficult to be modeled due to its dependence on two parameters.

In this part of the Thesis we provide more intuitive notions of complexity and prove their utility in order to analyze physical and chemical quantum systems described by continuous probability distributions. Firstly, in Chapter 5 we introduce the notion of complexity and some of its possible definitions based on different aspects of Information Theory, focussing our attention in the so-called "product complexities". Then, in Chapter 6, we obtain some analytical properties and uncertainty relationships of these the complexity measures. In Chapter 7, the hydrogenic d-dimensional systems have been analyzed in terms of complexity. Finally, in Chapter 8, we study some selected molecular systems in order to find the relation between complexity and other chemical properties such as hardness, softness, ionization potential, reactivity of molecules, etc.

Chapter 5

The concept of complexity

The problem of understanding and characterizing complexity in a quantitative way is a vast and rapidly developing subject. Although various interpretations of the term have arised in different disciplines, no comprehensive discussion has yet been attempted. Usually, complexity is understood as a general indicator of pattern, structure and correlation in systems or processes, but its quantitative characterization is a very important subject of research and it has received considerable attention over the past years [292, 293].

The characterization of complexity, attending to the aforementioned general descriptors, cannot be unique and must be adequate for the type of structure or process we deal with, the nature and the goal of the description we are looking for, as well as for the level or scale of the observation that we use.

Based on the ideas described in the Introduction, the notion of complexity in Physics arises [294, 295] by considering the perfect crystal (completely ordered with centered probability distribution around a prevailing state of perfect symmetry) and the isolated ideal gas (completely disordered, because the system can be found in any of its accessible states with the same probability), as examples of simple models and therefore as systems with zero complexity [91]. Any other system would be in between these two extreme cases.

The mathematical formulation of complexity has to be designed in such a way that it fulfils, at least, the two following properties:

- to reach the minimum value for the two extreme probability distributions (the least complex ones), corresponding to perfect order (mathematically represented by a Dirac-delta for a continuous variable) and maximum disorder (associated with a highly flat distribution),
- to be invariant under replication, translation and scaling transformations.

Recently a class of complexity measures has been propossed as a product of two factors measuring, respectively, order and disorder on the given systems or, equivalently, localization and delocalization [91, 296]. Concepts such as entropy or information are frequently present in the proposals for characterizing complexity, but it is known that other ingredients capturing qualities beyond randomness are also necessary. In fact, as previously mentioned, one would wish to detect also clustering or pattern.

Due to its significant role in the information theory, probably the most popular candidate for being one of the coupled factors which give rise to complexity is the Shannon entropy S, but there exist other useful spreading and information-theoretic measures such as, for instance, the disequilibrium D, the Fisher information I and the variance, V. All of them have been used in the first part of this Thesis, where its utility to describe physical and chemical properties of the systems has been discussed in detail.

5.1 Measures of complexity

The way to define complexity is not unique, and consequently there exits various candidates that can be used as complexity measures. In this Thesis we focus our attention in those defined in terms of two complementary factors in order to quantify simultaneously the order/disorder, localization/delocalization and randomness or uncertainty of the system under study; namely, the LMC shape, Fisher-Shannon, Cramér-Rao and generalized Rényi complexities.

LMC shape complexity

The *LMC shape complexity*, $C(LMC)$, was introduced in 1995 by López-Ruiz, Mancini and Calbet [91] although, later on, it has been criticized [297], modified [298, 299] and generalized [300] leading to a useful estimator which reaches minimal values for both extremely ordered and disordered limits (i.e., for the Dirac-delta distribution and for the highly flat ones, respectively) satisfying also the desirable properties of invariance under scaling transformation, translation and replication [301, 302]. The utility of this improved complexity has been clearly shown in many different fields [208, 283, 290] allowing reliable detection of periodic, quasiperiodic, linear stochastic and chaotic dynamics [91, 301, 302].

The LMC measure is built up as the product of two important information-theoretic quantities, namely the so-called disequilibrium D (also known as self-similarity [303] or information energy [304]), which quantifies the departure of the probability density from uniformity [91], and the Shannon entropy S, which is a general measure of randomness or uncertainty of the probability density [16, 32]. Both global quantities are closely

related to the measure of spread of a probability distribution:

$$C(LMC) \equiv D \times e^{S}, \tag{5.1}$$

where, for a given distribution $\rho(\vec{r})$ the disequilibrium is

$$D\left[\rho\right] \equiv \langle\rho\rangle = \int \rho^2(\vec{r}) d\vec{r}, \tag{5.2}$$

and the Shannon entropy is given by

$$S\left[\rho\right] = -\int \rho(\vec{r}) \ln \rho(\vec{r}) d\vec{r}. \tag{5.3}$$

Then, this composite information-theoretic quantity measures the complexity of the system by means of a combined balance of the average height of the probability density $\rho(\vec{r})$ (as given by $D\left[\rho\right]$) and its total bulk extent (as given by $S\left[\rho\right]$). It is worthy to point out that both quantities D and S employed to define the $C(LMC)$ complexity posses a global character.

Fisher-Shannon complexity

The *Fisher-Shannon complexity*, $C(FS)$, involves a global information measures and a local one, the Fisher information [3, 37]. The properties of the Fisher information make this measure to be an appropriate candidate with the aim of defining a complexity measure in terms of complementary global and local factors.

Although the Fisher-Shannon product has been employed as a measure of atomic correlation [203], its definition as a statistical complexity measure is quite recent [305, 306]. This quantity combines the global character (by considering the distribution as a whole) and the local one (in terms of the gradient of the distribution), respectively, preserving also the aforementioned desirable properties associated to the complexity concept. It is defined as

$$C(FS) \equiv I \times J, \tag{5.4}$$

where I is the Fisher information given by

$$I[\rho] = \int \rho(\vec{r}) \left|\vec{\nabla} \ln \rho(\vec{r})\right|^2 d\vec{r}, \tag{5.5}$$

and J is the so-called *power Shannon entropy*

$$J\left[\rho\right] = \frac{1}{2\pi e} e^{\frac{2}{d}S[\rho]}, \tag{5.6}$$

where d is the dimension of the system. The definition of J has been chosen in order to preserve the general properties of complexity, in particular the scaling invariance,

including a constant factor in order to simplify the expression of its universal lower bound, as described below.

Comparing the FS and the LMC complexities, we can observe that the Fisher information now replaces the disequilibrium in order to quantify the level of organization of the system. The FS complexity expression arises from the isoperimetric d-dimensional inequality $I \times J \geq d$ [64, 307] providing a universal lower bound to the FS complexity. This measure has been used in several applications, in particular let us mention those concerning atomic distributions in position and momentum spaces, where the FS complexity is shown to provide relevant information on atomic shell structure and ionization processes; as well, it is also strongly related to different structural properties of many-fermion systems [281, 305, 306, 308].

Cramér-Rao complexity

The well known Cramér-Rao bound $I \times V \geq d^2$ (where d is the dimension of the space) [64, 307], leads us to consider a new complexity measure, given by the *Cramér-Rao product* as:

$$C(CR) \equiv I \times V, \tag{5.7}$$

where the strong connection between both the local and global level of uncertainty is manifested again. As in the Fisher-Shannon case, the local character is provided by using the Fisher information while the Shannon entropy is replaced by the variance, which is also a global measure. This product has been considered in different contexts [281, 308, 309].

Generalized Rényi-like complexities

Now, the previously introduced product-like complexities are generalized by replacing the Shannon entropy functional by a more general and powerful magnitude as the Rényi entropy. Therefore we deal with a one-parameter (to be denoted by α) generalized complexity which weights different regions of the distributions according to the value of α. The LMC and FS complexities are particular cases of these so-called Rényi complexities.

Specifically the so-called *Shape-Rényi complexity* (SR), characterized as a difference between the α-order Rényi entropy and the second order one (expressed in terms of the Disequilibrium, D), has been extended to continuous systems [310], theoretically studied, and tested for the binary symmetric channel (BSC) and the logistic map [301]. A more extended family of generalized complexity measures has been proposed, and rigorous bounds, geometrical properties and several applications have been also studied [311]. It is defined by

$$SR^{(\alpha)} \equiv D \times e^{R^{(\alpha)}}, \tag{5.8}$$

where D is the disequilibrium (see, Eq. (5.2)) and $R^{(\alpha)}$ is the Rényi entropy.

The Rényi entropy is a global measure and plays a similar role to those of other density functionals as descriptors of the uncertainty on a distribution. It is defined by

$$R^{(\alpha)}[\rho] = \frac{1}{1-\alpha} \ln \omega^{(\alpha)}[\rho] \tag{5.9}$$

where the quantity ω_α is the so-called "α-order entropic moment" of a given density $\rho(\vec{r})$:

$$\omega^{(\alpha)}[\rho] = \int \rho^\alpha(\vec{r}) d\vec{r}, \tag{5.10}$$

which have been also employed in diverse fields, specially remarkable being their meaning for some specific α values in the development of the Density Functional Theory [101] (e.g. Thomas-Fermi kinetic and exchange energies) as well as the own disequilibrium [83, 91]. The normalization to unity of the distribution can be expressed as $\omega^{(1)} = 1$, and the disequilibrium defined by Eq. (5.2) can be expressed as $D = \omega^{(2)}$.

The allowed range of values for the characteristic parameter α of the Rényi entropy is determined by the convergence conditions on the integral in Eq. (5.10), arising from the short- and long-range behaviours of the distribution $\rho(\vec{r})$. Apart from the necessary (but not sufficient) condition $\alpha > 0$ for the finiteness of $R^{(\alpha)}$, the particular value $\alpha = 1$ appears as a limiting case, because both the numerator and the denominator in Eq. (5.9) vanish, the limit giving rise to

$$R^{(1)}[\rho] = S[\rho] = -\int \rho(\vec{r}) \ln \rho(\vec{r}) d\vec{r}, \tag{5.11}$$

that is, the Rényi entropy of order 1 is the Shannon entropy S or, in other words, the Rényi entropy $R^{(\alpha)}$ represents an extension or generalization of the Shannon entropy.

The power α of the distribution in Eq. (5.10), where $\omega^{(\alpha)}$ is defined, allows us to enhance or diminish, by increasing or decreasing its value, the relative contribution of the integrand over different regions to the whole integral and, consequently, to the entropic moments and the Rényi entropy $R^{(\alpha)}$. Higher values of α make the function $\rho^\alpha(\vec{r})$ to concentrate around the local maxima of the distribution, while the lower values have the effect of smoothing that function over its whole domain. It is in that sense that the parameter α provides us with a powerful tool in order to get information on the structure of the distribution by means of the Rényi entropy.

The Fisher-Shannon complexity defined before can be also generalized in terms of the Rényi entropy. The *Fisher-Rényi complexity* (FR) is defined by simply replacing the Shannon entropy, i.e., the global factor in the expression of the Fisher-Shannon complexity, by the Rényi entropy. Some rigorous properties for this entropic product, also called Fisher-Rényi product, have been recently obtained [312]. The FR complexity is

defined as

$$FR^{(\alpha)} \equiv IJ^{(\alpha)}, \tag{5.12}$$

where

$$J^{(\alpha)}[\rho] = \frac{1}{2\pi e} \exp\left\{\frac{2}{3} R^{(\alpha)}[\rho]\right\}, \tag{5.13}$$

is the 'α-order power entropy' for the three-dimensional case.

Some comments are in order: (i) the particular cases $SR^{(1)}$ and $FR^{(1)}$ corresponding to $\alpha = 1$ provide, respectively, the expressions of the LMC and FS complexities, (ii) all relevant invariance properties of LMC and FS also remain for arbitrary $\alpha > 0$, (iii) the weighting effect of the parameter α over specific regions, as previously mentioned for the Rényi entropy, now translates into the associated complexities, and (iv) attending to its definition, the composing factors of the second order Shape-Rényi complexity are one the inverse of each other, and consequently $SR^{(2)} = 1$.

Other Rényi products have been also considered in the literature, for which different properties are known for very specific α ranges [312] ($\alpha < 1$) such as, e.g. bounds and uncertainty-like relationships. The analysis of those properties is not within the aims of the present study, in which a much wider interval for the α parameter is considered.

5.2 Comparison between complexities

As mentioned before, there is no agreement about the definition of complexity, its characterization can not be univocal and must be adequate for the problem we are dealing with. In this Chapter we have considered some measures, i.e., the LMC, FS and CR complexities, which will be used in the following chapters to analyze atomic and molecular systems.

In order to clarify the differences between these complexity measures, two example are depicted in Figures 5.1 and 5.2 and the values of their corresponding complexities are given in Tables 5.1 and 5.2, respectively.

In Figure 5.1 two exponential-like functions are shown, one of them, $g(x)$, modified by a sinusoidal perturbation. As we discussed in Chapter 1, in this figure we can clearly distinguish through the differences between the complexity based on global information measures, i.e., the LMC complexity, and the other ones which have a local component, the Fisher information, i.e., the Fisher-Shannon and the Cramer-Rao complexities. Their corresponding values have been obtained in Table 5.1

We can observe that if we use the LMC complexity to determine which function is more complex, we do not get so much information, what is due to the fact that this quantity is defined in terms of a global measure, i.e., the Shannon entropy and the disequilibrium,

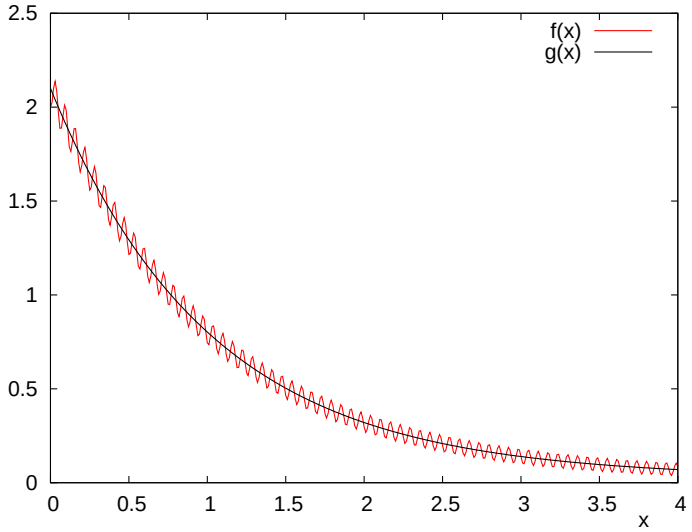

FIGURE 5.1: Representation of $f(x) \sim e^{-ax}$ and $g(x) \sim e^{-ax} + \epsilon \quad sin^2 nx$.

Function	$C(LMC)$	$C(FS)$	$C(CR)$
$f(x)$	1.0362	528.079	292.564
$g(x)$	1.0371	0.13384	0.07407

TABLE 5.1: Complexity measures of $f(x) \sim e^{-ax}$ and $g(x) \sim e^{-ax} + \epsilon sin^2 nx$

and, as we discussed in Section 1.3, these functions have a similar global behaviour. On the other hand, when we use a complexity measure composed by a very strong local information measure such as Fisher information, the results are very different. In this case, we can conclude that $g(x)$ is much more complex than $f(x)$ in a "local sense".

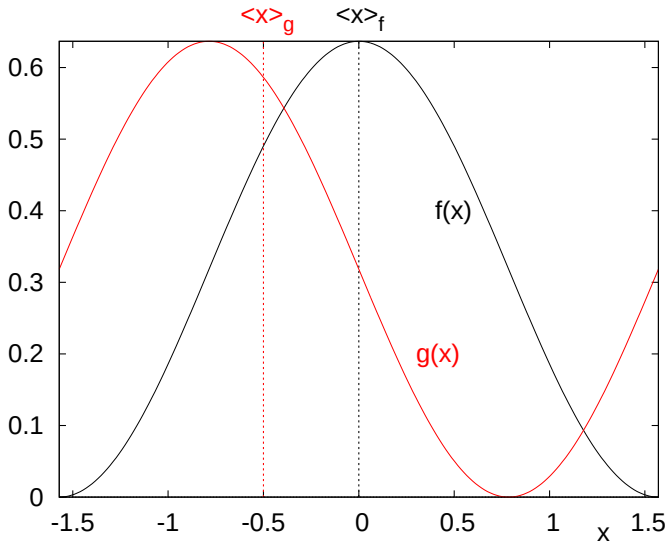

FIGURE 5.2: Representation of $f(x) = \frac{2}{\pi}\cos^2(x)$ and $g(x) = \frac{2}{\pi}\cos^2\left(x + \frac{\pi}{4}\right)$.

In Figure 5.2 two cosine functions are depicted. As we discussed in Chapter 1, these functions have the same Shannon entropy but their variances are different because their

centroids are located at different points. As a consequence, their Cramér-Rao complexities are different, as illustrated by the values contained in Table 5.2

Function	$C(LMC)$	$C(FS)$	$C(CR)$
$f(x)$	3.4672	1.2513	1.2899
$g(x)$	3.4672	1.2513	4.2899

TABLE 5.2: Complexity measures of $f(x) = \frac{2}{\pi}\cos^2(x)$ and $g(x) = \frac{2}{\pi}\cos^2\left(x + \frac{\pi}{4}\right)$

Chapter 6

Analytical properties and generalization of complexity measures. Applications to neutral atoms.

Numerous studies on complexity have been carried out in order to better understand the structural characteristics of the analyzed distributions. Most of such studies have been done attending to the numerical values displayed by the complexity measures for specific distributions, each complexity having its own characteristics. However, it would be also very useful to have at our disposal rigorous properties on the complexity measuresof general validity for arbitrary density functions. Due to this aim, the first part of this Chapter, Section 6.1, is devoted to the obtention of new properties and statistical interpretations of the different studied complexities, and to the derivation of uncertainty-like products which related the complexities in both conjugated spaces.

For illustration, an analysis of different relationships among information-theoretic quantities will be carried out for a large set of atomic systems in both position ($\vec{r}$) and momentum ($\vec{p}$) spaces. Consequently, we will deal with densities whose domain are the three-dimensional ($d = 3$) space. Studies on complexity has been also done in previous works, mainly by computing their numerical values [208], but very scarcely as in the present Section, in which rigorous relationships among different complexities and/or other information magnitudes are obtained, being valid for arbitrary systems and dimensionalities.

It is also worthy to mention that (i) the product or phase space distribution $f(\vec{r}, \vec{p}) \equiv \rho(\vec{r})\gamma(\vec{p})$ will be also considered in order to have a more complete informational description of the system, and (ii) for its analysis in atomic systems, it will be sufficient to

deal with the spherically averaged densities $\rho(r)$ and $\gamma(p)$, for which the independent variable range is the non-negative real line $[0, \infty)$.

In the second part of this Chapter, Section 6.2, we will analyze the advantages of using the generalized complexity measures $SR^{(\alpha)}$ and $FR^{(\alpha)}$ (see Eqs (5.8) and (5.12)), instead of the LMC and Fisher-Shannon complexities. In doing so, an analysis throughout the whole Periodic Table of elements is carried out. To the best of our knowledge, in fact, this is the first time in which the SR complexity is considered and analyzed for atoms. The same also occurs with the FR complexity, apart from recently derived results [312], mainly concerning uncertainty-like relationships but not the atomic structure and the shell-filling process.

6.1 Properties and uncertainty-like inequalities on complexity measures

In this Section, several properties on complexity measures are obtained by using exclusively their mathematical definitions, and being consequently of universal validity. Among those properties, we should remark the lower bounds in terms of one or two expectation values, uncertainty relations, etc.

6.1.1 Rigorous properties

Contrary to the case of the isolated factors which define complexity measures, namely, Shannon entropy, disequilibrium, Fisher information and variance, not many rigorous properties and /or relationships on complexity are known. Concerning the aforementioned functionals, it is worthy to mention, among others, the variational upper and/or lower bounds on each factor in terms of radial expectation values of the density [51, 313], as well as different uncertainty-like relationships.

In this subsection, different rigorous properties on the LMC, Fisher-Shannon and Cramér-Rao complexities will be obtained, being valid for arbitrary d-dimensional distributions. In some cases (as it is well known for the Fisher-Shannon and Cramér-Rao complexities), there exist lower bounds given as universal constant values (not necessarily dependent on the dimensionality). However, such a value in the case of LMC complexity has been only shown to exist for the one-dimensional case [298] (i.e. for densities having as domain the real line), what is generalized for arbitrary dimensionality in the present work. Other results are here expressed as bounds in terms of expectation values and/or density functionals. A numerical analysis of the accuracy displayed by the aforementioned bounds will be also carried out for the one-particle position and momentum densities of atomic systems within a Hartree-Fock framework.

Starting with the LMC complexity $C(LMC) = D \times e^S$, let us firstly observe that it can be also expressed in terms of entropic moments $\omega^{(q)}$. In doing so, it is convenient to define the function

$$f(q) \equiv \ln \omega^{(q)}, \tag{6.1}$$

which, due to the normalization constraint $\omega^{(1)} = 1$, takes the particular value $f(1) = 0$. Additionally, let us write the LMC complexity as $C(LMC) = \exp\{\ln D + S\}$.

Attending to the definition of S and D, it is easy to check that $S = -f'(1)$, i.e. minus the slope of the function $f(q)$ at $q = 1$, and

$$\ln D = \ln \omega^{(2)} = f(2) = \frac{f(2) - f(1)}{2 - 1}, \tag{6.2}$$

where the normalization constraint has been taken into account. Last equality is written in order to point out that $\ln D$ represents the slope of the straight line connecting the (two) points of the curve $f(q)$ at $q = 1$ and $q = 2$. Finally, and having in mind the convexity of $f(q)$ (or equivalently, the log-convexity of entropic moments $\omega^{(q)}$ as can be easily shown by using Hölder's inequality), it is concluded that the single exponent on $C(LMC)$ written as above is non-negative and, consequently, that $C(LMC) \geq 1$.

Up to now, this bound for the LMC complexity was only demostrated for the one dimensional case [298]. This is the first time, to the best of our knowledge, that a universal (i.e. valid for any d-dimensional distribution) constant lower bound on LMC complexity is obtained.

Moreover, from this proof it is immediately concluded that the equality $C(LMC) = 1$ is only reached for uniform distributions with a finite volume support. In doing so, it is enough to observe that equality is only possible for a linear $f(q)$ over the range $1 \leq q \leq 2$. Such a linearity translates on entropic moments as $\omega^{(q)} = D^{q-1}$ (where the values $\omega^{(1)} = 1$ and $\omega^{(2)} = D$ have been considered). This means that

$$\int \left(\frac{\rho(\vec{r})}{D} \right)^q d\vec{r} = \frac{1}{D}. \tag{6.3}$$

The non-dependence on 'q' of the right-hand-side requires the fraction on the integral to take only the values 0 or 1. Then, the density has the constant value $\rho(\vec{r}) = D$ on its whole support Λ apart from, at most, a zero-measure set of points, being the volume of the support $1/D$ in order to fulfil the normalization condition.

It is remarkable that lowest LMC complexity corresponds to step-like distributions over a finite volume set Λ, which are precisely the maximum-entropy ones among those with domain Λ. Then, necessarily they also minimize the disequilibrium, as it is also well-known when dealing with finite-size domains.

In summary, uniform distributions simultaneously minimize the disequilibrium D (i.e. localization) and maximize the Shannon entropy, and consequently the exponential entropy e^S (i.e. delocalization). But the joint effect of the two opposite ones on each factor of the $C(LMC)$ complexity is dominated by the minimizer one (i.e. the disequilibrium), giving rise to the minimum LMC complexity for uniform densities.

So, it should be expected that the higher $C(LMC)$ values are, the more far from uniformity the density is. To have an idea on the validity of this remark as well as on the comparison of complexity to the unity lower bound, we show in Figure 6.1 the values of LMC complexity for the position and momentum densities, $\rho(\vec{r})$ and $\gamma(\vec{p})$ respectively, for neutral atoms with nuclear charge from $Z = 1$ to $Z = 103$. The discontinuities in the curves correspond to their decomposition according to the different periods conforming the whole Periodic Table, as will be also done for drawing the rest of figures in this Section.

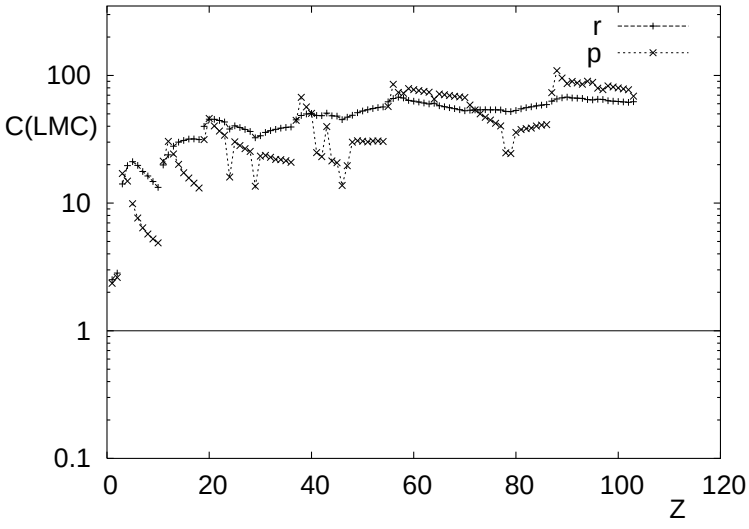

FIGURE 6.1: LMC complexities $C(LMC)$ in position and momentum spaces for neutral atoms with nuclear charge from $Z = 1$ to $Z = 103$. Atomic units are used.

It is clearly observed that, apart from being all values in both spaces above unity, there appear different pieces in each curve corresponding to electronic filling of specific subshells, displaying monotonic behaviors within each subshell which are opposite (increasing or decreasing) when comparing both conjugated spaces. This can be interpreted in terms of the uncertainty principle (which will be also analyzed in next subsections), in such a way that a higher delocalization in one space is associated to a higher localization in the conjugated one.

Additionally, higher values of complexity for heavy atoms are due to the lost of uniformity because of the increase in the level of shell structure, image with exactly corresponds to the intuitive notion of complexity of a system.

Let us now center our attention on the Fisher-Shannon complexity $C(FS) = I \times J$. The inequality $I \times J \geq d$ [59], which provides a lower bound on the product of both quantities, is consequently written in terms of the Fisher-Shannon complexity, as

$$C_r(FS) \geq d, \qquad C_p(FS) \geq d, \qquad C_{rp}(FS) \geq 2\pi e d^2, \tag{6.4}$$

where d is the dimension of the space, and last inequality contains an additional factor apart from the product of complexities in conjugated spaces because of the definition of the power entropy J_{rp} in the product space. It is worthy to mention that the above inequalities are valid for arbitrary distributions on d-dimensional spaces, in the same line as the lower bound $C(LMC) \geq 1$ previously obtained for LMC complexities independently of the space we are dealing with.

The numerical analysis of Figure 6.2 for $C(FS)$ is now carried out similarly as done in Figure 6.1 for $C(LMC)$, by considering exactly the same systems and spaces. Now, the lower bound is stablished by the three-dimensional ($d = 3$) space as domain of the distributions. Similar comments to those of the previous figure, concerning the behavior in terms of the nuclear charge Z, can be also done.

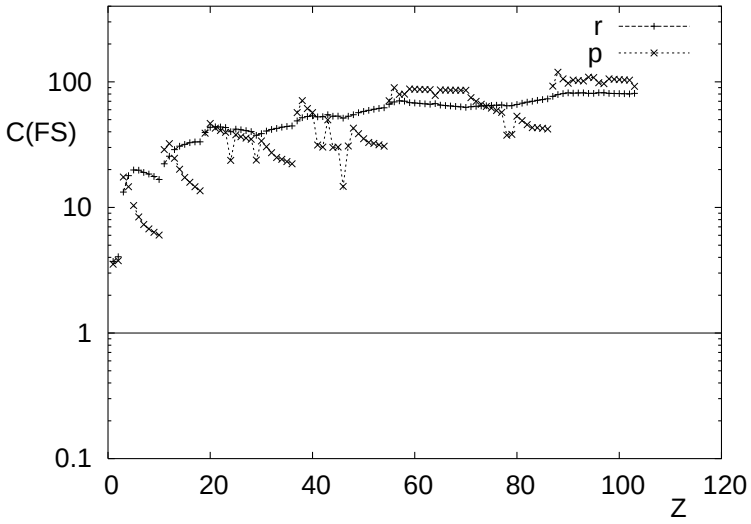

FIGURE 6.2: Fisher-Shannon complexities $C(FS)$ in position and momentum spaces for neutral atoms with nuclear charge from $Z = 1$ to $Z = 103$. Atomic units are used.

In spite of the different characteristics of the two components of the Fisher-Shannon complexity $C(FS) = I \times J$, it is known a result which provides a connection between both information measures $I(\rho)$ and $J(\rho)$ which, as we are going to show, can be also expressed and interpreted in terms of complexities. The above mentioned connection arises from the so-called effect of *gaussian perturbation*, and it provides information on the variation suffered by the information content of a distribution ρ when adding a small-amplitude gaussian one. Concerning the Fisher and Shannon measures, it is known that

$$\frac{d}{d\epsilon} S\left[\rho + \sqrt{\epsilon}\rho_G\right]\Big|_{\epsilon=0} = \frac{1}{2} I\left[\rho\right], \tag{6.5}$$

as shown by de Bruijn [64], where ρ_G denotes the standard gaussian distribution with mean 0 and variance 1. In this sense, the Fisher information could be interpreted as a measure of the variation of Shannon entropy of the initial density under a gaussian perturbation.

Keeping in mind this result, let us consider the power entropy of the perturbed distribution $\rho_\epsilon \equiv \rho + \sqrt{\epsilon}\rho_G$, namely

$$J\left[\rho_\epsilon\right] = \frac{1}{2\pi e} e^{\frac{2}{d} S[\rho_\epsilon]}. \tag{6.6}$$

Carrying out the same derivation and limiting operations as in Eq. (6.5), but on the power entropy $J(\rho_\epsilon)$ instead of the Shannon entropy $S(\rho_\epsilon)$, it is immediate to check that

$$C(FS) = d \cdot \left[\frac{d}{d\epsilon} J(\rho + \sqrt{\epsilon}\rho_G)\Big|_{\epsilon=0}\right], \tag{6.7}$$

what gives rise to an additional interpretation on the Fisher-Shannon complexity: it represents the variation of the power entropy J of a given density ρ when perturbed by a gaussian distribution ρ_G. So, the interpretation of the Fisher information (a single measure of information) according to the process of gaussian perturbation is now extended to the interpretation, for the same process, in terms of FS complexity.

Concerning the Cramér-Rao complexity $C(CR)$, we next show that it can be also bounded from below in terms of radial expectation values of the density. This kind of upper and/or lower bounds are extensively found in the literature for different single-density functionals, such as the Shannon entropy [51] or entropic moments [313], but such is not the case for complexities, mainly because of being constructed as a product of two different factors, what extremely involves the bounding procedure as compared to its application for single density functionals.

Here we are going to take advantage of the non-negativity of the so-called "relative Fisher information" between two functions. In what follows, and for the sake of simplicity, we will restrict ourselves to spherically symmetric densities, as is the case of the present study in atomic systems.

In doing so, let us consider the non-negative integral

$$\int \rho(\vec{r}) \left(\frac{d}{dr} \ln \frac{\rho(r)}{f(r)}\right)^2 d\vec{r} \geq 0, \tag{6.8}$$

where $f(r)$ is a (not necessarily normalized to unity) function, on which some conditions will be impossed below. By only carrying out the processes of derivation and squaring,

and defining

$$F(r) \equiv \frac{f'(r)}{f(r)}, \tag{6.9}$$

it is not difficult to find the relationship

$$\bar{I}_r \geq -\left\langle F^2(r)\right\rangle - 2\left\langle F'(r)\right\rangle - 2(d-1)\left\langle \frac{F(r)}{r}\right\rangle, \tag{6.10}$$

where $\bar{I}_r$ refers to the Fisher information of the spherically averaged density $\rho(r)$, and the function $F(r)$ has to fulfil the condition $r^{d-1}\rho(r)F(r)\Big|_0^\infty = 0$ for the finiteness of the expectation values.

For an appropriate choice of $F(r)$ the above expression provides a lower bound on the Fisher information in terms of radial expectation values $\left\langle r^k\right\rangle$ of the density $\rho(\vec{r})$. Let us consider a choice of $F(r)$ for which the right-hand-side of Eq. (6.10) consists of a rational function in which the denominator is the variance $V_r = \langle r^2\rangle - \langle r\rangle^2$ and, consequently, the inequality transforms into a lower bound of the Cramér-Rao complexity $C_r(CR)$. Such a $F(r)$ is given by

$$F(r) = -\alpha\beta r^{\alpha-1} - \nu\gamma r^{\gamma-1}, \tag{6.11}$$

where $\{\alpha, \beta, \gamma, \nu\}$ are parameters to be determined below.

First, we optimize the resulting bound on the parameters (β, ν) and then we consider the particular case $(\alpha = 2, \gamma = 1)$, giving rise to

$$C_r(CR) \geq d^2 + (d-1)\langle r^{-1}\rangle\left[(d-1)\langle r^2\rangle\langle r^{-1}\rangle - 2d\langle r\rangle\right], \tag{6.12}$$

which provides the desired lower bound to the position space CR complexity.

Some comments are in order: (i) a similar bound for the corresponding quantity in the conjugated space is obtained by considering the momentum density, and (ii) some radial expectation values (in both spaces) are specially relevant from a physical point of view. It is well known [314], for instance that, for atomic systems, $\langle r^{-1}\rangle$ is essentially the electron-nucleus attraction energy, $\langle r^2\rangle$ is related to the diamagnetic susceptibility [314], $\langle p^{-1}\rangle$ is twice the height of the peak of the Comptom profile [315], and $\langle p^2\rangle$ is twice the kinetic energy [315]. So, such a different quantities, physically relevant and/or experimentally accessible, provide also information on the Cramér-Rao complexity of atomic systems.

In Figure 6.3, a numerical computation of $C_p(CR)$ (momentum space) and the above mentioned particular bound (with $d = 3$ and momentum expectation values) are displayed for neutral atoms throughout the Periodic Table, with nuclear charges from $Z = 1$ to $Z = 103$. It is clearly observed the similar trends followed by the exact complexity and its lower bound. Both curves display a structure strongly related to the shell-filling process as revealed by analyzing the location of extrema. A similar figure is obtained for

the corresponding quantities in position space, being consequently also valid the same comments as given above.

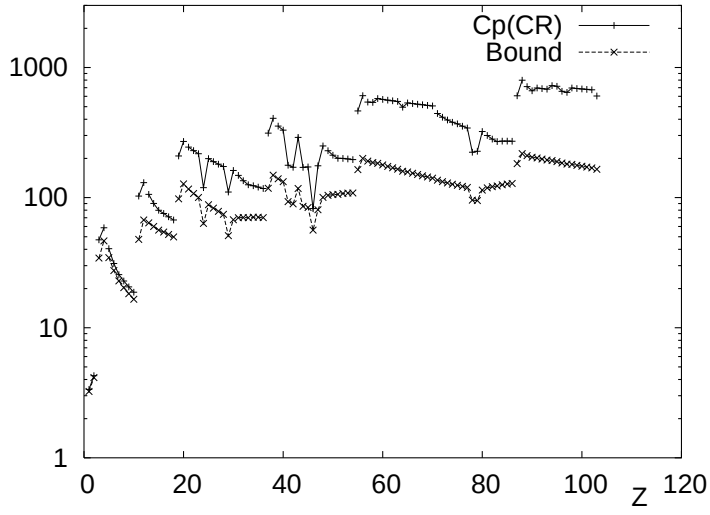

FIGURE 6.3: Cramér-Rao complexity $C_p(CR)$ in momentum space, and lower bound in terms of radial expectation values, for neutral atoms with nuclear charge from $Z = 1$ to $Z = 103$. Atomic units are used.

It is also worthy to mention that, contrary to the analyzed multielectronic systems, none of the three complexities depends on the nuclear charge Z for one-electron systems (hydrogenic atoms), although the individual factors do (e.g. D_r is proportional to Z^3 and I_r to Z^2, and inversely in the conjugated space). In this sense, it is interesting to comment that such complexities can be analytically determined, their values being

$$C_r(LMC) = \frac{e^3}{8} = 2.5107, \qquad C_p(LMC) = \frac{66}{e^{10/3}} = 2.3545, \tag{6.13}$$

$$C_r(FS) = \frac{2e}{\pi^{1/3}} = 3.712, \qquad C_p(FS) = \frac{48(2\pi)^{1/3}}{e^{29/9}} = 3.5311, \tag{6.14}$$

$$C_r(CR) = 3, \qquad C_p(CR) = 12\left(1 - \frac{64}{9\pi^2}\right) = 3.354. \tag{6.15}$$

As observed before, the multielectronic character of the systems makes their complexities to increase considerably as compared to those of the corresponding one-electron ions.

6.1.2 Uncertainty-like inequalities

It is natural to look for the existence of uncertainty-like relationships on the complexities considered in the present work attending to those known for some density functionals and expectation values. It appears very interesting to find rigorous and universal relationships among conjugated complexities. So, in spite of existing well known uncertainty

inequalities on most of the individual factors composing complexities, such is not the case of the complexities themselves. The main reason is that, usually, the two inequalities associated with each factor work in opposite directions, making consequently impossible to combine both together in order to obtain a coherent bound on the whole complexity.

In this subsection, different uncertainty-like complexity inequalities are obtained, all them of universal validity, i.e., the hold for any pair of functions related via Fourier tansform in the same way as the one-particle densities in the conjugated spaces do.

Let us also remark that, for the particular case of analyzing products of complexities $C_r \times C_p$, such a study is equivalent to consider the product or phase space complexity C_{rp}. However, the simple product operation of complexities is not at all the only way of getting uncertainty-like relationships, appearing also interesting to deal with quotients of complexities or of some of their powers, among others.

In this sense, it is worthy to mention that the ratio between the Fisher-Shannon and Cramér-Rao complexities on a given space can be bounded in terms of the so-called "radial uncertainty products", expressed in terms, as mentioned above, of radial expectation values in both conjugated spaces. In doing so, let us consider the ratio $C(FS)/C(CR)$ (in any space) which, attending to the definition of both complexities, turns out to be J/V in the considered space. For simplicity, let us consider the position space ratio J_r/V_r, keeping in mind that all results obtained below will be also valid for the conjugated space quantities. The BBM inequality Eq. (1.34) between Shannon entropies can be written in terms of the power entropies as $J_r \times J_p \geq (\pi e)^{d-1}/2$, giving rise to a lower bound on the numerator J_r in terms of the power entropy J_p. On the other hand, upper bounds on the power entropy J_p in terms of any non-negative order radial expectation value $\langle p^\alpha \rangle$ are also well known [51]. Both inequalities together provide a lower bound on J_r in terms of any $\langle p^\alpha \rangle$ with $\alpha > 0$.

Concerning the denominator V_r on the studied ratio, it is immediate from its definition that $1/V_r \geq 1/\langle r^2 \rangle$. Finally, combining both lower bounds results in the relationship

$$C_r(FS) \geq \frac{e^{1-\frac{2}{\alpha}}}{2} \left(\frac{d}{\alpha}\right)^{2/\alpha} \left(\frac{\alpha\Gamma(d/2)}{2\Gamma(d/\alpha)}\right)^{2/d} \frac{1}{\langle r^2 \rangle \langle p^\alpha \rangle^{2/\alpha}} C_r(CR), \tag{6.16}$$

for any $\alpha > 0$ and similarly in the conjugated space by appropriately replacing the involved densities and variables. A numerical analysis of the above inequality is carried out (in position space) in Figure 6.4 throughout the Periodic Table, for the particular case $\alpha = 1$. As in previous figures, it is again observed the similar shape displayed by both the exact Fisher-Shannon complexity and its lower bound in terms of Cramér-Rao complexity and the chosen uncertainty product.

Let us finally remark an uncertainty-like inequality on the LMC complexity product $C_r(LMC) \times C_p(LMC) = C_{rp}(LMC)$ in terms of arbitrary order uncertainty products of radial expectation values. In order to obtain it, let us remember that the factors

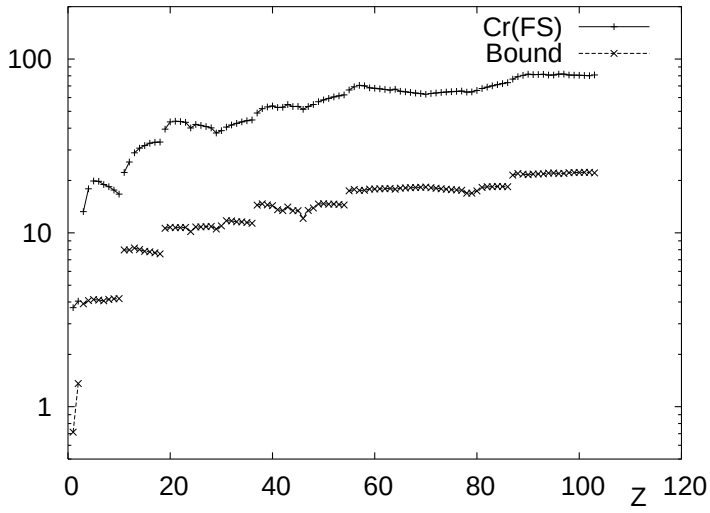

FIGURE 6.4: Fisher-Shannon complexity $C_r(FS)$ in momentum space and lower bound in terms of Cramér-Rao complexity $C_r(CR)$, for neutral atoms with nuclear charge from $Z = 1$ to $Z = 103$. Atomic units are used.

appearing in the product space complexity consist of (i) the exponential entropy on rp-space, bounded from below by means of the BBM inequality, and (ii) the disequilibrium in both position and momentum spaces which are known to be bounded from below in terms of two arbitrary radial expectation values of the associated density [313]. Choosing in both spaces as one radial constraint the normalization, the resulting bound on the uncertainty LMC complexity product results in

$$C_r(LMC) \times C_p(LMC) \geq e^d \Gamma^2(d/2)(d+\alpha)(d+\beta) \left(\frac{d}{d+2\alpha}\right)^{1+\frac{d}{\alpha}} \times \left(\frac{d}{d+2\beta}\right)^{1+\frac{d}{\beta}} \frac{1}{\langle r^\alpha \rangle^{d/\alpha} \langle p^\beta \rangle^{d/\beta}}, \tag{6.17}$$

for radial expectation values of orders α, $\beta > -d/2$ in d-dimensional conjugated spaces. This result confirms the existence of a strong relationship between complexity uncertainty and uncertainty products in terms of radial expectation values. So, the knowledge of an uncertainty product imposses a constraint on the minimal value the LMC complexity product can reach.

Complexities of information-extremizer distributions

For completeness, we obtain the values of complexities for extreme information distributions constrained by a given radial expectation value (apart from normalization) analized in the Chapter 4. Let us denote the complexities of the extremizer distributions (whose

expressions are identical independently of the space considered) by using the subscript to specify the extremized functional (e.g. $C_S(LMC)$ refers to LMC complexity of the distribution which maximizes S, and similarly for the other complexities and extremized functionals). It is very remarkable that, although the individual factors of each complexity depends on the value of the constraint $\langle r^\alpha \rangle$, the complexity itself does not in any case. The obtained expressions are given below:

$$C_S(LMC) = (e/2)^{d/\alpha} \tag{6.18}$$

$$C_S(FS) = \frac{\alpha^{2-\frac{2}{d}} \Gamma\left(\frac{d-2}{\alpha}+2\right) e^{\frac{2}{\alpha}-1} \left[2\Gamma(d/\alpha)\right]^{\frac{2}{d}-1}}{\Gamma^{2/d}(d/2)} \tag{6.19}$$

$$C_S(CR) = \alpha^2 \frac{\Gamma\left(\frac{d-2}{\alpha}+2\right)}{\Gamma(d/\alpha)} \left[\frac{\Gamma\left(\frac{d+2}{\alpha}\right)}{\Gamma(d/\alpha)} - \left(\frac{\Gamma\left(\frac{d+1}{\alpha}\right)}{\Gamma(d/\alpha)}\right)^2\right] \tag{6.20}$$

$$C_I(LMC) = e^3/8, \qquad C_I(FS) = \frac{2e}{\pi^{1/3}}, \qquad C_I(CR) = 3 \tag{6.21}$$

$$C_T(LMC) = \frac{B\left(\frac{d}{\alpha}, \frac{q+1}{q-1}\right)}{B\left(\frac{d}{\alpha}, \frac{q}{q-1}\right)} \exp\left\{\frac{1}{q-1}\left[\Psi\left(\frac{q}{q-1}+\frac{d}{\alpha}\right) - \Psi\left(\frac{q}{q-1}\right)\right]\right\} \tag{6.22}$$

$$\begin{aligned} C_T(FS) \;=\; & \frac{\alpha^{2-\frac{2}{d}}}{(q-1)^2\Gamma^{2/d}(d/2)} \frac{B\left(2+\frac{d-2}{\alpha}, \frac{2-q}{q-1}\right)}{\left[2B\left(\frac{d}{\alpha}, \frac{q}{q-1}\right)\right]^{1-\frac{2}{d}}} \\ & \times \exp\left\{\frac{2}{d(q-1}\left[\Psi\left(\frac{q}{q-1}+\frac{d}{\alpha}\right) - \Psi\left(\frac{q}{q-1}\right)\right] - 1\right\} \end{aligned} \tag{6.23}$$

$$C_T(CR) = \left(\frac{\alpha}{q-1}\right)^2 \frac{\Gamma\left(\frac{d}{\alpha}+\frac{q}{q-1}\right)}{\Gamma\left(\frac{d}{\alpha}\right)} \left[\frac{\Gamma\left(\frac{d+2}{\alpha}\right)}{\Gamma\left(\frac{d+2}{\alpha}+\frac{q}{q-1}\right)} - \frac{\Gamma^2\left(\frac{d+1}{\alpha}\right)\Gamma\left(\frac{d}{\alpha}+\frac{q}{q-1}\right)}{\Gamma^2\left(\frac{d+1}{\alpha}+\frac{q}{q-1}\right)\Gamma\left(\frac{d}{\alpha}\right)}\right] \tag{6.24}$$

where $B(x,y)$ denotes the beta function and $\Psi(x) = \dfrac{\Gamma'(x)}{\Gamma(x)}$ the digamma function; last two equations are valid only for the range of the Tsallis entropy order $1 < q < 2$, because those two complexities contain the Fisher information I of the maximum Tsallis entropy distribution, which integral only converges within such a range. Let us remark that the maximization of the Tsallis entropy $T^{(q=2)}$ is equivalent to the minimization of the disequilibrium D. So, the corresponding LMC complexity of the minimum disequilibrium distribution is

$$C_D(LMC) = \frac{2\alpha}{2\alpha+d} \exp\left\{\Psi\left(2+\frac{d}{\alpha}\right) - \Psi(2)\right\} \tag{6.25}$$

which corresponds to the particular value $q = 2$ in Eq. (6.22).

Some comments are in order: (i) as previously mentioned, it is observed that the final expressions for these analytical complexities do not depend on the constraint value $\langle r^\alpha \rangle$, but only on its order; (ii) it still remains the problem of finding the *maximum/minimum complexity distribution* under such constraints; that is, it is not guaranteed that the distribution that maximizes (minimizes) one factor of complexity be the same that also extremizes the whole complexity; and (iii) it would be also possible to consider a higher number of constraints, but in such a case the extremizer distribution (i.e. the solution of the associated variational problem) would not be analytically obtained and, consequently, the same would happen with complexity, for which the Lagrange multipliers, characteristics of the variational method, must be numerically determined.

6.2 Fisher-Rényi and Shape-Rényi complexities

The next purpose is to analyze numerically the Shape-Rényi and Fisher-Rényi complexities, defined in the Chapter 5, of the one-particle densities in position and momentum spaces, $\rho(\vec{r})$ and $\gamma(\vec{p})$ respectively, for neutral atoms throughout the Periodic Table, their nuclear charge ranging from $Z = 1$ to $Z = 103$.

The Shape-Rényi complexity in position and momentum spaces, to be denoted by $SR_r^{(\alpha)}$ and $SR_p^{(\alpha)}$ respectively, are shown for these atomic systems in Figures 6.5(a) (position) and 6.5(b) (momentum), for diverse values of the parameter α within the range $0.4 \leq \alpha \leq 3.6$. It is worthy to point out that for atomic systems the exponential long-range behavior of the position space density [316] allows any non-negative value $\alpha > 0$, while the momentum space one as p^{-8} [270] imposses the constraint $\alpha > 3/8 = 0.375$.

A first look at Figure 6.5 allows us to observe relevant differences between the structural characteristics of the Shape-Rényi complexity $SR^{(\alpha)}$ after comparing the curves corresponding to both conjugated spaces. The position space measure $SR_r^{(\alpha)}$ (Figure 6.5(a)) displays a much richer structure when dealing with very low values of α, reaching a higher smoothness and monotonicity as α increases. In those cases where the presence of local extrema is more apparent, a detailed analysis of their location reveals that they correspond either to closed shell systems or to atoms suffering the so-called anomalous shell-filling. These two characteristics depend on the occupation number of the outermost or valence atomic subshell, where the aforementioned exponential behavior of $\rho(r)$ makes the density values to be much smaller as compared to those of the core region. Consequently, powering the density to a small α value enhances the relative contribution of the valence region, revealing the properties associated to the shell-filling process. Specially relevant is the strength of peaks for systems with 's' valence subshell as compared to other values of the angular momentum quantum number. It is additionally observed that changes of $SR^{(\alpha)}$ in both spaces as increasing the nuclear charge (i.e. between

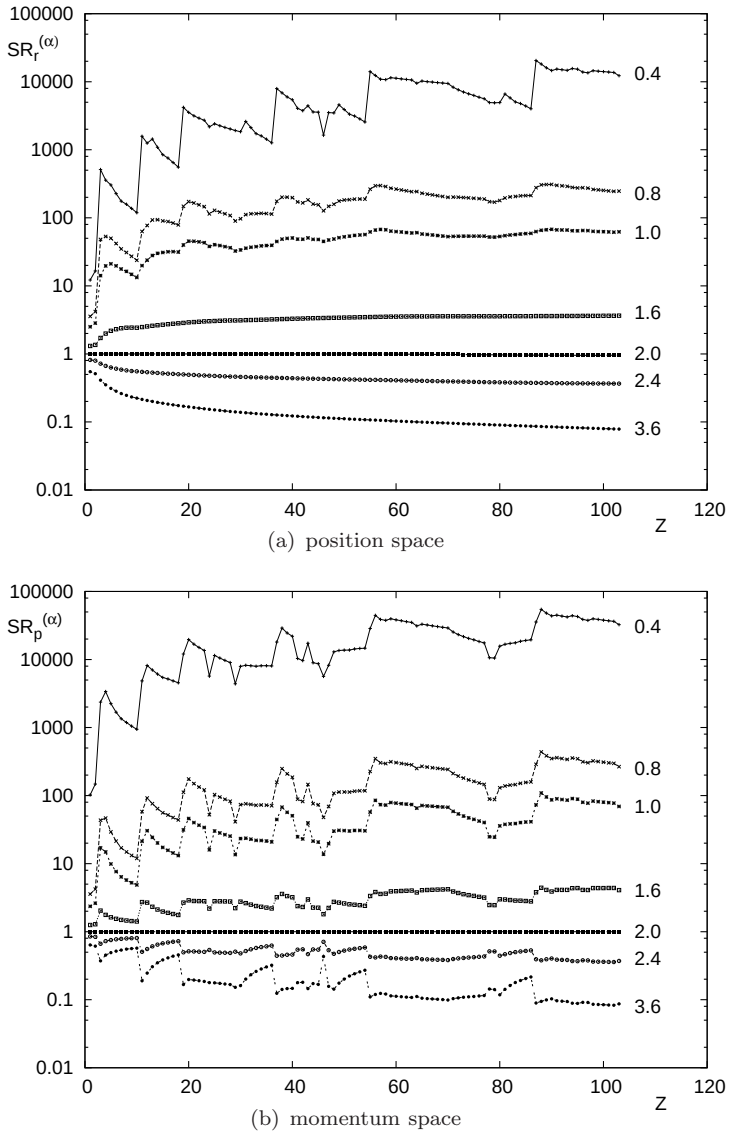

FIGURE 6.5: Shape-Rényi complexity $SR^{(\alpha)}$ for $\alpha = 0.4, 0.8, 1.0, 1.6, 2.0, 2.4, 3.6$ in (a) position space and (b) momentum space. Atomic units are used.

consecutive systems) become smaller as far as considering heavier atoms, being much more apparent for light ones.

The same study in momentum space (Figure 6.5(b)) provides similar conclusions in what concerns the location of extrema and its interpretation in terms of the shell structure. The main difference when comparing it to the position space curves is that such a structure is displayed independently of the α value considered, being much more apparent again for lower α's. Nevertheless, even for high α values such a structure can be also observed under a much smaller scale. Again the reason for finding this behavior can be understood having in mind that the valence region is populated by low speed electrons, represented in terms of the momentum density $\gamma(p)$ by its value around the origin (i.e. close to $p = 0$). The momentum density in that region reaches high enough values in

order to provide information on the valence electrons even without carrying out the enhancement operation by lowering the α parameter.

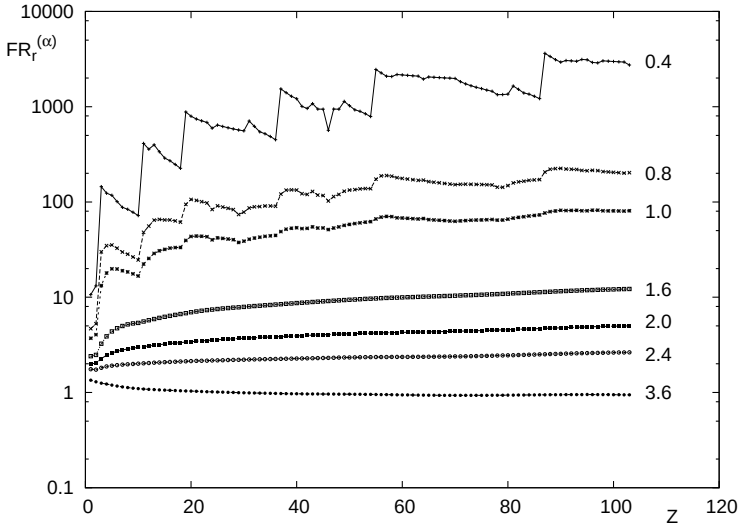

(a) position space

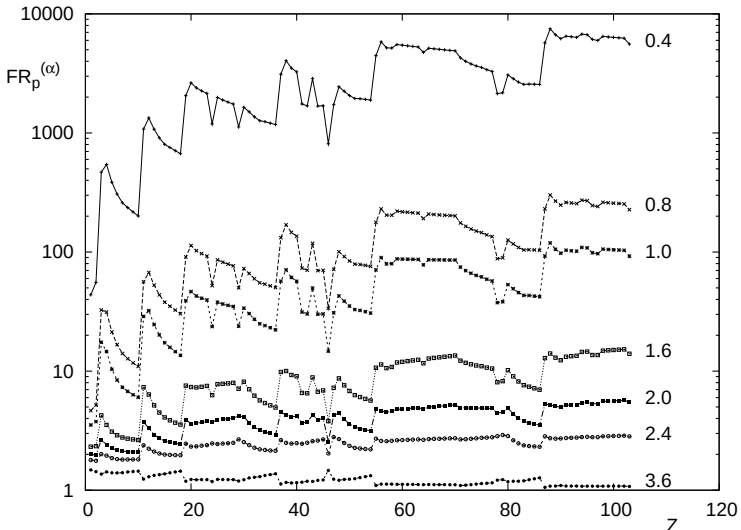

(b) momentum space

FIGURE 6.6: Fisher-Rényi complexity $FR^{(\alpha)}$ for $\alpha = 0.4, 0.8, 1.0, 1.6, 2.0, 2.4, 3.6$ in (a) position space and (b) momentum space. Atomic units are used.

Similar comments to those arising from the analysis of the figure corresponding to the Shape-Rényi complexity $SR^{(\alpha)}$ in both conjugated spaces remain also valid for the Fisher-Rényi complexity $FR^{(\alpha)}$ as observed in the Figure 6.6, at least in what concerns location of extrema and level of structure in each space. The Figure 6.6 is composed similarly as the Figure 6.5, i.e. position (Figure 6.6(a)) and momentum (Figure 6.6(b)) spaces. At this point it is worthy to remember the very different character of the factors involved as measures of order for each complexity, namely the disequilibrium and the Fisher information respectively. In spite of such a difference, the complexities themselves display a very similar structure for all the α values here considered. Nevertheless,

a detailed analysis reveals the aforementioned 'local sensitivity' of the Fisher-Rényi complexity $FR^{(\alpha)}$ as compared to the Shape-Rényi one $SR^{(\alpha)}$ in the magnitude of their variations for closed shells and anomalous shell-filling systems, especially in the momentum space, not so apparent in the position one.

It should be pointed out the role played by the Rényi complexities SR and FR as compared to the individual factors composing them. It is well known the monotonic and structureless behavior of e.g. the disequilibrium D_r or the Fisher entropy I_r in position space [305], as also recently observed for the Rényi entropy $R_p^{(\alpha)}$ with $\alpha > 1$ [73].

The study of the Figure 6.5 and 6.6 reveals not only the interest of considering different values of the Rényi parameter α in order to obtain a more complete information on the structure of the density in different atomic regions from the Rényi-like complexities, but also the usefulness of dealing simultaneously with both conjuated spaces.

6.2.1 Rényi information planes

Far beyond the Shape-Rényi and Fisher-Rényi atomic complexities as descriptors of the shell-filling pattern and information content, it appears also relevant the study of the contribution to the whole complexity of each of its composing factors, in order to analyse the location of all atomic systems here considered in the corresponding order-disorder plane substented by the individual factors. In this way, systems belonging to similar complexity values can be also classified attending to their disequilibrium/order on one hand, and to their uncertainty/disorder on the other.

For illustration, the corresponding $I - J^{(\alpha)}$ and $D - L^{(\alpha)}$ planes are shown in Figures 6.7 and 6.8, respectively, in the position space for the first case (i.e. $I_r - J_r^{(\alpha)}$ in Figure 6.7) and in the momentum one for the other (i.e. $D_p - L_p^{(\alpha)}$ in Figure 6.8). Similar conclusions are obtained for the other planes: for a given space, both planes look similar, the differences being mainly associated to the global and local character of the involved factors, as will be explained when discussing the Figures 6.7 and 6.8 in detail. Nevertheless, it should be remarked that momentum space planes appear more involved than the position ones. As mentioned in the previous Section, the information content of the atomic systems is mainly governed by the nuclear region in position space and by the valence subshells in the momentum one. Adding electrons to the atomic systems constitutes a process which follows rules (shell-filling pattern) not as simple as merely increasing the nuclear charge. Such a difference is also displayed in the corresponding information planes.

Figure 6.7 displays the Fisher-Rényi plane in position space, for different values of the parameter α. The main two comments arising from the analysis of this figure are: (i) as observed for the position space complexities, the atomic shell structure is displayed, also

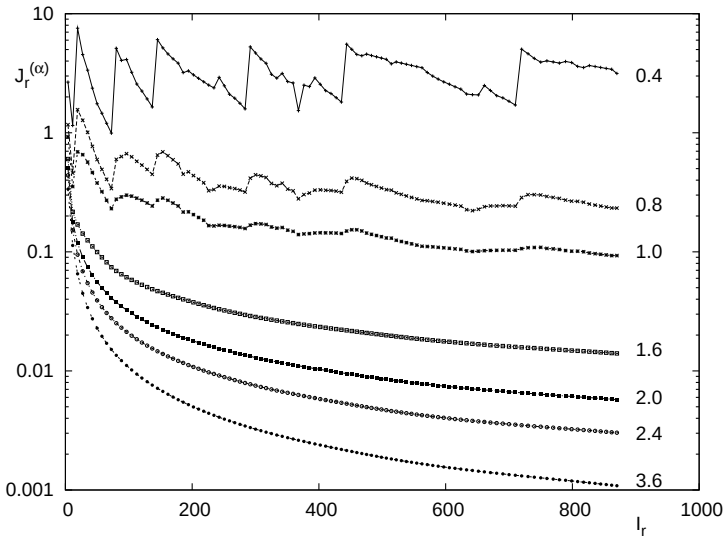

FIGURE 6.7: Fisher-Rényi plane $I - J^{(\alpha)}$ in position space, for $\alpha = 0.4, 1.0, 2.0, 3.6$. Atomic units are used.

in the information planes, for low α values, the curves being very smooth and almost monotonic for higher ones; the location of peaks corresponding to local extrema are associated to the characteristics of the atomic shell-filling, and (ii) all curves display a similar trend of large Fisher information and low power entropy for heavy atoms, which can be interpreted as a relevant increase of gradient at the origin as the electron cloud concentrates around the nuclear region when the nuclear charge increases, while in other regions the electron density spreads almost uniformly, increasing consequently the power entropy.

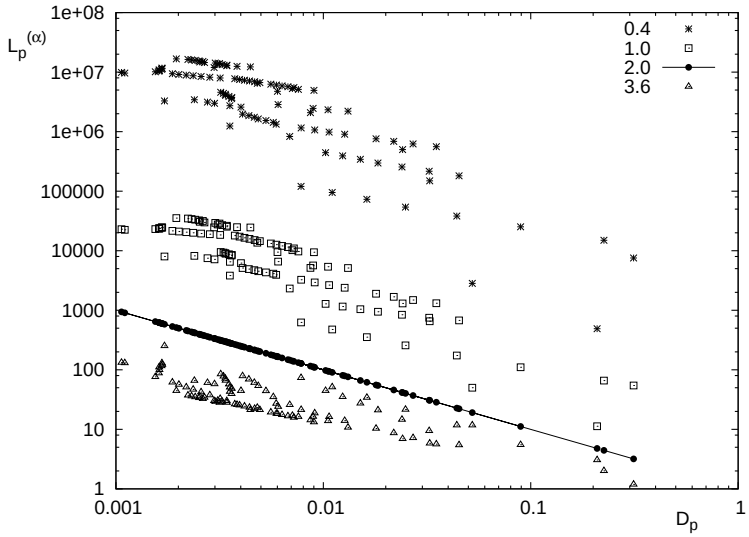

FIGURE 6.8: Shape-Rényi plane $D - L^{(\alpha)}$ in momentum space for $\alpha = 0.4, 0.8, 1.0, 1.6, 2.0, 2.4, 3.6$. Atomic units are used.

The aforementioned involvement in momentum space as a consequence of the shell-filling process is clearly observed in Figure 6.8, where the location of the different atomic systems in the momentum $D - L^{(\alpha)}$ plane for a given value of the parameter α are displayed as a 'cloud', instead of a curve as in previous figures (apart from the trivial case $\alpha = 2$ with a constant $SR^{(\alpha)}$ product). Nevertheless, it is observed a general trend for each α value, in the sense that heavy systems concentrate around the upper-left region, corresponding to low disequilibrium and high exponential entropy (i.e. low order and high uncertainty). Additionally, the distance between consecutive systems becomes shorter as increasing their nuclear charge. In what concerns the dependence on α, it is observed that the clouds are ordered from above to below as increasing α, belonging to different bands, parallel to the unity product line.

A comparison between Figures 6.7 and 6.8 perfectly shows the complementary character of the two conjugated spaces as well as that of the contributing individual factors to the whole complexity in both information planes. In this sense, it is worthy to remark that heavy systems are located, in the position space $I - J$ plane, in the lower right corner, corresponding to a high localization and a low entropy. Opposite trends, however, are observed in momentum space $D - L$ plane.

As in the complexity figures, it is also possible to distinguish the shell-filling patterns for low α in momentum space, more clearly for inner subshells (i.e. 1s, 2s, 2p). Nevertheless, the same can be also observed for additional subshells by employing an appropriate scale in the figure.

6.3 Conclusions

In this Chapter we have obtained a set of rigorous properties and uncertainty-like inequalities on complexity measures, which have been also analyzed numerically for neutral atomic systems. We can conclude that the complexity measures are useful quantities in order to interpret different structural properties of atomic systems. Attending to the main complexity definitions in terms of the Shannon entropy, the Fisher information and the variance, several rigorous properties have been obtained. Such properties include universal bounds, limiting expressions, relationships among themselves and/or radial expectation values and uncertainty products, as well as the exact values for specific functions (e.g. hydrogenic densities and information-extremizer distributions). All results here obtained are valid for arbitrary systems, being numerically tested in atomic systems for the sake of completeness.

On the other hand, in Section 6.2, the Shape-Rényi and Fisher-Rényi complexities generalize the well-known ones LMC and FS respectively, previously employed for analyzing atomic densities, including them as particular cases. The characteristic parameter of the Rényi complexities allows us to modify the relative weight of the distribution within

specific regions of physical interest. The numerical study carried out in the present work provides relevant information on the atomic shell structure as well as the uncertainty and disequilibrium patterns in both conjugated spaces for neutral atoms throughout the whole Periodic Table. The complementary role played by the involved information measures, of very different character, appears highly relevant especially when dealing simultaneously with the position and momentum distributions. Each one behaves in a characteristic fashion according to the nuclear charge of the involved systems, as well as to their shell-structure and the groups they belong to.

Chapter 7

Complexity analysis of d-dimensional hydrogenic systems

A basic problem in information theory of natural systems is the identification of the proper quantifier(s) of their complexity and internal disorder at their physical states. Presently this aim remains open not only for a complicated system, such as e.g. a nucleic acid (either DNA or its single-strand lackey, RNA) in its natural state, but also for the simplest quantum-mechanical realistic systems, including the hydrogenic atom.

The internal disorder of a system, which is manifest in the non-uniformity of the quantum-mechanical density and in the so distinctive hierarchy of its physical states, is being increasingly investigated beyond the root-mean-square or standard deviation (also called Heisenberg measure) by means of various information-theoretic quantities; firstly, by means of the Shannon entropy [53, 161, 169], and later on, by other information and/or spreading measures such as the Fisher information and the power and logarithmic moments [146], as described in Chapter 2 (see also Ref. [317]) where the information theory of d-dimensional hydrogenic systems is reviewed in detail.

Just recently, further complementary insights have been shown to be obtained in the three-dimensional Hydrogen atom at arbitrary states by means of composite information-theoretic measures, such as the Fisher-Shannon and the LMC complexities. In particular, Sañudo and López-Ruiz [318] have found some numerical evidence that, contrary to the energy, both the Fisher-Shannon measure and the LMC complexity in position space do not present any accidental degeneracy (i.e. they do depend on the orbital quantum number l); moreover, they reach their minimal values at the circular states (i.e., those with the highest l). In fact, the position Shannon entropy by itself possesses also these two characteristics as it has been numerically observed long ago [53], where the dependence on the magnetic quantum number m is additionally studied for various physical states.

In this Chapter we provide (Section 7.1) the analytical methodology required to calculate the LMC or shape complexity of the stationary states for the d-dimensional hydrogenic system in the two conjugated position and momentum spaces, and then we apply it to a special class of physical states which includes the ground state and the circular states (i.e. states with the highest hyperangular momenta allowed within a given electronic manifold). After describing the known expressions of the quantum-mechanical density of the system in both spaces, we show that the computation of their LMC complexities for arbitrary d-dimensional hydrogenic stationary states boils down to the evaluation of some entropic functionals of Laguerre and Gegenbauer polynomials.

In order to get the final expressions of these complexity measures in terms of the dimensionality d and the quantum numbers characterizing the physical state under consideration, we need to compute the values of these polynomial entropic functionals what is, in general, a formidable open task. However, in subsection 7.1.1, we succeed to do it for the important cases of ground and circular states. It seems that for the latter ones the shape complexity reaches its minimal value, at least in the three-dimensional case as indicated above. It is also shown that the results obtained always fulfil the uncertainty relation satisfied by the position and momentum shape complexities obtained in Chapter 6. In subsection 7.1.2 we numericaly analyze the results obtained before in terms of the dimensionality of the systems. After the study for arbitrary dimensions, we focus our interest in the obtention of the complexity measures of the three-dimensional Hydrogen atoms. In Section 7.2 we compare the LMC and the Fisher-Shannon complexities in order to check which quantity better describes the internal disorder of these systems. Some upper bounds to the Fisher-Shannon complexity will be given. The last application within this Chapter is the study of the complexity measures in a Klein-Gordon single-particle system, Section 7.3, carried out in order to analyze the relativistic effects in the degree of complexity for hydrogenic systems. Finally, some conclusions are given in Section 7.4.

7.1 Multidimensional hydrogenic systems

The hydrogenic orbitals (i.e., the solutions of the non-relativistic, time-independent Schrödinger equation describing the quantum mechanics for the motion of an electron in the Coulomb field of a nucleus with charge $+Z$) corresponding to stationary states of the hydrogenic system in the configuration space are characterized within the infinite-nuclear-mass approximation by the energetic eigenvalues

$$E = -\frac{Z^2}{2\eta^2}, \tag{7.1}$$

and the eigenfunctions $\Psi_{n,l,\{\mu\}}(\vec{r})$, which provides us with the quantum-mechanical probability density of this system in position space:

$$\rho_{n,l,\{\mu\}}(\vec{r}) = \left|\Psi_{n,l,\{\mu\}}(\vec{r})\right|^2 = R^2_{n,l}(r)\left|\mathcal{Y}_{l,\{\mu\}}(\Omega_d)\right|^2, \tag{7.2}$$

where n is the principal quantum number and $(l,\{\mu\}) \equiv (l=\mu_1,\mu_2,...,\mu_{d-1})$ denote the hyperquantum numbers associated to the angular variables $\Omega_{d-1} \equiv (\theta_1,\theta_2,...,\theta_{d-1}\equiv\varphi)$, which may have all values consistent with the inequalities $l \equiv \mu_1 \geq \mu_2 \geq ... \geq |\mu_{d-1}| \equiv |m| \geq 0$.

The radial function is given by

$$R_{n,l}(r) = \left(\frac{\lambda^{-d}}{2\eta}\right)^{1/2}\left[\frac{\omega_{2L+1}(\hat{r})}{\hat{r}^{d-2}}\right]^{1/2}\tilde{\mathcal{L}}^{2L+1}_{\eta-L-1}(\hat{r}), \tag{7.3}$$

where $\tilde{\mathcal{L}}^{\alpha}_{k}(x)$ denotes the Laguerre polynomial of degree k and parameter α, orthonormal with respect to the weight function $\omega_\alpha(x) = x^\alpha e^{-x}$, the adimensional parameter $\hat{r} = \dfrac{r}{\lambda}$ with $\lambda = \dfrac{\eta}{2Z}$, the grand principal quantum number η and the grand orbital angular momentum hyperquantum number L are

$$\eta = n + \frac{d-3}{2}; \quad n = 1,2,3,..., \quad \text{and} \quad L = l + \frac{d-3}{2}, \quad l = 0,1,2,... \tag{7.4}$$

verifying $\eta - L - 1 = n - l - 1$.

The angular part $\mathcal{Y}_{l,\{\mu\}}(\Omega_d)$ is given by the hyperspherical harmonics [153, 319]

$$\mathcal{Y}_{l,\{\mu\}}(\Omega_d) = \frac{1}{\sqrt{2\pi}}e^{im\varphi}\prod_{j=1}^{d-2}\tilde{C}^{\alpha_j+\mu_{j+1}}_{\mu_j-\mu_{j+1}}(\cos\theta_j)(\sin\theta_j)^{\mu_{j+1}}, \tag{7.5}$$

with $\alpha_j = \frac{1}{2}(d-j-1)$ and $\tilde{C}^{\lambda}_{k}(x)$ denotes the orthonormal Gegenbauer polynomials of degree k and parameter λ.

In momentum space the eigenfunction of the system is the d-dimensional Fourier transforms of the wavefunction in position space [134, 151, 153, 317], which square provides the probability density in momentum space:

$$\gamma(\vec{p}) = \left|\tilde{\Psi}_{n,l,\{\mu\}}(\vec{p})\right|^2 = \mathcal{M}^2_{n,l}(p)\left[\mathcal{Y}_{l\{\mu\}}(\Omega_d)\right]^2, \tag{7.6}$$

where the radial part is

$$\begin{aligned}\mathcal{M}_{n.l}(p) &= 2^{L+2}\left(\frac{\eta}{Z}\right)^{d/2}\frac{(\eta\tilde{p})^l}{(1+\eta^2\tilde{p}^2)^{L+2}}\tilde{C}^{L+1}_{\eta-L-1}\left(\frac{1-\eta^2\tilde{p}^2}{1+\eta^2\tilde{p}^2}\right) \\ &= \left(\frac{\eta}{Z}\right)^{d/2}(1+y)^{3/2}\left(\frac{1+y}{1-y}\right)^{\frac{d-2}{4}}\omega^{*1/2}_{L+1}(y)\tilde{C}^{L+1}_{\eta-L-1}(y),\end{aligned} \tag{7.7}$$

with $y = \dfrac{1-\eta^2\tilde{p}^2}{1+\eta^2\tilde{p}^2}$ and $\tilde{p} = \dfrac{p}{Z}$. The symbol $\tilde{C}_m^{\alpha}(x)$ denotes the Gegenbauer polynomial of order k and parameter α orthonormal with respect to the weight function $\omega_{\alpha}^{*} = (1-x^2)^{\alpha-\frac{1}{2}}$ on the interval $[-1,+1]$. The angular part is again an hyperspherical harmonic as in the position case, given by Eq. (7.5), but with the angular variables of the vector $\vec{p}$.

Let us remember the expression of the LMC complexity in position space:

$$C_r(LMC) = D\left[\rho\right] \times e^{S[\rho]} \tag{7.8}$$

where $D\left[\rho\right]$ is the disequilibrium and $S\left[\rho\right]$ is the Shannon entropy. The expression for the momentum complexity $C_p(LMC)$ is analogous considering $\gamma(\vec{p})$. So, the calculation of the LMC or shape complexity of the position and momentum hydrogenic densities ultimately reduces to the evaluation of some entropic functionals of Laguerre and Gegenbauer polynomials.

Position space

Let us first calculate the disequilibrium $D\left[\rho\right]$. From Eq. (7.2) one obtains that

$$D\left[\rho\right] = \int \rho(\vec{r})^2 d\vec{r} = \frac{2^{d-2}}{\eta^{d+2}} Z^d K_1\left(d,\eta,L\right) K_2\left(l,\{\mu\}\right), \tag{7.9}$$

where

$$K_1\left(d,\eta,L\right) = \int_0^{\infty} x^{-d-5} \left\{ \omega_{2L+1}(x) \left[\tilde{\mathcal{L}}_{\eta-L-1}^{2L+1}(x)\right]^2 \right\}^2 dx \tag{7.10}$$

and

$$K_2\left(l,\{\mu\}\right) = \int_{\Omega} \left|\mathcal{Y}_{l\{\mu\}}\left(\Omega_{d-1}\right)\right|^4 d\Omega_{d-1} \tag{7.11}$$

The Shannon entropy of $\rho\left(\vec{r}\right)$ has been shown to have the following expression:

$$S\left[\rho\right] = S\left[R_{nl}\right] + S\left[\mathcal{Y}_{l\{\mu\}}\right], \tag{7.12}$$

with the radial part

$$\begin{aligned} S\left[R_{n,l}\right] &= -\int_0^{\infty} r^{d-1} R_{n,l}^2(r) \log R_{n,l}^2 dr \\ &= A(n,l,d) + \frac{1}{2\eta} E_1\left[\tilde{\mathcal{L}}_{\eta-L-1}^{2L+1}\right] - d\ln Z, \end{aligned} \tag{7.13}$$

and the angular part

$$S\left[\mathcal{Y}_{l,\{\mu\}}\right] = -\int_{S_{d-1}} \left|\mathcal{Y}_{l,\{\mu\}}\left(\Omega_d\right)\right|^2 \ln\left|\mathcal{Y}_{l,\{\mu\}}\left(\Omega_d\right)\right|^2 d\Omega_d$$
$$= B(l,\{\mu\},d) + \sum_{j=1}^{d-2} E_2\left[\tilde{C}^{\alpha_j+\mu_{j+1}}_{\mu_j-\mu_{j+1}}\right], \tag{7.14}$$

where $A(n,l,d)$ and $B(l,\{\mu\},d)$ have the values

$$A(n,l,d) = -2l\left[\frac{2\eta-2L-1}{2\eta}+\psi(\eta+L+1)\right]+\frac{3\eta^2-L(L+1)}{\eta}+-\ln\left[\frac{2^{d-1}}{\eta^{d+1}}\right], \tag{7.15}$$

and

$$B(l,\{\mu\},d) = \ln 2\pi - 2\sum_{j=1}^{d-2}\mu_{j+1}$$
$$\times\left[\psi(2\alpha_j+\mu_j+\mu_{j+1})-\psi(\alpha_j+\mu_j)-\ln 2-\frac{1}{2(\alpha_j+\mu_j)}\right], \tag{7.16}$$

with $\psi(x)=\dfrac{\Gamma^{'}(x)}{\Gamma(x)}$ the digamma function. The entropic functionals $E_i\left[\tilde{y}_n\right]$, $i=1$ and 2, of the polynomials $\{\tilde{y}_n\}$, orthonormal with respect to the weight function $\omega(x)$, are defined [169, 170] by

$$E_1\left[\tilde{y}_n\right] = -\int_0^\infty x\omega(x)\tilde{y}_n^2(x)\ln\tilde{y}_n^2(x)dx, \tag{7.17}$$

and

$$E_2\left[\tilde{y}_n\right] = -\int_{-1}^{+1} \omega(x)\tilde{y}_n^2(x)\ln\tilde{y}_n^2(x)dx, \tag{7.18}$$

respectively.

Finally, from Eqs. (7.8), (7.9) and (7.12)-(7.14), we obtain the following value for the position LMC complexity of our system:

$$C_r(LMC) = \frac{2^{d-2}}{\eta^{d+2}}K_1\left(d,\eta,L\right)K_2\left(L,\{\mu\}\right) \tag{7.19}$$
$$\times\exp\left[A(n,l,d)+\frac{1}{2\eta}E_1\left[\tilde{L}^{2L+1}_{\eta-L-1}\right]+S\left[\mathcal{Y}_{l,\{\mu\}}\right]\right],$$

where the entropy of the hyperspherical harmonics $S\left[\mathcal{Y}_{l,\{\mu\}}\right]$, given by Eq. (7.14), is controlled by the entropy of Gegenbauer polynomials $E_2\left[\tilde{C}^{\alpha}_{k}\right]$ defined by Eq. (7.18). It is worthy to remark that the position complexity $C\left[\rho\right]$ in a hydrogenic system does not depend on the strength of the Coulomb potential, that is, on the nuclear charge Z (as discussed in the previous Chapter, Section 6.1).

Momentum space

The LMC complexity of the momentum probability density $\gamma(\vec{p})$ is given by $C_p(LMC) = D[\gamma] \times e^{S[\gamma]}$, where the momentum averaging density or disequilibrium $D[\gamma]$ can be obtained from Eq. (7.6) as follows:

$$D[\gamma] = \int \gamma^2(\vec{p})\, d\vec{p} = \frac{2^{4L+8}\eta^d}{Z^d} K_3(d,\eta,L)\, K_2(l,\{\mu\}), \tag{7.20}$$

with K_2 being given by Eq. (7.11), and K_3 can be expressed as

$$K_3(d,\eta,L) = \int_0^\infty \frac{y^{4l+d-1}}{(1+y^2)^{4L+8}} \left[\tilde{C}^{L+1}_{\eta-L-1}\left(\frac{1-y^2}{1+y^2}\right)\right]^4 dy. \tag{7.21}$$

On the other hand, the momentum Shannon entropy $S[\gamma]$ can be calculated in a similar way as in the position case. We obtain

$$\begin{aligned} S[\gamma] &= -\int \gamma(\vec{p}) \ln \gamma(\vec{p})\, d\vec{p} = S[\mathcal{M}_{nl}] + S\left[\mathcal{Y}_{l,\{\mu\}}\right] \\ &= F(n,l,d) + E_2\left[\tilde{C}^{L+1}_{\eta-L-1}\right] + d\ln Z + S\left[\mathcal{Y}_{l,\{\mu\}}\right], \end{aligned} \tag{7.22}$$

where $F(n,l,d)$ is given by the expression

$$\begin{aligned} F(n,l,d) = &-\ln\frac{\eta^d}{2^{2L+4}} - (2L+4)\left[\psi(\eta+L+1) - \psi(\eta)\right] \\ &+ \frac{L+2}{\eta} - (d+1)\left[1 - \frac{2\eta(2L+1)}{4\eta^2-1}\right]. \end{aligned} \tag{7.23}$$

Then, from Eqs. (7.20) and (7.22) we finally have the value for the momentum LMC complexity

$$\begin{aligned} C_p(LMC) = &\, 2^{4L+8}\eta^d K_3(d,\eta,L)\, K_2(L,\{\mu\}) \\ &\times \exp\left\{F(n,l,d) + E_2\left[\tilde{C}^{L+1}_{\eta-L-1}\right] + S\left[\mathcal{Y}_{l,\{\mu\}}\right]\right\}. \end{aligned} \tag{7.24}$$

Notice that, here again, this momentum quantity does not not depend on the nuclear charge Z. Moreover the momentum complexity $C_p(LMC)$ is essentially controlled by the entropy of the Gegenbauer polynomials $E_2\left[\tilde{C}^{\alpha}_{k}\right]$, since the entropy of hyperspherical harmonics $S\left[\mathcal{Y}_{l,\{\mu\}}\right]$ reduces to that of these polynomials according to Eq. (7.14).

7.1.1 LMC complexity of ground and circular states

Here we apply the general expressions (7.19) and (7.24) previously found for the position and momentum shape complexities of an arbitrary physical state of the d-dimensional

hydrogenic system, for the cases of the ground state ($n = 1, \mu_i = 0, \forall i = 1, \cdots, d-1$) and the circular states. A circular state is a single-electron state with the highest hyperangular momenta allowed within a given electronic manifold, i.e. a state with hyperangular momentum quantum numbers $\mu_i = n - 1$ for all $i = 1, ..., d-1$.

Ground state

In this case $\eta - L - 1 = 0$, so that the Laguerre polynomial involved in the radial wavefunction is a constant. Then, the probability density of the ground state in position space given by Eqs. (7.2), (7.3) and (7.5), reduces as follows:

$$\rho_{g.s.}(\vec{r}) = \left(\frac{2Z}{d-1}\right)^d \frac{1}{\pi^{\frac{d-1}{2}}\Gamma\left(\frac{d+1}{2}\right)} e^{-\frac{4Z}{d-1}r}, \tag{7.25}$$

which has been also found by other authors (see e.g. Ref. [126]).

The expressions (7.9)-(7.11), which provide the averaging density of an arbitrary quantum-mechanical state, reduce to the value

$$D\left[\rho_{g.s.}\right] = \frac{Z^d}{(d-1)^d} \frac{1}{\pi^{\frac{d-1}{2}}\Gamma\left(\frac{d+1}{2}\right)}, \tag{7.26}$$

for the ground-state averaging density. Moreover, the angular part of the entropy is

$$S\left[\mathcal{Y}_{0,\{0\}}\right] = \ln \frac{2\pi^{d/2}}{\Gamma\left(\frac{d}{2}\right)}, \tag{7.27}$$

so that it has the value $\ln 2\pi$ and $\ln 4\pi$ for $d = 2$ and 3, respectively. Then, the formulas (7.12)-(7.18) of the Shannon entropy for arbitrary physical state of our system simplify the total Shannon entropy as

$$S\left[\rho_{g.s.}\right] = \ln\left[\frac{(d-1)^d}{2^d}\pi^{\frac{d-1}{2}}\Gamma\left(\frac{d+1}{2}\right)\right] + d - d\ln Z, \tag{7.28}$$

for the ground-state. Finally, from Eq. (7.19) or from its own definition together with Eqs. (7.26)-(7.28) we obtain the position LMC complexity of the d-dimensional hydrogenic ground state, having the value

$$C_r(LMC)(g.s.) = \left(\frac{e}{2}\right)^d \tag{7.29}$$

In momentum space we can operate in a similar way. First we have determined the ground-state probability density

$$\gamma_{g.s.}(\vec{p}) = \frac{(d-1)^d \Gamma\left(\frac{d+1}{2}\right)}{Z^d \pi^{\frac{d+1}{2}}} \frac{1}{\left(1+\frac{(d-1)^2}{4}\tilde{p}^2\right)^{d+1}}, \tag{7.30}$$

which has been also given by Aquilanti et al [134], among others. Then, we have obtained the values

$$D\left[\gamma_{g.s.}\right] = \left(\frac{2d-2}{Z}\right)^d \frac{1}{\pi^{\frac{d+2}{2}}} \frac{\Gamma^2\left(\frac{d+1}{2}\right)\Gamma\left(2+\frac{3d}{2}\right)}{\Gamma\left(2d+2\right)}, \tag{7.31}$$

for the momentum averaging density directly from Eqs. (7.20)-(7.21), and

$$S\left[\gamma_{g.s.}\right] = \ln \frac{\pi^{\frac{d+1}{2}}}{(d-1)^d \Gamma\left(\frac{d+1}{2}\right)} + (d+1)\left[\psi(d+1) - \psi\left(\frac{d}{2}+1\right)\right] + d\ln Z, \tag{7.32}$$

for the momentum Shannon entropy, from Eqs. (7.22)-(7.23). Finally. from Eq. (7.24) or by means of Eqs. (7.31)-(7.32) we have the expression

$$C_p(LMC)(g.s.) = \frac{2^d \Gamma\left(\frac{d+1}{2}\right)\Gamma\left(2+\frac{3d}{2}\right)}{\pi^{1/2}\Gamma\left(2d+2\right)} \times \exp\left\{(d+1)\left[\psi\left(d+1\right) - \psi\left(\frac{d+2}{2}\right)\right]\right\}, \tag{7.33}$$

for the ground-state d-dimensional hydrogenic LMC complexity in momentum space. In particular, this quantity has the values

$$C_p(LMC)(g.s.; d=2) = \frac{2e^{3/2}}{5} = 1.7926, \tag{7.34}$$

$$C_p(LMC)(g.s.; d=3) = \frac{66}{e^{10/3}} = 2.3545, \tag{7.35}$$

$$C_p(LMC)(g.s.; d=4) = \frac{e^{35/12}}{6} = 3.0799, \tag{7.36}$$

for the ground-state hydrogenic system with dimensionalities $d = 2, 3$ and 4, respectively. Let us here mention that the three-dimensional value agrees with that calculated in Ref. [298].

Circular states

Following a parallel process with circular states, we have obtained

$$\rho_{c.s.}(\vec{r}) = \frac{2^{d+2-2n} Z^d}{\pi^{\frac{d-1}{2}}(2n+d-3)^d \Gamma(n)\Gamma\left(n+\frac{d-1}{2}\right)} e^{-\frac{r}{\lambda}} \left(\frac{r}{\lambda}\right)^{2n-2} \prod_{j=1}^{d-2} \left(\sin\theta_j\right)^{2n-2}, \tag{7.37}$$

for the position probability density, and

$$\gamma_{c.s.}(\vec{p}) = \frac{2^{2n-2}(2n+d-3)^d \Gamma\left(n+\frac{d-1}{2}\right)}{Z^d \pi^{\frac{d+1}{2}} \Gamma(n)} \frac{(\eta p/Z)^{2n-2}}{(1+\frac{\eta^2 p^2}{Z^2})^{2n+d-1}} \prod_{j=1}^{d-2} (\sin\theta_j)^{2n-2}, \quad (7.38)$$

for the momentum probability density of a d-dimensional hydrogenic circular state with principal quantum number n. Moreover, we have found the values

$$D\left[\rho_{c.s.}\right] = \frac{Z^d \Gamma\left(n-\frac{1}{2}\right) \Gamma\left(2n+\frac{d-3}{2}\right)}{2^{2n-2}\pi^{\frac{d}{2}}(2n+d-3)^d \Gamma\left(n\right) \Gamma^2\left(n+\frac{d-1}{2}\right)}, \quad (7.39)$$

and

$$D\left[\gamma_{c.s.}\right] = \frac{2^{4n+d-4}(2n+d-3)^d \Gamma^2\left(n+\frac{d-1}{2}\right) \Gamma\left(2n-1\right) \Gamma\left(2n+\frac{3d}{2}\right)}{Z^d \pi^{\frac{d+2}{2}} \Gamma^2\left(n\right) \Gamma\left(4n+2d-2\right)}, \quad (7.40)$$

for the position and momentum averaging densities of circular states. On the other hand, we have also been able to express the position and momentum entropies as

$$\begin{aligned} S\left[\rho_{c.s.}\right] = {} & 2n+d-2-(n-1)\left[\psi(n)+\psi\left(n+\frac{d-1}{2}\right)\right] - d\ln 2 \\ & + \ln\left[(2n+d-3)^d \pi^{\frac{d-1}{2}} \Gamma(n) \Gamma\left(n+\frac{d-1}{2}\right)\right] - d\ln Z, \end{aligned} \quad (7.41)$$

and

$$S\left[\gamma_{c.s.}\right] = A(n,d) + \ln\left[\frac{2^{d+1} Z^d \pi^{\frac{d+1}{2}} \Gamma(n)}{(2n+d-3)^d \Gamma\left(n+\frac{d-1}{2}\right)}\right], \quad (7.42)$$

where the constant $A(n,d)$ is given by

$$\begin{aligned} A(n,d) = {} & \frac{2n+d-1}{2n+d-3} - \frac{d+1}{2n+d-2} - (n-1)\psi(n) \\ & - \left(\frac{d+1}{2}\right)\psi\left(n+\frac{d-2}{2}\right) + \left(n+\frac{d-1}{2}\right)\psi\left(n+\frac{d-3}{2}\right). \end{aligned} \quad (7.43)$$

Finally, from Eqs. (7.39)-(7.42) or equivalently from Eqs. (7.19) and (7.24) we get the values

$$\begin{aligned} C_r(LMC)(c.s.) = {} & \frac{\Gamma\left(n-\frac{1}{2}\right) \Gamma\left(2n+\frac{d-3}{2}\right)}{2^{2n+d-2}\pi^{1/2}\Gamma\left(n+\frac{d-1}{2}\right)} \\ & \times \exp\left\{2n+d-2-(n-1)\left[\psi(n)+\psi\left(n+\frac{d-1}{2}\right)\right]\right\}, \end{aligned} \quad (7.44)$$

and

$$C_p(LMC)(c.s.) = \frac{2^{4n+2d-3}\Gamma\left(n+\frac{d-1}{2}\right)\Gamma(2n-1)\Gamma\left(2n+\frac{3d}{2}\right)}{\pi^{1/2}\Gamma(n)\Gamma(4n+2d-2)} \exp\left[A(n,d)\right], \quad (7.45)$$

for the position and momentum LMC complexity of a d-dimensional hydrogenic system in an arbitrary circular state. It is worthwhile remarking, for checking purposes, that Eqs. (7.44) and (7.45) reduce to Eqs. (7.29) and (7.33), respectively, in case that $n = 1$, as expected; in this sense we have to use the duplication and recurrence properties of the digamma function, namely: $\psi(2z) = \frac{1}{2}\left[\psi(z) + \psi\left(z + \frac{1}{2}\right)\right] + \ln 2$ and $\psi(z+1) = \psi(z) + \frac{1}{z}$.

7.1.2 Numerical study and dependene on the dimensionality

Here we discuss the general complexity expressions previously obtained, in terms of (i) the dimensionality for a given circular state (i.e., for fixed n), and (ii) the principal quantum number n for a given dimensionality d.

Let us begin with the dimensional analysis of the position and momentum complexities for circular states given by Eqs. (7.44) and (7.45), respectively. The position complexity considered as a function of the dimensionality is plotted in Figure (7.1) for the ground state (n=1) and the circular states with $n = 2$ and 3. It displays a parabolic growth for all states as d increases.

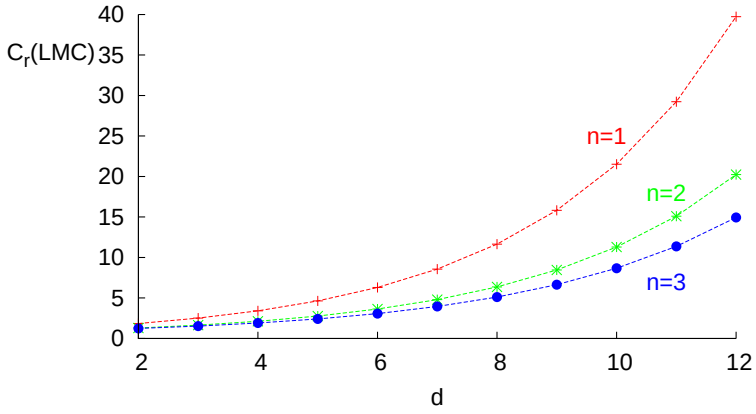

FIGURE 7.1: Dependence of the LMC complexity in position space on the dimension d for three circular states. Atomic units are used.

The LMC complexity of the momentum density appears to have a strong ressemblance with the position one, mainly because the two basic ingredients of each complexity have opposite behaviours as d varies. This is clearly shown in Figure (7.2), where the Shannon entropies $S[\rho]$ and $S[\gamma]$ as well as the logarithm of the position and momentum values of the disequilibrium are plotted for the ground state against d. Let us keep in mind that $C_r(LMC) = \exp(S[\rho] + \ln D[\rho])$ in position space and similarly in momentum space. We observe that the Shannon entropies and the disequilibrium logarithmic measures have opposite behaviours in the two reciprocal spaces, so that the combined exponential effect which gives rise to the corresponding complexities is very similar qualitatively and at least quantitatively. Moreover it happens that, for a given dimensionality, the relative

contribution of the disequilibrium (entropic power) is smaller than that of the entropic power (disequilibrium) in position (momentum) space. This indicates that the relative contribution of the bulk extent of the position (momentum) probability density is more powerful (less) than its average height.

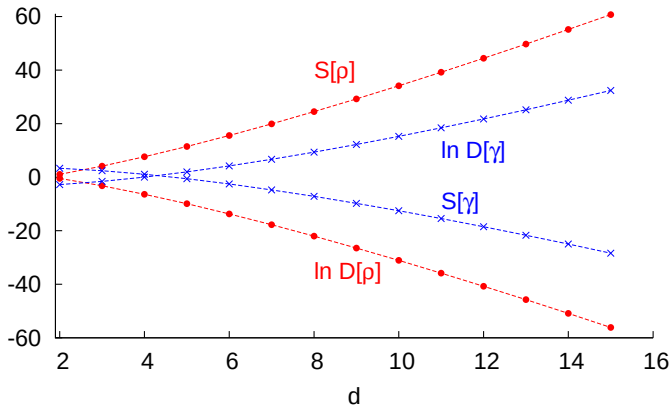

FIGURE 7.2: Ground state Shannon entropy ($S[\rho]$, $S[\gamma]$) and disequilibrium ($D[\rho]$, $D[\gamma]$) in position and momentum spaces as a function of the dimension d. Atomic units are used.

In addition, from Figure (7.1), we observe that the inequalities

$$C_d[\rho_{c.s.}; n=3] < C_d[\rho_{c.s.}; n=2] < C_d[\rho_{g.s.}]$$

are fulfiled in position space, and similarly in the momentum one, i.e. for a given dimension of the hydrogenic systems, the highest value of the LMC complexity is reached for the ground state.

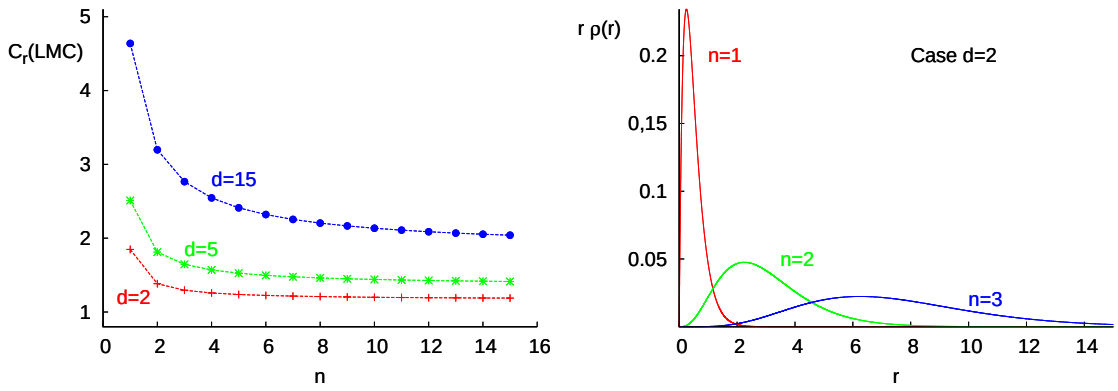

FIGURE 7.3: (Left) Dependence of the position LMC complexity of circular states on the principal quantum number n for various dimensionalities. (Right) Radial probability density in position space for various two-dimensional circular states.

This decreasing phenomenon of the complexity for the circular states when the quantum number n increases, can be more clearly observed in the left graph of Figure (7.3) where the values of the position complexity for the states with n = 1-15 are given at the dimensionalities d = 2, 5 and 15. Therein we remark that when the quantum number n increases, the radial density behaves so that its maximum height decreases and its spreading increases at different rates in such a way that, in overall, occurs the phenomenon pointed out by this chain of inequalities; namely, the larger n is, the smaller is the LMC complexity of the corresponding circular state.

These dimensional and energetic (quantum number n) behaviours of the position complexity turn out to be a delicate overall balance of the average height and the bulk spreading of the system given by its two information-theoretic ingredients: the disequilibrium $D[\rho]$ and the Shannon entropic power, respectively.

Now we look for the dimensional (i.e., with $d \to \infty$) limit, and the high energy or Rydberg ($n \to \infty$) limit of the position and momentum complexities of the system. The former one plays a relevant role in the dimensional scaling methods in atomic and molecular physics [126], and the latter one for the Rydberg states which lie down at the region where the transition classical-quantum takes place. The large d limit is close to (but not the same) the conventional classical limit obtained as $\hbar \to 0$ for a fixed dimension [126].

For the ground state, whose energy is $E_{g.s.} = -2\left(\frac{Z}{d-1}\right)^2$, the position complexity is, according to Eq. (7.29), $C_r(LMC)(g.s.) = \left(\frac{e}{2}\right)^d$. So that at the pseudoclassical limit, in which the electron is located at a fixed radial distance, the energy vanishes while the position complexity diverges. In momentum space, the LMC complexity given by Eq. (7.33) has the asymtotic behaviour

$$C_p(LMC)(g.s.) \sim \frac{3^{\frac{3}{2}(d-1)}}{2^{2d-\frac{3}{2}}\sqrt{e}}, \qquad d \to \infty \tag{7.46}$$

for the pseudoclassical limit.

A similar asymptotic analysis of Eq. (7.44) has allowed us to find the following limiting values for the position LMC complexity of a general circular state (characterized by the quantum number n):

$$C_r(LMC)(c.s.) \sim \left(\frac{e}{2}\right)^{d+2n-2} e^{(1-n)\psi(n)} \frac{\Gamma\left(n-\frac{1}{2}\right)}{\sqrt{\pi}}, \qquad d \to \infty \tag{7.47}$$

at the dimensional limit, and the value

$$C_r(LMC)(c.s.) \sim \left(\frac{e}{2}\right)^{\frac{d-1}{2}}, \qquad n \gg 1 \tag{7.48}$$

for the circular Rydberg states of a d-dimensional hydrogenic system.

Operating with Eq. (7.45) in a parallel way, we have obtained the expressions

$$C_p(LMC)(c.s.) \sim \left(\frac{3^{3/2}}{4}\right)^d \frac{3^{2n-\frac{1}{2}}\Gamma(2n-1)}{2^{4n-\frac{5}{2}}\Gamma(n)} e^{(1-n)\psi(n)-\frac{1}{2}}, \qquad d \to \infty \quad (7.49)$$

for the momentum LMC complexity of a circular state with quantum number n at the pseudoclassical limit, and

$$C_p(LMC)(c.s.) \sim \left(\frac{e}{2}\right)^{\frac{d-1}{2}}, \qquad n \gg 1 \quad (7.50)$$

for the momentum LMC complexity of a circular Rydberg state.

Let us also make some comments about the uncertainty products of the position and momentum LMC complexities $C[\rho] \times C[\gamma]$ for the ground and circular states. The general expressions are readily obtained from Eqs. (7.29) and (7.44) in position space, and from Eqs. (7.33) and (7.45) in momentum space. Consequently, this uncertainty product behaves as

$$C_r(LMC)(c.s.) \times C_p(LMC)(c.s.) \sim \left(\frac{e}{2}\right)^{d-1}, \qquad n \gg 1 \quad (7.51)$$

at the Rydberg limit, and as

$$C_r(LMC)(c.s.) \times C_p(LMC)(c.s.) \sim \left(\frac{3^{3/2}e}{2^3}\right)^d \frac{3^{2n-\frac{1}{2}}}{2^{4n-\frac{5}{2}}} \frac{\Gamma^2\left(n-\frac{1}{2}\right)}{\pi} e^{2n-\frac{5}{2}-2(n-1)\psi(n)}, d \to \infty \quad (7.52)$$

at the high dimensional limit for circular states, where Eqs. (7.47)-(7.50) have been taken into account. The last expression yields

$$C_r(LMC)(g.s.) \times C_p(LMC)(g.s.) \sim \left(\frac{3^{3/2}e}{2^3}\right)^d \left(\frac{3}{2e^{1/3}}\right)^{\frac{3}{2}}, \qquad d \to \infty \quad (7.53)$$

for the ground state uncertainty product. Finally, for completeness, let us remark that the complexity uncertainty product is always not below $\frac{e}{2} = 1.359$.

7.2 Three-dimensional hydrogenic systems

There does not stil exist any quantity to properly measure the rich variety of three-dimensional geometries of the hydrogenic orbitals, which are characterized by means of three integer numbers: the principal, orbital and magnetic/azimuthal quantum numbers, usually denoted by n, l and m, respectively. This is a particular case of the systems studied in the previous Section 7.1 taking $d = 3$.

We use the LMC, Fisher-Shannon and Cramér-Rao complexities to quantify the structure and the internal disorder of these systems in position space. These measures quantify different facets of the internal structure of the system which are manifest in the diverse three-dimensional geometries of its orbitals. The Fisher-Shannon measure grasps the oscillatory nature of the electronic cloud together with its total extent in the configuration space. The Cramér-Rao quantity takes also into account the gradient content but toghether with the electronic spreading around the centroid. The LMC complexity quantifies the combined effects of the average height and the total spreading of the probability density, so being insensitive to the electronic oscillations.

Let us briefly advance that here we find that the Fisher-Shannon measure turns out to be the most appropriate one to describe the (intuitive) complexity of the three dimensional geometry of hydrogenic orbitals.

For the three-dimensional case, i.e., taking $d = 3$ in Eqs. (7.2)-(7.5), one has that the probability density in position space is given by

$$\rho(\vec{r}) = |\Psi_{n,l,m}(\vec{r})|^2 = R^2_{n,l}(r)\,|Y_{l,m}(\Omega)|^2 \tag{7.54}$$

where $n = 1, 2, ...$ is the principal quantum number, $l = 0, 1, ..., n-1$ is the angular quantum number and $m = -l, -l+1, ..., l-1, l$, the magnetic quantum number, and $r = |\vec{r}|$ with the solid angle Ω defined by the angular coordinates (θ, φ). The radial component, duly normalized to unity, is given by

$$R_{n,l}(r) = \frac{2Z^{3/2}}{n^2}\left[\frac{\omega_{2l+1}(\tilde{r})}{\tilde{r}}\right]^{1/2} \tilde{\mathcal{L}}^{2l+1}_{n-l-1}(\tilde{r}), \tag{7.55}$$

with $\tilde{r} = \dfrac{2Zr}{n}$, and $\tilde{\mathcal{L}}^{\alpha}_{k}(x)$ denote the Laguerre polynomials orthonormal with respect to the weight function $\omega_\alpha(x) = x^\alpha e^{-x}$ on the interval $[0, \infty)$; that is, they satisfy the orthogonality relation

$$\int_0^\infty \omega_\alpha(x)\tilde{\mathcal{L}}^{\alpha}_{n}(x)\tilde{\mathcal{L}}^{\alpha}_{m}(x)dx = \delta_{nm} \tag{7.56}$$

The angular factor $Y_{l,m}(\theta, \varphi)$ is the renowned spherical harmonic which describes the bulky shape of the system, which is given by

$$Y_{l,m}(\theta, \varphi) = \frac{1}{\sqrt{2\pi}} e^{im\varphi}\tilde{\mathcal{C}}^{m+1/2}_{l-m}(\cos\theta)\,(\sin\theta)^m\,, \tag{7.57}$$

where $\{\tilde{\mathcal{C}}^{\lambda}_{k}(x)\}$ denotes the Gegenbauer or ultraspherical polynomials, which are orthonormal with respect to the weight function $(1-x^2)^{\lambda-1/2}$ on the interval $[-1, +1]$.

Then, the probability of finding the electron within the volume element $d\vec{r}$ centered in $\vec{r}$ can be expresed as

$$\rho(\vec{r})d\vec{r} = D_{n,l}(r)dr \times \Theta_{l,m}(\theta)d\theta d\varphi, \tag{7.58}$$

where

$$D_{n,l} = R^2_{n,l}(r)r^2, \qquad \text{and} \qquad \Theta_{l,m}(\theta) = |Y_{l,n}(\theta,\varphi)|^2 \sin\theta \tag{7.59}$$

are the known radial and angular probability densities, respectively.

7.2.1 Complexity measures of hydrogenic orbitals in position space

Let us here discuss, both analytically and numerically, the three complexity measures analized in this Part II (i.e. CR, FS and LMC) for a general hydrogenic orbital with quantum numbers (n, l, m). Next, (a) the Cramér-Rao measure is given explicitly, (b) the Fisher-Shannon measure is shown to quadratically depend on the principal quantum number n, and (c) the LMC complexity is carefully analyzed in terms of the quantum numbers. In this way we considerably extend the recent finding of Sañudo and López-Ruíz [318] relative to the fact that the Fisher-Shannon and LMC complexities have their minimum values for the orbitals with the highest orbital momentum.

The Cramér-Rao complexity has the value

$$C_r(CR) = I[\rho] \times V[\rho] = \frac{n-|m|}{n^3}\left[n^2(n^2+2) - l^2(l+1)^2\right], \tag{7.60}$$

where we have taken into account that, for the three-dimensional hydrogenic systems, we have

$$V[\rho] = \frac{n^2(n^2+2) - l^2(l+1)^2}{4Z^2}, \tag{7.61}$$

for the variance, and

$$I[\rho] = \frac{4Z^2}{n^3}(n-|m|), \tag{7.62}$$

for the Fisher information.

To obtain the Fisher-Shannon measure, it is necessary to calculate the Shannon entropy given by Eqs. (7.12)-(7.16) with $d = 3$,

$$S[\rho] = \tilde{A}(n,l,m) + \frac{1}{2n}E_1\left(\tilde{\mathcal{L}}^{2l+1}_{n-l-1}\right) + E_2\left(\tilde{C}^{|m|+1/2}_{l-|m|}\right), \tag{7.63}$$

where

$$\tilde{A}(n,l,m) = \ln\left(2^{2|m|-1}\pi n^4\right) + \frac{3n^2 - l(l+1)}{n} - 2l\left[\frac{2n-2l-1}{2n} + \psi(n+l+1)\right] - 2|m|\left[\psi(l+m+1) - \psi(l+1/2) - \frac{1}{2l+1}\right], \tag{7.64}$$

and the integrals E_1 and E_2 are given by Eqs. (7.17) and (7.18) respectively.

So, the Fisher-Shannon complexity has the value

$$C_r(FS) = I[\rho] \times \frac{1}{2\pi e}e^{\frac{2}{3}S[\rho]} = \frac{4(n-|m|)}{n^3}\frac{1}{2\pi e}e^{\frac{2}{3}B(n,l,m)}, \tag{7.65}$$

where

$$B(n,l,m) = A(n,l,m) + \frac{1}{2n} E_1\left(\tilde{\mathcal{L}}_{n-l-1}^{2l+1}\right) + E_2\left(\tilde{\mathcal{C}}_{l-|m|}^{|m|+1/2}\right). \tag{7.66}$$

For the LMC complexity, it is necessary to derive the disequilibrium from Eqs. (7.9)-(7.11) with $d = 3$:

$$\begin{aligned} D\left[\rho\right] &= \int \rho(\vec{r})^2 d\vec{r} = \int_0^\infty r^2 \left|R_{n,l}(r)\right|^4 \times \int_\Omega \left|Y_{l,m}(\Omega)\right|^4 d\Omega \\ &= D\left[R_{n,l}\right] \times D\left[Y_{l,m}\right] = Z^3 D(n,l,m), \end{aligned} \tag{7.67}$$

where

$$\begin{aligned} D(n,l,m) = \frac{(2l+1)^2}{2^{4n}\pi n^5} \sum_{k=0}^{n_r} \binom{2n_r-2k}{n_r-k}^2 \frac{(k+1)_k}{k!} \frac{\Gamma\left(4l+2k+3\right)}{\Gamma^2\left(2l+k+2\right)} \\ \times \sum_{l'=0}^{2l} (2l'+1) \begin{pmatrix} l & l & l' \\ 0 & 0 & 0 \end{pmatrix}^2 \begin{pmatrix} l & l & l' \\ m & m & -2m \end{pmatrix}^2, \end{aligned} \tag{7.68}$$

with $n_r \equiv n - l - 1$, and the $3j$-symbols [320] have been used.

The radial part, $D\left[R_{n,l}\right]$, of the disequilibrium is given by Eq. (7.10) for $d = 3$:

$$D\left[R_{n,l}\right] = \frac{Z^3 2^{2-4n}}{n^5} \sum_{k=0}^{n_r} \binom{2n_r-2k}{n_r-k}^2 \frac{(k+1)_k}{k!} \frac{\Gamma\left(4l+2k+3\right)}{\Gamma^2\left(2l+k+2\right)}, \tag{7.69}$$

and Eq. (7.11) provides the angular part, $D\left[Y_{l,m}\right]$,

$$\begin{aligned} D\left[Y_{l,m}\right] &= \int_0^{2\pi} d\phi \int_0^\pi \sin\theta d\theta \left|Y_{lm}\left(\theta,\phi\right)\right|^4 \\ &= \sum_{l'=0}^{2l} \left(\frac{\hat{l}^2 \hat{l'}}{\sqrt{4\pi}}\right)^2 \begin{pmatrix} l & l & l' \\ 0 & 0 & 0 \end{pmatrix}^2 \begin{pmatrix} l & l & l' \\ m & m & -2m \end{pmatrix}^2, \end{aligned} \tag{7.70}$$

where the linearization formulas

$$\left[\mathcal{L}_{n_r}^{2l+1}(x)\right]^2 = \frac{\Gamma(2l+n_r+2)}{2^{2n_r} n_r!} \sum_{k=0}^{n_r} \binom{2n_r-2k}{n_r-k} \frac{(2k)!}{k!} \frac{1}{\Gamma(2l+2+k)} \mathcal{L}_{2k}^{4l+2}(2x), \tag{7.71}$$

and

$$\left|Y_{lm}\left(\Omega\right)\right|^2 = \sum_{l'=0}^{2l} \frac{\hat{l}^2 \hat{l'}}{\sqrt{4\pi}} \begin{pmatrix} l & l & l' \\ 0 & 0 & 0 \end{pmatrix} \begin{pmatrix} l & l & l' \\ m & m & -2m \end{pmatrix} Y_{l',2m}^*\left(\Omega\right), \tag{7.72}$$

with $\hat{a} = \sqrt{2a+1}$ have been considered. Taking into account the integral

$$\int_\Omega Y_{l_1,m_1}\left(\Omega\right) Y_{l_2,m_2}\left(\Omega\right) Y_{l_3,m_3}^*\left(\Omega\right) d\Omega = \frac{\hat{l_1}\hat{l_2}\hat{l_3}}{\sqrt{4\pi}} \begin{pmatrix} l_1 & l_2 & l_3 \\ 0 & 0 & 0 \end{pmatrix} \begin{pmatrix} l_1 & l_2 & l_3 \\ m_1 & m_2 & m_3 \end{pmatrix}, \tag{7.73}$$

and the orthogonality relation for the Laguerre polynomials, one straightforwardly obtains the results provided by Eqs. (7.69) and (7.70)

Then, taking into account Eqs. (7.63), (7.66) and (7.67) one has the value

$$C_r(LMC) = D\left[\rho\right] e^{S[\rho]} = D(n,l,m)e^{B(n,l,m)}. \tag{7.74}$$

In particular, for the ground state ($n = 1$, $l = m = 0$) we have the values

$$C_r(CR)(g.s) = 3, \qquad C_r(FS)(g.s.) = \frac{2e}{\pi^{1/3}}, \qquad C_r(LMC)(g.s.) = \frac{e^3}{8}, \tag{7.75}$$

for the three composite information-theoretic measures mentioned above. Let us highlight that neither of the three complexities depend on the nuclear charge. Moreover, it is known that $C(FS) \geq 3$ for all three-dimensional densities [59, 64] but also $C(CR) \geq 9$ for any hydrogenic orbital as one can easily prove from Eq. (7.60).

Let us now discuss the numerical results for the Fisher-Shannon, Cramér-Rao and LMC complexity measures of hydrogenic atoms for various specific orbitals in terms of their corresponding quantum numbers (n, l, m). To make possible the mutual comparison among these measures, and in order to avoid difficulties regarding physical dimensions, we study the dependence of the ratio between the measures $C_r(LMC)(n,l,m) \equiv C(n,l,m)$ of the orbital we are interested in and the corresponding measure $C_r(LMC)(1,0,0) \equiv C(1,0,0) \equiv C_r(LMC)(g.s.)$ of the ground state, that is:

$$\zeta(n,l,m) \equiv \frac{C(n,l,m)}{C(1,0,0)}, \tag{7.76}$$

on the three quantum numbers. The results are shown in Figures 7.4, 7.7 and 7.8, where the relative values of the three composite information-theoretic measures are plotted in terms of n, m and l, respectively.

More specifically, in Figure 7.4, we have plotted the three measures for various ns-states (i.e., with $l = m = 0$). Therein, we observe that (a) the Fisher-Shannon and Cramér-Rao measures have an increasing parabolic behaviour as n is increases while the LMC complexity is roughly constant, and (b) the inequalities

$$\zeta_{FS}(n,0,0) > \zeta_{CR}(n,0,0) > \zeta_{LMC}(n,0,0), \tag{7.77}$$

are fulfilled for any fixed n. Similar features are displayed by states (n,l,m) other than $(n,0,0)$. In order to both understand this behaviour and gain a deeper insight into the internal complexity of the hydrogenic atom, which is manifest in the three-dimensional geometry of its configuration orbitals (and so, in the spatial charge distribution density of the atom at different energies), we have drawn the radial $D_{n,l} = R^2_{n,l}(r)r^2$ and

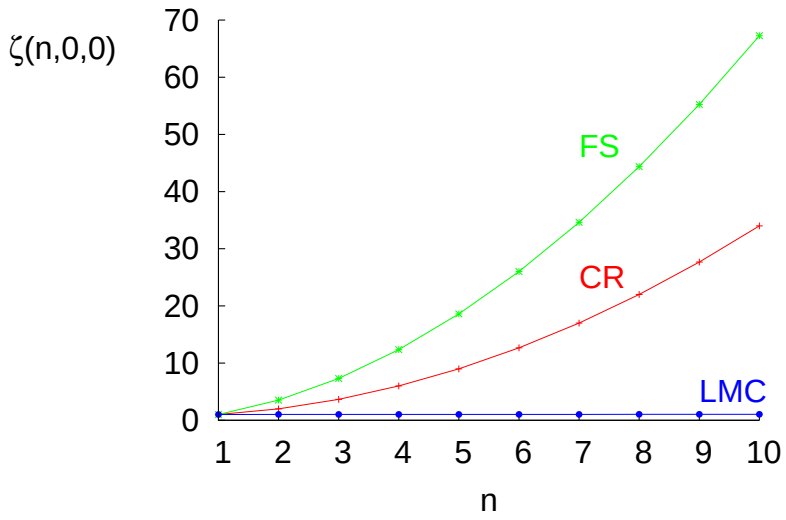

FIGURE 7.4: Relative Fisher-Shannon $\zeta_{FS}(n,0,0)$, Cramér-Rao $\zeta_{CR}(n,0,0)$ and LMC complexity $\zeta_{LMC}(n,0,0)$ ratios of the ten lowest hydrogenic states s as a function of n. See text.

angular $\Theta_{l,m}(\theta) = |Y_{l,m}(\theta,\varphi)|^2 \sin\theta$ densities (see Eq. (7.59)) in Figures 7.5 and 7.6, respectively, for the three lowest energetic levels of hydrogen.

From Figure 7.5 we realize that as n increases while keeping fixed l, both the oscillatory character (so, the gradient content and its associated Fisher information) and the spreading (so, the Shannon entropic power) of the radial density certainly grow while its variance hardly does so and the average height (which controls $D[\rho]$) clearly decreases. Taking into account these radial observations and the graph of $\Theta_{0,0}(\theta)$ at the top line of Figure 7.6, we can understand the parabolic growth of the Fisher-Shannon and Cramér-Rao measures as well as the lower value and relative constancy of the LMC complexity for ns states shown in Figure 7.4 when n is increasing. In fact, the gradient content (mainly because of its radial contribution) and the spreading of the radial density of these states contribute constructively to the Fisher-Shannon measure of Hydrogen, while the spreading and the average height almost cancel out one each other, making the LMC complexity to have a very small and almost constant value; we should say, for completeness, that $\zeta_{LMC}(n,0,0)$ increases from 1 to 1.04 when n varies from 1 to 10. In the Cramér-Rao case, the parabolic growth is almost due to the increasing behaviour of the gradient content, and consequently of its Fisher information ingredient.

Let us now explain and understand the linear decreasing behaviour of the Fisher-Shannon and Cramér-Rao measures as well as the practical constancy of the LMC complexity for the hydrogen orbital ($n = 20$, $l = 17$, m) when $|m|$ increases, as shown in Figure 7.7. These phenomena purely depend on the angular contribution due to the analytical form of the angular density $\Theta_{17,m}(\theta)$ since the radial contribution (i.e. that due to the radial density $R_{n,l}(r)$) remains constant when m varies. A straightforward

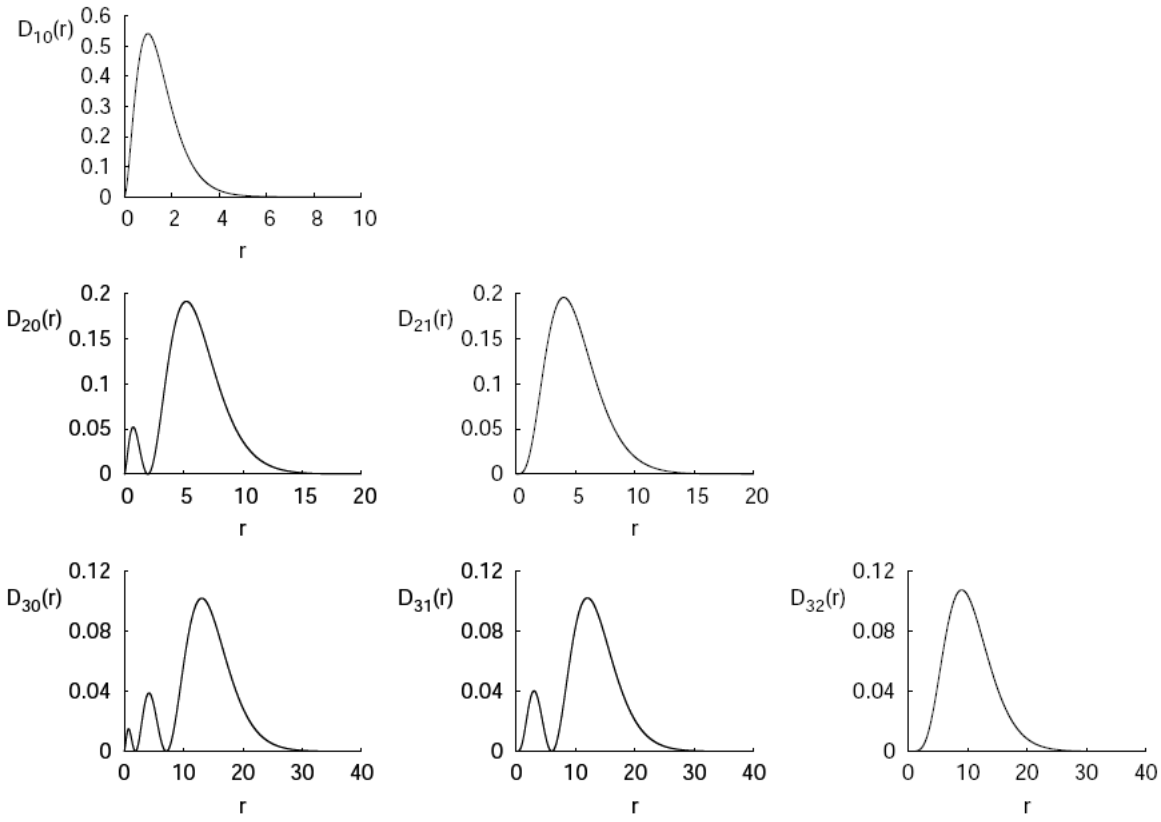

FIGURE 7.5: Radial distribution $D_{n,l} = R^2_{n,l}(r)r^2$ of all the electronic orbitals corresponding to the three lowest energy levels of Hydrogen. Atomic units have been used.

extrapolation of the graphs corresponding to the angular densities $\Theta_{l,m}(\theta)$ contained in Figure 7.6, shows that when l is fixed and $|m|$ increases, both the gradient content and spreading of this density decrease while the average height and the probability concentration around its centroid are roughly constant. Therefore, the Fisher-Shannon and Cramér-Rao ratios have a similar decreasing behaviour as shown in Figure 7.7 although with a stronger rate in the former case, because its two ingredients (Fisher information and Shannon entropic power) contribute constructively while in the Cramér-Rao case, one of the components (namely, the variance) does not contribute at all. Keep in mind, by the way, that the relations (7.61) and (7.62) show that the total variance does not depend on m and the Fisher information linearly decreases as $|m|$ increases, respectively. On the other hand, Figure 7.6 shows that the angular average height increases while the spreading decreases so that the overall combined contribution of these two ingredients to the LMC complexity remains roughly constant and very small when $|m|$ varies; in fact, $\zeta_{LMC}(20, 17, m)$ parabolically decreases from 1 to 0.6 when $|m|$ varies from 0 to 17.

In Figure 7.8 it is shown that the Fisher-Shannon and Cramér-Rao measures have a concave decreasing shape and the LMC complexity turns out to be comparatively constant for the orbital $(n = 20, l, m = 1)$ with arbitrary orbital quantum number l. We can

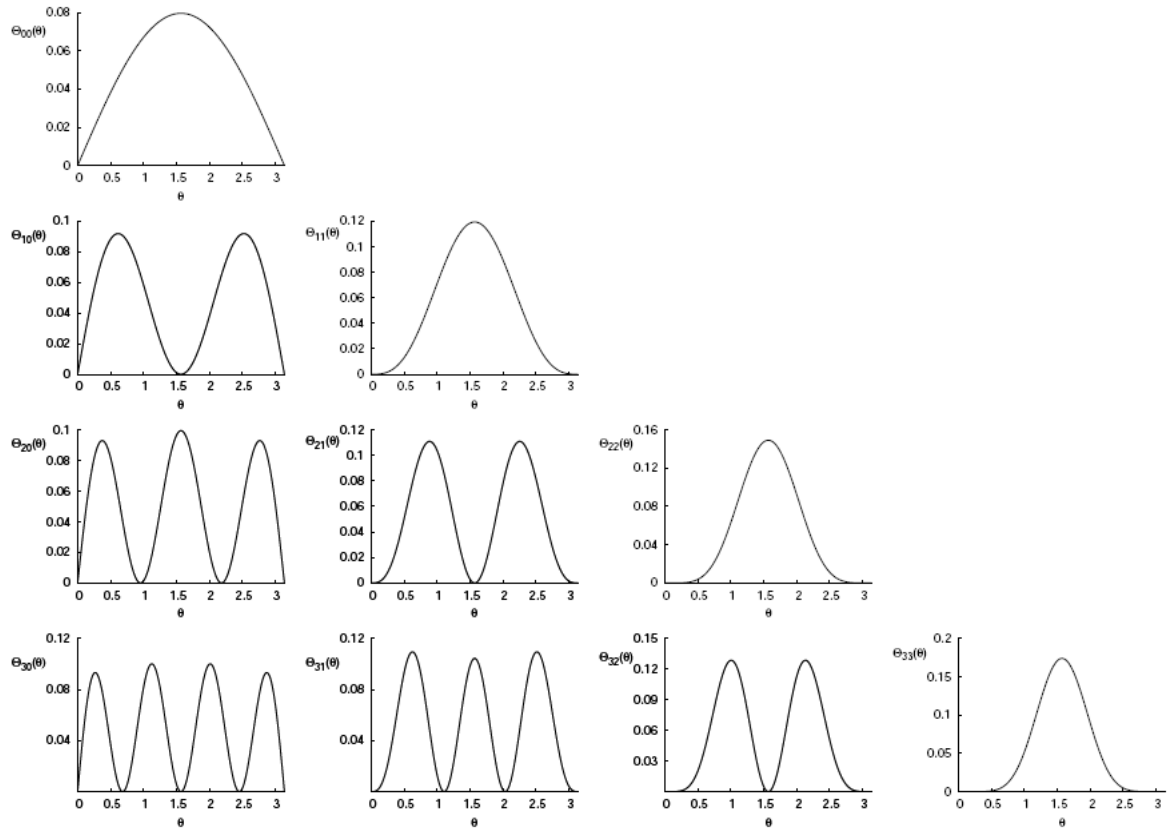

FIGURE 7.6: Angular distribution $\Theta_{l,m}(\theta) = |Y_{l,m}(\theta,\varphi)|^2 \sin\theta$ of all electronic orbitals corresponding to the four lowest lying energy levels of Hydrogen. Atomic units are used.

understand these phenomena by taking into account the graphs, duly extrapolated, of the rows of Figure 7.5 and the columns of Figure 7.6 where the radial density for fixed n and the angular density for fixed m are shown. Herein we realize that when l increases, (a) the radial gradient content decreases while the corresponding angular quantity increases, so that the gradient content of the total density $\rho(\vec{r})$ does not depend on l in accordance to its Fisher information as given by Eq. (7.62); (b) the radial and angular spreadings have decreasing and constant behaviours, respectively, so that the overall effect is that the Shannon entropic power of the total density $\rho(\vec{r})$ increases, (c) both the radial and the angular average height increase, so that the total averaging density $\rho(\vec{r})$ increases, and a similar phenomenon occurs with the concentration of the radial and angular probability clouds around their respective mean value, so that the total variance $V[\rho]$ decreases very quickly (as Eq. (7.61) analytically shows). Taking into account these observations into the relations (7.60), (7.65) and (7.74) which define the three composite information-theoretic measures under consideration, we can immediatly explain the decreasing dependence of the Fisher-Shannon and Cramér-Rao measures on the orbital quantum number as well as the approximate constancy of the LMC complexity, as illustrated in Figure 7.8; in fact, $\zeta_{LMC}(20,l,1)$ also decreases but within the

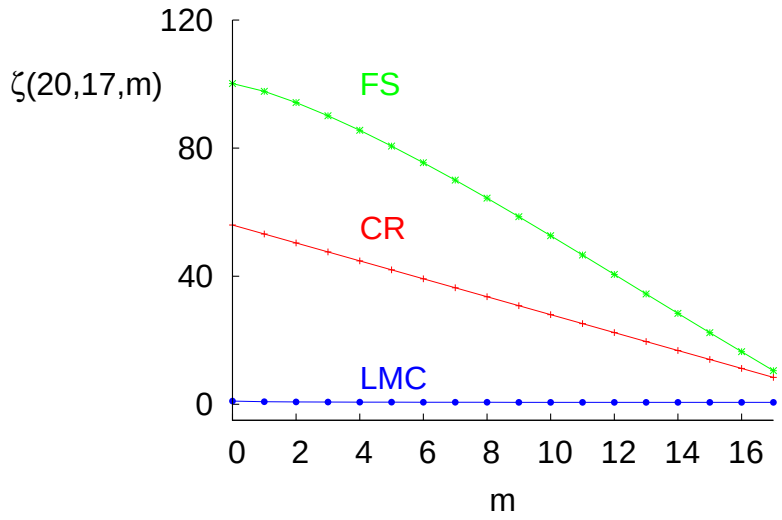

FIGURE 7.7: Relative Fisher-Shannon $\zeta_{FS}(20,17,m)$, Cramér-Rao $\zeta_{CR}(20,17,m)$ and *LMC* $\zeta_{LMC}(20,17,m)$ ratios of the manifold of hydrogenic levels with $n = 20$ and $l = 17$ as a function of the magnetic quantum number m. See text.

narrow interval $(1, 0.76)$ when l goes from 0 to 19.

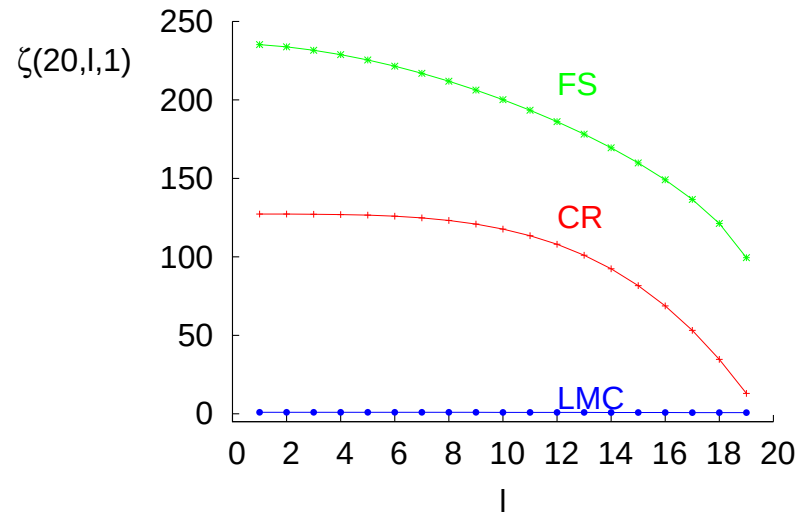

FIGURE 7.8: Relative Fisher-Shannon $\zeta_{FS}(20,l,1)$, Cramér-Rao $\zeta_{CR}(20,l,1)$ and LMC $\zeta_{LMC}(20,l,1)$ ratios of the hydrogenic states with $n = 20$ and $m = 1$ as a function of the orbital quantum number l. See text.

For completeness, we have numerically studied the dependence of the Fisher-Shannon measure on the principal quantum number n. We have found the accurate fit

$$C_r(FS)\,(n,l,m) = a_{lm}n^2 + b_{lm}n + c_{lm}$$

where the parameters a,b,c are given in Table 7.1 for two particular states with the corresponding correlation coefficient R of each fit. It would be extremely interesting to

	a	b	c	R
$C_r(FS)\,(n,0,0)$	0.565	1.202	-1.270	0.999996
$C_r(FS)\,(n,3,1)$	0.451	0.459	-4.672	0.999998

TABLE 7.1: Fit of the Fisher-Shannon measure for the hydrogenic orbitals $(n,l,m) = (n,0,0)$ and $(n,3,1)$

show this result from Eqs. (7.65)-(7.66) in a rigorous physico-mathematical way, what remains as an open problem which will we afforded elsewhere.

7.2.2 Upper bounds to the Fisher-Shannon and LMC complexities

We have seen previously that, contrary to the Cramér-Rao measure which expression can be calculated explicitly in terms of the quantum numbers (n,l,m), the Fisher-Shannon and the LMCcomplexities, Eqs. (7.65) and (7.74) respectively, have not yet been explicitly found. This is mainly because one of their two factors (namely, the Shannon entropic power) has not yet been determined analytically in terms of the quantum numbers. Here we will obtain rigorous upper bounds to these two composite information-theoretic measures in terms of the three quantum numbers of a generic hydrogenic orbital. Nevertheless, variational bounds to this information-theoretic quantity have been found [44, 49, 51] by means of one and two radial expectation values. In particular the upper bound

$$S\left[\rho\right] \leqslant \ln\left[8\pi\left(\frac{e\left\langle r\right\rangle}{3}\right)^{3}\right], \tag{7.78}$$

in terms of $\langle r\rangle$ is known, as a particular case of that $\langle r^{\alpha}\rangle$ with for arbitrary $\alpha > 0$

Then, taking into account that the expectation value $\langle r\rangle$ of the hydrogenic orbital (n,l,m) is given [156, 317] by

$$\left\langle r\right\rangle = \frac{1}{2Z}\left[3n^{2} - l(l+1)\right], \tag{7.79}$$

the bound on $S\left[\rho\right]$ reads as

$$S\left[\rho\right] \leqslant \ln\left\{\frac{\pi e^{3}}{27Z^{3}}\left[3n^{2} - l(l+1)\right]^{3}\right\}. \tag{7.80}$$

Now, from Eqs. (7.65), (7.74) and (7.80), we finally obtain the upper bounds

$$C_r(FS) \leqslant B_{FS} \equiv \frac{2e}{9\pi^{1/3}}\frac{n-|m|}{n^{3}}\left[3n^{2} - l(l+1)\right]^{2}, \tag{7.81}$$

to the Fisher-Shannon measure, and

$$C_r(LMC) \leqslant B_{LMC} = \frac{\pi e^{3}}{27}\left[3n^{2} - l(l+1)\right]^{3} \times D(n,l,m), \tag{7.82}$$

to the LMCcomplexity. It is worth noting that these two inequalities saturate at the ground state, having the values $\frac{2e}{\pi^{1/3}}$ and $\frac{e^3}{8}$ for the Fisher-Shannon and LMCcomplexity cases, respectively, when $n = 1$, $l = 0$, and $m = 0$.

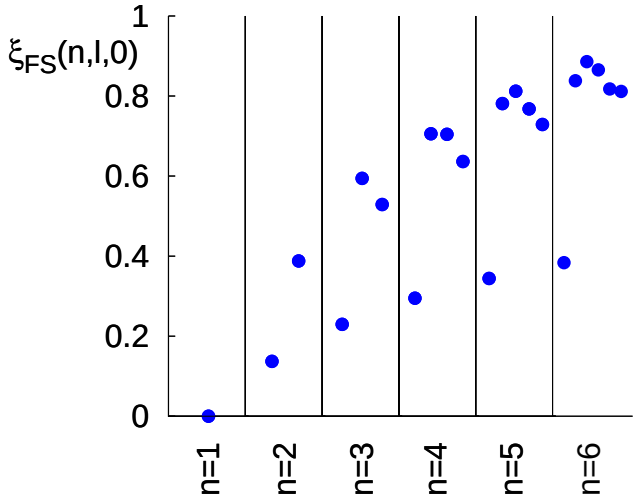

FIGURE 7.9: Dependence of the Fisher-Shannon ratio, $\xi_{FS}(n, l, 0)$, on the quantum numbers n and l.

In order to analyze the accuracy of the previous bounds on complexities, we plot in Figure 7.9 and Figure 7.10 the ratios

$$\xi_{FS}(n, l, m) = \frac{B_{FS} - C_{FS}[\rho]}{C_{FS}[\rho]}, \tag{7.83}$$

and

$$\xi_{LMC}(n, l, m) = \frac{B_{LMC} - C_{LMC}[\rho]}{C_{LMC}[\rho]}, \tag{7.84}$$

for the Fisher-Shannon and the LMC complexity measures, respectively, in the case (n, l, m) for $n = 1, 2, 3, 4, 5$ and 6, and all allowed values of l. Various observations are apparent. First, the two ratios vanish when $n = 1$ indicating the saturation of the inequalities (7.81) and (7.82) just mentioned. Second, for a manifold with fixed n the greatest accuracy occurs for the s states. Moreover, the accuracy of the bounds decreases when l increases up to the centroid of the manifold and then it decreases. Finally, the Fisher-Shannon bound is always more accurate than the LMC one for any hydrogenic orbital.

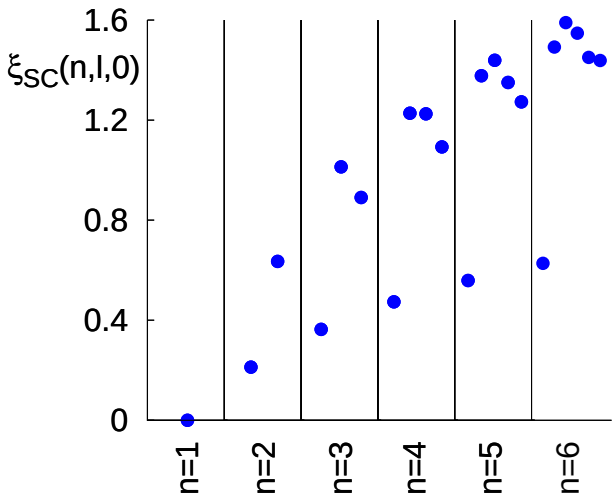

FIGURE 7.10: Dependence of the LMC complexity ratio, $\xi_{LMC}(n, l, 0)$, on the quantum numbers n and l.

7.3 Relativistic Klein-Gordon single-particle systems

Recently, the use of information-theoretical methods have been extended to take into account the relativistic effects in atomic physics. Relativistic quantum mechanics [321] tells us that special relativity provokes spatial modifications (severe at times) of the electron density of many-electron systems [283, 322–325], what produces fundamental and measurable changes in their physical properties. The qualitative and quantitative evaluation of the relativistic modification of the spatial redistribution of the electron density of ground and excited states in atomic and molecular systems by information-theoretic means is a widely open field. In the recent years the relativistic effects of various single and composite information-theoretic quantities of the ground state of hydrogenic [325] and neutral atoms [283, 324] have been investigated in different relativistic settings.

First Borgoo et al [283] (see also Ref. [322]) found that, in a Dirac-Fock setting, the LMC or shape complexity of the ground-state atoms (i) has an increasing dependence on the nuclear charge (also observed by Katriel and Sen [325] in Dirac ground-state hydrogenic systems), (ii) manifests shell and relativistic effects, the latter being specially relevant in the disequilibrium component (which indicates that they are dominated by the innermost orbital). Also, Sañudo and López-Ruiz [324] (see also Ref. [323]) show a similar trend for both $LMC$and Fisher-Shannon complexities in a different setting which uses the fractional occupation probabilities of electrons in atomic orbitals instead of the continuous electronic wavefunctions; so, they use discrete forms for the information-theoretic ingredients of the complexities. Moreover, their results allow to identify the shell structure of noble gases and the anomalous shell filling of some specific elements;

this phenomenon is specially striking in the Fisher-Shannon case as the authors explicitly point out.

This Section contributes to this recent field with the quantification, by means of the Fisher-Shannon complexity, of the relativistic compression of both ground and excited states of the Klein-Gordon single-particle wavefunctions in a Coulombian well. This magnitude is used to quantify the relativistic charge spreading of Klein-Gordon particles moving in a Coulomb potential $V(\vec{r}) = -\dfrac{Ze^2}{r}$. We study the dependence of these quantities on the potential strength Z and on the quantum numbers (n, l, m) which characterize the stationary states of a spinless relativistic particle with a negative electric charge.

The Klein-Gordon wave equation was introduced in 1926 and constituted the first theoretical description of particle dynamics in a relativistic quantum setting [326–329]. Since then, the study of its properties for different potentials of various dimensionalities has been a subject of increasing interest [129, 330, 331]. Many efforts were addressed to obtain the spectrum of energy levels and the ordinary moments or expectation values $\langle r^k \rangle$ of the charge distribution of numerous single-particle systems (such as e.g. muonic and pionic atoms [332]). Only recently, Chen and Dong [330] have been able to obtain explicit expressions for these moments and some off-diagonal matrix elements of r^k for a Klein-Gordon single-particle of mass m_0 in the Coulomb potential $V(\vec{r}) = -\dfrac{Ze^2}{r}$. These authors, however, do not use the Lorentz-Invariant (LI) Klein-Gordon charge density

$$\rho_{LI}(\vec{r}) = \frac{e}{m_0 c^2} \left[\epsilon - V(r)\right] \left|\Psi_{nlm}(\vec{r})\right|^2, \tag{7.85}$$

but instead the Non-Lorentz-Invariant (NLI) expression $\rho_{NLI}(\vec{r}) = \left|\Psi_{nlm}(\vec{r})\right|^2$ as in the non-relativistic case, where ϵ and $\Psi(\vec{r})$ denote the physical solutions of the Klein-Gordon equation [129, 330]

$$\left[\epsilon - V(r)\right] \psi(\vec{r}) = (-\hbar^2 c^2 \nabla^2 + m_0^2 c^4)\psi(\vec{r}), \tag{7.86}$$

which characterizes the wavefunctions $\Psi_{nlm}(\vec{r}, t) = \psi_{nlm}(\vec{r}) exp\left(-\dfrac{i}{\hbar}\epsilon t\right)$ of the stationary states of our system. In spherical coordinates $\vec{r} = (r, \theta, \phi)$, the eigenfunction is given by $\psi(r, \theta, \psi) = r^{-1} u(r) Y_{lm}(\theta, \phi)$, where the Y-symbol denotes the spherical harmonics of order (l, m). Performing the change $r \to s$, with $s = \beta r$ in Eq. (7.86), and using the notations

$$\beta \equiv \frac{2}{\hbar c}\sqrt{m_0^2 c^4 - \epsilon^2}; \qquad \lambda \equiv \frac{2\epsilon Z e^2}{\hbar^2 c^2 \beta}, \tag{7.87}$$

one has the radial Klein-Gordon equation

$$\frac{d^2 u(s)}{ds^2} - \left[\frac{l'(l'+1)}{s^2} - \frac{\lambda}{s} + \frac{1}{4}\right] u(s) = 0, \tag{7.88}$$

where the following additional notations

$$l' = \sqrt{\left(l+\frac{1}{2}\right)^2 - \gamma^2} - \frac{1}{2}, \qquad \text{with} \quad \gamma \equiv Z\alpha, \tag{7.89}$$

have also been used, being the fine structure constant $\alpha \equiv \dfrac{e^2}{\hbar c}$. It is known [129] that the bound states have the energy eigenvalues

$$\epsilon = \frac{m_0 c^2}{\sqrt{1+\left(\frac{\gamma}{n-l+l'}\right)^2}}, \tag{7.90}$$

and the eigenfunctions

$$u_{nl}(s) = \mathscr{N} s^{(l'+1)} e^{-\frac{s}{2}} \widetilde{L}^{2l'+1}_{n-l-1}(s). \tag{7.91}$$

To preserve Lorentz invariance, according to the relativistic quantum mechanics [321], we calculate the constant $\mathscr{N}$ by taking into account the charge conservation $\displaystyle\int_{\mathbb{R}^3} \rho(\vec{r}) d^2 r = e$, which yields the value [333]

$$\mathscr{N}^2 = \frac{m_0 c^2 \gamma}{\hbar c} \frac{1}{(n+l'-l)^2+\gamma^2}. \tag{7.92}$$

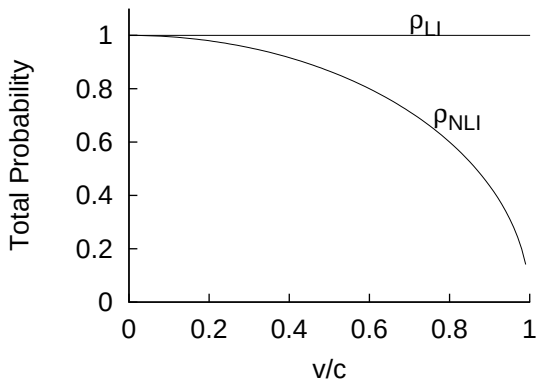

FIGURE 7.11: Normalization of the charge density for the Lorentz invariant (LI) and the non-Lorentz invariant (NLI) charge densities

Let us emphasize that the resulting Lorentz-invariant charge density $\rho_{LI}(\vec{r})$ given by Eqs. (7.85)-(7.92) is always (i.e., for any observer's velocity v) appropriately normalized, while the non-Lorentz-invariant density $\rho_{NLI}(\vec{r})$ used by Cheng and Dong [330] is not. This is numerically illustrated in Figure 7.11 for a pionic atom with nuclear charge $Z = 68$ in the infinite nuclear mass approximation (π^- -meson mass=273.132054 a.u.).

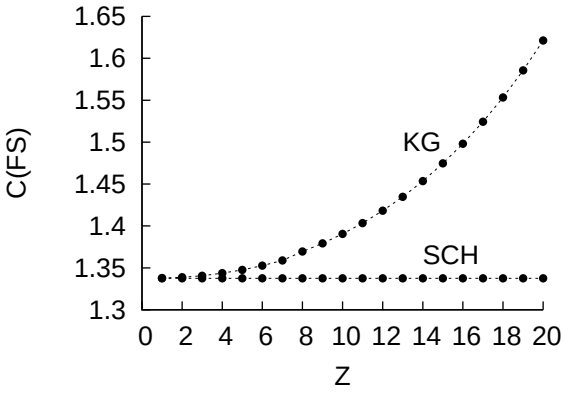

FIGURE 7.12: Fisher-Shannon complexity for the ground state Klein-Gordon (KG) and Schrödinger (SCH) pionic atom in terms of the nuclear charge Z (atomic units are used).

Let us now numerically discuss the relativistic effects in the Fisher-Shannon complexity for a pionic system. First, we center our attention in the dependence on the nuclear charge of the system. As we can observe in Figure 7.12, the Fisher-Shannon complexity of the Klein-Gordon case depends on the nuclear charge Z, contrary to the non-relativistic description. The Schrödinger or non-relativistic value of the Fisher-Shannon complexity has been recently shown to be independent of the nuclear charge Z for any hydrogenic system, (see Eqs. (6.13)-(6.15) of Chapter 6). It is apparent that this quantity is a very appropriate indicator of the relativistic effects as has been recently pointed out by Sañudo and López-Ruiz [323, 324] in other relativistic settings. These effects becomes bigger when the nuclear charge increases, so the relativistic Fisher-Shannon complexity enhances. This behaviour is easy to understand because, when we take into account the relativistic effects, the charge probability density is more compressed towards the nucleus than in the non-relativistic case [321, 333].

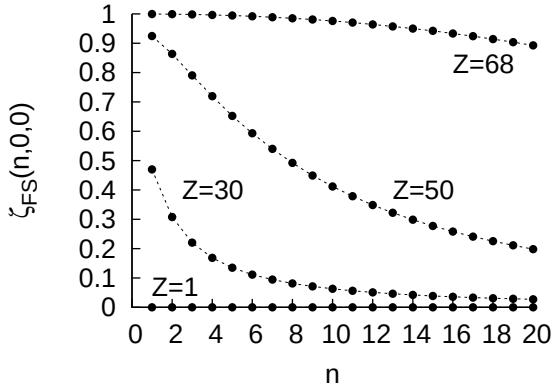

FIGURE 7.13: Relative Fisher-Shannon complexity for various ns-states of the Klein-Gordon and Schrödinger pionic atom.

To measure the relativistic effects we define the relative quantity $\zeta_{\rm FS} = 1 - \dfrac{C_{SCH}(FS)}{C_{KG}(FS)}$. This quantity varies from 0 to 1, so that $\zeta_{\rm FS} \sim 0$ when the relativistic effects are negligible and $\zeta_{\rm FS} \sim 1$ in the ultrarelativistic limit. In Figure 7.13 we can see the effects of the relativistic model for different values of the nuclear charge Z and various ns-states $(n, 0, 0)$.

First, we observe that the relativistic effects grow when the nuclear charge increases, not only for the ground state (as already pointed out) but also for all the excited states. Second, the relativistic effects decrease when the principal quantum number increases. Third, this decreasing behaviour with n has a strong dependence on Z, the decrease becoming slower as bigger is the nuclear charge.

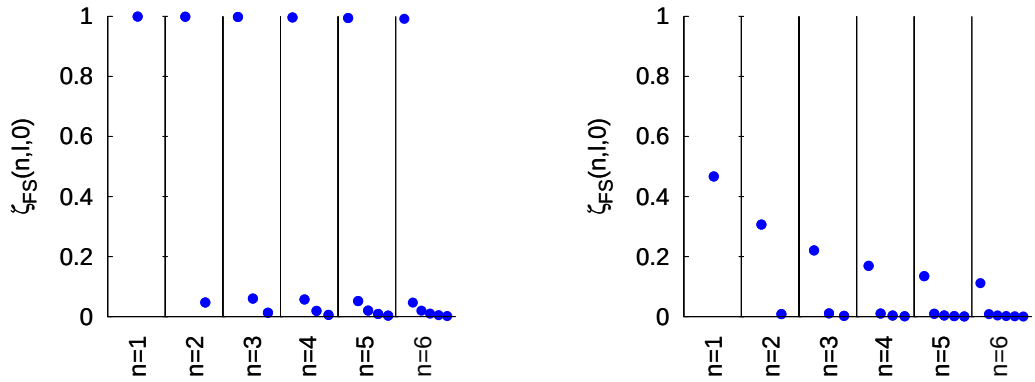

FIGURE 7.14: Relative Fisher-Shannon complexity for various states $(n, l, 0)$ of the Klein-Gordon and Schrödinger pionic atoms with $Z = 68$ (left) and $Z = 30$ (right).

In Figure 7.14 we can observe that the relativistic effects are practically negligible (points at the bottom) when the angular quantum number is different from zero even for large nuclear charge. This dependence on l is quantitatively more important than the dependence on the principal quantum number n.

Finally in Figure 7.15 we show the relative behaviour of the LMC complexity in the non-relativistic and relativistic Klein-Gordon cases in terms of the orbital quantum number l for various states $(n,\ l,\ 0)$ with fixed n. This behaviour is similar to that of the Fisher-Shannon case shown in Figure 7.14. Again, we observe that the relativistic effects are negligible for l other than 0, even for atoms with a large nuclear charge.

For completeness, let us point out that the relativistic effects are practically independent of the magnetic quantum number m for (Z, n, l) fixed.

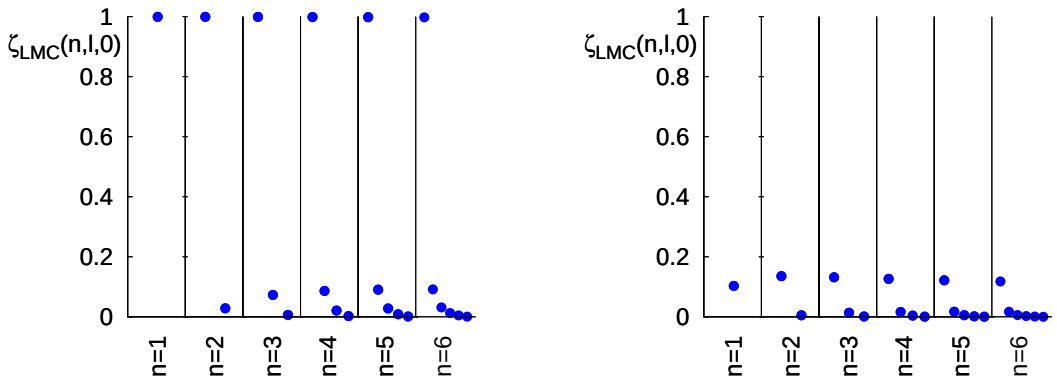

FIGURE 7.15: *LMC* complexity for various states $(n, l, 0)$ of the Klein-Gordon and Schrödinger pionic atoms with $Z = 68$ (left) and $Z = 30$ (right).

7.4 Conclusions

Firstly, in Section 7.1 the *LMC* shape complexity of the hydrogenic system in *d*-dimensional position and momentum spaces has been investigated. We have seen that the determination of the analytical expression of this complexity is a formidable open task, mainly because the analytical evaluation of the entropic functionals of the Laguerre and Gegenbauer polynomials, $E_1\left[\tilde{L}_k^{\alpha}\right]$ and $E_2\left[\tilde{C}_k^{\alpha}\right]$, involved in the calculation of the Shannon entropy, has not yet been accomplished. The general methodology presented here is used to find explicit expressions for the position and momentum complexities of the ground and circular states in terms of the dimensionality and the principal quantum number. Then, these information-theoretic quantities are numerically discussed for various states and dimensionalities as well as for the dimensional and high-lying energy (Rydberg) limits. Briefly, we find that both position and momentum complexities increase (decrease) when the dimensionality (the quantum number of the state) increases. This phenomenon is the result of a delicate balance of the average height and the bulk spreading of the system given by their two information-theoretic ingredients, the disequilibrium and the entropic power, respectively. Finally, the uncertainty product of the position and momentum *LMC* shape complexities is examined.

In Section 7.2, we particularized the *d*-dimensional problem to $d = 3$ studing the complexity measures for the hydrogenic atoms in three dimensions. We have investigated both analytically and numerically the complexity of hydrogenic atoms which gives rise to the great diversity of three-dimensional geometries for its configuration orbitals (n, l, m). This is done by means of the Fisher-Shannon, the Cramér-Rao and the *LMC* complexities. After analyzing the dependence of these three composite quantities in terms of the quantum numbers n, l and m, it is found that: (i) when (l, m) are fixed, all complexities have an increasing behaviour as a function of the principal quantum number n, with a rate of growth which is higher in the Cramér-Rao and (even more relevant)

Fisher-Shannon cases; this is mainly because of the increasingly strong radial oscillating nature (when n gets bigger), what is appropriately grasped by the Fisher ingredient of these two composite quantities; (ii) the three complexities decrease when the magnetic quantum number $|m|$ increases, and the decreasing rate is much faster in the Cramér-Rao case and more emphatically in the Fisher-Shannon case; this is basically due to the increasingly weak angular oscillating nature when $|m|$ decreases, what provokes the lowering of the Fisher ingredient of these two quantities; and (ii) all of them decrease when the orbital quantum number l is increasing, and again , the decreasing rate is much faster in the Cramér-Rao and Fisher-Shannon cases; here, however, the physical interpretation is much more involved as it is duly explained in subsection 7.2.1. Finally, in subsection 7.2.2, we have used some variational bounds to the Shannon entropy to find sharp, saturating upper bounds to the Fisher-Shannon measure and to the LMC complexity.

In Section 7.3, we have explored relativistic effects on the behaviour of the Fisher-Shannon complexity of pionic systems with nuclear charge Z in the Klein-Gordon framework. We have done it for both ground and excited states. First we found that the relativistic Fisher-Shannon complexity grows when the nuclear charge increases in contrast with its constancy in the non-relativistic case for both ground and excited states. A similar behaviour has been recently observed in the case of the ground state of systems governed by the Dirac equation [283, 322–324]. We found that this trend remains for excited states in a damped way, so that the relativistic effects enhance with Z for a given (n, l, m) state and, for a given Z, decrease when the principal and/or orbital quantum numbers are increasing. Let us also highlight that the non-relativistic limits at large principal quantum number n for a given Z (see Figs. 7.15) and at small values of Z (see Fig. 7.12) are reached. On the other hand it is pertinent to underline that the finite nuclear volume effects are very tiny for any information-theoretic and complexity measure because of their macroscopic character.

Let us remind finally that we have also investigated the relativistic Klein-Gordon effects in pionic atoms by means of the LMC shape complexity [91] $C(LMC) = D[\rho] \times \exp S[\rho]$. We found that the relativistic effects are also identified by this quantity but more slightly as compared to the Fisher-Shannon complexity $C(FS)$. Apparently this is because of the property of locality of $C(FS)$ coming through its gradient-dependent Fisher ingredient, which graphs much better the (strong) oscillatory condition of the pionic densities.

Chapter 8

Molecular complexity

The goal of this Chapter is to perform an information-theoretical analysis by use of complexity measures in order to analyze and quantify the information content of a set of ninety two molecular systems of different chemical type. Focus will be set on the recognition of patterns of uncertainty, order, and organization by employing several molecular properties such as energy, ionization potential, hardness and electrophilicity. Different complexity measures and informational planes of those molecules will be analyzed in terms of their chemical properties, number of electrons or geometrical features.

The organization of these Chapter is as follows: in Section 8.1 we defined the complexity measures along with their information-theoretic components and the chemical properties considered throughout the study. In Section 8.2 we compute information measures as well as the Fisher-Shannon and the LMC complexities. These information quantities are computed in position and momentum spaces, as well as in the joint product space that contains more complete information about the system. Additionally, the Fisher-Shannon $(I - J)$ and the disequilibrium-Shannon $(D - L)$ planes are studied to identify pattern and organization.

8.1 Information-theoretic measures, complexities and chemical properties

In the independent-particle approximation the total density distribution in a molecule is a sum of contributions from electrons in each of the occupied orbitals. This is the case in both $r-$ and $p-$space, position and momentum spaces respectively. In momentum space, the total electron density, $\gamma(\vec{p})$, is obtained through the molecular momentals (momentum-space orbitals) $\varphi_i(\vec{p})$, and similarly for the position-space density, $\rho(\vec{r})$, through the molecular position-space orbitals $\phi_i(\vec{r})$. The momentals can be obtained by

three-dimensional Fourier transforma of the corresponding orbitals, and conversely:

$$\varphi_i(\vec{p}) = (2\pi)^{-3/2} \int d\vec{r} \exp\left(-i\vec{p}\cdot\vec{r}\right) \phi_i(\vec{r}) \tag{8.1}$$

Standard procedures for performing the Fourier transform of position space orbitals generated by ab-initio methods have been described [213]. The orbitals employed in ab-initio methods are linear combinations of atomic basis functions and since analytic expressions are known for the Fourier transforms of such basis functions [214], the transformations of the total molecular electronic wavefunction from position to momentum space is computationally straightforward [215].

As we defined in Chapter 5, the LMC complexity is given by:

$$C_r(LMC) = D_r \times e^{S_r} = D_r \times L_r, \tag{8.2}$$

in position space, where D_r is the disequilibrium, and also the exponential entropy $L_r = e^{S_r}$ is defined. Similar expressions for the LMC complexity measure in the conjugated momentum space might be defined for a distribution $\gamma(\vec{p})$:

$$C_p(LMC) = D_p \times e^{S_p} = D_p \times L_p. \tag{8.3}$$

The FS complexity in position space, $C_r(FS)$, is defined as

$$C_r(FS) = I_r \times J_r, \tag{8.4}$$

and similarly

$$C_p(FS) = I_p \times J_p, \tag{8.5}$$

in momentum space.

Aside of the analysis of the position and momentum information measures, we have considered useful to study these magnitudes in the product, rp-space, characterized by the probability density $f(\vec{r},\vec{p}) = \rho(\vec{r})\gamma(\vec{p})$, where the complexity measures verify

$$C_{rp}(LMC) = D_{rp} \times L_{rp} = C_r(LMC) \times C_p(LMC), \tag{8.6}$$

and

$$C_{rp}(FS) = I_{rp} \times J_{rp} = C_r(FS) \times C_p(FS). \tag{8.7}$$

Last equality in both Eqs. (8.6) and (8.7) arise straightforwardly from the complexity definitions in the individual spaces.

From the above two equations, it is clear that the features and patterns of both LMC and FS complexity measures in the product space will be determined by those of each

conjugated space. However, the numerical analyses carried out in the next Section, reveal that the momentum space contribution plays a more relevant role as compared to the position one for the study of the molecular systems here considered.

With the purpose of organizing and characterizing the complexity features of the molecular systems under study, we have computed several reactivity properties such as the ionization potential (IP), the total dipole moment, the hardness (η) and the electrophilicity index (ω). These properties were obtained at the density functional theory (DFT) level, by use of the Janak's theorem [219], analogous to the Koopmans' theorem [218], for relating the first vertical ionization energy and the electron affinity to the HOMO and LUMO energies, which are necessary to calculate the conceptual DFT properties. The hardness (η) was obtained within this framework [101] through

$$\eta = \frac{1}{S} \sim \frac{\epsilon_{LUMO} - \epsilon_{HOMO}}{2} \tag{8.8}$$

where ϵ denotes the frontier molecular orbital energies and S the softness of the system. It is worth mentioning that the factor 1/2 in Eq. (8.8) was included originally to make symmetrical the hardness definition with the chemical potential [101, 334]

$$\mu = \left(\frac{\partial E}{\partial N}\right)_{v(\vec{r})} = \frac{\epsilon_{LUMO} + \epsilon_{HOMO}}{2}, \tag{8.9}$$

although it has been recently disowned it [335, 336]. In general terms, the chemical hardness and softness are good descriptor of chemical reactivity, i.e., whereas the former has been employed [217, 335, 336] as a measure of the reactivity of a molecule in the sense of the resistance to changes in its electron distribution, hence molecules with larger values of η are interpreted as less reactive molecules, the S index quantifies the polarizability of the molecule [220–223]; thus soft molecules are more polarizable and possess predisposition to acquire additional electronic charge [224]. The chemical hardness η is a central quantity for the study of reactivity through the hard and soft acids and bases principle [225–227].

The electrophilicity index [337], ω, allows a quantitative classification of the global electrophilic nature of a molecule within a relative scale. The electrophilicity index of a system in terms of its chemical potential and hardness is given by the expression

$$\omega = \frac{\mu^2}{2\eta} \tag{8.10}$$

The electrophilicity is also a useful descriptor of chemical reactivity, which quantifies the global electrophilic power of the molecules [224] (predisposition to acquire an additional electronic charge).

8.2 Complexity measures and information planes of molecular systems

The set of molecules chosen for the study includes different types of chemical organic and inorganic systems (aliphatic compounds, hydrocarbons, aromatic, alcohols, ethers, ketones). The set includes a variety of closed shell systems, radicals, isomers as well as molecules with heavy atoms such as sulphur, chlorine, magnesium and phosphorous. The geometries needed for the single point energy calculations above referred were obtained through experimental data from standard databases [338]. The molecular set might be organized by isoelectronic groups as follows (N is the number of electrons):
N-10: NH_3 (ammonia)
N-12: $LiOH$ (lithium hydroxide)
N-14: HBO (boron hydride oxide), Li_2O (dilithium oxide)
N-15: HCO (formyl radical), NO (nitric oxide)
N-16: H_2CO (formaldehyde), NHO (nitrosyl hydride), O_2 (oxygen)
N-17: CH_3O (methoxy radical)
N-18: CH_3NH_2 (methyl amine), CH_3OH (methyl alcohol), H_2O_2 (hydrogen peroxide), NH_2OH (hydroxylamine)
N-20: $NaOH$ (sodium hydroxide)
N-21: BO_2 (boron dioxide), C_3H_3 (radical propargyl), $MgOH$ (magnesium hydroxide), $HCCO$ (ketenyl radical)
N-22: C_3H_4 (cyclopropene), CH_2CCH_2 (allene), CH_3CCH (propyne), CH_2NN (diazomethane), CH_2CO (ketene), CH_3CN (acetonitrile), CH_3NC (methyl isocyanide), CO_2 (carbon dioxide), FCN (cyanogen fluoride), HBS (hydrogen boron sulfide), $HCCOH$ (ethynol), $HCNO$ (fulminic acid), HN_3 (hydrogen azide), $HNCO$ (isocyanic acid), $HOCN$ (cyanic acid), N_2O (nitrous oxide), NH_2CN (cyanamide)
N-23: NO_2 (nitrogen dioxide), NS (mononitrogen monosulfide), PO (phosphorus monoxide), C_3H_5 (allyl radical), CH_3CO (acetyl radical)
N-24: C_2H_4O (ethylene oxide), C_3H_6 (cyclopropane), CF_2 (difluoromethyleeletrone), CH_2O_2 (dioxirane), C_2H_5N (aziridine), CH_3CHO (acetaldehyde), $CHONH_2$ (formamide), FNO (nitrosyl fluoride), H_2CS (thioformaldehyde), $HCOOH$ (formic acid), HNO_2 (nitrous acid) $NHCHNH_2$ (aminomethanimine), O_3 (ozone), SO (sulfur monoxide)
N-25: $CH_2CH_2CH_3$ (npropyl radical), CH_3CHCH_3 (isopropyl radical), CH_3OO (methylperoxy radical), FO_2 (dioxygen monofluoride), NF_2 (difluoroamino radical), CH_3CHOH (ethoxy radical), CH_3S (thiomethoxy)
N-26: C_3H_8 (propane), $CH_3CH_2NH_2$ (ethylamine), CH_3CH_2OH (ethanol), CH_3NHCH_3 (dimethylamine), CH_3OCH_3 (dimethyl ether), CH_3OOH (methyl peroxide), F_2O (difluorine monoxide)
N-30: $ClCN$ (chlorocyanogen), OCS (carbonyl sulfide), SiO_2 (silicon dioxide)
N-31: PO_2 (phosphorus dioxide), PS (phosphorus sulfide)

N-32: $ClNO$ (nitrosyl chloride), S_2 (sulfur diatomic), SO_2 (sulfur dioxide)
N-33: ClO_2 (chlorine dioxide), $OClO$ (chlorine dioxide)
N-34: CH_3CH_2SH (ethanethiol), CH_3SCH_3 (dimethyl sulfide), H_2S_2 (hydrogen sulfide), SF_2 (sulfur difluoride)
N-38: CS_2 (carbon disulfide)
N-40: CCl_2 (dichloromethylene), S_2O (sulfur monoxide)
N-46: $MgCl_2$ (magnesium dichloride)
N-48: S_3 (sulfur trimer), $SiCl_2$ (dichlorosilylene)
N-49: ClS_2 (sulfur chloride)

The electronic structure calculations performed in the present study for the whole set of molecules were carried out with the Gaussian 03 suite of programs [229] at the CISD/6-311++G(3df,2p) level of theory. For this ser of molecules we have calculated all information and complexity measures in both position and momentum spaces as well as in the product space by employing the necessary software along with 3D numerical integration routines [230, 231] and the DGRID suite of programs [215]. As mentioned above, the values of the conceptual DFT properties have been obtained at the B3LYP/6-311++G(3df,2p) level of theory. All calculated quantities in this study are given in atomic units, their values might be consulted in the supplementary material: Table B.1 (molecular properties), Table B.2 (complexity measures) and Table B.3 (information plane measures) in the Appendix B.

8.2.1 Complexity measures

In contrast with the atomic case, where the complexities possess a high level of natural organization provided by periodical properties [305, 306], the molecular case requires some sort of organization which could be affected by many factors (structural, energetic, entropic, etc). So that we have analyzed the molecular complexities $C(LMC)$ and $C(FS)$ as functions of the main chemical properties of interest, i.e., the total energy, the dipole moment, the ionization potential, the hardness and the electrophilicity, establishing a link between the different complexity measures and the chemical properties so as to provide an insight into their organization, order and uncertainty features.

In Figure 8.1, we have plotted the $C(FS)$ and $C(LMC)$ as a function of the total energy of the molecules in the product space (rp). Firstly, it may be observed from this Figure that both complexity measures in this space possess a similar behavior. Secondly, a general trend is observed in that molecules with higher energy correspond to higher complexity values, for both $C(LMC)$ and $C(FS)$, as compared to the ones which possess lower energies. Note that, regarding the set of molecules studied in this work, they are grouped together according to four energy intervals: $E > -400$, $E \in [-700, -400]$, $E \in [-1000, -700)$, and $E < -1000$. In this Figure we have labeled the molecules which correspond to the maximum and minimum values of $C_{rp}(FS)$ within each group,

noting that they coincide with the corresponding extremal $C_{rp}(LMC)$ values. It is worth noting that the maximum values correspond with molecules that contain one heavy atom at least, and that the minimum complexities correspond with molecules having similar chemical geometry.

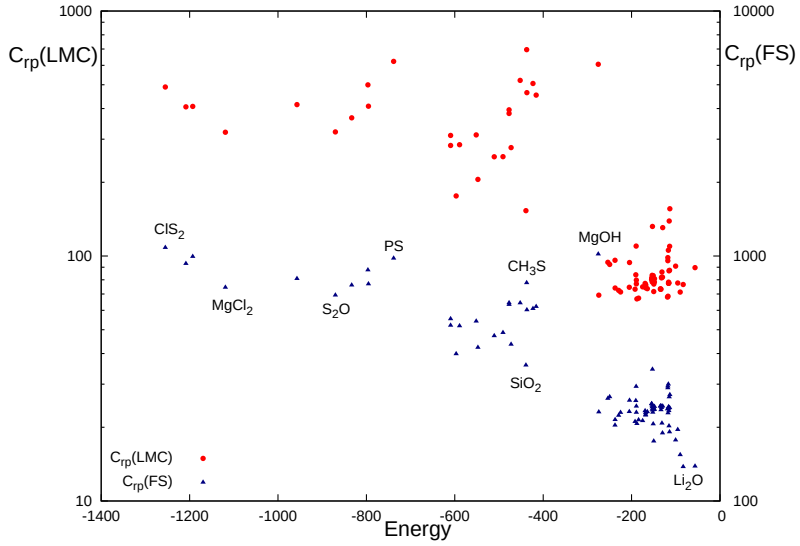

FIGURE 8.1: $C(LMC)$ (red circles) and $C(FS)$ (blue triangles) complexities as a function of the total energy for the set of ninety two molecules in the product space (rp). Atomic units are used.

In view of the results shown in this Figure it seems that the molecular complexity is also affected by several other chemical factors, such as the molecular structure (e.g. lower complexity values in each group, energy-wise, corresponds with molecules of similar geometry), composition (e.g. higher complexity corresponds with molecules containing heavy atoms), chemical functionality, reactivity, etc. Note that each complexity consists of two factors, one of them always defined in terns of the Shannon entropy S, whereas the other characterizes more specifically the corresponding complexity measure in terms of a global quantity (disequilibrium D) for $C_{rp}(LMC)$ and a local one (Fisher information I) for $C_{rp}(FS)$. Nevertheless, there are no relevant structural differences between both complexities, based either on D or I.

In Figure 8.2 we have plotted the complexity values for the $C_{rp}(LMC)$ and $C_{rp}(FS)$ measures as a function of the number of electrons in the product space (note that both complexities measures are in a double-X axes). We may observe from Figure 8.2 that both complexity measures behave in a similar fashion, i.e., molecules with lower number of electrons ($N < 26$) possess low complexities whereas molecules with larger number of electrons ($N > 26$) possess larger complexity values. A few exceptions may be noticed from Figure 8.2, i.e., molecules with low number of electrons and higher complexities correspond to those containing heavier atoms: CH_3S, $MgOH$, NS and HBS for $C_{rp}(LMC)$, and, $MgOH$ and CH_3S for $C_{rp}(FS)$, as also observed before

when discussing the analysis based on the total energy. It is worth mentioning, similarly to the case of the results in Figure 8.1, that several other factors may affect the molecular complexities as it was discussed above.

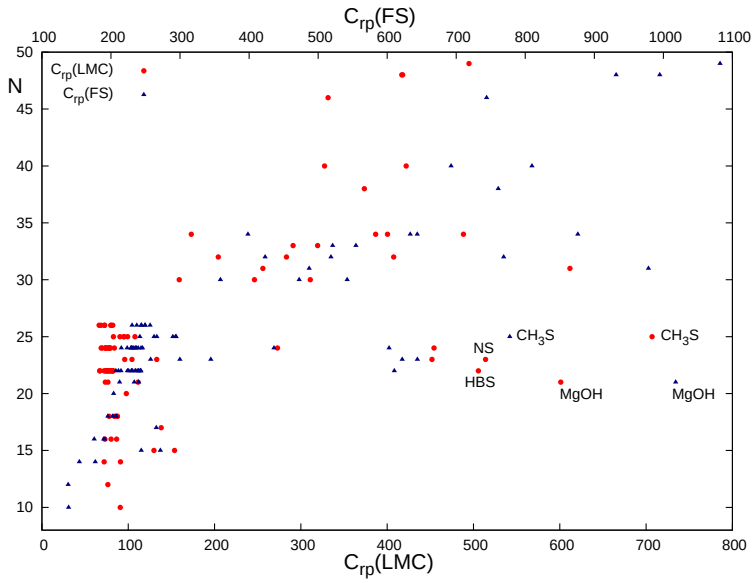

FIGURE 8.2: $C(LMC)$ (red circles) and $C(FS)$ (blue triangles) complexity as a function of the number of electrons (N) for the set of ninety two molecules in the product space (rp). Atomic units are used.

In order to analyze the influence of the chemical reactivity on the complexities for the set of studied molecules, we have plotted in Figure 8.3 the hardness values versus the LMC and FS complexities in the product space (rp) for those molecules. The general observations are that the LMC and FS complexities behave in the same way, both indicating a clear relationship with the hardness and hence with the chemical reactivity of the molecules. Besides, it might be observed that as the hardness increases, the complexity values decrease. This fact illustrates that molecules which are chemically more stable (resistant to changes in the electron distribution) possess low complexity values; thus the chemical reactivity seems to be directly related to the complexity in that higher values of $C(LMC)$ and $C(FS)$ correspond with more reactive systems, with very few exceptions which again correspond to molecules with heavier atoms as we mentioned before (CH_3S, PS, $MgOH$ for $C(LMC)$ and ClS_2, $MgOH$, S_3 for $C(FS)$). It is worth mentioning that a similar analysis for the dipole moment (in Table B.1 Appendix B) might be performed and so we note that molecules with higher complexity possess lower the dipole moment, hence corresponding to those that are more polarizable, and so the most reactive ones (which in this case correspond to those containing heavier atoms).

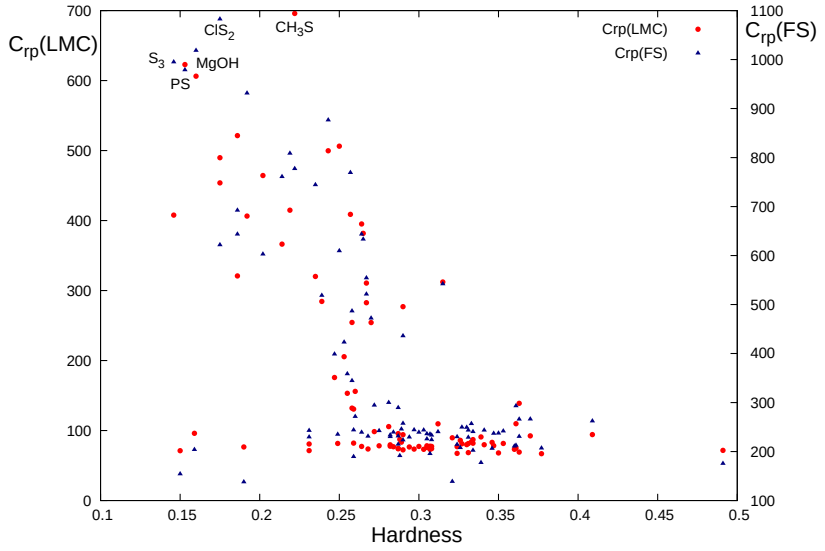

FIGURE 8.3: $C(LMC)$ (red circles) and $C(FS)$ (blue triangles) complexity as a function of the hardness for the set of ninety two molecules in the product space (rp). Atomic units are used.

The ionization potential (IP) is now employed as an indicator of the chemical stability of the molecules, analyzing the relation among their IP and the complexities. In Figure 8.4 it may be observed that molecules with higher IP values (more stable ones) are located at the right-hand-side of the Figure, indicating that stability is related to the molecular complexities in that higher LMC and FS complexities correspond to more reactive molecules (which are less stable).

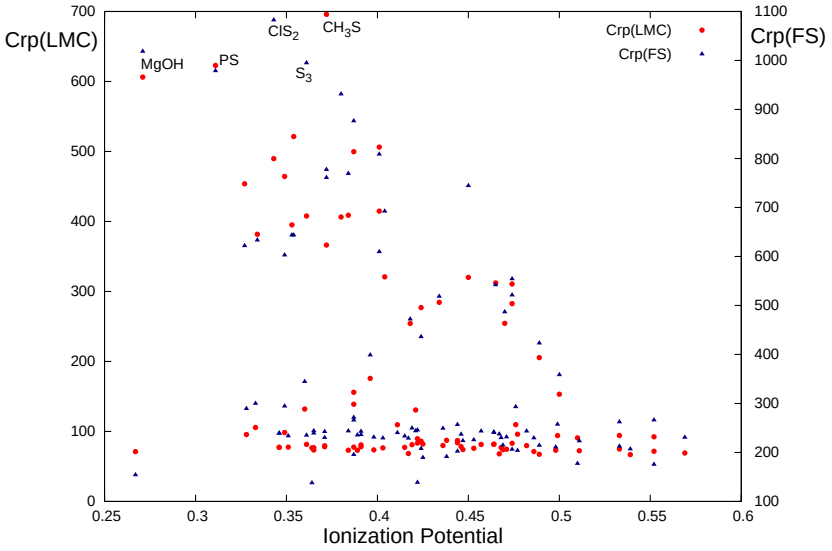

FIGURE 8.4: $C(LMC)$ (red circle) and $C(FS)$ (blue triangles) complexity as a function of the ionization potential for the set of ninety two molecules in the product space (rp). Atomic units are used.

The electrophilicity index is an useful indicator of chemical reactivity, quantifying the global electrophilic power of the molecules, as mentioned above. Thus, we have found interesting to study the complexities, $C(LMC)$ and $C(FS)$, as a function of the electrophilicity in the product space (see Table B.1 in Appendix B). In contrast with the other analyzed properties, the electrophilicity (affected by both the hardness and the chemical potential, see Eq. (8.10)), displays a more complicated behaviour in that molecules with lower values of complexity are associated with molecules possessing lower electrophilicity, except for the $NaOH$ molecule which is highly electropilic.

It is worthy to remark that all conclusions obtained from the analysis performed in the product space 'rp' remain valid also when considering the momentum space 'p' alone, while in position space the above discussed behaviours are not so relevant as compared to the momentum ones. Nevertheless, most of the structural features observed in the Figures are better displayed in the product than in the momentum space, as a consequence of the joint effect arising when dealing simultaneously with the position variable essentially by shifting away both complexities.

8.2.2 Information planes

In the search of pattern and organization we have analyzed the set of studied molecules, through features such as their energy and the number of electrons by plotting the contribution of each one of the information measures D (order) and L (uncertainty) to the total LMC complexity, and I (organization) and J (uncertainty) to the FS complexity. Thus, in Figures 8.5 and 8.6 we analyze the behavior of the energy in the $D_p - L_p$ and $I_p - J_p$ planes, while in Figures 8.7 and 8.8 the effect of the number of electrons in the $D_r - L_r$ and $I_p - J_p$ planes is displayed. For the energetic analysis of the information planes, we have found more useful to depict the corresponding ones to the momentum space, since the momentum density is directly related to the energy.

In Figure 8.5, we have plotted (in a double-logarithmic scale) the $D_p - L_p$ plane for the set of molecules which are grouped together and labeled according to the energy intervals they belong to, as observed in Figure 8.1, i.e., E_{400} for molecules with $E > -400$ a.u., E_{700} for $E \in [-700, -400]$ a.u., E_{1000} for $E \in [-1000, -700]$ a.u., and E_{1400} for molecules with $E < -1000$ a.u.. From Figure 8.5 it is observed that the $D - L$ plane is clearly divided into two regions according to the $D \times L \geq 1$ inequality [103] (valid for position, momentum as well as product spaces), and the region below the line (equality) corresponds to the forbidden region.. Parallel lines to this bound represent isocomplexity lines, where an increase (decrease) in uncertainty, L_p, along them is compensated by a proportional decrease (increase) of order (disequilibrium D_p), and higher deviations from this frontier are associated to higher LMC complexities. The general observation from this set of molecules is that groups with different energies are somewhat separated into different regions. So, molecules with higher energies possess the highest values of

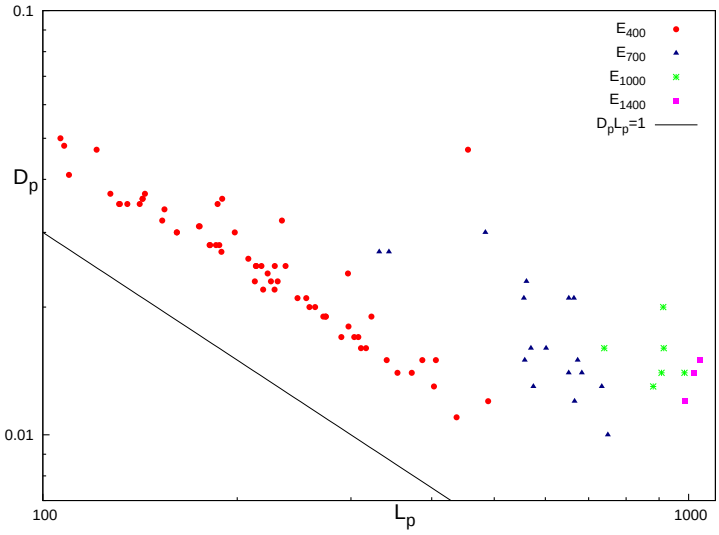

FIGURE 8.5: Disequilibrium-Shannon plane ($D_p - L_p$) in momentum space for energetically different groups: E_{400} for molecules with $E \geq -400$ (red circles), E_{700} for $E \in [-700, -400]$ (blue triangles),E_{1000} for $E \in [-1000, -700]$ (green stars) and E_{1400} for molecules with $E \leq -1000$ (magenta box). Double-logarithmic scale. Lower bound ($D_p \times L_p = 1$) is depicted by the black line. Atomic units are used.

L_p (more uncertainty), whereas the disequilibrium values are distributed over a wider range of values for all the groups energy-wise. So it seems that the energy is related to the uncertainty of the systems either for L_p in Figure 8.5 as for J_p in Figure 8.6 (discussed below). An interesting feature that is worthy to comment from this Figure is that low energy molecules behave more linearly and they appear located closer to the bound than higher energy molecules, i.e., more energetic molecules seem to deviate from the isocomplexity lines. This observation deserves a deeper study with a larger number of molecules and a wider range of energy.

In Figure 8.6 we have plotted (in a double-logarithmic scale) the $I_p - J_p$ plane for the same set of groups energy-wires. At this point it is worth mentioning that there is a rigorous lower bound to the associated FS complexity, namely $C(FS) = I \times J \geq$ constant (the constant being 3 for the individual spaces and $18\pi e$ for the product space). Figure 8.6 indicates a division of the $I_p - J_p$ plane into two regions where the straight line $I \times J =$ constant (drawn in the plane) divides it into an "allowed" (upper) and a "forbidden" (lower) regions. Similar observations as those discusssed in Figure 8.5 apply also in this case, i.e. those groups with larger energy values possess larger uncertainty as measured by the J_p values, whereas for organization, as measured through I_p, a wide spread is observed over the studied range of values. A similar conjecture as the one discussed above for the $D_p - L_p$ plane might apply in this case in that lower energy molecules seems to obey a linear behavior (isocomplexity lines).

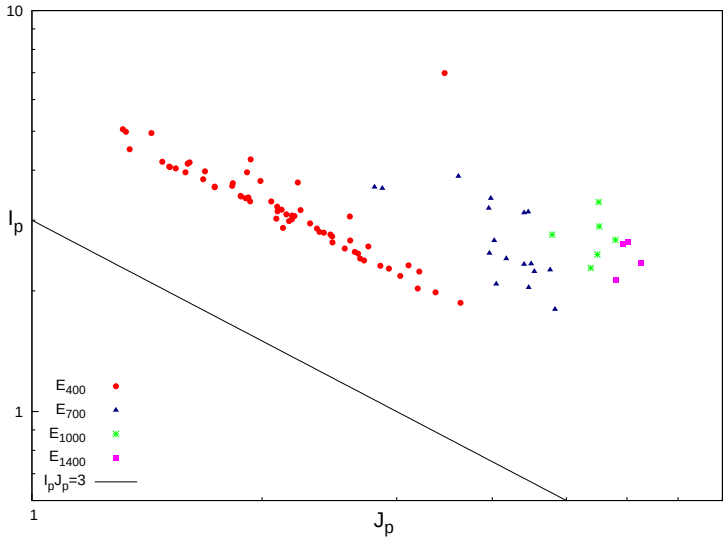

FIGURE 8.6: Fisher-Shannon plane ($I_p - J_p$) in momentum space for energetically different groups: E_{400} for molecules with $E \geq -400$ (red circles), E_{700} for $E \in [-700, -400]$ (blue triangles),E_{1000} for $E \in [-1000, -700]$ (green stars) and E_{1400} for molecules with $E \leq -1000$ (magenta box). Double-logarithmic scale. Lower bound ($I_p \times J_p = 3$) is depicted by the black line. Atomic units are used.

Our analysis continues with the study of the information planes for the isoelectronic series. In Figure 8.7 the components of the LMC complexity in position space are depicted (in a double-logarithmic scale), for the series with N=22, 24, 25 and 26 electrons denoted by N22, N24, N25 and N26 in the Figure, respectively, in the $D_r - L_r$ plane. In this case each isoelectronic series follows a trajectory which shows a linear behaviour (similar trends are observed in momentum space $D_p - L_p$) with correlation coefficients closed to one: N22 (0.989), N24 (0.991), N25 (0.989), N26 (0.981). Systems that are not in the isocomplexity lines belong to molecules with higher complexity values (in Table B.2 of Appendix B), which possess heavier atoms. This behavior means that in position space, higher complexity is due to higher disequilibrium values (higher order) and lower uncertainty L_r. It is interesting to mention that the opposite behavior is observed in momentum space (not depicted), i.e, higher complexity values correspond with lower disequilibrium and higher uncertainty. This opposite trends observed in both conjugated spaces can be explain as follows: A lower Shannon entropy in posicion space corresponds to a more concentrated charge density in some regions, which translates into a higher spreading of electron momentum density, giving rise to a higher Shannon entropy in such space. The same comment applies for the trends of the disequilibrium. It is also worthy to note that all isocomplexity lines, representing the isoelectronic molecular series with N= 22, 24, 25 and 26 electrons, show large deviations (higher LMC complexities) from the rigorous lower bound as it may be observed from Figure 8.7 in position space.

Proceeding with the analysis of the pattern and organization for the isoelectronic series, we have analyzed the contribution of each one of the information measures I and J

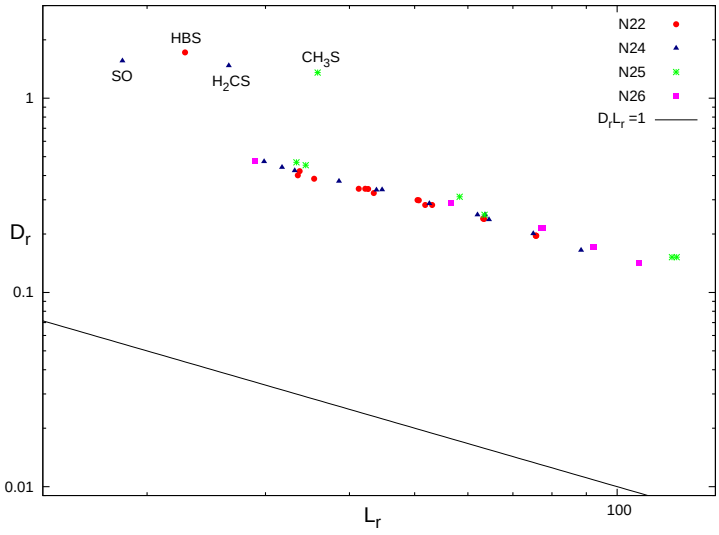

FIGURE 8.7: Disequilibrium-Shannon plane ($D_r - L_r$) in position space of the isoelectronic series of 22 (red circles), 24 (blue triangles), 25 (green stars) and 26 (magenta box) electrons. Double-logarithmic scale. Lower bound ($D_r \times L_r = 1$) is depicted by the black line. Molecules with large energy values are shown at the upper left corner of the Figure. Atomic units are used.

to the total FS complexity. This is done in Figure 8.8 for some of the isoelectronic molecular series with N= 22, 24, 25 and 26 electrons in the momentum space through the information plane $I_p - J_p$. Parallel lines to the constant $I \times J = 3$ represent isocomplexity lines, and higher deviations from this frontier are associated with higher FS complexities. Along these lines, an increase (decrease) in uncertainty (J) gets balanced by a proportional decrease (increase) of accuracy (I). Such a parallel shape is displayed by all isoelectronic series in momentum space, as shown in Figure 8.8, and we have verified their linear behaviour by a linear regression analysis with correlations coefficients: N22 (0.989), N24 (0.994), N25 (0.993), N26 (0.998). Notice that systems that are not in the isocomplexity lines belong to higher complexity molecules as we have previously discussed. They include heavier atoms, as observed from Figure 8.7, possessing higher values of J_p (more uncertainty) which provokes their higher complexity. It is also worth noting that all isocomplexity lines representing the isoelectronic molecular series show large deviations (higher FS complexities) from the rigorous lower bound ($I \times J = 3$) as it may be observed from the Figure. On the other hand, in the conjugated position space $I_r - J_r$ (not depicted), we may observe a similar trend, i.e., each isoelectronic series possess a linear behaviour except for the molecules with highest complexity values which are not in this isocomplexity lines, having lower values of J_r and higher values of I_r in contrast with Figure 8.8.

Notwithstanding that not all information products are good candidates to form complexity measures, i.e., preserving the desirable properties of invariance under scaling transformation, translation and replication, we have found interesting to study the plane

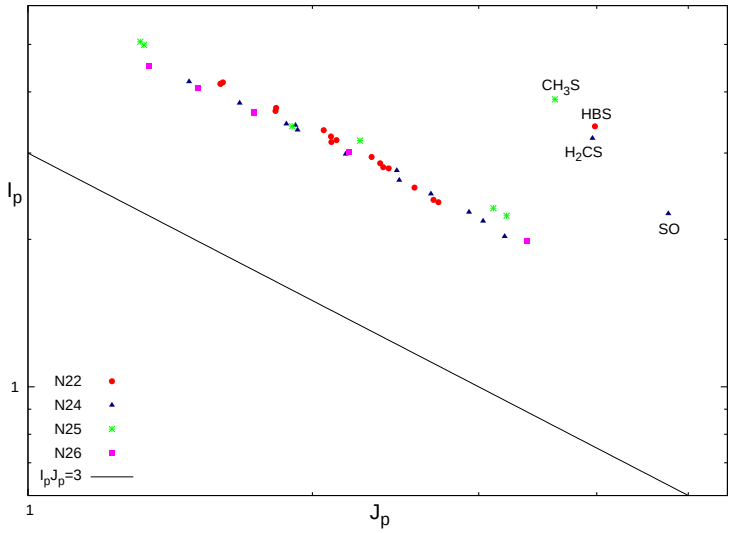

FIGURE 8.8: Fisher-Shannon plane ($I_p - J_p$) in momentum space of the isoelectronic series of 22 (red circles), 24 (blue triangles), 25 (green stars) and 26 (magenta box) electrons. Double-logarithmic scale. Lower bound ($I_p \times J_p = 3$) is depicted by the black line. Molecules with large energy values are shown at the upper left corner of the Figure. Atomic units are used.

$I - D$, with the purpose of analyzing patterns of order-organization. Note that this product fails to be invariant under scaling transformations [302]. Thus, in Figures 8.9 and 8.10 we have plotted the $I - D$ planes in momentum and position spaces, respectively, for the set of groups, energy-wires, studied above, and for some of the isoelectronic series with N= 22, 24, 25 and 26 electrons, respectively.

It can be observed from Figure 8.9 that there exists a relationship between order (disequilibrium) and organization (Fisher information) for the set of studied molecules in momentum space, within the $I_p - D_p$ plane, i.e., molecules with higher values of D_p possess higher I_p values. It is apparent from the Figure that a linear relationship between I and D is obeyed at least for these groups of energetically similar molecules. This linear behavior is observed for all molecules of the lowest energetic group except for $MgOH$ which is within the most complex ones as quantified in terms of $C(LMC)$ and $C(FS)$. To the best of our knowledge, this is the first time that such an apparent linear behavior between D and I has been studied.

A similar linear behavior might be observed from Figure 8.10 in the corresponding $I_r - D_r$ plane, showing a positive slope for all isoelectronic molecular series which means that, as the molecular order increases (higher D), their organization also increases (higher I). Interestingly, Figure 8.10 shows that $I - D$ plane is useful to detect molecular patterns of order-organization except for molecules of higher complexity (SO, HBS, H_2CS, CH_3S) which do not fit with the simple linear description of order-organization.

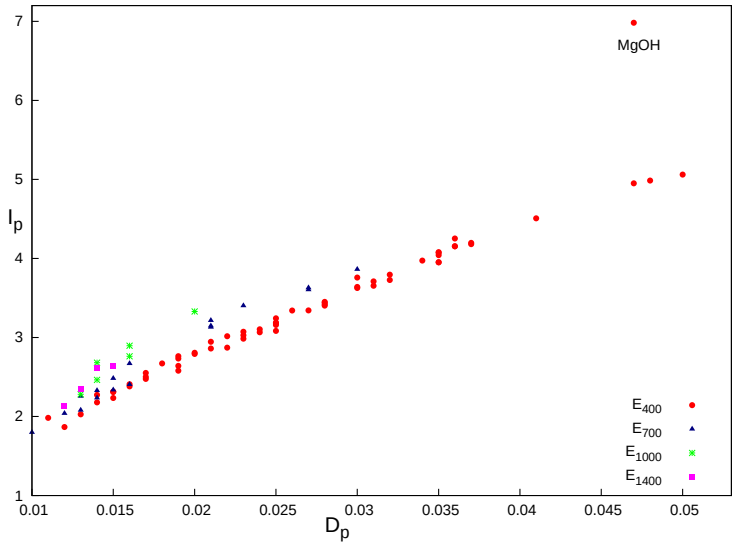

FIGURE 8.9: Fisher-Disequilibrium plane $(I_p - D_p)$ in momentum space for energetically different groups: E_{400} for molecules with $E \geq -400$ (red circles), E_{700} for $E \in [-700, -400]$ (blue triangles),E_{1000} for $E \in [-1000, -700]$ (green stars) and E_{1400} for molecules with $E \leq -1000$ (magenta box). Double-logarithmic scale. Atomic units are used.

(a) Chemical properties

Molecule	Energy	Ionization Potential	Hardness	Electrophilicity
$HCNO$	-168.134	0.403	0.294	0.02 0
$HNCO$	-168.261	0.447	0.308	0.031
$HOCN$	-168.223	0.453	0.305	0.036

(b) Complexity measures

Molecule	$C_{rp}(LMC)$	$C_{rp}(FS)$
$HCNO$	76.453	229.303
$HNCO$	74.159	223.889
$HOCN$	75.922	225.656

TABLE 8.1: (a) Chemical properties and (b) complexity measures for the isomers $HCNO$, $HNCO$ and $HOCN$ in atomic units (a.u.)

Finally, we have found useful to analyze the particular case of three isoelectronic isomers: $HCNO$ (fulminic acid), $HNCO$ (isocyanic acid) and $HOCN$ (cyanic acid) in order to analyze their chemical properties with respect to their complexity values. From an experimental side it is known that cyanic and isocyanic acids are isomers of fulminic acid $(H - C = N - O)$ which is an unstable compound [339]. From Table 8.1 we may corroborate that this is indeed the case in that fulminic acid possess the lowest ionization potential (less stability) but larger values for the complexity measures. According to our discussion above for the chemical properties this is indeed a more reactive molecule (lowest hardness value).

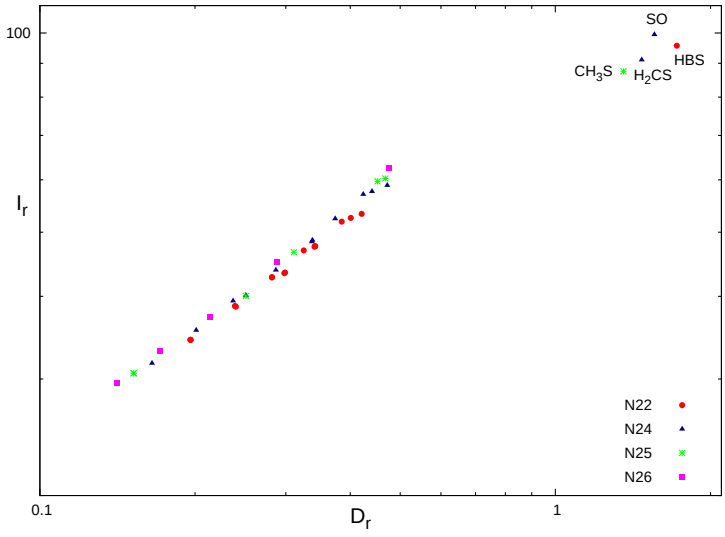

FIGURE 8.10: Fisher-Disequilibrium plane ($I_r - D_r$) in position space of the isoelectronic series of 22 (red circles), 24 (blue triangles), 25 (green stars) and 26 (magenta box) electrons. Double-logarithmic scale. Atomic units are used.

8.3 Conclusions

In this Chapter we have investigated the internal disorder of 92 molecules by means of five composite information-theoretic tools: the Fisher-Shannon and LMC shape complexities as well as three information planes. It is required the study of these measures in both position and momentum spaces in order to obtain a more complete description of the information-theoretic interpretation of the molecular systems.

Our results show that, although molecular complexities display general trends, these meaures are affected by several chemical factors, such as the molecular structure (e.g., lower complexity values corresponds with molecules of similar geometry), composition (e.g., higher complexity correspond with molecules with heavy atoms), chemical functionality, reactivity, etc. On the other hand, the information planes exhibit chemically significant patterns of structure and organization. We can conclude that the energy of the systems is related to its uncertainty throughtout L_p in the DL information plane and J_p in the IJ one.

Nevertheless, it is necessary to study a larger set of molecules with a wider range of energies in order to corroborate our conclusions.

Part III

Divergence measures of atomic systems and processes

Introduction

Throughout Parts I and II of this Thesis, we have tried to quantify information features of a given distribution, associated to a physical or chemical system, in terms of different information and complexity measures. It is also interesting to have at our disposal other density functionals which enable us to measure the "distance" and/or similarity among them. In probability, statistics and information theory different approaches have dealt with the aim of establishing quantitative measures among two or more distribution functions in order to quantify how different these distribution are, giving rise to a variety of measures of divergence, a concept which will be described later. Each one has its own properties and characteristics, which make them more or less useful attending to the kind of problem, system or process as well as the interpretation we are dealing with [64, 340–347]. In particular, the usefulness of some of them has been widely proved in the study, for instance, of different physical and chemical systems and processes in terms of meaningful and relevant distributions in their description.

Exploring quantitatively the level of similarity/dissimilarity between two different systems in terms of meaningful distributions appears actually as a very interesting field. There exists an extensive literature on measures of similarity and dissimilarity between probability densities [347, 348], which have been used in a wide variety of scientific fields including, for instance, sequence analysis [349], pattern recognition [350], diversity [351], classification [352], homology [353], neural networks [354], computational linguistics [355] or quantum theory [356].

The recent explosion in the knowledge based on chemical research has given rise to a surge of interest in chemical similarity. Molecular modelling, quantitative structure activity relationship (QSAR) and quantum information are relevant examples of such an interest [357, 358]. Chemical similarity is oftenly described as an inverse of a measure of distance in the appropriate space. In particular, the Quantum Similarity Theory (QST) [359] was originally developed in order to establish quantitative comparisons between molecular systems by means of their fundamental structural magnitudes, i.e. electron density functions. The obvious motivation arised upon the guess that studying the differences between the electronic charge densities of these species could be related to differences between their respective physical and chemical properties, according to the Density Functional Theory and the Hohenberg-Kohn theorem [101].

The main aim of this Part is to analyze the ability of the most important divergence measures, defined in the next chapter (Chapter 9), such as the Jensen-like and the Fisher divergences, in the study of dissimilarity between atomic systems, as compared to other well-known comparative measures, such as the Quadratic Distance (QD) and the Quantum Similarity Index (QSI). The universality of the methods here employed allows their application not only to atomic systems, but also to many others such as, for instance, molecules and clusters, as well as to the analysis of physical and chemical processes such as ionization and reactions.

The structure of this Part is the following: firstly, in Chapter 9, different divergence measures will be defined giving not only their mathematical formulation in terms of information measures such as Shannon entropy or Fisher information, but also discussing their meanings. In Chapters 10 and 11, the dissimilarity or divergence between neutral atoms throughout the Periodic Table in terms of their one-particle densities will be studied, as well as the dissimilarity between neutral species and their corresponding ions in both conjugated position and momentum spaces. This study is carried out in terms of the Jensen-like (i.e., Jensen-Shannon, Jensen-Rényi and Jensen-Tsallis) and Fisher divergences, as well as the quadratic distance and the quantum similarity index. Finally, in Chapter 12, other applications of these divergence measures will be shown in order to prove their utility in numerous physical problems of different nature.

Chapter 9

The concept of divergence

In this part of the Thesis we use the concept of divergence in order to quantify the dissimilarities among two or more distributions. In doing so, some requirements on the mathematical formulation of any divergence measure must be fulfilled, namely (i) the divergence between two distributions ρ_1 and ρ_2 has to be non-negative, (ii) this quantity vanishes only when $\rho_1 = \rho_2$, and (iii) it has to be symmetric, i.e., the divergence between ρ_1 and ρ_2 is equal to the divergence between ρ_2 and ρ_1

These properties allow us to employ the divergence as a measure of the "distance" between distributions, although we are aware that they do not necessarily verify the triangular inequality, according to the mathematical properties required for any distance. In such a case, these kind of functionals is known as semi-metric [360] instead of metrics as in the case of the usual distance.

Let us now define the different measures which will be used in the following chapters as divergence and dissimilarity measures.

9.1 Quadratic distance

The concept of distance between distributions finds its roots in the same concept associated to a coupled of elements in a vectorial space, constituting in fact an extension of it. Supplying an appropriate norm on the space in such a way of giving rise to a metric or distance leads us to the best known and deeply studied L^2 space, in which the distance between two vectors is given by the square root of the scalar product of the difference vector with itself. Considering the space of finite norm distributions defined over the whole three-dimensional space (and consequently with $d = 3$ in what followss), and normalizing each one to unity, the simplest and most intuitive dissimilarity measure is the *Quadratic Distance* (QD), given by the norm (defined by the Lebesgue integral

on the domain Δ common to both distributions) of their difference:

$$QD(\rho_1,\rho_2) \equiv \left(\int_\Delta [\rho_1(\vec{r}) - \rho_2(\vec{r})]^2 d\vec{r}\right)^{1/2}, \tag{9.1}$$

with the normalization $\int_\Delta \rho_1(\vec{r})d\vec{r} = \int_\Delta \rho_2(\vec{r})d\vec{r} = 1$.

Among all the well-known properties that any distance verifies, let us remark that (i) it is non-negative for any pair of distributions, and (ii) the minimal value zero is reached if and only if both functions are identical. Having these properties in mind, it is clear that the QD values provide us with an indicator of similarity between densities.

Different applications of this quantity have been carried out in several fields such as atomic [361] and molecular [303] chemistry and physics, among others.

9.2 Quantum similarity index

The Quantum Similarity Technique is based on overlap integrals and the use of the *Quantum Similarity Index* (QSI) to measure the closeness of two distributions $\rho_1(\vec{r})$ and $\rho_2(\vec{r})$. The QSI is defined as

$$QSI(\rho_1,\rho_2) \equiv \frac{\int_\Delta \rho_1(\vec{r})\rho_2(\vec{r})d\vec{r}}{\sqrt{\int_\Delta \rho_1^2(\vec{r})d\vec{r}\int_\Delta \rho_2^2(\vec{r})d\vec{r}}}, \tag{9.2}$$

where the numerator is refereed as the 'Quantum Similarity Measure' (QSM) of ρ_1 and ρ_2, while the denominator normalizes the QSM in terms of the corresponding disequilibriums defined and used in previous chapters (see Eq.(1.21)). The main properties of this measure, apart from symmetry under exchange of distributions, are: (i) it ranges over the bounded interval $(0, 1]$ and (ii) the maximum value 1 is only reached for identical distributions.

Its definition arises from the molecular research field [359], but later on the QSI has been widely applied in many different problems and subjects in order to establish a comparative measure as indicator of similarity between both distributions over the basis of the aforementioned main properties [361–364].

Let us remark here the different character of both measures QD and QSI, in spite of being defined in terms of exactly the same integrals, attending to the boundness of the QSI contrary to the unbounded character of QD. This comment can be also expressed in terms of the saturation values (those corresponding to identical distributions), being 0 (minimum) for QD and 1 (maximum) for QSI.

9.3 Kullback-Leibler distance

Apart from the above discussed dissimilarity measures defined in terms of overlap integrals, there exist additional comparative measures, some of them arising at a first step from fundamental information-theoretic functionals of distribution, such as the Shannon, Rényi and Tsallis entropies and Fisher information, as well as their later extensions for establishing information-theoretic-based comparisons among distributions, as is the case of the Kullback-Leibler relative or cross entropy [341] and the relative Fisher information [365].

Probably the pioneering and most relevant divergence measure introduced within the information theory is the so-called *Kullback-Leibler divergence* (KL) or relative entropy [341]. It is defined as

$$KL(\rho_1, \rho_2) \equiv \int_\Delta \rho_1(\vec{r}) \ln \frac{\rho_1(\vec{r})}{\rho_2(\vec{r})} d\vec{r}, \tag{9.3}$$

having its roots in the Shannon entropy [16],

$$S(\rho) \equiv -\int_\Delta \rho(\vec{r}) \ln \rho(\vec{r}) d\vec{r}, \tag{9.4}$$

The main properties of this quantity are: (i) the KL is always non-negative if the normalization of both distributions are identical, i.e. $\int_\Delta \rho_1(\vec{r})d\vec{r} = \int_\Delta \rho_2(\vec{r})d\vec{r}$, (ii) the minimum value $KL(\rho_1, \rho_2) = 0$ is reached only for $\rho_1(\vec{r}) = \rho_2(\vec{r})$, (ii) the Shannon entropy, $S(\rho)$, can be obtained by taking $\rho_2 = 1$ in the KL expression, so, we can give a new interpretation for the Shannon entopy, as the relative entropy of ρ_1 with respect to the uniform distribution.

The non-negativity of KL relative entropy together with the minimal zero value for identical distributions enable us to think on this measure in terms of similarity or distance between two probability measures. In other words, this quantity can be considered as a measure of how different the two distributions are attending to their global spreading. However, the absence of symmetry of the KL divergence induces its symmetrized version $KLS(\rho_1, \rho_2) \equiv KL(\rho_1, \rho_2) + KL(\rho_2, \rho_1)$, in order to get an appropriate interpretation of this quantity as an information distance. Both divergences KL and KLS have been widely studied, finding applications in a great variety of fields such as, for instance, minimum cross entropy estimation techniques [366] or indexing and image retrieval [367].

This divergence measure (KL), also called "information gain", is related to other important quantities studied in Information Theory, and it has been extensively used in Bayesian updating through the minimum-cross-entropy principle [4], where is usually employed by choosing an 'a priori' or reference density ρ_2 in order to quantify the extent to which ρ_1 differs from the reference ρ_2. Another recent and important application belongs to the field of Quantum Information Theory, where the relative entropy can be

used as a measure of distinguishability between quantum systems and therefore as a quantum entanglement measure [368].

9.4 Jensen-like divergences

In this section, divergences based on global information measures (e.g. Shannon, Rényi and Tsallis entropies) will be defined. As will be discussed later the global character of the basic entropic measures translates also into the arising divergence.

Jensen-Shannon divergence

An information-based measure of divergence, strongly related to both the Shannon and the relative entropies (defined in the previous section), is the so-called *Jensen-Shannon divergence* (JSD). It is characterized for quantifying the Shannon "entropy excess" of a couple of distributions with respect to the mixture of their respective entropies. More specifically, it is given by [369, 370]

$$JSD(\rho_1, \rho_2) \equiv S\left(\frac{\rho_1 + \rho_2}{2}\right) - \frac{1}{2}\left[S(\rho_1) + S(\rho_2)\right] \tag{9.5}$$

$$= \frac{1}{2}\left[KL\left(\rho_1, \frac{\rho_1 + \rho_2}{2}\right) + KL\left(\rho_2, \frac{\rho_1 + \rho_2}{2}\right)\right], \tag{9.6}$$

the mathematical definition clarifying the above interpretation as entropy excess of the mean density with respect to the mean entropy of the involved distributions. Last equality arises straightforwardly from the definition of KL, providing an additional interpretation of JSD as the mean "distance" (understood in terms of KL) of each density to the mean one.

Apart from preserving the global character of the Shannon entropy, the JSD possesses the main properties required for a measure to be interpreted as an informational distance, namely non-negativity (as a consequence of the convexity of the $S(\rho)$ functional), symmetry and the minimum value zero being reached only when $\rho_1 = \rho_2$.

It quantifies, in fact, the statistical dependence among an arbitrary number of probability distributions (as will be shown below) and there are some important reasons because of many researchers choose JSD as a measure of divergence. Among them: (i) it is a smoothed version of the Kullback-Leibler divergence and hence it shares its mathematical properties as well as its intuitive interpretability [64], (ii) it provides direct interpretations in the framework of statistical physics, information theory or mathematical statistics [371], (iii) the JSD is related to other information-theoretical functionals (special case of the Jensen difference [360] and the Csiszár divergence [344]) and it is the square of a metric [372], (iv) the JSD can be generalized to measure the distance

among more than two distributions, and (v) it is possible to assign different weights to the distributions, which allows us to take into account different sizes, masses, charges,... of the objects we are comparing (e.g. different lengths of the subsequences in DNA analyses or different subshells or parts in atomic or molecular similarity analyses [371]). However its use in the framework of quantum information theory [356, 358] or in the study of multielectronic systems [373, 374] is very recent.

The interpretation of JSD remains also valid if one considers an arbitrary number M of distributions $\{\rho_1, \ldots, \rho_M\}$ as well as density and entropy means calculated by considering non-uniform weights, defining their Jensen-Shannon Divergence JSD as follows:

$$JSD\left(\{\omega_j, \rho_j\}_{j=1}^{M}\right) \equiv S\left(\bar{\rho}\right) - \sum_{j=1}^{M} \omega_j S(\rho_j) \tag{9.7}$$

where

$$\bar{\rho} = \sum_{j=1}^{M} \omega_j \rho_j, \tag{9.8}$$

is the mean density and the weights ω_j $(j = 1, \ldots, M)$ verify $\sum_{j=1}^{M} \omega_j = 1$. It is immediate to observe that the present definition reduces to the initial one (Eqs. (9.5)) by only considering the particular case $M = 2$ and $\omega_1 = \omega_2 = 1/2$.

Some comments are in order: (i) the aforementioned properties for the $M = 2$ uniformly weighted JSD divergence also remain for the above generalization, and (ii) the same is also true for the expression of JSD as the mean of the associated KL relative entropies:

$$JSD(\{\omega_j, \rho_j\}_{j=1}^{M}) = \sum_{j=1}^{M} \omega_j \cdot KL\left(\rho_j, \bar{\rho}\right). \tag{9.9}$$

This generalization also provides a measure of global distance among the elements of a given set of distributions or, equivalently, of the mean distance from each element to the mean distribution.

During past years researchers have been interested towards rigorous properties and parametric generalizations of this divergence information measure. In particular, and only for discrete probability distributions, Lin and Wong derived some basic properties for JSD [345, 375] and later on they also provided some identities and inequalities [376]. Taneja introduced [347, 348] two scalar parametric generalizations of JSD . More recently, Lamberti and Majtey have investigated and generalized the properties of JDS in the framework of non-extensive Tsallis statistics [34, 372, 377].

Jensen-Rényi divergence

As pointed out in Chapter 1, the Shannon entropy S constitutes a particular case of the so-called Rényi entropy of order q [33]

$$R^{(q)}[\rho] = \frac{1}{1-q} \ln \omega^{(q)}[\rho], \tag{9.10}$$

with $\omega^{(q)}[\rho] \equiv \int \rho^q(\vec{r}) d\vec{r}$ being the entropic moment of order q of the distribution $\rho(\vec{r})$.

Replacing the Shannon entropy by the Rényi one in the JSD definition (9.5) gives rise to a new double-density functional, the *Jensen-Rényi divergence* [360] given by

$$JRD^{(q)}(\rho_1, \rho_2) \equiv R^{(q)}\left(\frac{\rho_1 + \rho_2}{2}\right) - \frac{1}{2}\left[R^{(q)}(\rho_1) + R^{(q)}(\rho_2)\right], \tag{9.11}$$

in such a way that $JRD^{(1)} = JSD$, the new divergence generalizing the previously introduced JSD one. Scarce applications of the JRD measure have been carried out, only in fields (to the best of our knowledge) such as image registration [378, 379] or document categorization [380].

The non-negativity of $JRD^{(q)}$ is guaranteed only for $0 < q < 1$, constraint which arises from the convex/concave character of the frequency moments $\omega^{(q)}$ according to the value of q. This parameter acts by smoothing the integrands for lower q values and then enhancing the relative contribution of the outermost region for the particular case of atomic system.

So, the $JRD^{(q)}$ allows us to establish a comparisong among densities according to their similarity within specific regions of their common domain.

In a similar way that in the case of JSD as given by Eq. (9.7), we can extend the JRD definition by considering an arbitrary number of M distributions and by weighting each density according to the desired criteria. This generalization gives rise to

$$JRD^{(q)}\left(\{\omega_i, \rho_i\}_{i=1}^M\right) \equiv R^{(q)}(\bar{\rho}) - \sum_{i=1}^{M} \omega_i R^{(q)}(\rho_i), \tag{9.12}$$

with $\bar{\rho} = \sum_{i=1}^{M} \omega_i \rho_i$ and $\sum_{i=1}^{M} \omega_i = 1$. The same properties previously mentioned regarding the definition (9.11) remain.

Jensen-Tsallis divergence

Other generalization of the Shannon entropy (see Section 1.1) is given by the so-called Tsallis entropy of order q [34],

$$T^{(q)}(\rho) \equiv \frac{1-\omega^{(q)}(\rho)}{q-1}, \tag{9.13}$$

also based, as in the case of the Rényi entropy, on the entropic moment of order q of the distribution $\rho(\vec{r})$.

Replacing the Shannon entropy by the Tsallis one in the JSD definition gives rise to a new double-density functional, the *Jensen-Tsallis divergence* of order q [381, 382]

$$JTD^{(q)}(\rho_1,\rho_2) = T^{(q)}\left(\frac{\rho_1+\rho_2}{2}\right) - \frac{1}{2}\left[T^{(q)}(\rho_1) + T^{(q)}(\rho_2)\right], \tag{9.14}$$

in such a way that $JTD^{(1)} = JSD$. The non-extensive character of the Tsallis entropy (i.e. for a system composed by two or more parts, the total Tsallis entropy of a system is not the sum of the Tsallis entropies of its parts) remains to the JTD. Non-extensive divergences closely related to the JTD divergence above defined have been applied in the fields of symbolic sequence segmentation [377], geological or medical image registration [381] and machine learning techniques [382].

Contrary to the case of JRD, which non-negativity is only guaranteed for $0 < q < 1$, such a property is veryfied for JTD for arbitrary q, where the only constraints on the value of q arise from the convergence of the involved frequency moments according to the long- and short-range behaviors of the distributions, as also happens with the Rényi relative entropy even for order q below 1. This parameter acts in JTD exactly in the same way as for JRD. That is, the main feature of the Jensen-Tsallis divergence $JTD^{(q)}$ as compared to other ones and, particularly, to the Jensen-Shannon divergence JSD, is its capability of enhancing/diminishing the relative contribution of different regions within the domain of the distributions under comparison.

As in the case of previous Jensen-like divergences, the JTD can be extended by considering M different distributions:

$$JTD^{(q)}\left(\{\omega_i,\rho_i\}_{i=1}^{M}\right) \equiv T^{(q)}(\bar{\rho}) - \sum_{i=1}^{M}\omega_i T^{(q)}(\rho_i), \tag{9.15}$$

with $\bar{\rho} = \sum_{i=1}^{M}\omega_i\rho_i$ and $\sum_{i=1}^{M}\omega_i = 1$. The same properties previously mentioned, arising from the definition (9.14), still remain.

9.5 Fisher divergence

It is worthy to point out that the global character of the Shannon entropy translates also into the divergences KLS, JSD and its generalizations JRD and JTD, as also occurs with QD and QSI due to the involved integrals in their definition (for further details, see Chapter 1 where all information measures had been defined and analyzed). However, it would be also of great interest to dispose of divergence measures displaying a deeper local character, namely their values being more sensitive to the aforementioned strong local changes. As we have studied in previous chapters, the main quantity having such a characteristic (in what concerns measures on a single distribution) is the Fisher information I [3, 37], defined as

$$I(\rho) = \int_{\Delta} \rho(\vec{r}) |\vec{\nabla} \ln \rho(\vec{r})|^2 d\vec{r}, \tag{9.16}$$

Attending to the characteristics of Shannon and Fisher functionals, and having in mind the definition given by Eq. (9.3) of the Shannon-based global comparison KL between two distributions, a measure of local character based on the Fisher information concept can be also built up in a similar way, namely

$$FD(\rho_1, \rho_2) \equiv \int_{\Delta} \rho_1(\vec{r}) \left| \vec{\nabla} \ln \frac{\rho_1(\vec{r})}{\rho_2(\vec{r})} \right|^2 d\vec{r} + \int \rho_2(\vec{r}) \left| \vec{\nabla} \ln \frac{\rho_2(\vec{r})}{\rho_1(\vec{r})} \right|^2 d\vec{r}, \tag{9.17}$$

which will be referred as *Fisher Divergence* (FD) in what follows, according to the concept of divergence among distributions, previously introduced by other authors in the information-theoretical context [346, 347]. From the FD definition, it is immediately observed that it preserves the aforementioned properties desirable for establishing the quantitative comparison, namely symmetry, non-negativity and saturation for identical distributions.

It is worthy to point out that each individual term of the FD definition is known as *relative Fisher information*, which scarce applications have been carried out with similar aims to those of the Kullback-Leibler relative entropy, that is, to perform a comparison of a distribution with respect to an a priori one [365, 383].

9.6 Comparison between Jensen-Shannon and Fisher divergences

In the previous sections we have defined different divergence measures, in particular the Jensen-Shannon, JSD, and Fisher, FD divergences, defined in terms of the Shannon entropy and Fisher information, respectively. Both of them give us a glance about how

different two distributions are, but in different ways. In order to get a better understanding on those differences, suppose we want to compare two different persons "according to" some specific characteristic, i.e. height, weight, hair's colour, eye's colour... A similar situation arises when dealing with quantum systems and the probability distributions, being the main reason because it is useful to have at our disposal a variety of divergence measures according to the characteristics upon which base the comparison.

The Jensen-Shannon divergence is defined in terms of the Shannon entropy, which is a global measure (we discussed the meaning of global and local character of the information measures in Chapter 1), so this divergence gives us an idea about how similar or different two distribution are over their whole domain. On the other hand, the Fisher divergence is based on a local information measure, the Fisher information, so, in this case the divergence quantifies the differences between two distributions in more detail at a smaller-scale. Additionally, the generalizations, JRD and JTD allows to enhance specific regions in order to quantify the strength of the divergence.

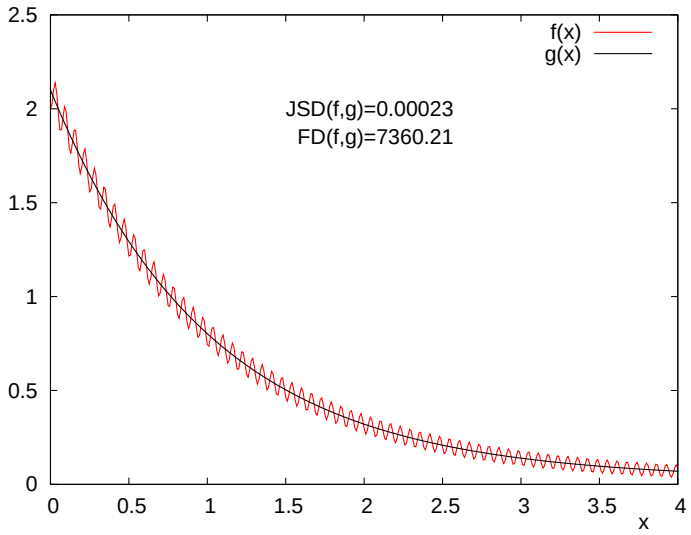

FIGURE 9.1: JSD and FD for $f(x) \sim e^{-ax}$ and $g(x) \sim e^{-ax} + \epsilon sin^2 nx$.

As an example, two elementary functions are depicted in Figure 9.1. We can observe that both distributions have the same global behaviour and consequently their JSD has a small value. However, if we observe the figure in more detail, we can distinguish that $g(x)$ has an oscillatory behaviour due to its sine-type perturbation that $f(x)$ does not have. Hence, the FD is very high because this divergence accurately detects the local changes in the probability distributions.

Chapter 10

Fisher and Jensen-Shannon divergences of neutral atoms and ionization processes

Finding appropriate ways of comparing two or more systems among themselves in terms of representative distribution functions appears very interesting, especially in order to describe the similarity among relevant physical and chemical properties of the systems in terms of their corresponding distributions. Such is for instance the case of atomic systems, where the aim is to analyze the correlation among their similarity in terms of one-particle densities and meaningful properties such as shell structure, the total number of electrons or the atomic ionization potential (AIP).

The aim of this Chapter is to study, by using the previously introduced relative measures (see Chapter 9), the dissimilarities between electronic densities corresponding to neutral atoms and/or ions in both conjugated spaces. This chapter is structured as follows: Section 10.1 is devoted to the numerical analysis of Fisher (subsection 10.1.1) and Jensen-Shannon (subsection 10.1.2) divergences among one-particle densities, in position and momentum spaces for neutral atoms throughout the Periodic Table, including a study of the results as compared to those provided by other information measures, such as the quadratic distance QD or the relative entropy KLS, providing the appropriate interpretation from a physical point of view. In Section 10.2, we carry out a dissimilarity analysis for simple, but strongly organized N-electron systems ($N \leq 54$) such as neutral atoms and their singly charged ions, exploring their outer electronic layer and studying the features inherent to the process of gain or loss of one electron for an atom keeping its nuclear charge Z. The relationship between the atomic ionization potential (AIP) and the dissimilarity measures among neutral systems and charged species is also studied. In Section 10.3 we explore the core region of atoms by computing the isoelectronic variation of these information divergences of over a fairly extended range of nuclear

charge Z values. The results obtained by means of these divergence measures (FD and JSD) are also compared to those obtained with quantum similarity techniques (QST) based on overlap measures. Finally, the conclusions and main results are collected in the last section, Section 10.4

10.1 Divergence measures of neutral atoms

In this section we study the similarities among atomic one-particle densities by means of two different measures, namely JSD and FD divergences which posses a global and a local character, respectively. The results provided by both measures are interpreted in terms of relevant physical characteristics of the systems under study.

10.1.1 Fisher divergence

The main aim in this subsection is the numerical study of the Fisher divergence (FD)

$$FD(\rho_1,\rho_2) \equiv \int \rho_1(\vec{r}) \left| \vec{\nabla} \ln \frac{\rho_1(\vec{r})}{\rho_2(\vec{r})} \right|^2 d\vec{r} + \int \rho_2(\vec{r}) \left| \vec{\nabla} \ln \frac{\rho_2(\vec{r})}{\rho_1(\vec{r})} \right|^2 d\vec{r}, \tag{10.1}$$

between pairs of atomic electron densities, either in position or momentum spaces, $\rho(\vec{r})$ and $\gamma(\vec{p})$ respectively, as well as to provide an appropriate physical interpretation of the FD values. First of all, let us remember that the one-particle densities $\rho(\vec{r})$ and $\gamma(\vec{p})$ are obtained from the total wavefunction $\Psi(\vec{r},\vec{r}_2,\ldots,\vec{r}_N)$ of the N-electron atom, and its Fourier transform $\tilde{\Psi}(\vec{p},\vec{p}_2,\ldots,\vec{p}_N)$, by integrating $|\Psi|^2$ and $|\tilde{\Psi}|^2$ on all variables except the first one. Additionally, the spherical averages $\rho(r)$ and $\gamma(p)$ of the aforementioned one-particle densities are quite enough for the density-based study of isolated atomic systems.

In order to clarify the notation, all quantities considered in what follows will be denoted by adding a subscript to determine the space they belong to (except for results or expressions of general validity in both conjugated spaces), while systems will be referred by means of their nuclear charge Z. For illustration, $FD_r(3,5)$ will denote the Fisher divergence in position or r-space between the neutral atoms with nuclear charges $Z=3$ and $Z=5$.

The numerical analysis has been carried out by using Near-Hartree-Fock wavefunctions [269] for neutral atoms with nuclear charge $Z=1-103$. First, let us show the Fisher divergence in position space $FD_r(Z,Z')$ between each atom Z' belonging to a given group as compared to each one within the whole Periodic Table $Z=1-103$. For illustration, the associated curves (as functions of Z) are displayed in Figure 10.1(a) for noble gases (i.e. $Z'=2,10,18,36,54,86$) in position space. It is observed that all curves (corresponding to the systems of the chosen group) behave in a similar fashion, firstly

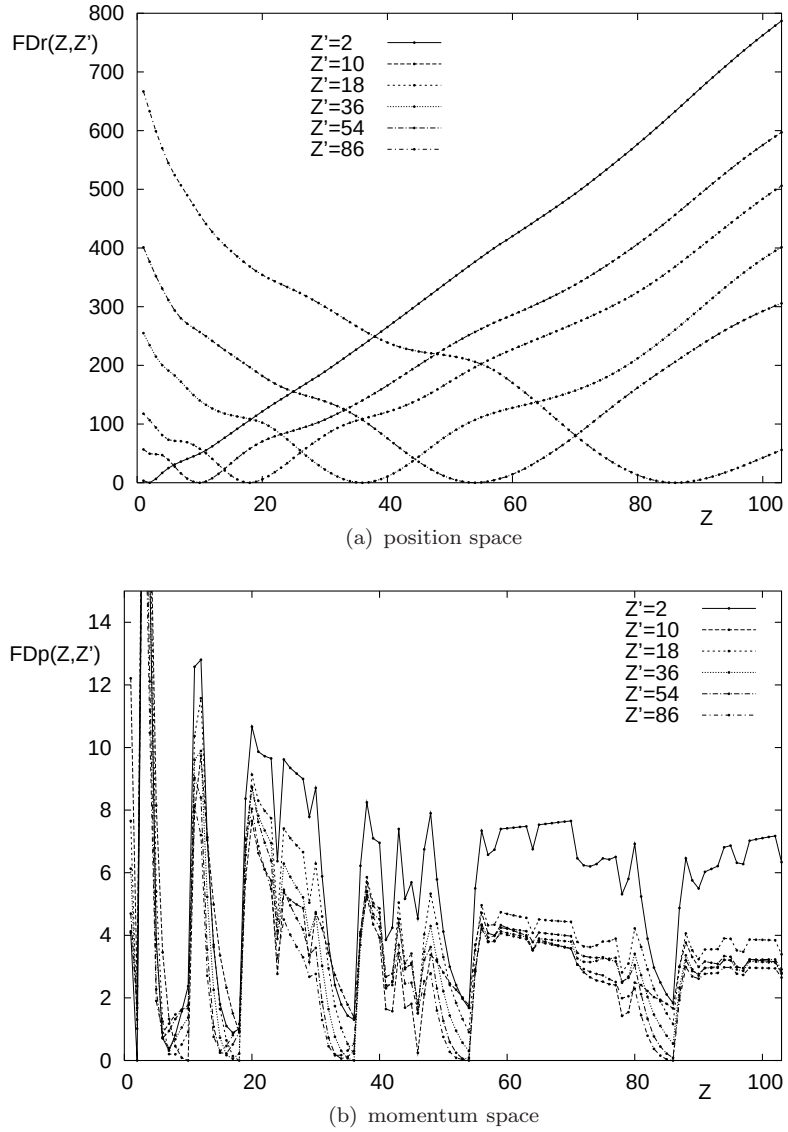

(a) position space

(b) momentum space

FIGURE 10.1: Fisher divergence $FD(Z, Z')$ of noble gases ($Z' = 2, 10, 18, 36, 54, 86$) for $Z = 1 - 103$ in (a) position and (b) momentum spaces. Atomic units are used.

decreasing monotonically until reaching the minimal zero value for $Z = Z'$, and then monotonically increasing as Z increases. Such a behavior is displayed not only for all systems of the present group, but also for all other groups of the Periodic Table. This fact can be interpreted, attending to the meaning of divergence associated to the FD definition, in the sense that $FD_r(Z, Z')$ mostly depends on how different the atomic nuclear charges Z and Z' are. However, no information on other physically relevant characteristics (e.g. shell-filling, periodicity,...) is obtained by means of $FD_r(Z, Z')$.

The previous unimodal shapes in Figure 10.1(a) strongly differ from those displayed when performing a similar comparison in terms of the Fisher divergence $FD_p(Z, Z')$ in momentum space as given in Figure 10.1(b) for the previously chosen group, namely noble gases; next comments corresponding to this group remain also valid for all groups

of the Periodic Table. Now, a significant number of local extrema (maxima and minima) appear in all curves, which behavior is consequently far from the previously mentioned systematically unimodal one in position space.

Focussing our attention on minima (intuitively associated to the concept of close or similar densities) it is observed, at a first glance, the existence of a small number of clearly distinguishable minima located at (roughly) the same positions for all curves, as well as a higher number of not so deep/enhanced peaks along them. Concerning the most relevant minima, they are located at the values of the nuclear charges Z of the systems conforming the group under study. This situation is much more in accordance with the aforementioned interpretation of a divergence between atomic distributions as a measure of their distance or dissimilarity interpreted in terms of their main physical characteristics, because the $FD_p(Z, Z')$ values are highly conditioned by the valence orbital quantum number l and its occupancy or, equivalently, by the groups the atoms under consideration belong to. So, and contrary to the position space divergence FD_r, the momentum space one FD_p is shown to be able of providing information on physical properties of neutral atoms beyond the mere difference between their nuclear charges.

Apart from the deeper peaks associated to comparisons between members belonging to the same group of the Periodic Table, there also appear a set of much smaller local extrema for specific values of the nuclear charge Z, a common feature of all curves characterized by a Z'. Most of those peaks occur when one of the systems under consideration is an atom suffering of the so-called anomalous shell-filling. The appearance of those peaks for these 'anomalous cases' is systematic, in the sense of being displaying independently of the other system which is being compared to.

The similar behavior of all elements belonging to the same group is a common feature of all groups within the Periodic Table. For all of them, moreover, increasing the nuclear charge of contiguous atoms makes their difference in momentum space (attending to the divergence values) to decrease, that is, similar trends are displayed by contiguous systems belonging to different groups. In particular, filling a 'p' subshell and even more for the 'd' and 'f' ones provides lower values of the divergence among themselves. For instance, transition metals as well as lantanides and actinides display very similar trends within their periods.

The differences between the FD behaviors in position and momentum spaces arise from the asymptotic behaviors of the involved densities. In position space, the atomic density $\rho(r)$ has an exponentially decreasing behavior, so that the values of the involved integrals are mainly determined by the regions surrounding the nuclei, where the density behavior is governed by the nuclear charge Z. However, the low-speed regions for small linear momentum p, where it roughly reaches the highest values, are associated to the outermost subshells (valence ones), being consequently those mainly determining the FD values, according to the main contribution of the momentum density.

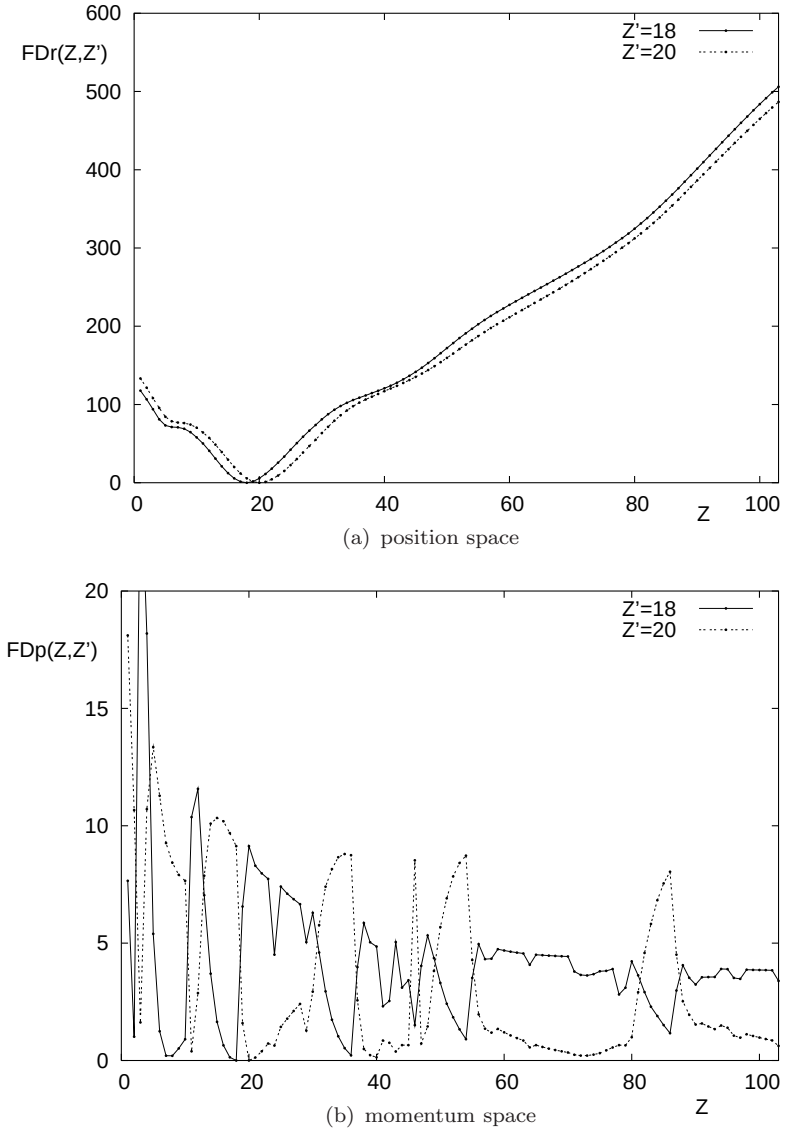

(a) position space

(b) momentum space

FIGURE 10.2: Fisher divergence $FD(Z, Z')$ of Ar ($Z' = 18$) and Ca ($Z' = 20$) for $Z = 1 - 103$ in (a) position and (b) momentum spaces. Atomic units are used.

Some conclusions of the previous comments are emphasized by analysing the structural behaviors of curves corresponding to Fisher divergences of elements belonging to different groups. In doing so, let us choose a couple of them as done in Figures 10.2(a) and 10.2(b), corresponding to their divergences with respect to other systems, in both conjugated position and momentum spaces, respectively. Let us consider two systems similar in what concerns the values of their nuclear charges but significantly different according to their valence orbitals, such as for instance Argon and Calcium ($Z' = 18$ and $Z' = 20$,respectively) as done in those figures. Concerning their position space divergences $FD_r(Z, Z')$ as functions within the range $Z = 1 - 103$ for each Z', it is observed in Figure 10.2(a) how both curves display almost identical shapes, differing roughly by a small shift according to the closeness of their nuclear charges 18 and 20, which is also the distance between the locations of their absolute minima being $20 - 18 = 2$. This figure

corroborates the above comment concerning position space FD_r divergences, in the sense that they are mainly determined by the nuclear charges of the involved systems, much more than on their physical or chemical properties. However, a similar analysis based on Figure 10.2(b) where the momentum space divergences are displayed for the same systems shows a strongly different behavior of the $FD_p(Z, Z')$ function even for systems with very close values of their nuclear charges. In the present example the chosen systems belong to different groups, being the outermost subshell $3p^6$ for $Z' = 18$ (noble gas) and $4s^2$ for $Z' = 20$ (alkaline earth). That difference between their valence subshells strongly determine the associated FD_p values according to the shell structure of the atom they are compared to. In a similar way as explained in comments of Figure 10.1(b) for the role of the momentum space divergence FD_p, it can now be also concluded that main minima correspond (with very few exceptions) to systems belonging to the same group, while other extrema are mostly associated to the anomalous shell-filling process.

A brief global conclusion obtained from the analysis of all figures discussed up to now in the present subsection is that the Fisher divergence in momentum space $FD_p(Z, Z')$ for neutral atoms displays a structural richness which is clearly related to the shell filling process and structure, while the same measure in position space loses such an information content as shown by its unimodal behavior for all atomic systems.

Concerning the last conclusion, it is natural to wonder on the quality of the just analyzed Fisher divergence as compared to the quadratic distance QD given by

$$QD(\rho_1, \rho_2) \equiv \left(\int [\rho_1(\vec{r}) - \rho_2(\vec{r})]^2 \, d\vec{r} \right)^{1/2}. \tag{10.2}$$

Among this kind of studies, it is worthy to remark those only carried out in position space [362, 384] as well as other more complete ones just recently published involving additionally the momentum and the phase spaces [361, 364]. In the present work, we have carried out for the QD distance a similar analysis as that performed with the FD divergence. Again, the previously mentioned unimodal shape for the $QD_r(Z, Z')$ curves is displayed in position space, a richer structure being obtained in the momentum one. So, and for comparison purposes, we will restrict ourselves to the FD_p and QD_p quantities, in order to analysis the characteristic structural patterns of both them.

From a systematic comparison of the curves $FD_p(Z, Z')$ and $QD_p(Z, Z')$ as functions of Z for a fixed Z', it is concluded that their resemblances and differences are strongly determined by the specific Z' atomic value chosen for comparing them, as well as by the range which the Z values belong to. This can be clearly observed in Figures 10.3(a) and 10.3(b), correponding to $Z' = 9$ and $Z' = 5$ respectively. The main structure of both curves in Figure 10.3(a) for $Z' = 9$ (properly scaled in order to carried out an useful comparison) is very similar over almost the whole Periodic Table. All peaks appear to be of the same kind (maximum or minimum), whether for cases corresponding to atoms

of the same group as $Z' = 9$ whether for those associated to the anomalous shell filling. However, a strongly different behavior is observed in Figure 10.3(b) for the $Z' = 5$ atom. It is clearly observed how the Fisher divergence $FD_p(Z, 5)$ displays an enhanced sensitivity associated to the shell structure as compared to that shown by the quadratic distance $QD_p(Z, 5)$.

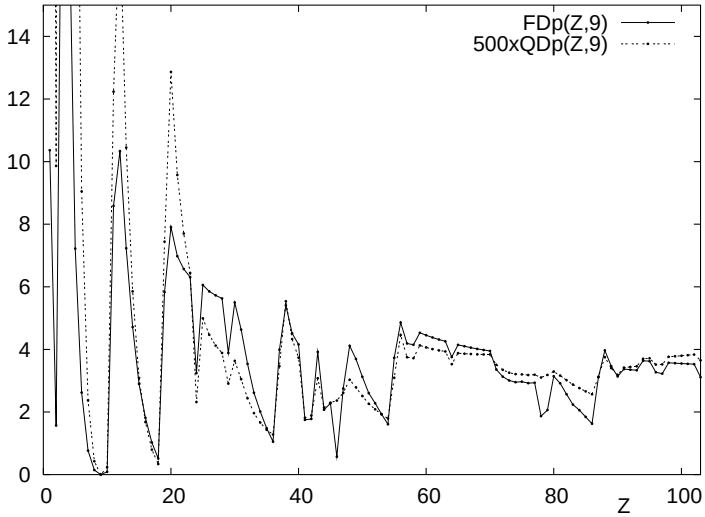

(a) F ($Z' = 9$)

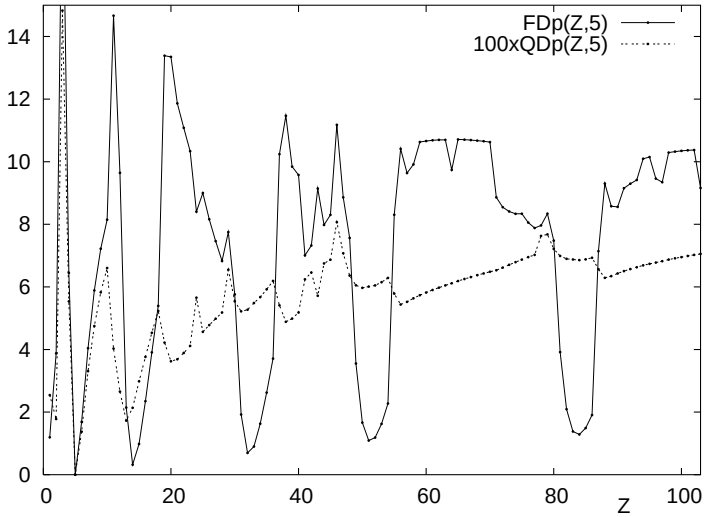

(b) B ($Z' = 5$)

FIGURE 10.3: Fisher divergence $FD_p(Z, Z')$ and quadratic distance $QD_p(Z, Z')$ in momentum space for $Z = 1 - 103$ of (a) F ($Z' = 9$) and (b) B ($Z' = 5$). Atomic units are used.

10.1.2 Jensen-Shannon divergence

As mentioned in the previous chapter, two of the most popular ways (apart from the quadratic distance) of defining global quantitative measures of dissimilarity among distribution functions are the Jensen-Shannon divergence (JSD)

$$JSD(\rho_1, \rho_2) = S\left(\frac{\rho_1 + \rho_2}{2}\right) - \frac{1}{2}\left[S(\rho_1) + S(\rho_2)\right], \tag{10.3}$$

and the symmetrized Kullback-Leibler entropy (KLS).

$$KLS(\rho_1, \rho_2) = \int \rho_1(\vec{r}) \ln \frac{\rho_1(\vec{r})}{\rho_2(\vec{r})} d\vec{r} + \int \rho_2(\vec{r}) \ln \frac{\rho_2(\vec{r})}{\rho_1 \vec{r})} d\vec{r}. \tag{10.4}$$

Attending to the aim of the present work, namely the analysis of different measures in order to compare atomic electron densities in both position and momentum spaces as well as the interpretation of the corresponding results from a physical point of view, it appears natural to carry out a similar study to that developed in the previous subsection for the Fisher divergence (FD), now in terms of the above mentioned quantities of global character, opposite to the local one of FD.

In doing so, let us first analyze the $JSD(Z, Z')$ curves (as functions of Z) for each value Z' corresponding again, for illustration, to noble gases in position (Figure 10.4(a)) and momentum (Figure 10.4(b)) spaces, in a similar fashion as done for FD. Now it is worthy to remark the roughly similar structure of the JSD measure for any Z' through the whole Periodic Table independently of the space considered. This similarity strongly differs from the corresponding behavior of the FD divergence as remarked in the previous section. An important conclusion on this result is that the position space JSD_r divergence provides much more information on the atomic structural properties than the quadratic distance or the FD divergence, being far from their position space unimodality. Location of main extrema of $JSD(Z, Z')$ still remains determined by the shell-filling process following similar patterns to those of the FD_p divergence in momentum space, but also appearing now in position one for the JSD_r divergence, in spite of not being so ordered, narrow and deep as in the FD_p case.

Restricting ourselves to the momentum space, it is clearly revealed the higher content of information of the Fisher divergence FD on the atomic shell-filling process than that provided by the Jensen-Shannon divergence JSD, being again better displayed in momentum space the structural richness of atomic systems by means of the local divergence FD as compared to the global one JSD.

Similar comments are also valid for all other groups in the Periodic Table, as well as for the symmetrized Kullback-Leibler entropy $KLS(Z, Z')$ in both spaces. In order to have an idea of the behavior of the KLS relative measure, the corresponding values are

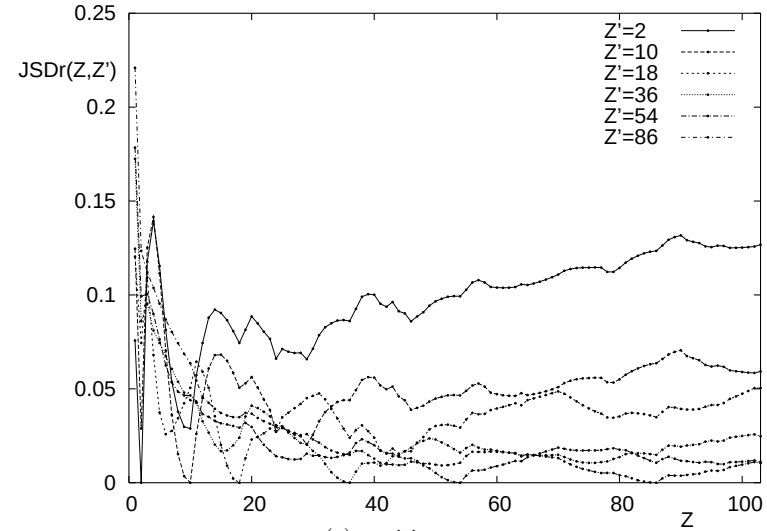

(a) position space

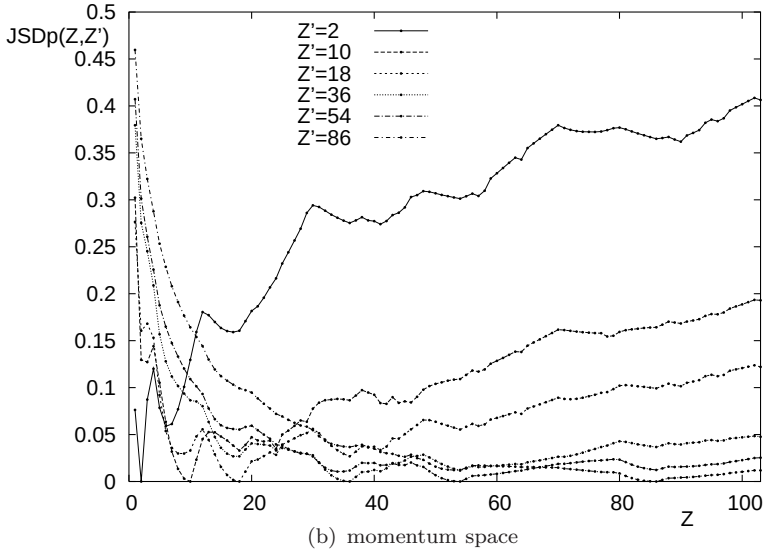

(b) momentum space

FIGURE 10.4: Jensen-Shannon divergence $JSD(Z, Z')$ of noble gases ($Z' = 2, 10, 18, 36, 54, 86$) for $Z = 1 - 103$ in (a) position and (b) momentum spaces. Atomic units are used.

displayed in Figures 10.5(a) and 10.5(b) in position and momentum spaces, respectively. Similarly as ocurred with the JSD divergence, the shell-filling pattern is clearly displayed in both spaces, even more clearly in position space when dealing with heavy systems. In any case, location of extrema in both cases appears again determined by the shell structure of the involved atoms. The present analysis widely generalizes and improves the only previous one, to the best of our knowledge, carried out in order to compare atomic distributions [385], where the KL relative entropy, as well as the quadratic and L^1 distances, were employed to the study of consecutive atoms.

The reason of JSD and KLS displaying relevant structure in both conjugated spaces, as opposite to the FD case where only in momentum space was observed, arises from their

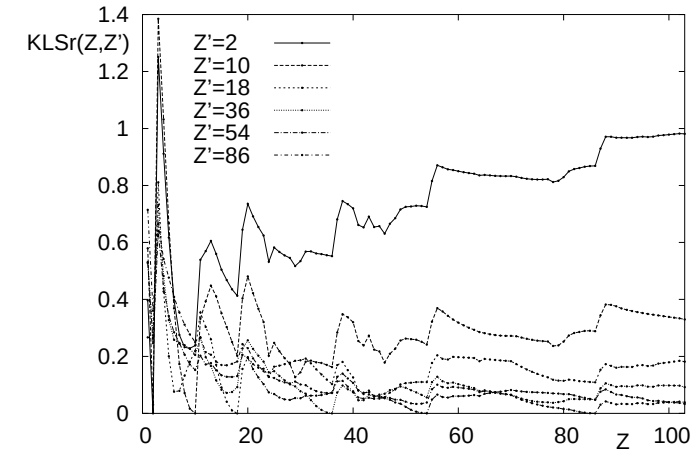

(a) position space

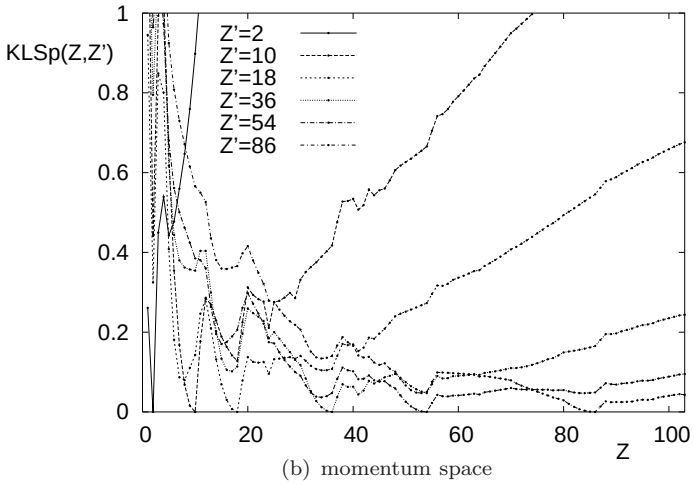

(b) momentum space

FIGURE 10.5: Symmetrized Kullback-Leibler entropy $KLS(Z, Z')$ of noble gases ($Z' = 2, 10, 18, 36, 54, 86$) for $Z = 1 - 103$ in (a) position and (b) momentum spaces. Atomic units are used.

definition in terms of a logarithmic functional, being consequently determined by the behavior of the compared densities over the whole domain with a balanced quantification on short- and long-range regions.

So, it can be concluded that the measures of global character JSD_r and KLS_r in position space provides more information than the local character measure FD_r, while the level of structure of the same quantities in momentum space appears appreciably higher for the Fisher divergence FD_p than for the global Jensen-Shannon and Kullback-Leibler ones.

10.2 Divergence analysis of monoionization processes

In this section we focus in the outer electronic layer of the atom in order to study the dissimilarities between the neutral systems and the singly charged ones, with identical

nuclear charge, by means of their corresponding electronic densities. In doing so we calculate the Jensen-Shannon and Fisher divergences, given by Eqs. (10.3) and (10.1) respectively, associated to the corresponding densities involved in the monoionization processes, to analyse a set of 150 atomic systems including anions, neutral species and cations, with a number of electrons up to $N = 54$.

We also compute, for the sake of completeness, the Quadratic distance (Eq. (10.2)) and the Quantum similarity index (QSI):

$$QSI(\rho_1, \rho_2) \equiv \frac{\int \rho_1(\vec{r})\rho_2(\vec{r})d\vec{r}}{\sqrt{\int \rho_1^2(\vec{r})d\vec{r} \int \rho_2^2(\vec{r})d\vec{r}}}, \tag{10.5}$$

in order to better interpret and compare the aforementioned systems and processes. Let us start with these two quantities. We have computed, in r and p spaces, QD and QSI between neutral species ($N = 1 - 54$) and their singly charged cations (NC pairs) or anions (AN pairs) as well as between anions and cations (AC). The results confirm and expand some basic and preliminary results obtained for these charged systems [364].

Concerning position space, all computed values of QD_r, for the aforementioned pairs of atomic systems, as shown in Figure 10.6(a), provide very smooth curves versus Z, whatever the type of ionization process suffered by the atom might be. The monotonic decreasing behaviour of the curves shows how QD_r between atoms and ions are simply smaller as the nuclear charge Z grows. Therefore QD in position space masks any information concerning periodicity properties, groups of the Periodic Table which the systems belong to and the characteristics of the outermost subshell involved in the ionization.

However, results are completely different in momentum space where the shell structure of the Periodic Table is clearly displayed in Figure 10.6(b). The ranges of values for QD_p are strongly dependent on the orbital angular momentum 'l' of the subshells affected by the change on the number of electrons, and the great structure of the curves in this space contrasts deeply with the monotonous behaviour displayed in position space. These very different trends in the conjugated spaces are shown in Figure 10.6 for the three studied processes: $A \to N$, $N \to C$ and $A \to C$ by removing one or two electrons. It is worthy to note also that (i) the three curves in momentum space (Figure 10.6(b)) are completely fitted, in spite of their picked structure, (ii) distances between these three couples are ordered, for fixed Z, in the sense that $QD(AN) < QD(NC) < QD(AC)$ in both spaces, and (iii) an average decreasing trend, with the size of the atom, modulates this rich structure, i.e. changes in the ionization processes of heavy atoms are, overall, smaller than those suffered by light atoms.

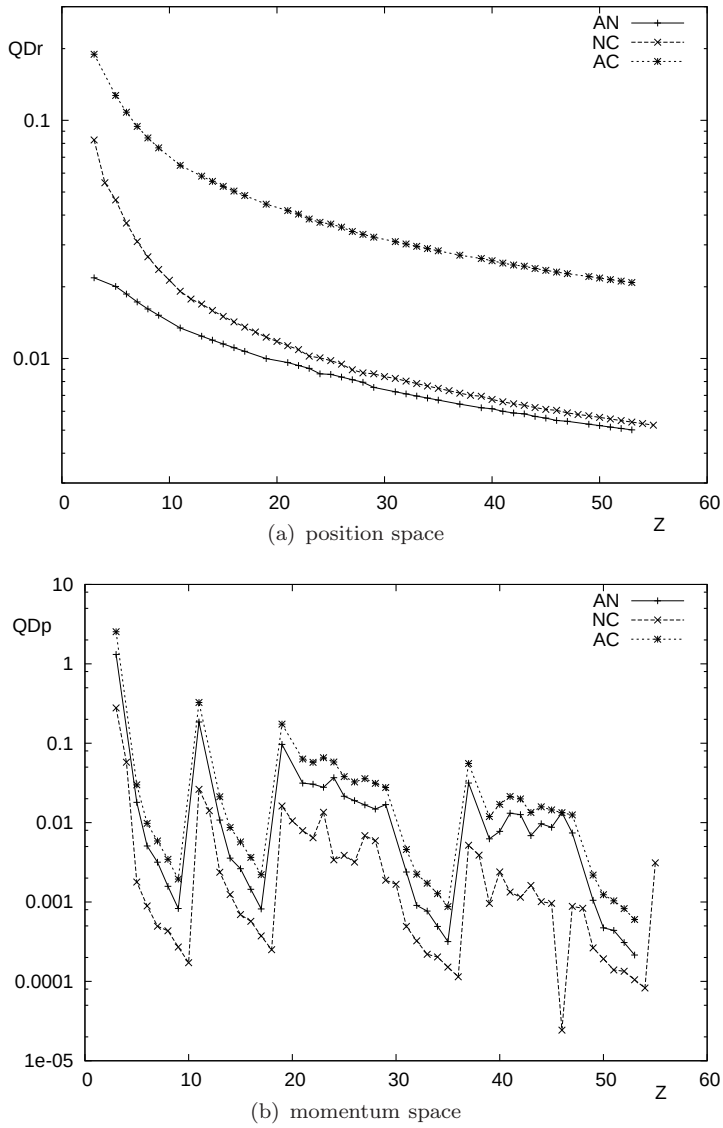

FIGURE 10.6: Quadratic distance QD among neutral atoms (N) and singly charged anions (A) and cations (C) with nuclear charge Z in (a) position and (b) momentum spaces. Atomic units are used.

Analogous results are found for the corresponding quantum similarity index (QSI), where all computed values, in position space, almost reach the maximum value 1, whereas a much richer structure is displayed in p space, as shown in Figure 10.7, for illustration, in the NC process. As expected, minimum values of QSI_p correspond, overall, with maximum ones of QD_p. Besides, the atomic ionization potential (AIP), which is the basic experimental magnitude to be considered according to the physical process we are studying, is also displayed in the figure. It is worthy to mention here the coincidence of minima for QSI_p with relevant ones for AIP (corresponding to ionization related to 's' valence subshells), and also the apparent constant (almost equal to 1) values of QSI_p for atoms suffering ionizations in 'p' subshells.

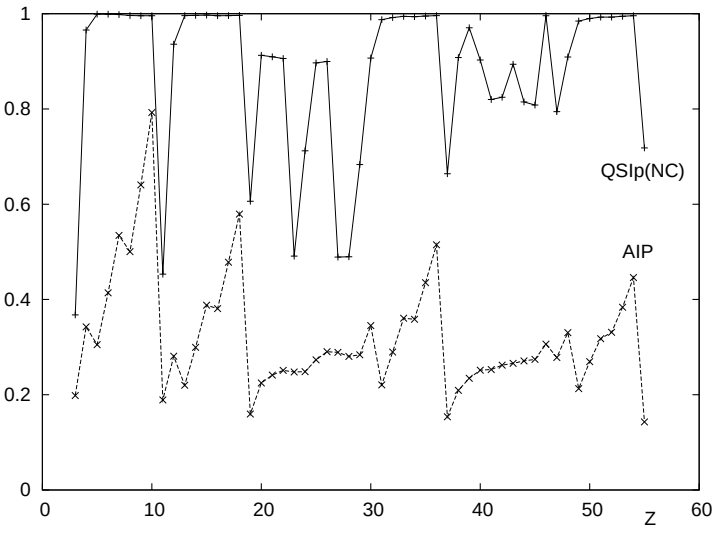

FIGURE 10.7: Quantum similarity index $QSI_p(NC)$ between neutral atoms (N) and singly charged cations (C), and atomic ionization potential AIP of neutral atoms with nuclear charge Z. Atomic units are used.

The strong differences found concerning the level of structure for both the QD and QSI measures in the two conjugated spaces are understood by analyzing their definitons as well as the short- and long-range behaviors of the one-particle densities. The exponential decrease of the position space density $\rho(r)$ makes the values of the three overlap integrals to be mainly quantified by the region around the nucleus, where the nuclear charge Z determines the value of the density. Consequently, both QD_r and QSI_r are strongly dependent on the nuclear charge of the compared systems, much more than on the outermost regions where the valence subshell determine the most relevant physical and chemical properties. On the other hand, such a valence region corresponds to the low-speed electrons, i.e. those associated with the momentum density around the origin and, consequently, to the main contributions on evaluating the overlap integrals for the corresponding QD_p and QSI_p measures.

Figures 10.8(a) and 10.8(b) show, in r and p spaces respectively, the results obtained by comparing the informational divergences before defined, namely FD and JSD, when an electron is removed from the neutral species ($N \rightarrow C$), as well as the atomic ionization potential AIP needed for performing such a process. We note first that both divergences display in position space a notable structure in contrast to QD (Figure 10.6) and QSI measures, and second that, in spite of being of very different character (local (FD) or global (JSD) ones), both divergences not only follow similar general trends in the two conjugated spaces, but each one also belong to a similar range of values independently of the considered space. These are new and important facts that reveal the power of these two divergences over those computed by QST.

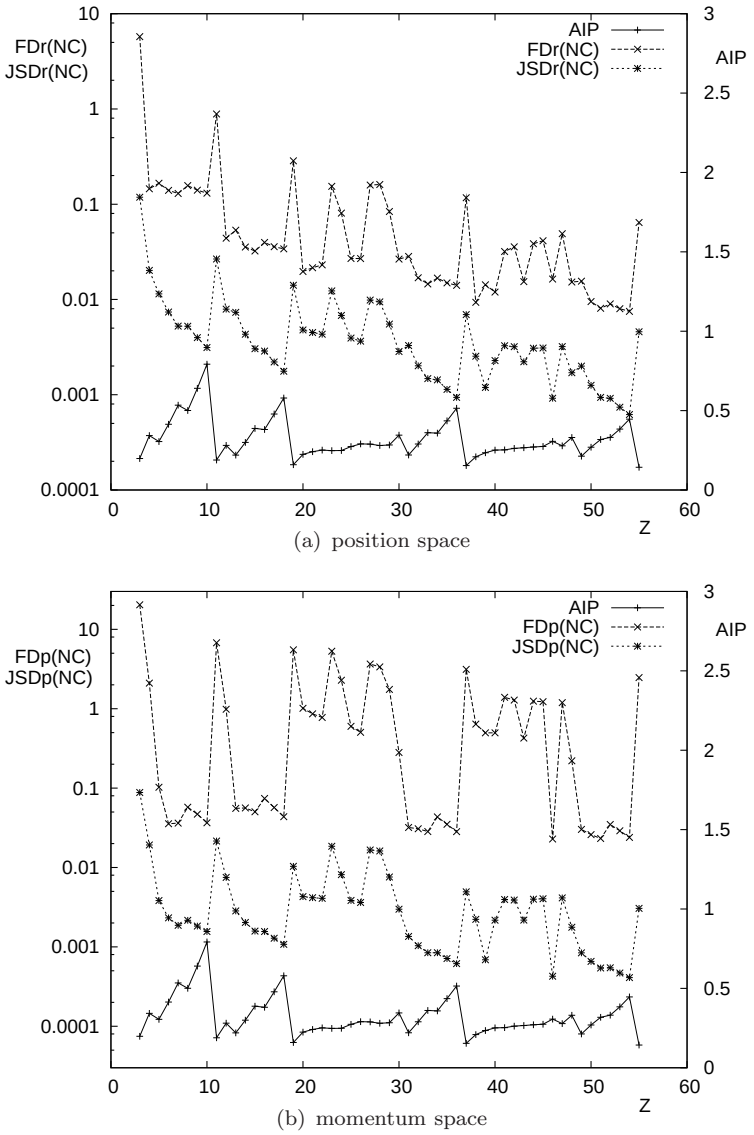

FIGURE 10.8: Fisher and Jensen-Shannon divergences, FD(NC) and JSD(NC), between neutral atoms (N) and singly charged cations (C) in (a) position and (b) momentum spaces, and atomic ionization potential AIP of neutral atoms with nuclear charge Z. Atomic units are used.

Carrying out the same analysis for other ionization processes, namely those in which the compared systems are a singly charged anion and the resulting one after removing one ($A \to N$) or two ($A \to C$) electrons (the neutral atom or the singly charged cation, respectively), similar conclusions are obtained.

However it is important to note and to analyze the pointed and fluctuant structure of these divergences within each period by comparing their extremal values to those of AIP. In Table 10.1, values of the nuclear charge Z for which the divergences considered in this work display local extrema are given. In addition, minimum values of the AIP are associated to systems with a single electron in the valence subshell, making consequently such a subshell to disappear after ionization, and the resulting system to strongly differ

Measure		**N ⟶ C**	**A ⟶ N**	**A ⟶ C**
AIP	(s)	3,11,19,23,28,37,47,55		
	(p,d)	5,8,13,16,31,34,49		
FD_r	(s)	3,11,19,23,28,37,42,45,47,55	3,11,19,24,37,41,45	3,11,19,24,29,37,42,47
	(p,d)	5,8,13,16,31,34,39,49	6,14,32,50,53	8,16,34,52
JSD_r	(s)	3,11,19,23,27,37,41,45,47,55	3,11,19,24,29,37,42,44,46	3,11,19,23,27,37,41,44
	(p,d)	31,49		
FD_p	(s)	3,11,19,23,27,37,41,44,47,55	3,11,19,37,46	3,11,19,23,27,37,41,44
	(p,d)	25,33,40,43,51	33,51	
JSD_p	(s)	3,11,19,23,27,37,41,45,47,55	3,11,19,24,29,37,42,44,46	3,11,19,23,27,37,41,44
	(p,d)	8,52	7,15,33,51	
QD_p	(s)	3,11,19,23,25,27,37,40,43,47,55	3,11,19,24,29,37,41,44,46	3,11,19,23,27,37,41,44
	(p,d)			
QSI_p	(s)	3,11,19,23,27,37,41,45,47,55	3,11,19,24,29,37,42,44,46	3,11,19,24,29,37,42,47
	(p,d)	16,34,52	7,15,33,51	8,15

TABLE 10.1: Nuclear charge Z of local extrema for the atomic ionization potential AIP of neutral atoms and/or the Fisher and Jensen-Shannon divergences in position (FD_r and JSD_r) and momentum (FD_p and JSD_p) spaces, and the quadratic distance QD_p and the quantum similarity index QSI_p in momentum space, for ionization processes among neutral atoms (N) and singly charged anions (A) and cations (C). Atomic units are used.

from the initial one. This relevant difference is usually revealed in terms of a high divergence and dissimilarity between the initial and the final system.

Attending to the above discussion, the Table 10.1 contains the values of Z for which both the AIP and the QSI_p display local minima, and also those corresponding to local maxima of momentum space QD_p as well the divergences FD and JSD in both position and momentum spaces. Let us remember at this point the structureless of both QD and QSI in position space, being consequently not included in the table. Additionally, two cases have been distinguished according to the involvement of any 's' electron on the ionization process or else only 'p' and 'd' ones. This is done because of the relevant role played by the first ones in conditioning the associated divergence and similarity values.

However, there is only one exception for the rules previously given in order to choose the kind of extrema (maxima or minima) to be considered: instead of maxima, the Z values provided for the $FD_r(AN)$ divergence correspond to its minima. The fact that this particular quantity displayed such a behavior can be explained attending to the long-range behavior of the position space atomic densities. Denoting by ϵ the AIP of a given system (for the sake of simplicity), it is well-known [316, 386] that the charge density behaves as $\rho(r) \sim e^{-\sqrt{8\epsilon}r}$ for large r. The FD definition given by Eq. (10.1) allows to assert that $FD(\rho_1, \rho_2) \sim (\epsilon_1 - \epsilon_2)^2$. For alkaline metals, the AN process makes a completely filled 's' valence subshell to become half-filled, while the other two processes (NC and AC) completely remove the initial non-empty 's' subshell, giving rise to a final closed-shell system (namely the singly charged cation) with a much higher AIP than the initial system (with s valence subshell) in the AN process. So, the difference between their AIP, which determines the behavior of the FD divergence, is much higher

when the final system is a cation than a neutral atom. In this analysis it has been essential the presence of the logarithmic derivative in the FD definition, which provides the aforementioned dependence on the ionization potential in position space. This is not the case neither for the momentum space nor for other measures.

In all the aforementioned cases there exist a strong correlation also with the structure displayed by the atomic ionization potential AIP in the NC ionization process in which an 's' electron is removed, as shown in the corresponding column of the table, as well as in Figures 10.8(a) and 10.8(b). However, the same is not true when the removed electron is of 'p' or 'd' type, where such a connection with the AIP extrema only remains for the position space Fisher divergence FD_r. Concerning the QST and divergence measures, these comments are also valid for the AN and AC ionization processes.

The above mentioned goodness of the Fisher divergence in position space FD_r on displaying such a richer structure as compared to the other measures as well as the divergence in momentum space, can be better understood by turning up to the long-range behavior of the charge density in terms of the atomic ionization potential, being the connection between the extrema of FD_r and AIP the closest one within the magnitudes enclosed in the Table 10.1.

In order to better interpret the number and location of extrema of these quantities, the corresponding ionization processes are detailed in the Table 10.2 for all systems considered in the present section. It is observed the systematic presence of the alkaline atoms ($Z = 3, 11, 19, 37, 55$) for which only 's' electrons are removed from the initial system. Additionally, many of the other extrema shown in the Table 10.1 correspond to systems involved in the so-called 'anomalous shell-filling' as well as for ionizations concerning non-valence subshells (see Table 10.2). Sometimes there appear extrema for processes involving 'p' subshells when they become half-filled or completely removed after the ionization.

Let us remark here that some recent works have dealt previously with the correlation between information measures and the atomic ionization potential, according to its role in describing the single ionization processes [308, 364]. The net Fisher information measure, defined as the product of both the position and momentum Fisher information, is found to be correlated, at least qualitatively, with the inverse of the experimental ionization potential [387], as similarly shown to occur with Onicescu information energy [208]. However, those and other works only deal with pairs of neutral systems within a given model, or a unique system described within different models [385], contrary to the case considered in the present work, namely the dissimilarities between neutral and charged species.

Z	**A**	$\longrightarrow$	**N**	$\longrightarrow$	**C**
3-4	$2s^{j+1}$	$\longrightarrow$	$2s^{j}$	$\longrightarrow$	$2s^{j-1}$
5-10	$2p^{j+1}$	$\longrightarrow$	$2p^{j}$	$\longrightarrow$	$2p^{j-1}$
11-12	$3s^{j+1}$	$\longrightarrow$	$3s^{j}$	$\longrightarrow$	$3s^{j-1}$
13-18	$3p^{j+1}$	$\longrightarrow$	$3p^{j}$	$\longrightarrow$	$3p^{j-1}$
19-20	$4s^{j+1}$	$\longrightarrow$	$4s^{j}$	$\longrightarrow$	$4s^{j-1}$
21-22,25-26,30	$4s^{2}3d^{j+1}$	$\longrightarrow$	$4s^{2}3d^{j}$	$\longrightarrow$	$4s^{1}3d^{j}$
23,27-28	$4s^{2}3d^{j+1}$	$\longrightarrow$	$4s^{2}3d^{j}$	$\longrightarrow$	$4s^{0}3d^{j+1}$
24,29	$4s^{2}3d^{j}$	$\longrightarrow$	$4s^{1}3d^{j}$	$\longrightarrow$	$4s^{0}3d^{j}$
31-36	$4p^{j+1}$	$\longrightarrow$	$4p^{j}$	$\longrightarrow$	$4p^{j-1}$
37-38	$5s^{j+1}$	$\longrightarrow$	$5s^{j}$	$\longrightarrow$	$5s^{j-1}$
39	$5s^{2}4d^{1}5p^{1}$	$\longrightarrow$	$5s^{2}4d^{1}$	$\longrightarrow$	$5s^{2}4d^{0}$
40,43,48	$5s^{2}4d^{j+1}$	$\longrightarrow$	$5s^{2}4d^{j}$	$\longrightarrow$	$5s^{1}4d^{j}$
41-42,44-45,47	$5s^{2}4d^{j}$	$\longrightarrow$	$5s^{1}4d^{j}$	$\longrightarrow$	$5s^{0}4d^{j}$
46	$5s^{2}4d^{9}$	$\longrightarrow$	$5s^{0}4d^{10}$	$\longrightarrow$	$5s^{0}4d^{9}$
49-54	$5p^{j+1}$	$\longrightarrow$	$5p^{j}$	$\longrightarrow$	$5p^{j-1}$
55			$6s^{1}$	$\longrightarrow$	$6s^{0}$

TABLE 10.2: Initial and final occupation numbers of outermost atomic subshells for some ionization processes among neutral atoms (N) and singly charged anions (A) and cations (C).

10.3 Divergence analysis of isoelectronic series

The isoelectronic series provide a well-known benchmark for the study of atoms and molecules. In this section results concerning the application of the informational divergences previously defined, are provided. We have analyzed nine atomic isoelectronic series, each one composed of a neutral atom and some of its cations. Each series consists of 21 systems, all of them with equal number of electrons N and their nuclear charge running from $Z = N$ to $Z = N + 20$. In this way we study how these divergence measures characterize, from the informational point of view, this set of 189 different systems, corresponding to the series with $N = 2 - 10$. On one hand, the effect of increasing/decreasing the nuclear charge is studied and, on the other, the electronic organization of each isoelectronic series is investigated. In doing so, the previously employed comparative measures (QSI, QD, FD and JSD) between the neutral species ($Z = N$) and each member of the isoelectronic series ($Z = N + 1, \ldots, N + 20$) have been computed.

Double Figure 10.9 shows the global Jensen-Shannon divergence (JSD) in r and p spaces. This global divergence works similarly in position and momentum space.

Some monotonic trends are also shown in these figures: (i) the divergence between the neutral system and each member of the isoelectronic series increases with Z, as it should be expected, showing that distances from neutrals increase when the nuclear charge becomes larger, (ii) this increasing behaviour with the size of the nucleus is progressively less notable, and (iii) the location of each isoelectronic curve is ordered according to N,

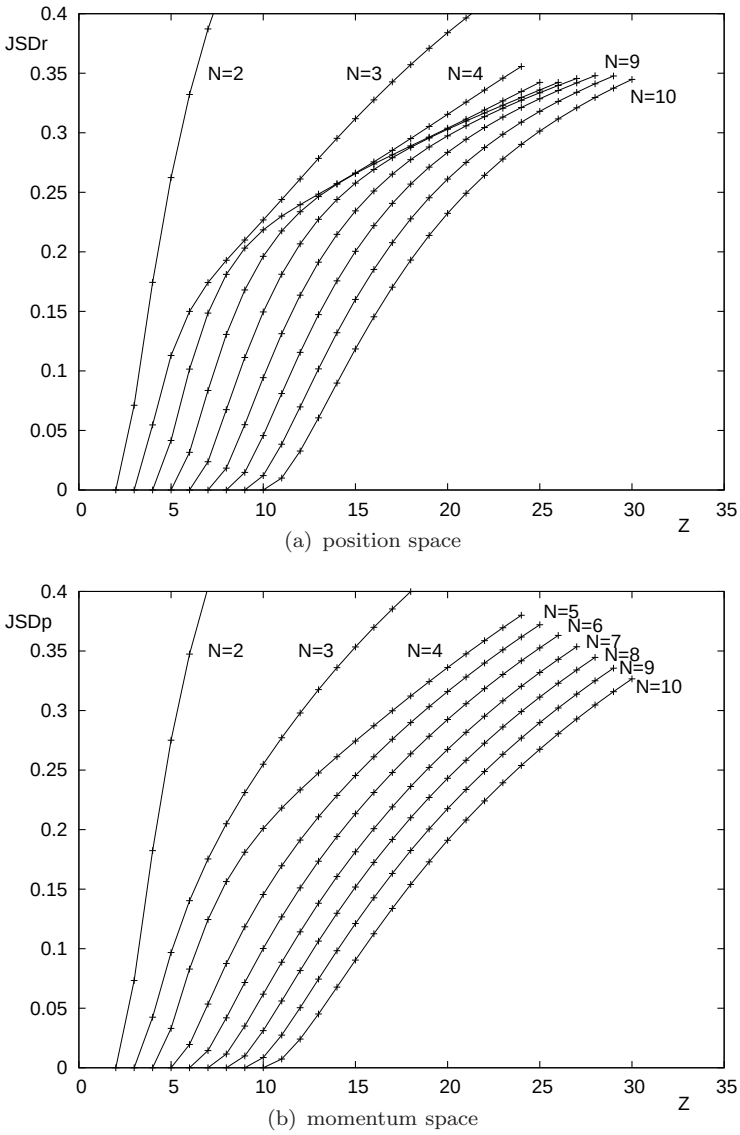

FIGURE 10.9: Jensen-Shannon divergence JSD between N-electron neutral atoms and cations for the isoelectronic series with $N = 2 - 10$ and nuclear charge Z within the range $N \leq Z \leq N + 20$ for each series, in (a) position and (b) momentum spaces. Atomic units are used.

so that divergences decrease with the number of electrons, N for fixed Z. In other words the value of the divergence is smaller when the size of the electronic cloud for both neutral and cation is bigger.

Double Figure 10.10 shows the Fisher divergence (FD) for the same isoelectronic series studied above. In this case it is important to note a very different behaviour as compared to that of JSD . First of all the trends of this local divergence, FD, in r and p spaces are very different, as FD_r displays a clearly increasing behaviour with Z, but FD_p tends towards a constant value when the size of the nucleus grows. Besides, FD_r has the following characteristics: (i) within each series, it increases with Z, as JSD_r does, but now this increase is progressively more notable according to the size of the nucleus and

(ii) a monotonic decreasing ordering of the isoelectronic curves with N is once again observed. On the other hand, the most important characteristics of FD_p are: (i) it increases at a lesser extent as the nucleus becomes larger, and at the end of the series it is almost unsensitive to the size of the nucleus, and (ii) the monotonic behaviour of the curves with N is broken by the $N = 2$ isoelectronic series.

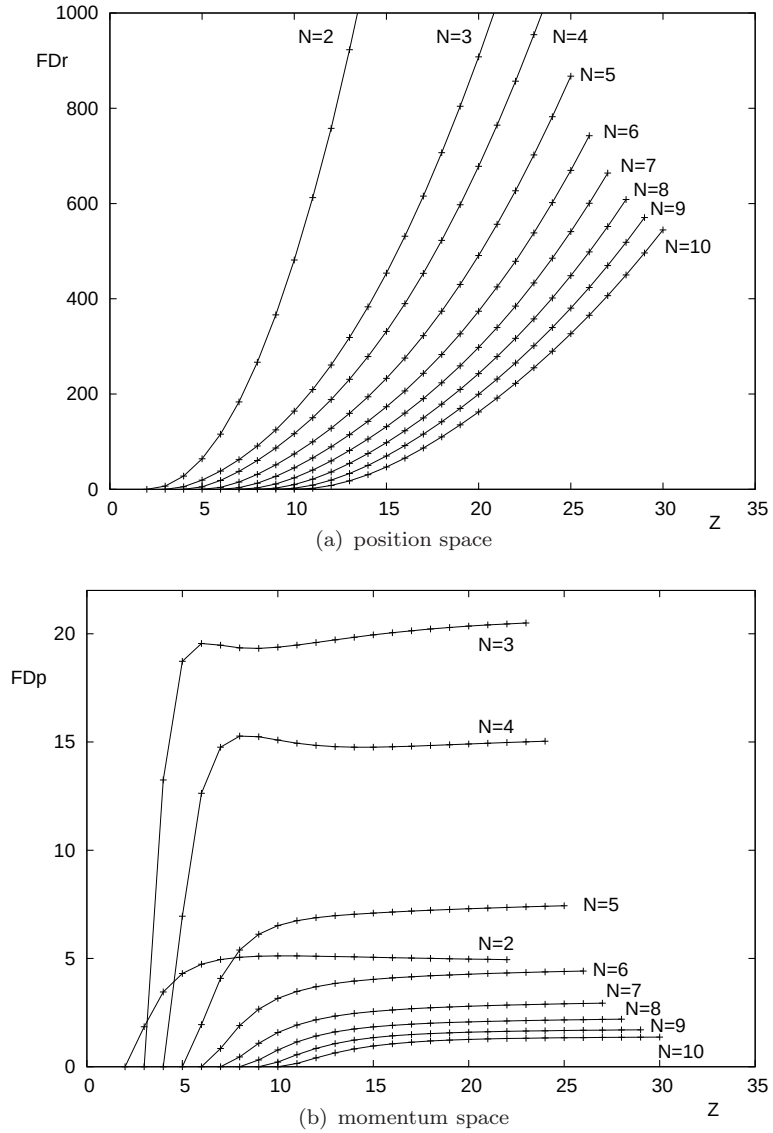

FIGURE 10.10: Fisher divergence FD between N-electron neutral atoms and cations for the isoelectronic series with $N = 2 - 10$ and nuclear charge Z within the range $N \leq Z \leq N + 20$ for each series, in (a) position and (b) momentum spaces. Atomic units are used.

This much more sensitive trend of FD versus JSD can be understood if we look at the local character of this divergence in comparison to the global one of JSD. In this sense, FD is much more sensitive to the local characteristics (near the origin, asymptotic behaviour, etc.) of the densities under comparison. In particular, it is worthy to remember the hydrogen-like behavior of the position space density around

the nucleus, which translates into the so-called 'cusp condition' [388], valid for any atomic system:

$$\frac{\rho'(0)}{\rho(0)} = -2Z, \tag{10.6}$$

which reveals a proportionality of the logarithmic derivative at the nucleus and the nuclear charge. Taking into account that the main relative contribution to the integrals defining FD_r comes from the region surrounding the nucleus (due to the fast exponential decay of the density), the aforementioned condition translates into a dependence of such a divergence between these systems on their nuclear charges as

$$FD(\rho_1, \rho_2) \sim (Z_1 - Z_2)^2 \tag{10.7}$$

which makes, as expected, the Fisher divergence to considerably increase when comparing the neutral system with a highly charged one. In fact, increasing the nuclear charge makes absolute value of the slope for the logarithmic derivative of the density around the nucleus to proportionaly increase and, consequently, also the Fisher information itself due to the high 'content of gradient' in that region. Additionally, it is worthy to point out how both divergences FD and JSD behave in a strongly different or similar fashion according to the space we are dealing with, namely position or momentum, respectively.

Similar comments on the QD and QSI measures can be done concerning monotonicity and ordering of the curves. In fact, the shape of the quadratic distance QD is found to be very similar to that of the Fisher divergence, sharing also the previously discussed opposite trends in both conjugated spaces. In what concerns the quantum similarity index QSI, it displays a monotonically decreasing behavior as the nuclear charge increases. This means that the similarity index along a given isoelectronic series mainly depends on the difference between the nuclear charge of the systems under consideration.

10.4 Conclusions

In this Chapter we have considered diferent divergence and dissimilarity measures, i.e. FD, JSD, KLS, QD and QSI, with the aim of analyzing the similarity and discrepancy among neutral and/or ionized atoms throughout the Periodic Table. These systems have been considered as an appropriate benchmark due to their strong hierarchical organization. The studied divergences have been shown to provide relevant information on the atomic shell structure and other physically relevant properties.

In particular, in Section 10.1 we have center our attention in the neutral systems, obtaining that the Fisher divergence, in spite of its local character, is almost unsensitive (as also happens with the QD and the QSI measures) to the atomic shell structure

when dealing with the corresponding position space distributions, constituting only in fact a measure of how close the compared systems are located at the Periodic Table, independently of the groups they belong to be different or the same. On the other hand, the situation absolutely differs from that one when dealing with the momentum space, where both the QD and the FD measures clearly show the complex organization and the shell-filling patterns at the Periodic Table. Now a strong similarity among members of the same atomic group is displayed, as well as relevant differences among systems owning valence subshells with different occupation and/or quantum numbers. Higher resolution is displayed by FD as compared to QD, especially for large Z systems. Concerning the global divergences KLS and JSD, they are shown to be quantities displaying a non trivial structure in position space, at a similar level to that provided in momentum space. Nevertheless, such a structure is much softer as compared to that of the momentum space Fisher divergence FD. Attending to the last comment, it appears much better to consider the simultaneous analysis in both conjugated spaces of all divergences here studied in order to exploit the information content and structural richness of the atomic systems.

As an immediate consequence of the above discussed characteristics, it appears strongly relevant to consider the complementary use of both spaces attending to the chosen divergence or comparative measure between atomic densities, especially for interpreting the results according to relevant physical and/or chemical properties such as those related to their shell structure, among others.

In Section 10.2, a comparison of ionized and neutral atomic systems have been carried out. We can conclude that the Quantum Similarity Techniques provides only relevant information on periodicity properties and shell structure when dealing with one-particle densities in momentum space. However, the corresponding values in position space are only concerned by, at most, how large the nuclear charge is. On the contrary the divergences measures defined and computed in this section, i.e. FD and JSD, explore deeply, in both conjugated spaces, the changes suffered by the atoms on their shell structure as a consequence of the ionization, by changing either the number of electrons or the nuclear charge.

These dissimilarity measures clearly show the complex organization and the shell-filling patterns at the Periodic Table. Specially remarkable is the correlation found between extrema of the atomic ionization potential and those of the divergences. Besides a thorough analysis of changes suffered on the subshells from which an electron is removed is done and they are also related to the values of the divergence measures. Characteristic features in the divergences accompanying the ionization process, by adding or removing electrons, are identified, and the physical reasons for the observed patterns are described. In particular, it has been shown the relevant role played, among other characteristics, by the angular momentum quantum number of the removed electron in the ionization process, the significance in many cases of the anomalous shell filling, as well as the

value of the atomic ionization potential as related to the Fisher and Jensen-Shannon divergences and the QST measures.

Concerning the similar study of the dependence on the nuclear charge Z when keeping fixed the number of electrons N along different isoelectronic series (analyzed in Section 10.3), the divergence among neutral atoms and cations increases as the difference between the nuclear charges of both systems becomes larger. In this case, no shell filling properties are displayed since both atomic systems under comparison have identical occupation numbers.

Chapter 11

Generalized Jensen divergences and dissimilarity of atomic electron densities

In this chapter we analyze the divergence of neutral atomic systems in terms of the generalized Jensen divergences, i.e. those defined in terms of generalizations of the Shannon entropy, such as the Rényi (Section 11.1) and Tsallis (Section 11.2) entropies. The corresponding divergences are given by:

$$JRD^{(q)}\left(\rho_1,\rho_2\right) \equiv R^{(q)}\left(\frac{\rho_1+\rho_2}{2}\right) - \frac{1}{2}\left[R^{(q)}\left(\rho_1\right) + R^{(q)}\left(\rho_2\right)\right], \tag{11.1}$$

and

$$JTD^{(q)}\left(\rho_1,\rho_2\right) = T^{(q)}\left(\frac{\rho_1+\rho_2}{2}\right) - \frac{1}{2}\left[T^{(q)}\left(\rho_1\right) + T^{(q)}\left(\rho_2\right)\right], \tag{11.2}$$

respectively.

To the best of our knowledge, the only relative measure with a characteristic parameter applied in the past for atomic systems is the relative Rényi entropy [312], by comparing atomic densities to hydrogen-like ones.

11.1 Jensen-Rényi divergence

Let us consider, firstly, the Jensen-Rényi divergence, JRD, applied to the study of neutral atoms throught the Periodic Table with nuclear charges $Z = 1 - 103$. The computations of $JRD^{(q)}$ for the particular values $q = 0.4, 0.8$, as compared to the limiting case $q \to 1$ which corresponds to JSD, provides the results shown in Figure 11.1 for the divergence between Krypton (nuclear charge $Z = 36$) and all neutral atoms throughout

the Periodic Table. The chosen values of q comply with the constraint $0 < q < 1$ which guarantees the non-negativity of JRD. Additionally, the constraint $q > 3/8$ in momentum space arising from the corresponding density has been taken into account.

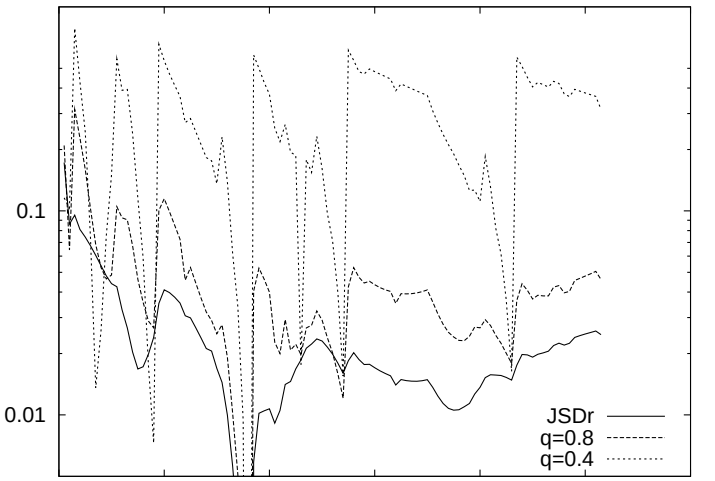

(a) Position space

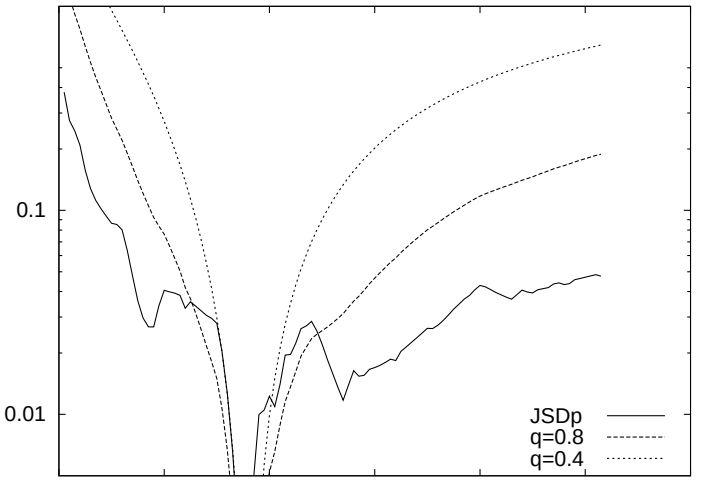

(b) Momentum space

FIGURE 11.1: Jensen-Rényi divergence $JRD^{(q)}$ for $q = 0.4, 0.8$ and Jensen-Shannon divergence $JSD = JRD^{(1)}$ between the one-particle densities of Krypton (nuclear charge $Z = 36$) and those of neutral atoms with $Z = 1 - 103$, in (a) position and (b) momentum spaces. Atomic units are used.

According to the definition of the JRD in terms of the Rényi entropy, Eq. (11.1), it is clearly observed that lowering the value of the parameter q below 1 enhances different contributions of the density domain according to the considered space (position or momentum) in an opposite way: enhancing the valence region in position space and the nuclear region in the momentum one. This is a consequence of the structural properties of both one-particle atomic densities, for which their maximum values are located at the origin systematically in position space, and frequently very close to it in the momentum

one. As explained before, the valence subshell is far from the nucleus as compared to the other ones, and the exponential decrease of the density makes the contribution of such a region to the JRD value to be very small, unless enhancing it by powering the density with a small exponent q. The Figure 11.1(a) reveals that, in order to get shell-filling patterns by means of $JRD^{(q)}$ in position space, low values of the parameter q are required.

The opposite trend is observed in the Figure 11.1(b), similarly justified as previously. The momentum density around the origin quantifies the relative number of electrons with low linear momentum 'p', which are just those located in the outermost region. Consequently, the contribution of that region is now diminished when lowering 'p'.

Concerning the momentum space, the value $q = 1$ appears as 'almost critical', in the sense that going down only up to $q = 0.8$ makes the previous structure to disappear almost completely.

So, the role played by the value of the parameter q allows one to obtain a higher level of information on the shell-filling effects according to the space which the density considered belongs to.

The discussion concerning the specific structure of the curves displayed in this figure can be carried out in a similar fashion to that of Figures in the previous section. That is, the location of the main minima corresponds to systems belonging to the same atomic group of Krypton (i.e. noble gases), while other minor ones are mostly associated to systems suffering the 'anomalous shell-filling'. This comment is valid for the JRD in both conjugated spaces, for those q values for which such a structure is displayed.

11.2 Jensen-Tsallis divergence

Now, let us consider a given neutral system for computing its $JTD^{(q)}$ divergence with respect to all neutral atoms throught the Periodic Table with nuclear charges $Z = 1-103$. This will be done for several values of the parameter q as well as in both conjugated spaces. For illustration, we choose as initial system the Mg atom ($Z = 12$) and the values $q = 0.6, 1.0, 1.4, 2.0,$ as well as $q = 0.2$ in position space. Let us remark that the last value is not allowed in momentum space, where the convergence conditions for $T^{(q)}$ require $q > 3/8 = 0.375$ due to the long-range behavior of the momentum density as p^{-8} [270], while the exponential decrease for the position density [316] guarantees the convergence for any $q > 0$.

The corresponding JTD curves are displayed in Figure 11.2, for position and momentum spaces (Figures 11.2(a) and 11.2(b), respectively). Some comments are in order. In both spaces, it is clearly observed that the structure of the curves strongly depends on the value of q. In fact, if we consider the smoothest curve in a figure (understood according

to the number and enhancement of local extrema), varying the q value in a monotone way provokes the curves to increase their level of structure progressively, as measured by the number of extrema and their enhancement. After crossing a critical value, the succesive curves lose the rough unimodal shape, keeping always their minimal value zero at $Z = 12$. In fact, the value $q = 1$ which provides the Jensen-Shannon divergence through the equality $JTD^{(1)} = JSD$ appears very close to the critical one in both spaces, in spite of the number of extrema displayed by the JSD at this level. However, the aforementioned variation follows opposite trends in each space. While the highly structured curves are displayed for low q values in position space, the situation for momentum space is just the opposite, where higher values of q are required in order to depart from unimodality.

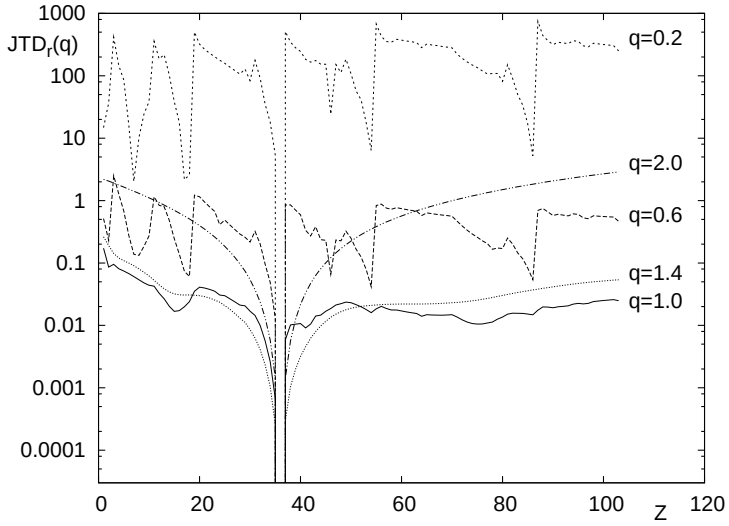

(a) position space

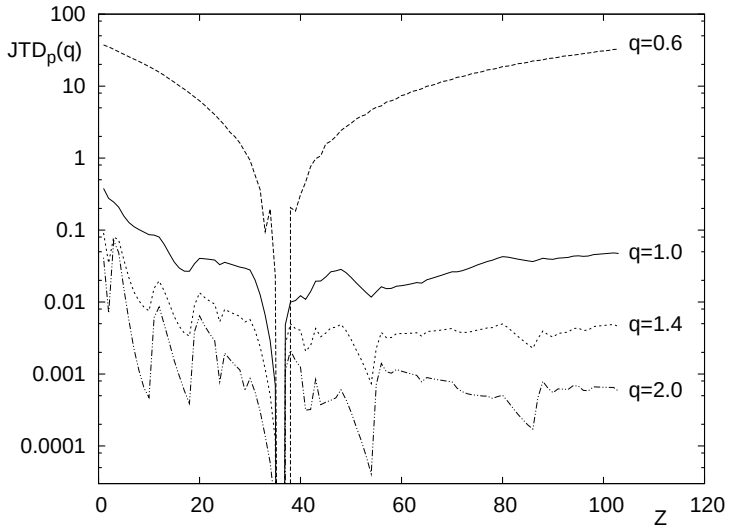

(b) momentum space

FIGURE 11.2: Jensen-Tsallis divergence $JTD^{(q)}$ between Mg (nuclear charge $Z = 12$) and all neutral atoms with the $Z = 1 - 103$, (a) in position space for $q = 0.2, 0.6, 1.0, 1.4, 2.0$, and (b) in momentum space for $q = 0.6, 1.0, 1.4, 2.0$. Atomic units are used.

A straighforward interpretation of the observed opposite behaviors noted above might be obtained by considering the physical meaning of the position and momentum densities, as well as their respective structural properties, previously described, especially concerning the values of the densities around the origin.

The differences between the short- and large-range values are enhanced if the power of the density within the integrand of $\omega^{(q)}(\rho)$ increases, making the value of JTD to be strongly determined by the region of the density around the origin. Conversely, decreasing the value of the parameter q smoothes the integrand, raising up the relative contribution of the outermost region.

Let us remember that the densities around the origin are associated to the surround of the nucleus (position space) and the outermost region (momentum space). This fact justifies the observed opposite trends in terms of q: as its value increases, the enhancement in position space corresponds to the nuclear region, whereas in momentum space corresponds to the valence one.

Taking into account that the shell-filling patterns are determined by the valence region, they are clearly observed in momentum space for large q. Then, the JTD divergence value is mainly based on the different characteristics of the systems under comparison according to their dissimilarity in what concerns shell-filling, while the comparison in position space is mainly determined by the values of their nuclear charges. Opposite trends are observed when decreasing the value of the parameter q. The same reasoning given above for explaining the JTD behavior as q increases also applies for the decreasing case. So that, the role played by the value of the parameter q allows one to obtain a higher level of information on the shell-filling effects, by enhancing the relative contribution of different specific regions according to the space we are dealing with. A continuous variation of q makes the contribution to the comparative measure of the outermost spatial region or, equivalently, of the valence subshell containing the low speed electrons, to vary also in a continuous way.

Concerning the structure of the curves displayed, their local extrema can be classified according to two different characteristics: (i) the lower JTD divergence when comparing an atomic system to another one belonging to the same group of the Periodic Table, and (ii) JTD values when one of the atoms under comparison belongs to the so-called anomalous shell-filling set of atomic systems. As will be shown below, this is a common feature in the study of dissimilarity based on the JTD divergence. The main achievement of the JTD in the present application is its ability to quantify the dissimilarity between atomic systems according to one of the more physically relevant characteristics, namely the shell-filling process, which determines most of the atomic chemical properties, being strongly related also to some experimentally accessible quantities, such as e.g. the first ionization potential [101].

The present comparative performance is far from the concept of distance among atoms according to the values of their nuclear charges, essentially interpreted as size or weight for neutral atoms. This fact is clearly displayed in the Figure 11.3, where the JTD of both $Z = 36, 38$ atoms along the Periodic Table is displayed. Those systems have been chosen in order to consider a couple of atoms with very similar nuclear charges but strongly different valence subshells as well as many other physical characterisitcs. In doing so, the JTD are given for $q = 0.5$ (below 1), $q = 1.5$ (above 1) and the limiting case $q = 1$ for which JTD turns out to be JSD. For the JSD divergence, there appear slight differences between the curves for $Z = 36$ and $Z = 38$, independently of the space considered. It is also worth noting that the range of values for JSD in both spaces is roughly the same.

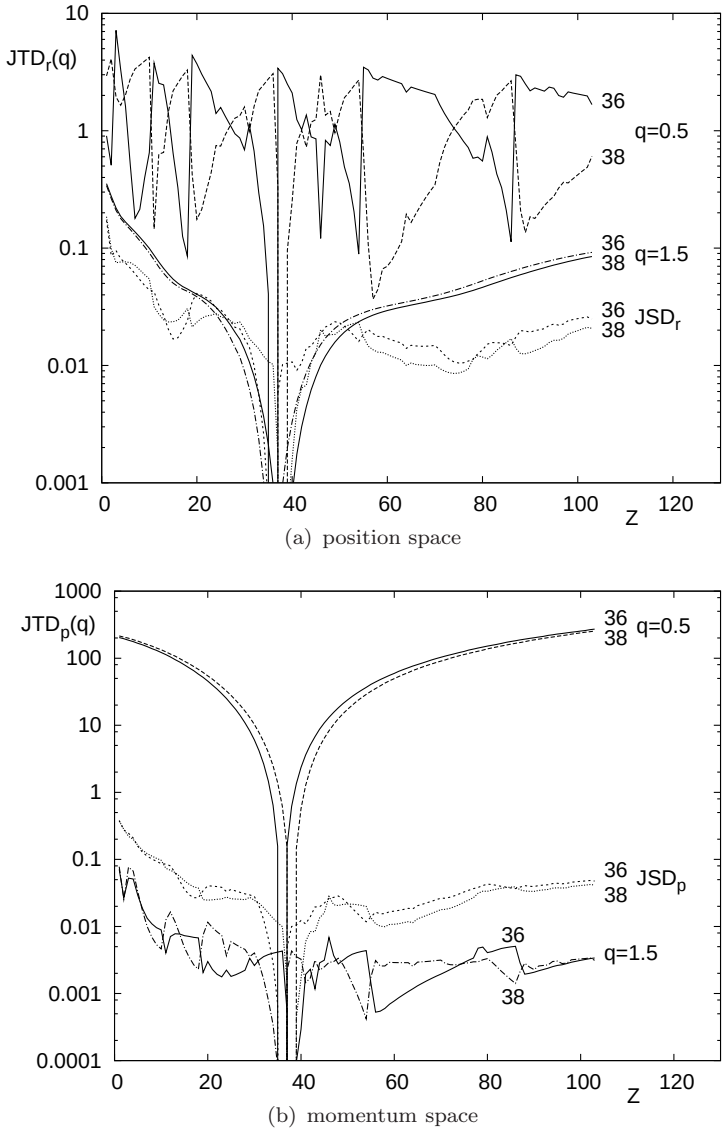

(a) position space

(b) momentum space

FIGURE 11.3: $JTD^{(q)}$ divergences of systems with nuclear charge $Z = 36$ (solid) and $Z = 38$ (dashed) with respect to all neutral atoms with $Z = 1 - 103$ for $q = 0.5, 1.0, 1.5$, in (a) position and (b) momentum spaces. Atomic units are used.

Dealing with position space in Figure 11.3(a), the JSD measure allows to observe a slight structure in the curves, which dissapears completely for the higher order divergence JTD ($q = 1.5$) but which extremely enhances for the low order $q = 0.5$, with both curves displaying in fact absolutely different structures and extrema at similar positions but with opposite maximum/minimum character. So it is concluded the convenience of dealing with low-order JTD in order to get relevant information on the valence characteristics. An opposite trend is displayed in Figure 11.3(b) for momentum space, where higher order JTD are the useful ones when analysing the aforementioned properties. In both spaces, the JTD curves progressively modify their shapes as the parameter q varies in a continuous form, making the number of extrema and their enhancement also to vary in a monotonic way.

In all cases, the appearance of local extrema in the curves is determined, as remarked in the discussion of Figure 11.3, by the groups of the Periodic Table which the atoms belong to. The divergence of a system with respect to an atom of the same group is smaller than that of its neighbors, displayed in the figures as apparent minima. In the present case, the valence orbital of $Z = 36$ is p^6, while for $Z = 38$ it is s^2. Those minima correspond, respectively, to atoms with identical valence orbital. Additional extrema, mainly minima, are associated with systems that suffer from the anomalous shell-filling effects.

The Figure 11.4 provides a corroboration of the previous observations. The curves correspond to the JTD values in position space of each atom belonging to the noble gases group, as compared to all the atomic systems throughout the Periodic Table. According to those comments, it should be expected a similar behavior for all the atoms belonging to the same group. A comparison between the cases $q = 1$ and $q = 0.2$ (Figures 11.4(a) and 11.4(b) respectively) makes once again to notice that, in spite of the similarity (at least roughly) among the shapes of the curves, they are almost identical for the low q order JTD as compared to the JSD. Similar observations can be noted from Figure 11.5 with regard to momentum space, where now the comparison between the Figure 11.5(a), corresponding to JSD, and a higher q order in Figure 11.5(b) makes the curves to get closer, with the only exception of the $Z = 2$ (Helium) one. The reason which justifies this exception is the different structure of the Helium, with an 's' valence subshell, as compared to the 'p' one for the others in the same group.

The analysis of the JTD divergence between atomic systems carried out above, regarding the relevancy of the considered divergence order q, the shell-structure of the systems under comparison as well as the information provided by the position and momentum densities allow us to consider this comparative measure as a powerful tool in order to appropriately quantify the dissimilarity of atomic systems, according to specific regions, on the basis of their respective one-particle densities.

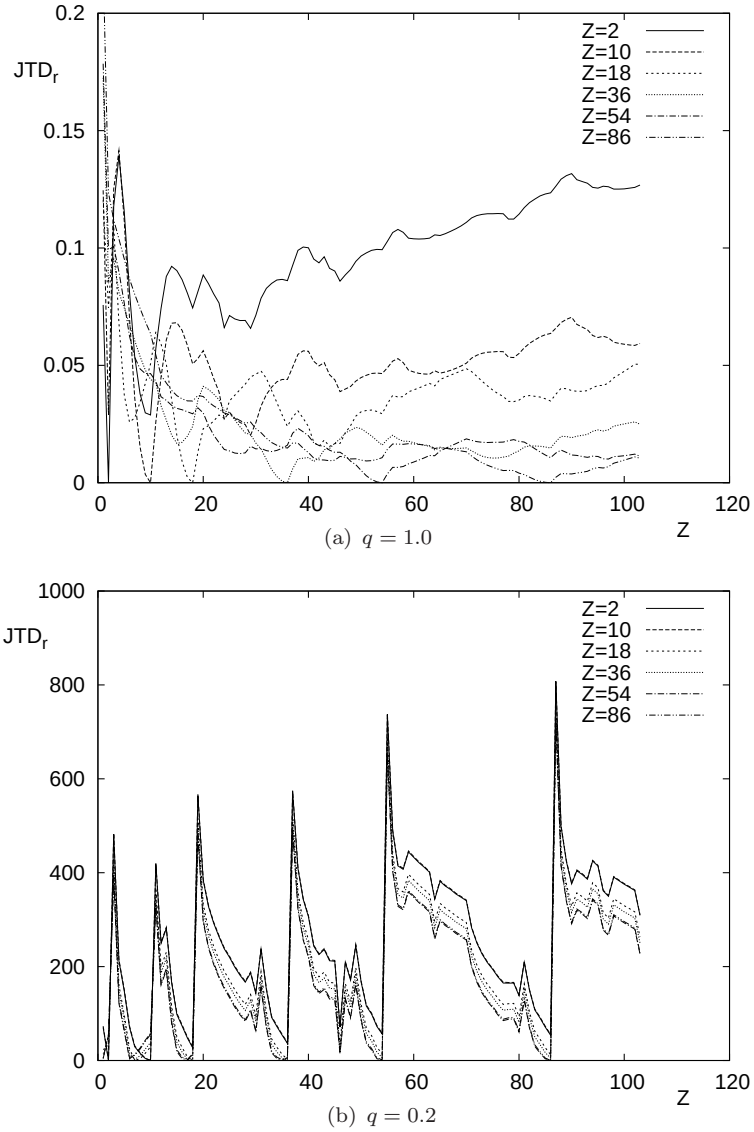

(a) $q = 1.0$

(b) $q = 0.2$

FIGURE 11.4: Jensen-Tsallis divergence in position space $JTD_r^{(q)}$ for the noble gases ($Z = 2, 10, 18, 36, 54, 86$) with respect to all neutral atoms with $Z = 1 - 103$, for (a) $q = 1.0$ and (b) $q = 0.2$. Atomic units are used.

It is worthy to remark that, in spite of the availability of other comparative measures, the JTD allows to perform a deeper and more detailed study as compared to other ones, such as JSD or KLS considered in the previous chapter. Attending to that comparison, the behavior of the JTD in the conjugated spaces deserves a relevant comment, concerning its capability to provide relevant information in both spaces, contrary to the case of many other measures, such as for instance the quadratic distance, the quantum similarity index and the Fisher divergence, which are not able to provide the aforementioned informational description when dealing with the position space, requiring to perform this type of analysis by means of the momentum space density.

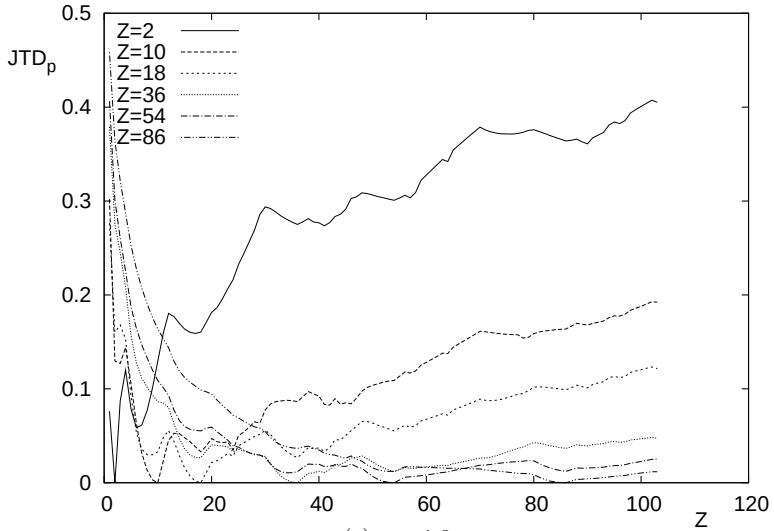

(a) $q = 1.0$

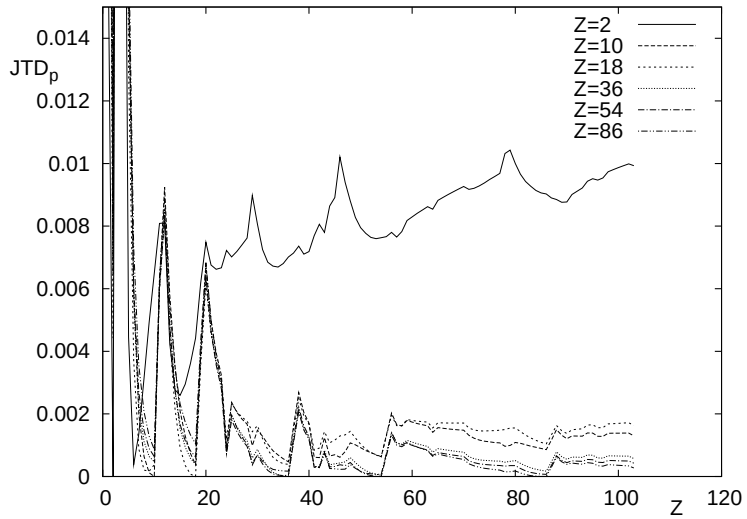

(b) $q = 2.5$

FIGURE 11.5: Jensen-Tsallis divergence in momentum space $JTD_p^{(q)}$ for the noble gases ($Z = 2, 10, 18, 36, 54, 86$) with respect to all neutral atoms with $Z = 1 - 103$, for (a) $q = 1.0$ and (b) $q = 2.5$. Atomic units are used.

11.3 Conclusions

In this Chapter we have proposed generalized divergence measures, based in concepts taken from the Information Theory, to study the dissimilarity among multielectronic distributions. It has been shown how the Jensen-Tsallis divergence JTD and Jensen-Rényi divergence JRD allow a deep introspection within the structure of the atomic one-particle densities.

In the first section of this chapter, Section 11.1 we have analyzed the information about the dissimilarity between neutral atomic systems given by the JRD, the other generalization of the Jensen-Shannon divergence. The Jensen-Rényi divergence (JRD) appears

capable of assigning different weights to specific regions of the electronic distribution domains in order to control the most important contributions of the electronic cloud to the atomic densities in position and momentum spaces. This generalized divergence provide information on the atomic shell structure and shell-filling patterns in both conjugated spaces as it occurs with the JTD.

From the Section 11.2, we can conclude that the JTD captures relevant differences in any of the conjugated spaces. This is not the case of other measures of divergence employed with multielectronic systems. The neutral atoms have constituted a benchmark for the present analysis, displaying their complex and hierarchical organization along the Periodic Table. The employment of the JTD (as we as the JRD) as a divergence measure can be applied not only to compare a couple of probability distributions, but also to an arbitrary number of them, even assigning different weights to each distribution considered as a whole, apart from the weighting effect of the characteristic parameter of JTD.

Further applications of this generalized divergence are actually being carried out for atoms and molecules, such as the comparisons among (i) distributions computed within different models for a given system, (ii) parts or components of the global system, (iii) atomic species involved in ionization processes, and (iv) initial and final products in chemical reactions. On the other hand, the generality of the techniques here employed allows the extension of this study to many relevant physical and chemical systems and/or processes. The results of those studies are being currently investigated in our laboratories and will be provided elsewhere.

We can conclude that, although both measures, i.e., JTD and JRD, are useful in order to determine the differences between neutral atoms in terms of their valence characteristics, we have obtained numerically a better description of the shell-filling proccess by means of JTD. On the other hand, the JRD has an advantage as compared to JTD, i.e., it is an extensive measure, namely, JRD is an additivity measure (for further detail, see Chapter 1, where the Rényi and Tsallis entropies were defined and discussed).

Chapter 12

Other applications of divergence measures

In this chapter we explore other applications of the divergence measures presented in the previous chapters, in particular for the Jensen-Shannon, Jensen-Rényi and Fisher divergences.

Firstly, in Section 12.1 we analyze the effects of the intereletronic repulsion in atoms by means of the divergence measures between the one-particle densities for a given systems, computed within two different models: Hartree-Fock (HF) and Bare Coulomb Field (BCF).

In Section 12.2 a study of the information content of atomic electron densities is carried out, by finding the contribution for a given atom of its composing subshells to the total atomic information and, similarly, the spread of information for selected sets of atoms, such as periods and groups within the Periodic Table as well as isoelectronic series is quantified.

12.1 Effect of the interelectronic repulsion on the information content of atomic densities

The interelectronic repulsion within atomic systems forbides to consider the global atom as a nucleus surrounded by a mere superposition of one-electron orbitals, each one governed exclusively by the electron-nucleus attraction potential which depth is given by the nuclear charge Z. Ignoring the repulsive forces is the basic feature of the so-called 'Bare Coulomb Field' (BCF) model [389] among others, in which the electron densities in both position and momentum spaces are determined by adding over all orbitals the corresponding hydrogen-like densities.

This section deals with the problem of quantifying the dissimilarity among atomic electron densities built up within different models, in order to establish a comparison to be interpreted according to the main differences between both models. Especially interesting appears the case in which the interelectronic repulsive force is taken into account in one model but not in the other, with the aim of analysing the most relevant informational characteristics, as will be described later, of the respective one-particle densities.

Different choices of models involving or not the electron-electron repulsion can be considered. Such is the case, for instance, of the BCF model in the non-repulsive case, but not the only one. At this point it is worthy to remark the well-known Kohn-Sham equations and the associated densities [101], where the Fermi statistics between the spin-like electrons remains after performing the appropriate manipulations. This framework, together with some additional models, will be also considered elsewhere with similar and complementary aims. For the main purposes of the present section, the quantitative comparisons between atomic densities are carried out by taking as reference non-repulsive densities the BCF ones. Similar comments concerning atomic densities arising from equations enclosing the repulsive terms can be also done, in the sense that different frameworks are susceptible of being employed, such as e.g., the Near-Hartree-Fock with or without relativistic corrections, configuration interaction, etc.

Some results have been rigorously proved concerning BCF densities. For instance, March showed that the electron charge density is a monotonically decreasing function for an arbitrary number of closed shells in the BCF case [389], and also the same property holds in the momentum space [390]. Additional results for the kinetic and total energies have been also obtained [391–393]. More recently computations for the atomic reciprocal form factor have been carried out in a BCF framework showing that this relevant quantity is spherically symmetric, positive and monotonically decreasing [394], and additional rigorous results have been also provided [395].

Instead of considering the BCF problem and solutions, more sophisticated models, such as e.g. the Hartree-Fock (HF) one [101], appear necessary in order to properly describe the atomic system by also considering the repulsive forces among electrons. Thinking on the N electron density in position space as a negatively charged cloud located around the nucleus with positive charge Z, it is immediate to realize that the interelectronic repulsion makes the cloud to increase its spread over the whole space and to decrease the mean speed of its constituents. This effect has an influence on the atomic position and momentum electron densities when taking into account the repulsive forces as compared to those built up from the purely attractive electron-nucleus potential. In this sense, it should be expected the repulsion to give rise, on one hand, to a more sparse position density and, on the other hand, to a momentum density more concentrated around the origin as center of the region of very low speeds.

The aforementioned intuitive notions on the effects of the repulsive forces among electrons on their representative one-particle densities in both position and momentum spaces would be desirable to be described not only qualitatively, as just done above, but also quantitatively by means of appropriate density functionals in order to quantify the specific level of sparsing of both the BCF (non-repulsive) and the HF (including repulsion) densities, and also by measuring in an appropriate way the 'distance' between both models in terms of the corresponding distributions.

The goal is to study the effect of the interelectronic repulsions on all neutral atoms throughout the Periodic Table by means of their electron HF and BCF densities $\rho(\mathbf{r})$ and $\gamma(\mathbf{p})$ in both conjugated spaces. The results will be analyze from a physical point of view according to relevant structural characteristics of the atomic densities, such as the shell-filling process. The BCF densities are easily built up in terms of hydrogen-like wavefunctions, while the numerical study throughout this work in the HF case will be carried out by using the accurate Near-Hartree-Fock wavefunctions of Koga et al [269]. In order to perform the aforementioned study, we will compute the quadratic distance (QD) and the quantum similarity index (QSI), as well as the Fisher (FD), Jensen-Shannon (JSD) and Jensen-Rényi (JRD) divergences.

12.1.1 The quantum similarity index and the quadratic distance

Let us start with the numerical analysis of QD given by

$$QD(\rho_1, \rho_2) \equiv \left\{ \int [\rho_1(\mathbf{r}) - \rho_2(\mathbf{r})]^2 d\mathbf{r} \right\}^{1/2} \tag{12.1}$$

and QSI defined as

$$QSI(\rho_1, \rho_2) \equiv \frac{\int \rho_1(\mathbf{r})\rho_2(\mathbf{r})d\mathbf{r}}{\sqrt{\int \rho_1^2(\mathbf{r})d\mathbf{r} \int \rho_2^2(\mathbf{r})d\mathbf{r}}}, \tag{12.2}$$

between the spherically averaged BCF and HF electron densities, in position and momentum spaces, $\rho(r)$ and $\gamma(p)$ respectively. In Figure 12.1(a), $QD_r(HF, BCF)$ is displayed for all neutral atoms with nuclear charge $Z = 1 - 103$, and similarly in Figure 12.1(b) for the momentum space (by only replacing the HF and BCF densities ρ by γ and, consequently, the variable 'r' by 'p'). First, we observe that the values in both figures have been drawn as piecewise curves, each piece corresponding to the periods which constitute the Periodic Table. This has been made in order to better interpret the results according to the shell-filling process. As should be expected, increasing the number of electrons makes the distance between both models also to increase, due to the higher effect of the electronic repulsion, as clearly observed in Figure 12.1(a).

In spite of the piecewise drawing procedure, the curve corresponding to $QD_r(HF, BCF)$ in Figure 12.1(a) appears almost continuous while $QD_p(HF, BCF)$ in Figure 12.1(b)

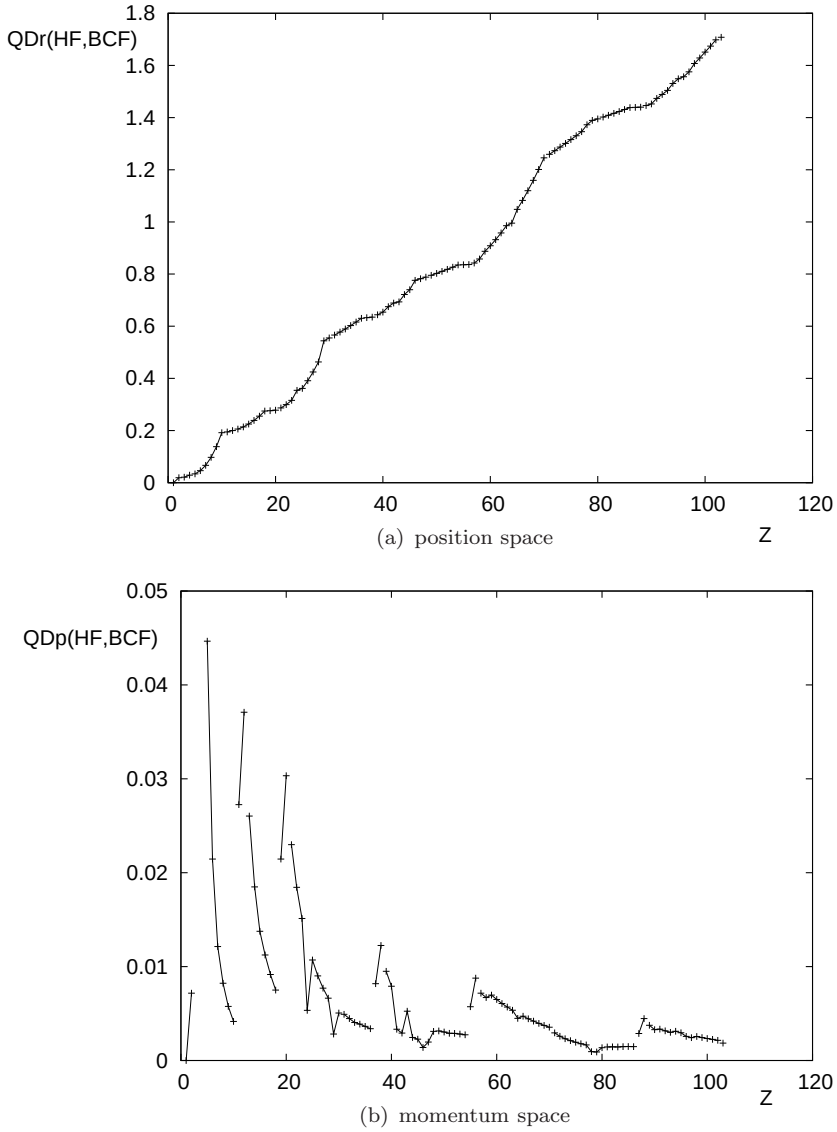

(a) position space

(b) momentum space

FIGURE 12.1: Quadratic distance $QD(HF, BCF)$ for neutral atoms with nuclear charge $Z = 1 - 103$ in (a) position and (b) momentum spaces. Atomic units are used.

clearly displays the aforementioned piecewise behaviour attending to the periods the atoms belong to. Nevertheless, the periodicity pattern can be also observed in position space, $QD_r(HF, BCF)$, not in terms of apparent discontinuities in the curve as occurs in momentum space, but as changes in its slope when moving from a period to the next one. These results are interpreted as follows: the main characteristic which share both models is the identical value of the nuclear charge Z, and also that the region around the nucleus is mainly governed by the attractive electron-nucleus potential as compared to the repulsive one. The last one is dominant over the first in the external region (valence subshell) which characterizes the periodicity patterns of the atomic systems. However, the fast decrease (exponential) of the charge densities makes the external subshells contribution to the integrals to be almost negligible. The opposite can be argued

in discussing Figure 12.1(b), where more slow electrons (close to $p = 0$) are just those of valence subshells which, consequently, carry a relevant contribution on computing the integrals. These comments can be better understood by observing Figures 12.2(a) and 12.2(b), where the involved one dimensional integrands (the functions integrated from 0 to ∞) are represented in order to appreciate their contribution to the global integrals. As previously mentioned, it is clearly observed that the relevant values of the three involved integral in position space, even for heavy atoms ($Z = 88$ as in Figure 12.2(a)) are strongly localized very close to the origin (i.e. the nucleus) displaying there almost identical values, while the differences among them in momentum space for the same atom (Figure 12.2(b)) are not only much stronger but also displayed over a much wider region.

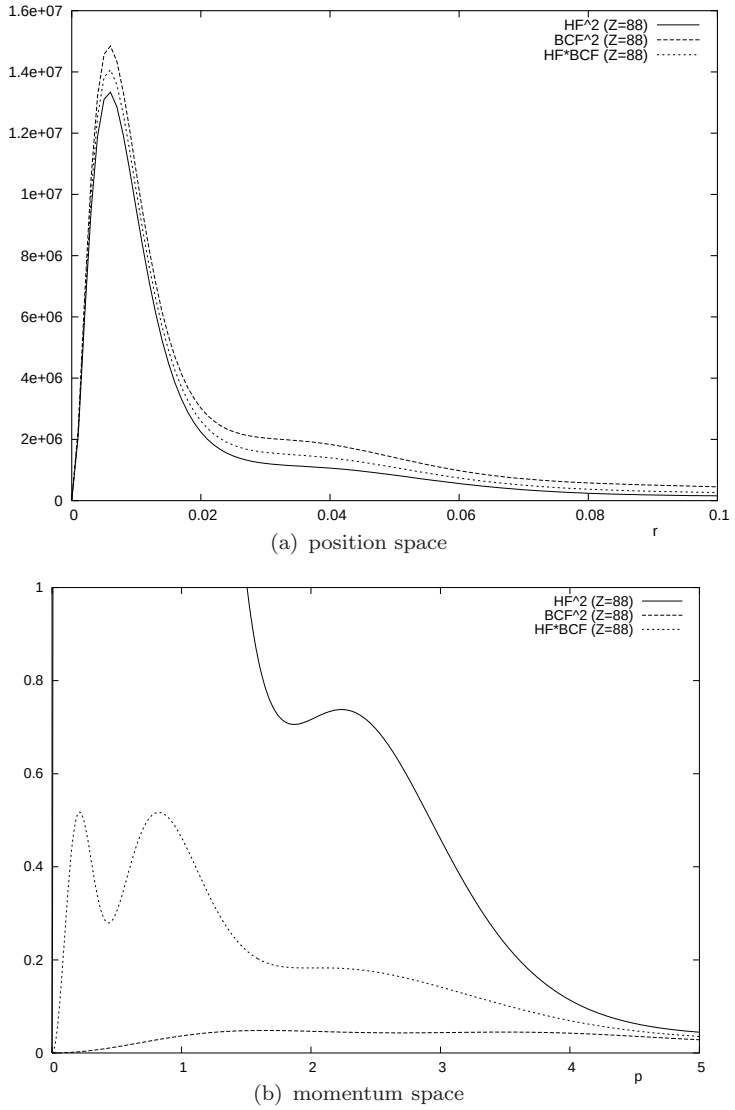

(a) position space

(b) momentum space

FIGURE 12.2: (a) Functions $4\pi r^2\rho^2_{HF}(r)$ (label HF^2), $4\pi r^2\rho^2_{BCF}(r)$ (label BCF^2), and $4\pi r^2\rho_{HF}(r)\rho_{BCF}(r)$ (label HF*BCF), defining overlap integrals for computing the $QD_r(HF, BCF)$ and $QSI_r(HF, BCF)$ for $Z = 88$ atom in position space, and (b) similarly for the momentum densities $\gamma(p)$. Atomic units are used.

A similar analysis is also carried out in terms of similarities QSI between the BCF and HF densities in both conjugated spaces. This is done attending to Figure 12.3, where $QSI(HF, BCF)$ are displayed again for $Z = 1 - 103$ in position and momentum spaces (Figure 12.3(a)). It is clearly observed that values of similarity between both models in position space are extremely close to the maximal value 1 and appear to be very little sensitive to the specific valence subshell of the considered systems, contrary to the momentum space case which have a decreasing trend and showing, additionally, the shell-filling patterns including the anomalous cases.

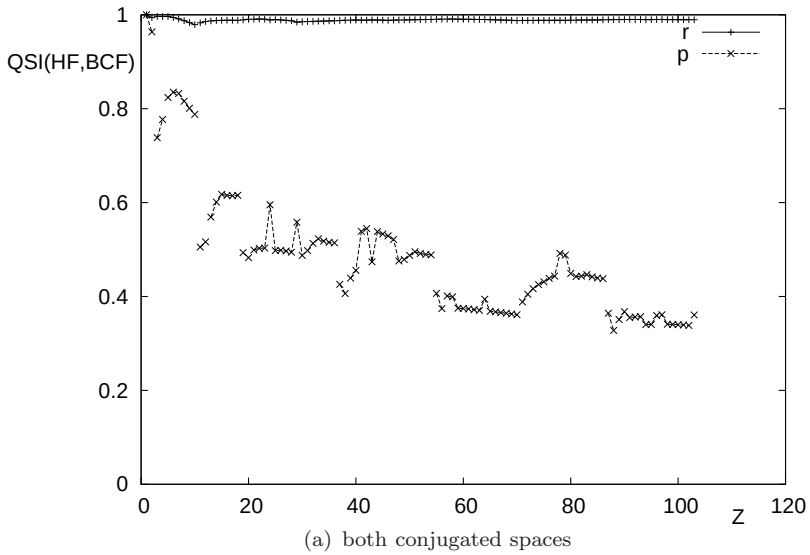

(a) both conjugated spaces

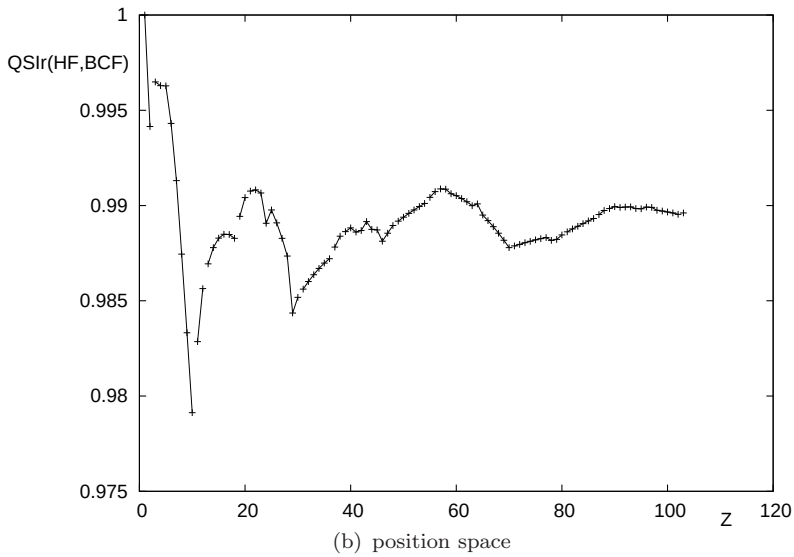

(b) position space

FIGURE 12.3: Quantum similarity index $QSI(HF, BCF)$ for neutral atoms with nuclear charge $Z = 1 - 103$ in (a) position and momentum spaces, and (b) close to 1 in position space. Atomic units are used.

Justifying these results requires again the previous interpretation concerning the quadratic distance QD attending to the behaviour of the involved integrals. In fact, the previous

discussion of Figure 12.2 regarding QD also applies to justify the result on QSI. Nevertheless, it is possible to observe the aforementioned structural characteristics also in position space by restricting ourselves to a much narrower interval for $QSI_r(HF, BCF)$, as shown in Figure 12.3(b) for values all above 0.975. From the analysis of both figures, it is worthy to point out that, in spite of QSI displaying periodicity patterns in both conjugated spaces, the position one appears to possesses a much smaller sensitivity in this sense than the momentum one.

It is worthy to point out that location of extrema in both QD and QSI in momentum space mostly belongs to noble gases ($Z = 10, 18, 36, 54, 86$) or atoms suffering anomalous shell-filling (e.g. $Z = 24, 29, 46, 64, 79, 93$), usually minima for QD being maxima for QSI .

Summarizing the results of the present subsection, it has been clearly shown that distances based on overlap integrals as QD and QSI in order to quantify the effects of the interelectronic repulsion in atomic systems are mainly determined by the nuclear charge Z in position space, displaying much richer information on shell structure when dealing with momentum space densities.

12.1.2 The Fisher, Jensen-Shannon and Jensen-Rényi Divergences

In this subsection, the Fisher divergence given by

$$FD(\rho_1, \rho_2) \equiv \int \rho_1(\vec{r}) \left| \vec{\nabla} \ln \frac{\rho_1(\vec{r})}{\rho_2(\vec{r})} \right|^2 d\vec{r} + \int \rho_2(\vec{r}) \left| \vec{\nabla} \ln \frac{\rho_2(\vec{r})}{\rho_1(\vec{r})} \right|^2 d\vec{r}, \tag{12.3}$$

and the Jensen-Shannon and Jensen-Rényi divergences defined as

$$JSD(\rho_1, \rho_2) = S\left(\frac{\rho_1 + \rho_2}{2}\right) - \frac{1}{2}\left[S(\rho_1) + S(\rho_2)\right], \tag{12.4}$$

and

$$JRD^{(q)}(\rho_1, \rho_2) \equiv R^{(q)}\left(\frac{\rho_1 + \rho_2}{2}\right) - \frac{1}{2}\left[R^{(q)}(\rho_1) + R^{(q)}(\rho_2)\right], \tag{12.5}$$

respectively, will be employed to compare the BCF and HF atomic densities in position and momentum spaces, in order to quantify the effect of the inter electronic repulsion on the information content of the densities as well as on the periodicity patterns.

The Fisher divergence $FD(HF, BCF)$ is displayed in Figures 12.4(a) (position space) and 12.4(b) (momentum space). Similarly to the previously studied quantities (subsection 12.1.1), monotonicity characters are opposite in both spaces, displaying an increasing behaviour in position space and decreasing in the momentum one mostly within each period. Again the overall behaviour in each space is the expected one in the sense of a higher number of electrons making more relevant the repulsive effect and expanding the charge cloud. Nevertheless, now shell-filling patterns can be clearly appreciated in

both conjugated spaces, while QSI and QD values appeared to be related to such a process only in momentum space. In what concerns location of extrema, most of them correspond (as also occurred with momentum space QD and QSI) to noble gases or anomalous shell-filling cases, maxima in position space corresponding to minima in the the momentum one and conversely.

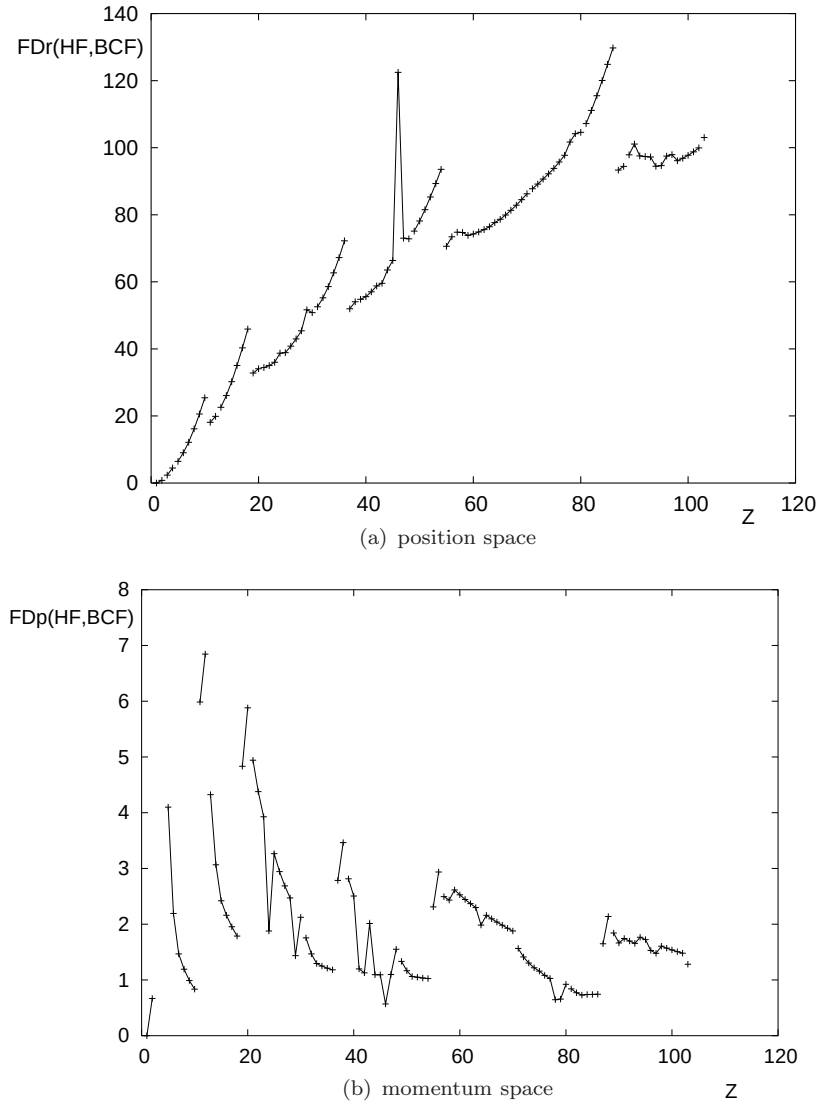

(a) position space

(b) momentum space

FIGURE 12.4: Fisher divergence $FD(HF, BCF)$ for neutral atoms with nuclear charge $Z = 1 - 103$ in (a) position and (b) momentum spaces. Atomic units are used.

Concerning the Jensen-Shannon divergence $JSD(HF, BCF)$ displayed in Figure 12.5 for both conjugated spaces, some comments are in order. First, the shell-filling process of the atomic systems is also revealed in both position and momentum spaces, the curves displaying a very similar shape. In fact, they differ roughly by a scaling factor and/or a small shift depending on the range of Z values considered (light, medium-size or heavy atoms). Nevertheless, the difference between JSD_r and JSD_p for a given Z is much smaller than those of all previously studied measures, some of them even belonging

to different magnitude orders. Again location of extrema corresponds mostly to noble gases and anomalous shell-filling systems, but now being of the same type (minimum or maximum) in both conjugated spaces, contrary to the opposite character for the FD_r and FD_p divergences.

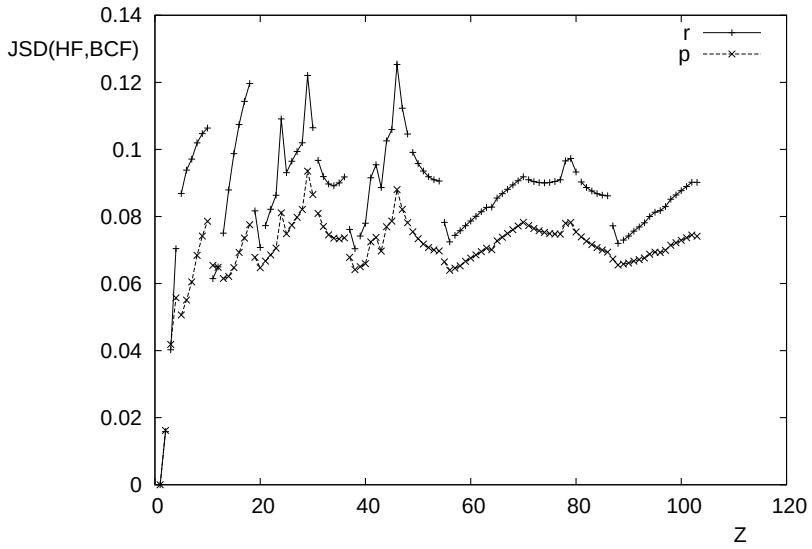

FIGURE 12.5: Jensen-Shannon divergence $JSD(HF, BCF)$ for neutral atoms with nuclear charge $Z = 1 - 103$ in position and momentum spaces. Atomic units are used.

For completeness, let us analyze one of the generalization of the JSD in terms of the Rényi entropy, the Jensen-Rényi divergence. In Figure 12.6, the $JRD^{(q)}$ for different values of q and the JSD between Hartree-Fock and Bare Coulomb Field densities are shown.

It is firstly observed, by comparing Figures 12.6(a) and 12.6(b), that the curves are ordered following opposite trends in each space. Divergences become higher as decreasing (increasing) q in position (momentum) space. The interelectronic repulsion mainly affects, consequently, the outermost region as compared to the nuclear one, as can be interpreted according to the results obtained in each space. This fact means that, as far as the interelectronic repulsion increases, the electrons start to separate out among themselves, but more easily in the outermost region due to their spreading there as compared to the vicinity of the nucleus.

Concerning the structural characteristics of the curves, it is also observed that also the extrema in each space follow different trends: local maxima appear in position space in the $q = 0.2$ curve for systems where a new subshell has been added, more apparently when such a subshell is of 's' type. This means that the single-electron valence orbitals are more sensitive to the effect of the repulsive forces than those with a higher occupation number. On the other hand, location of maxima in the momentum JSD curve are associated to closed-shell systems. Other q values make the extrema to progressively soften, even disappearing in some cases.

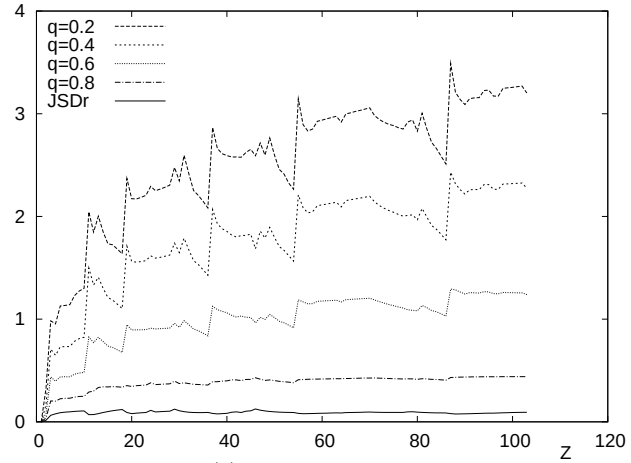

(a) Position space

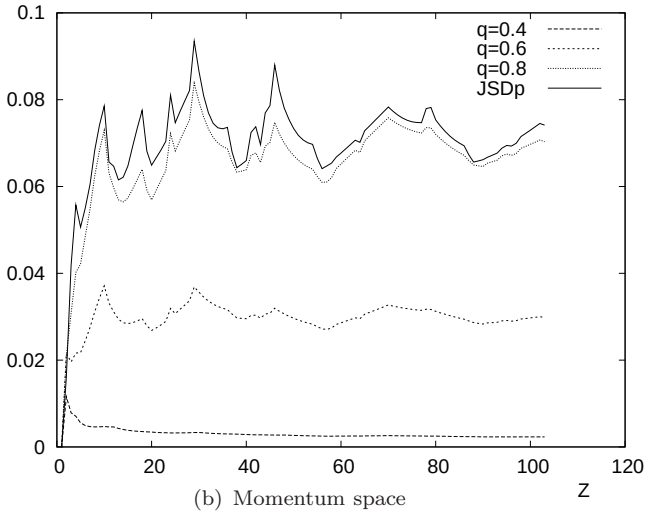

(b) Momentum space

FIGURE 12.6: Jensen-Rényi Divergence $JRD^{(q)}$ for $q = 0.2, 0.4, 0.6, 0.8$ and Jensen-Shannon divergence $JSD = JRD^{(1)}$ between the one-particle densities computed within Hartree-Fock (HF) and Bare Coulomb Field models (BCF), for neutral atoms with nuclear charge $Z = 1 - 103$, in (a) position and (b) momentum spaces. Atomic units are used.

The universality of the method here employed allows its application to the analysis of the effects arising by considering numerical computations or models other than the HF and BCF ones. This will be done elsewhere by considering correlated wavefunctions or relativistic effects, among others.

12.2 Entropy excess of atomic systems and sets with respect to their constituents

The main aim of this section is to employ generalized expressions of JSD starting from the initial definition given by Eq. (12.4) in order to build up the JSD divergence of an atomic one-particle density as the sum of those of each subshell, contributing to the

global charge according to their occupation numbers. After that, the global distributions for selected sets of atomic systems (e.g. groups, periods) are studied by means of the associated JSD divergences

The generalization of JSD can be expressed as

$$JSD(\{\omega_j, \rho_j\}_{j=1}^{M}) \equiv S\left(\sum_{j=1}^{M} \omega_j \rho_j\right) - \sum_{j=1}^{M} \omega_j S(\rho_j) \tag{12.6}$$

where the weights ω_j $(j = 1, \ldots, M)$ verify $\sum_{j=1}^{M} \omega_j = 1$. This extension is built up in two complementary ways: (i) by increasing the number of distributions under comparison, with JSD being interpreted as a 'mean spreading distance' among the constituents of a set with a number of functions higher than two, and (ii) by appropriately weighting the distributions to be compared according to their specific characteristics or those of the systems they represent, such as for instance their size or physical relevance. Let us notice the trivial equality $JSD = 0$ for the particular cas $M = 1$.

12.2.1 Jensen-Shannon divergence and atomic shell-filling

The spinless wavefunction of a N-electron atom and its Fourier transform, $\Psi(\vec{r}, \vec{r}_2, \ldots, \vec{r}_N)$ and $\tilde{\Psi}(\vec{p}, \vec{p}_2, \ldots, \vec{p}_N)$, respectively, allow to determine the one-particle densities in position and momentum spaces, $\rho(\vec{r}) = \int |\Psi|^2 d\vec{r}_2 \ldots d\vec{r}_N$ and $\gamma(\vec{p}) = \int |\tilde{\Psi}|^2 d\vec{p}_2 \ldots d\vec{p}_N$ respectively, both being essential quantities in the description and quantification of the main atomic properties. For most purposes it is sufficient to deal with their spherical averages $\rho(r)$ and $\gamma(p)$. In what follows, all expressions and numerical analyses are considered in both spaces.

The total density $\rho(r)$ is a linear combination of the (n, l)-subshell densities $\rho_{nl}(r)$. Considering the total density as well as each subshell density normalized to unity, the linear combination is

$$N\rho(r) = \sum_{nl} N_{nl} \rho_{nl}(r) \tag{12.7}$$

for the N electron atom, with N_{nl} being the number of electrons belonging to the (n,l) subshell, and $N_n l \leq 2(2l + 1)$ according to its occupation numbers. Consequently

$$N = \sum_{nl} N_{nl} \tag{12.8}$$

or equivalently

$$\sum_{nl} \omega_{nl} \equiv \sum_{nl} \frac{N_{nl}}{N} = 1 \tag{12.9}$$

where $\omega_{nl} \equiv \frac{N_{nl}}{N}$ will be refereed as '(n,l)-subshell relative weight' and represents the relative contribution of the subshell to the total charge.

According to the previous discussion, the density $\rho(r)$ of the whole atomic system can be considered as an appropriately weighted linear combination of its 'constituent pieces', i.e. the (n,l) subshell densities, the weights being determined by the subshell occupation numbers N_{nl} and the total number of electrons N of the whole system.

As for any arbitrary distribution, the internal disorder of each subshell density as well as that of the total density can be quantified by means of their corresponding Shannon entropies $S(\rho_{nl})$ and $S(\rho)$, respectively. An interesting question arising from the connection between subshell and total densities is: *to which extent the disorder of the global system is conditioned by the disorder of its constituents?* The solution to this problem can be better understood by analyzing Eq. (12.6), corresponding to the weighted JSD for a set of M distributions, with M being the number of occupied subshells..

The JSD definition should be considered as the difference between two quantities: the Shannon entropy of the total density and the mean entropy of its subshells. Taking into account the non-negativity of JSD, the aforementioned mean entropy constitutes a lower bound to the total entropy of the composite system. Consequently, JSD should be interpreted as the deviation (from above) of the total entropy from its allowed minimal value or, in other words, the 'entropy excess' of the whole system with respect to the entropies of the subsystems.

Attending to the saturation property of JSD (i.e. it reaches the minimal value for identical distributions), it is clear that lower JSD values will correspond to similar subshell distributions and, consequently, to similar subshell entropies, independently of their values being higher or lower. In order to make JSD reaching higher values it is needed to deal with strongly different values of subshell disorders or entropies. So, the JSD for the subshells of the considered atomic system provides additional information on how similar or different the internal disorders of the subshells composing the system are.

In Figure 12.7, the JSD divergences of the subshell densities for neutral atoms (i.e., $Z = N$) with nuclear charge $Z = 1 - 103$ in both position and momentum spaces are shown, denoted respectively as $JSD_r(Z)$ and $JSD_p(Z)$ for the sake of simplicity. In computing them, the accurate Near-Hartree-Fock wavefunctions of Koga et al [269, 396] have been employed.

Some comments are in order. It is firstly observed that the JSD values in both conjugated spaces belongs to a similar magnitude order and, in fact, to a not very wide interval excepting the trivial single-orbital cases, i.e. $Z = 1, 2$ for which $M = 1$. Furthermore, the shapes of both curves are almost identical, differing only (roughly) by a

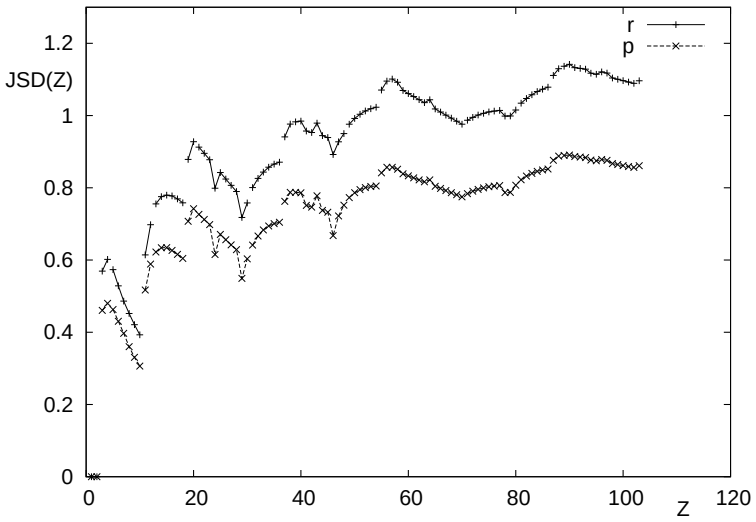

FIGURE 12.7: Jensen-Shannon divergence $JSD(Z)$ for the subshells of neutral atoms with nuclear charge $Z = 1 - 103$ in position (r) and momentum (p) spaces. Atomic units are used.

scaling constant. Also a strong relationship between location of extrema and the shell-filling process can be clearly appreciated. In fact, local extrema (maxima and minima) appear in both curves exactly at the same Z values. Most of them are associated to the so-called anomalous shell-filling, as opposite to the usual shell-filling pattern characterized by the successive addition of electrons to the outermost (valence) subshell, the inner ones (core) remaining completely occupied. Location of extrema appear determined by systems suffering the aforementioned anomalous process for which adding an electron to the valence subshell additionally makes an inner one (at least) to lose one or more electrons. Such is the case of the systems $Z = 24, 42, 57, 64, 78, 90, 96$. Nevertheless, additional extrema correspond to some closed shells atoms ($Z = 4, 10, 18, 20, 70, 102$). It is remarkable that, in both cases, the type of extrema (maximum or minimum) displayed is determined by the value of the 'l' quantum number of the 'anomalous' or the valence subshell, respectively. In the first case, maxima appear for systems having the outermost 's' subshell completely filled ($Z = 57, 64, 90, 96$) while minima occur for half-filled ones ($Z = 24, 42, 78$). Concerning systems with closed shells, maxima are associated to outermost 's' subshells ($Z = 4, 20$) and minima for 'p' ($Z = 10, 18$) and 'f' ($Z = 70, 102$) ones. The only exception to these rules is the maximum at $Z = 15$, corresponding to the half-filled '3p' subshell. No relevant structure is appreciated within the filling of 'd' subshells. The intrinsic divergence of atomic systems in both conjugated spaces appears to be strongly correlated with the shell filling patterns, providing information on relevant characteristics of such a process.

It can be consequently concluded that the level of disorder of the total system having as reference the internal disorders of the isolated subshells is strongly determined by specific physical characteristics (i.e. value of the 'l' quantum number) of the outermost subshells.

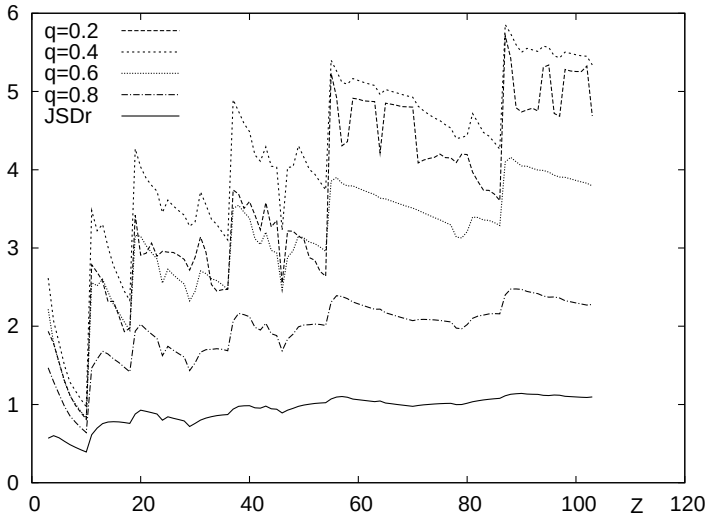

(a) Position space

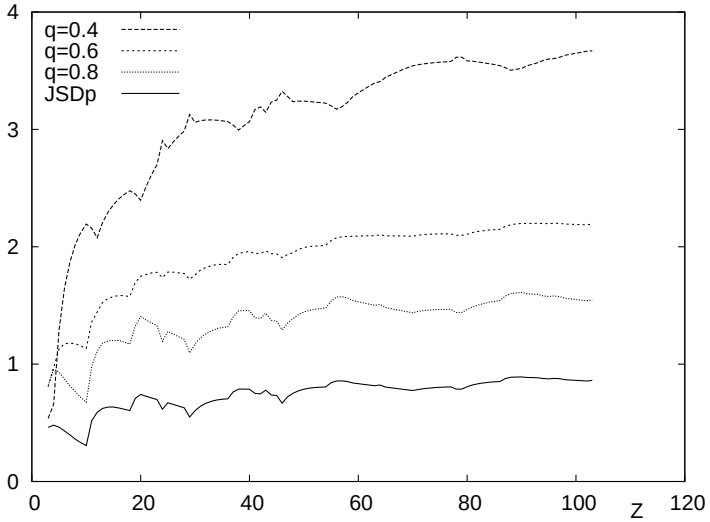

(b) Momentum space

FIGURE 12.8: Jensen-Rényi Divergence $JRD^{(q)}$ for some values of q and Jensen-Shannon divergence $JSD = JRD^{(1)}$ among the occupied subshells for all neutral atoms with nuclear charge $Z = 1 - 103$, in (a) position and (b) momentum spaces. Atomic units are used.

For completeness, let us consider one of the generalization of the JSD in terms of the Rényi entropy, the Jensen-Rényi divergence. Due to the similar characteristics of the Shannon and Rényi entropies, the JRD can be also extended for an arbitrary number M of distributions as

$$JRD^{(q)}\left(\{\omega_i, \rho_i\}_{i=1}^{M}\right) \equiv R^{(q)}\left(\sum_{i=1}^{M} \omega_i \rho_i\right) - \sum_{i=1}^{M} \omega_i R^{(q)}\left(\rho_i\right), \tag{12.10}$$

in order to analyze the advantages of using a divergence measure which depends on a parameter. The role played by such a parameter in the analysis of atomic densities has been previously discussed.

Now, the JRD divergences of the aforementioned collection of subshells have been computed for all neutral atoms with nuclear charge $Z = 1 - 103$, and their values are displayed in Figure 12.8.

Some comments are in order: (i) a general decreasing trend of the JRD divergence as q increases is observed in both conjugated spaces, almost systematic in momentum space with the corresponding curves ordered apart from few exceptions corresponding to light atoms. So, the Rényi entropy of the global system decreases, as compared to its lower bound given by the mean entropy of the subshells, when increasing q; (ii) according to the interpretation of low and large q values, the divergence among subshells is higher when enhancing the contribution of the densities around the origin, independently of the space considered. This fact suggests that the relevant feature for quantifying the global divergence is the region of higher density values instead of the shell-filling pattern; (iii) location of extrema within each curve does not follow a so systematic pattern as in the applications previously carried out. This is in accordance with the previous comment on the reasons for finding a higher or lower divergence. Similar conclusions are obtained from the analogous study in terms of JTD.

12.2.2 Jensen-Shannon divergence of atomic sets within the Periodic Table

Now, let us consider a collection of M atomic systems and their corresponding densities $(\rho_1, \dots \rho_M)$. Asking ourselves about their "closeness" in an information-theoretical sense, invites us to consider the Jensen-like divergences as a tool for quantifyed the "mean distance" among themselves. Considering equally weighted distributions will make their JSD to provide information on the spreading of their entropy values according to their shapes, instead to their size or normalization.

Different atomic sets are susceptible of being analyzed by means of JSD , attending to the main properties we are interested in. We will consider three interesting kind of sets, each possessing its own characteristics in order to provide information on their physical properties including the shell-filling process as well as the entropy dependence on the nuclear charge for fixed number of electrons.

Atomic groups of neutral systems

The Periodic Table of elements is divided into different groups, each one characterized by the valence subshell of the atoms according to the Aufbau principle. The elements of a given group are characterized by the angular quantum number 'l' of the corresponding valence subshell and its occupation number. Not all groups are composed by the same number of elements, according to the shell-filling rules.

For illustration, and in order to consider groups with a high enough number of elements, let us carry out a JSD analysis for sets of atomic distributions, each one corresponding to groups IA to VIIIA. They are characterized for having valence subshell of type 's' (IA and IIA) or 'p' (IIIA to VIIIA). The number of elements of these groups ranges between 5 and 7, and the principal quantum number within the interval $n = 1 - 7$. For comparison purposes, we will deal with sets of identical number M of elements, being $M = 5$ for all them corresponding to the values $n = 2 - 6$, which are the only ones common to all those groups. The aim of this study on JSD for a given group is to analyze to which extent the spreading of distributions for systems belonging to a given group is more or less similar.

The five-elements JSD values in both spaces for these groups are shown in Table 12.1. Some comments are in order. First, it is observed that all values of JSD_p belong to a very narrow interval, being wider for the position space ones. This means that the shapes of the position space densities within a given group are more sensitive to the valence subshell 'n' principal quantum number than the momentum ones. Additionally, there exist a general decreasing trend of JSD in both spaces as adding electrons to the valence subshell (in fact, such a decrease is strict in momentum space). In other words, the highly filled the valence subshells, more similar the densities are. Such an effect is more apparent in position than in momentum space. At this point, it is worthy to remark that filling up the valence subshell make the system to become progressively closer to a closed-shell system.

Group	JSD_r	JSD_p
IA (Z=3,11,19,37,55)	0.08258	0.04019
IIA (Z=4,12,20,38,56)	0.07544	0.03872
IIIA (Z=5,13,31,49,81)	0.08347	0.03755
IVA (Z=6,14,32,50,82)	0.07409	0.03626
VA (Z=7,15,33,51,83))	0.06635	0.03481
VIA (Z=8,16,34,52,84)	0.06047	0.03357
VIIA (Z=9,17,35,53,85)	0.05626	0.03259
VIIIA (Z=10,18,36,54,86)	0.05363	0.03202

TABLE 12.1: Jensen-Shannon divergence JSD for each of the groups IA-VIIIA of neutral atoms within the Periodic Table, in position (JSD_r) and momentum (JSD_p) spaces. Atomic units are used.

A physically relevant quantity, strongly associated to the shell-filling patterns, is the first atomic ionization potential (AIP), clearly dependent on the characteristics of the atomic valence subshell. We wonder about the relationship between such an experimentally accessible quantity and the JSD along a group, considered as a function of the principal quantum number n of the valence subshell (n, l) for fixed both l and occupation number. In order to check such a relationship, two different analysis are carried out in the next figures. In the Figure 12.9(a) the JSD in momentum space is depicted for groups IIIA up to VIIIA of the Periodic Table (all of them with 'p' as the outermost subshell). It

is observed from the figure that, within a given atomic group, the distance obtained in terms of JSD between the element with the smallest atomic number ($n = 2$) and the rest of them ($n = 3$ to 6) shows an increasing behaviour as n grows. In order to analyze the connection between the divergences in momentum space (12.9(a)) and the AIP, we have depicted in Figure 12.9(b) the values of the ionization potential of the elements belonging to a given group (IIIA to VIIIA) and we observe an opposite behaviour to that of JSD displayed in Figure 12.9(a), i.e. the JSD_p increases as the AIP decreases within each group.

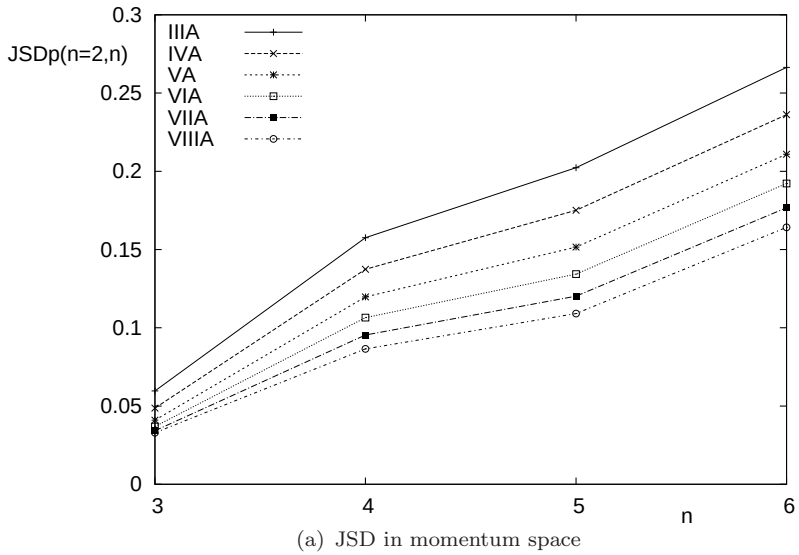

(a) JSD in momentum space

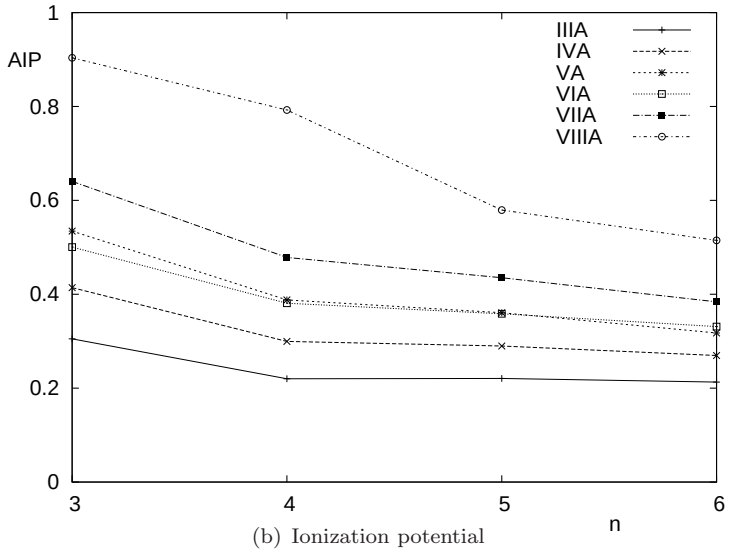

(b) Ionization potential

FIGURE 12.9: (a) Jensen-Shannon divergence in momentum space $JSD_p(n = 2, n)$ for groups IIIA to VIIIA of the Periodic Table, between the system with valence subshell principal quantum number $n = 2$ and each one of those with $n = 3 - 6$, and (b) atomic ionization potential AIP for the latter ones. Atomic units are used.

Atomic periods of neutral systems

After studying the dependence of JSD on the valence subshell principal quantum number 'n' keeping fixed its occupation number, let us now analyze the JSD values associated to all systems with the same valence subshell. In this case, the number of systems composing a given set depends on the value of the 'l' quantum number of the valence subshell, being 2, 6, 10 and 14 for types 's', 'p', 'd' and 'f', respectively.

In Table 12.2, the JSD values in conjugated spaces are given for each period (i.e., systems sharing the valence subshell) involved in the filling process for neutral atoms with nuclear charge $Z = 1 - 103$. In this table it is especially remarkable the almost identical values obtained independently of the space considered, with very few exceptions. The general trend again is a decreasing behaviour for increasing n principal quantum number keeping fixed the 'l' angular one. It is concluded that shapes of the densities in conjugated spaces for systems belonging to the same period become more similar for heavy than for light atoms.

Valence subshell	JSD_r	JSD_p
1s	0.07574	0.06936
2s	0.04112	0.04033
3s	0.00896	0.00893
4s	0.00432	0.00431
5s	0.00178	0.00178
6s	0.00110	0.00110
7s	0.00064	0.00064
2p	0.06337	0.05808
3p	0.02887	0.02829
4p	0.00765	0.00761
5p	0.00401	0.00400
6p	0.00179	0.00179
3d	0.01488	0.01452
4d	0.00938	0.00931
5d	0.00289	0.00289
4f	0.00473	0.00468
5f	0.00323	0.00322

TABLE 12.2: Jensen-Shannon divergence JSD for the set of neutral atoms with the same valence subshell within the Periodic Table, in position (JSD_r) and momentum (JSD_p) spaces. Atomic units are used.

The process of successively adding electrons to a closed-shell system, which can be interpreted as moving along a period, is also analyzed attending to the results displayed in Figure 12.10. The position space JSD_r between a noble gas and the following elements along the whole period just below such a system in the Periodic Table is observed to (roughly) display an unimodal shape. Starting to add electrons to the new subshell of the reference system makes the JSD to progressively increase as a consequence of a more noticeable dissimilarity, until reaching a maximum value (appreciably different

for each period) where the JSD starts to decrease as far as adding electrons makes the atom to get closer to another noble gas. Consequently, the divergence with respect to the preceding closed-shell system does not only depend on the number of additional electrons, but also on the distance to the next closed-shell atom. The very few and slight exceptions on the aforementioned unimodality are mostly associated to systems suffering the anomalous shell-filling, and the location of the 'maximal JSD system' tends to appear later as far as lower periods in the Periodic Table are considered.

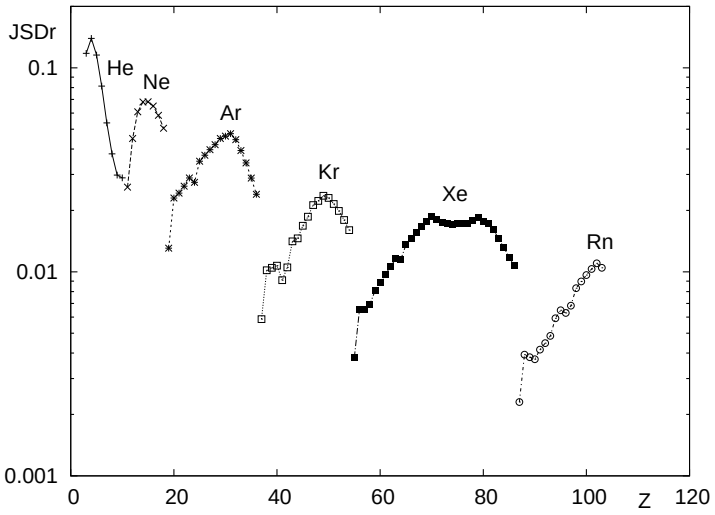

FIGURE 12.10: Position space Jensen-Shannon divergence JSD_r between a closed-shell system (He, Ne, Ar, Kr, Xe and Rn) and an open-shell one within its next period, with nuclear charge up to $Z = 103$. Atomic units are used.

Isoelectronic series

An isoelectronic series is a collection of atomic systems with identical number N of electrons but different nuclear (Z) or total ($Q \equiv Z - N$) charges. Let us consider the nine isoelectronic series with $N = 2 - 10$, each one composed by the corresponding neutral atom and its first twenty cations, the total charges ranging consequently within $Q = 0 - 20$. The Jensen-Shannon divergence JSD of a given series provides information on the extent to which the densities change when modifying the nuclear charge Z while keeping fixed the number of electrons. Previous studies on the physical characteristics of atomic systems belonging to a given isoelectronic series have been previously carried out [397], but usually by analyzing separately the isolated densities instead of by employing multi-density functionals as in the present work.

The divergence values $JSD(N)$ for $N = 2 - 10$ of all elements (twenty one) composing an N-electron series are shown in Figure 12.11 for position (r) and momentum (p) spaces. The main feature displayed in this figure is the decreasing trends of JSD in both conjugated spaces (with only one exception in position space) as increasing the number of electrons characterizing the series. This fact is in agreement with the discussion of

results corresponding to the previously studied atomic sets, in the sense that differences among the densities appear smaller for heavy atoms than for light ones. It should be pointed out that increasing N makes all systems conforming the series to increase their nuclear charge and, consequently, their masses. It is interesting to note that the range of values for JSD_r and JSD_p are not only similar but also very small, and in fact for the first two series are almost identical.

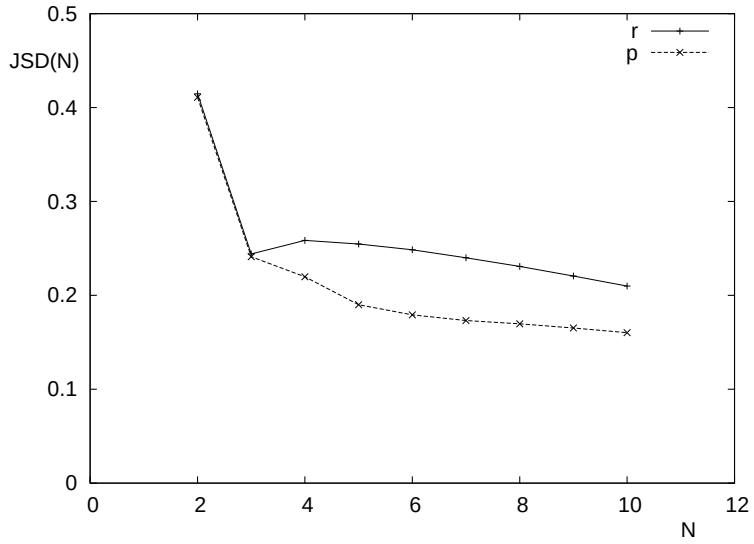

FIGURE 12.11: Jensen-Shannon divergence $JSD(N)$ for twenty-one elements isoelectronic series with $N = 2 - 10$ electrons, in position (r) and momentum (p) spaces. Atomic units are used.

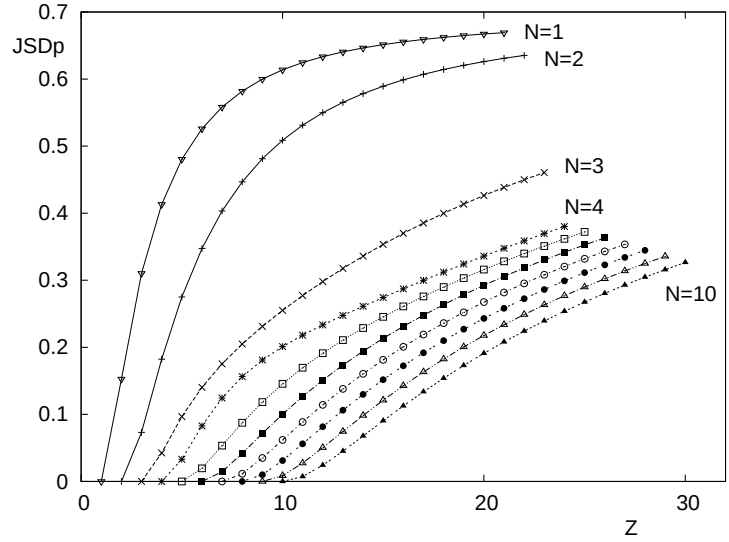

FIGURE 12.12: Momentum space Jensen-Shannon divergence JSD_p between a neutral N-electron atom and each of its successive twenty cations with nuclear charge $Z = N+1$ to $Z = N + 20$, for the isoelectronic series $N = 1 - 10$. Atomic units are used.

Similarly as done in the two previous subsections (groups and periods), a JSD analysis is carried out associated to the process of increasing the nuclear charge of an initial system, the neutral atom in the present case. In doing so, the momentum space JSD_p

between the neutral system and the successive ones obtained by increasing the nuclear charge is displayed in Figure 12.12. This is done for the isoelectronic series with a number of electrons $N = 1 - 10$, each series consisting of twenty one elements. The results are essentially the same in both spaces, and the most relevant conclusions are: (i) the series appear perfectly ordered, the higher JSD values corresponding to series with a lower number of electrons, (ii) increasing the nuclear charge quickly increases JSD, with the trend of reaching a limiting value after reaching a highly enough nuclear charge, and (iii) the $N = 1, 2$ series clearly distinguish from the others, as a consequence of possessing as valence subshell $1s$, the only one component of the systems in those series and consequently corresponding also to their core.

12.3 Conclusions

In this Chapter two different applications of the divergence measures have been analyzed. In the first section, Section 12.1, we have observed that the study of different distances or divergences allows us to gain a deeper physical insight on the relevance of the interelectronic repulsion in atomic systems as compared to the corresponding purely Coulomb ones. In order to obtain a complete informational description, it appears necessary to deal simultaneously with measures in position and momentum atomic densities. Nevertheless, Fisher and Jensen-Shannon divergences as well as the generalized Jensen-Rényi divergence provide relevant information in both conjugated spaces, while distances based on overlap integrals, such as the quadratic distance or the quantum similarity index, necessarily requires to employ momentum densities. Apart from the repulsive effect, the shell-filling patterns in Hartree-Fock framework are also clearly revealed in the just mentioned cases, not only attending to the specific valence subshell but additionally to its occupation number, the information measures detecting also the anomalous shell-filling.

From the second section, Sections 12.2, we can conclude that the generalized Jensen-Shannon divergence for arbitrary number of distributions and appropriate weights provide a very useful tool for quantifying the information content of a composite system, according to their decomposition in subshells, or of a set of whole systems, with respect to the information of their intrinsic constituents. The application in the study of many-electron systems within an information-theoretic framework reveals the strong connection between the divergence values in both position and momentum spaces, and relevant physical characteristics, such as (i) the atomic ionization potential, (ii) the shell-filling process in neutral atoms and (iii) the entropy excess dependence on the nuclear charge and the number of electrons.

It is also remarkable the very similar information (almost identical in some cases) provided by the JSD measure independently of the space we are dealing with, contrary

to the case of most comparative measures employed in the study of neutral atoms and ions, as also discussed in previous chapters..

The universality of the method here employed makes it susceptible to be used for the informational analysis of other relevant density functions, such as those describing molecular systems and or processes (e.g. reactions) also in the two conjugated spaces, as will be done elsewhere. Such a work will be also accompanied by the use of the generalized Jensen-Rényi and Jensen-Tsallis divergences, JRD and JTD, respectively.

Part IV

Appendices

Appendix A

Information-theoretic measures of hyperspherical harmonics

The hyperspherical harmonics $\mathcal{Y}_{l,\{\mu\}}(\Omega_d)$ were introduced and extensively studied by G. Green [398] and M.J.M. Hill [399] long ago. Later on authors have deeply investigated these objects as it is comprehensively discussed by J. Avery [153, 400]. They are the solutions of a very broad class of equations of a form into which numerous equations of the d-dimensional physics [126, 401] can be transformed, such as for instance Schrödinger equations for arbitrary D-dimensional central potentials and Bethe-Salpeter equations for some quark systems. Moreover they have been used for the analysis and interpretation of numerous atomic, molecular and nuclear phenomena which require the solution of the Schrödinger equation of a single-particle moving in a many-center quantum-mechanical potential or the Schrödinger equation of a finite many-particle system [319, 402–404].

The hyperspherical harmonics are the eigenfunctions of the operator Λ^2 which describes the square of the d-dimensional angular momentum operator,

$$\Lambda^2 = -\sum_{i=1}^{d-1} \frac{(\sin\theta_i)^{i+1-d}}{\left(\prod_{j=1}^{i-1}(\sin\theta_j)^2\right)} \frac{\partial}{\partial\theta_i}\left[(\sin\theta_i)^{d-i-1}\frac{\partial}{\partial\theta_i}\right], \tag{A.1}$$

where $(\theta_1, \theta_2, ..., \theta_{d-1}) \equiv \Omega_d$ represent the $d-1$ angular coordinates of the d-dimensional hypersphere S_{d-1} so that $0 \leq \theta_j \leq \pi$ for $j = 1, ..., d-2$, and $0 \leq \theta_{d-1} \leq 2\pi$. The eigensolutions of this operator are given by

$$\Lambda^2 \mathcal{Y}_{l,\{\mu\}}(\Omega_d) = l(l+d-2)\mathcal{Y}_{l,\{\mu\}}(\Omega_d), \tag{A.2}$$

where the $\mathcal{Y}$-symbol denotes the hyperspherical harmonics described by the $d-1$ natural numbers $l \equiv \mu_1$, $\{\mu_2, ..., \mu_{d-1} \equiv |m|\} \equiv \{\mu\}$ with values $l = 0, 1, 2, ...$ and $\mu_1 \geq \mu_2 \geq$

$... \geq \mu_{d-1}$. The hyperspherical harmonics are known to have the form

$$\mathcal{Y}_{l,\{\mu\}}(\Omega_d) = \frac{1}{\sqrt{2\pi}} e^{im\theta_{d-1}} \prod_{j=1}^{d-2} \hat{C}^{\alpha_j+\mu_{j+1}}_{\mu_j-\mu_{j+1}}(\cos\theta_j)\,(\sin\theta_j)^{\mu_{j+1}}\,, \tag{A.3}$$

with $2\alpha_j = d-j-1$, and $\hat{C}^{\lambda}_n(x)$, $\lambda > -\frac{1}{2}$, denotes the Gegenbauer polynomial of degree n and parameter λ which satisfies the orthonormalization condition

$$\int_{-1}^{1} \hat{C}^{\lambda}_n(x)\hat{C}^{\lambda}_m(x)\omega_\lambda(x)dx = \delta_{mn}, \tag{A.4}$$

where the weight function is given by

$$\omega_\lambda(x) = \left(1-x^2\right)^{\lambda-\frac{1}{2}}. \tag{A.5}$$

These objects are known to have numerous interesting properties [126, 153, 400, 403, 405, 406]; in particular they satistfy the orthogonality relation

$$\int_{S_d} \mathcal{Y}^*_{l,\{\mu\}}(\Omega_d)\mathcal{Y}_{l,\{\mu\}}(\Omega_d)d\Omega_d = \delta_{ll'}\delta_{\{\mu\}\{\mu'\}}, \tag{A.6}$$

where $d\Omega_d$ is the generalized solid angle element

$$d\Omega_d = \left(\prod_{j=1}^{d-2}(\sin\theta_j)^{2\alpha_j}d\theta_j\right)d\theta_{d-1}. \tag{A.7}$$

The spreading properties of the hyperspherical harmonics are best quantifued by means of the information-theoretic measures of the so-called *Born-Rakhmanov probability density* given by

$$\rho_{l\{\mu\}} = \left|\mathcal{Y}_{l,\{\mu\}}(\Omega_d)\right|^2 \tag{A.8}$$

In this appendix we have obtained the expressions of the information-theoretic measures of the hyperspherical harmonics in terms of their labeling indices, getting the explicit expressions for the Fisher information [3, 37]

$$I_{l,\{\mu\}}(d) = \int_{S_d} \frac{\left|\vec{\nabla}_\Omega \rho_{l\{\mu\}}\,(\Omega_d)\right|^2}{\rho_{l\{\mu\}}\,(\Omega_d)} d\Omega_d \tag{A.9}$$

where $\vec{\nabla}_\Omega$ denotes the angular $(d-1)$-dimensional gradient operator given by

$$\vec{\nabla}_\Omega = \sum_{i=0}^{d-1}\left(\prod_{k=1}^{i-1}\sin\theta_k\right)^{-1}\frac{\partial}{\partial\theta_i}\hat{\theta}_i, \tag{A.10}$$

and for the average density or inverse collision length [83, 313, 407]

$$W_{l,\{\mu\}}(d) = \int_{S_d} |\mathcal{Y}_{l,\{\mu\}}(\Omega_d)|^4 d\Omega_d, \tag{A.11}$$

in terms of the hyperquantum numbers which characterize the physical state under consideration.

We also give a lower bound for the Shannon entropy [32]

$$S_{l,\{\mu\}}(d) = -\int_{S_d} \rho_{l\{\mu\}}\left(\Omega_d\right) \ln \rho_{l\{\mu\}}\left(\Omega_d\right) d\Omega_d, \tag{A.12}$$

in terms of the hyperquantum numbers $l, \{\mu\}$.

A.1 Fisher information

This quantity, which is defined by Eqs. (A.9) and (A.10), can also be expressed as

$$\begin{aligned} I_{l,\{\mu\}}(d) &:= 4\int_{S_d} \left[\vec{\nabla}_\Omega |\mathcal{Y}_{l,\{\mu\}}(\theta_1,\theta_2,...,\theta_{d-2},0)|\right]^2 d\Omega_d = \\ &= 4\sum_{i=1}^{d-2} \int_{S_d} \left[\left(\prod_{k=1}^{i-1} \sin\theta_k\right)^{-1} \frac{\partial}{\partial\theta_i} \mathcal{Y}_{l,\{\mu\}}(\theta_1,\theta_2,...,\theta_{d-2},0)\right]^2 d\Omega_d = \\ &= 4\sum_{i=1}^{d-2} \left(\prod_{k=0}^{i-1} \int_0^\pi \left[\hat{C}^{\alpha_k+\mu_{k+1}}_{\mu_k-\mu_{k+1}}(\cos\theta_k)\right]^2 (\sin\theta_k)^{2\alpha_k+2\mu_{k+1}-1} d\theta_k\right) \\ &\quad \times \int_0^\pi \left[\frac{\partial}{\partial\theta_i}\left(\hat{C}^{\alpha_i+\mu_{i+1}}_{\mu_i-\mu_{i+1}}(\cos\theta_i)\cdot(\sin\theta_i)^{\mu_{i+1}}\right)\right]^2 (\sin\theta_i)^{2\alpha_i} d\theta_i, \end{aligned} \tag{A.13}$$

where we have taken into account the complex exponential dependence of the hyperspherical harmonics on the coordinate θ_{d-1}, as given by Eq. (A.3), for the first equality, the expression (A.10) for the second equality and the Gegenbauer normalization condition (A.4) for the last equality.

Taking into account that the Gegenbauer function $G_{\mu_j,\mu_{j+1}}(\theta_j) \equiv \hat{C}^{\alpha_j+\mu_{j+1}}_{\mu_j-\mu_{j+1}}(\cos\theta_j)(\sin\theta_j)^{\mu_{j+1}}$ fulfils the differential equation [408]

$$\frac{\partial}{\partial\theta_j}\left[(\sin\theta_j)^{2\alpha_j}\frac{\partial}{\partial\theta_j} G_{\mu_j,\mu_{j+1}}(\theta_j)\right] \tag{A.14}$$

$$= -(1-x_i^2)^{2\alpha_j}\left[\mu_j(\mu_j+2\alpha_j) - \frac{\mu_{j+1}(\mu_{j+1}+2\alpha_{j+1})}{\sin^2\theta_j}\right] G_{\mu_j,\mu_{j+1}}(\theta_j), \tag{A.15}$$

and making use of various algebraic properties of the hyperspherical harmonics [153, 400, 402, 403], one has that

$$I_{l,\{\mu\}}(d) = \sum_{i=1}^{D-2} \left\{ \mu_i(\mu_i + 2\alpha_i) - \mu_{i+1}(\mu_{i+1} + 2\alpha_{i+1}) \int_0^{\pi} \left[G_{n_i}^{\lambda_i}(\theta_i) \right]^2 (\sin\theta_i)^{2\alpha_{i+2}} d\theta_i \right\}. \tag{A.16}$$

Then, the use of the close connection of the Gegenbauer polynomials and the associated Legendre function $P_n^m(x)$ together with the expression

$$\int_{-1}^{1} (1-x^2)^{-1} \left[P_n^m(x) \right]^2 dx = \frac{(n+m)!}{m(n-m)!}, \tag{A.17}$$

has allowed us to finally find the following value for the Fisher information of the hyperspherical harmonics $\mathcal{Y}_{l,\{\mu\}}(\Omega)$:

$$\begin{aligned} I_{l,\{\mu\}}(d) &= 4 \sum_{i=1}^{d-2} \left[\mu_i(\mu_i + d - i - 1) - \mu_{i+1}(\mu_{i+1} + d - i - 2) \frac{2\mu_i + d - i - 1}{2\mu_{i+1} + d - i - 2} \right] \\ &\quad \times \frac{2\mu_1 + d - 2}{2\mu_i + d - i - 1} \qquad \text{(A.18)} \\ &= 4l(l + d - 2) - 2\mu_{d-1}(2l + d - 2) \qquad \text{(A.19)} \\ &= 4L(L+1) - 2\mu_{d-1}(2L+1) - (d-1)(d-3), \qquad \text{(A.20)} \end{aligned}$$

where we have used in the third inequality, for physical transparency purposes, the so-called grand angular momentum quantum number L defined by

$$L = l + \frac{d-3}{2}. \tag{A.21}$$

It turns out that the Fisher information of the hyperspherical harmonics only depends on the dimensionality of the hyperspace and the first and last labeling indices l and m. In particular, for $d = 3$ one has

$$I_{l,m}(3) = 4l(l+1) - 2|m|(2l+1), \tag{A.22}$$

for the Fisher information of the familiar three-dimensional spherical harmonics, which give the anisotropic character of the eigenfunctions of the central potentials. In this sense, the Fisher information can be considered as a measure of the angular, spatial or volume anisotropy of the stationary states of any spherically symmetric potential.

A.2 Average density

The average density, according to Eqs. (A.8), has the form given by Eq. (A.11). The use of Eq. (A.3) for the hyperspherical harmonics in terms of the Gegenbauer polynomials, and Eq. (A.7) for the generalized solid angle element allow us to transform this expression as follows:

$$\begin{aligned} W_{l,\{\mu\}}(d) &= \frac{1}{2\pi}\prod_{j=1}^{d-2}\int_{-1}^{+1} |\hat{C}^{\alpha_j+\mu_{j+1}}_{\mu_j-\mu_{j+1}}(x_j)|^4 \omega_{\alpha_j+2\mu_{j+1}}(x_j)dx_j \\ &= \frac{1}{2\pi}\prod_{j=1}^{d-2}\int_{-1}^{+1} |\hat{C}^{\lambda}_{n}(x_j)|^4 \omega_{\lambda+\mu_{j+1}}(x_j)dx_j, \end{aligned} \tag{A.23}$$

where we have performed the change of variable $\theta_j \rightarrow x_j = \cos\theta_j$ in the first equality, and the notation $\lambda = \alpha_j + \mu_{j+1}$ and $n = \mu_j - \mu_{j+1}$ in the second equality. To evaluate the integral involved in Eq. (A.23) we shall use twice the transformation

$$|\hat{C}^{\lambda}_{n}(x_j)|^2 \longrightarrow \hat{C}^{\lambda+\mu_{j+1}}_{2k}(x_j), \tag{A.24}$$

by means of the generalized Dougall linearization formula of the Gegenbauer polynomials [409], and the orthogonalization relation (A.4) for the Gegenbauer polynomials $\hat{C}^{\lambda+\mu_{j+1}}_{m}(x)$ orthogonal with respect to the weigth function $\omega_{\lambda+\mu_{j+1}}(x)$. The generalized Dougall formula for the orthogonal Gegenbauer polynomials $C^{\alpha}_{n}(x)$ is expressed as

$$[C^{\alpha}_{n}(x)]^2 = \sum_{k=0}^{n} a(\alpha,\beta,n;k) C^{\beta}_{2k}(x), \tag{A.25}$$

where the linearization coefficients are given by

$$\begin{aligned} a(\alpha,\beta,n;k) = {} & \frac{(2\alpha)_n}{(n!)^2}\binom{n}{k}\frac{(2k)!(k+2\alpha)_n(\alpha)_k(\beta+1/2)_k}{(2\beta)_{2k}(k+\beta)_k(\alpha+1/2)_k} \\ & \times {}_4F_3\left(\left.\begin{matrix} k-n, & k+n+2\alpha, & k+\alpha, & k+\beta+\frac{1}{2} \\ 2k+\beta+1, & k+2\alpha, & k+\alpha+\frac{1}{2} & \end{matrix}\right| 1\right). \end{aligned} \tag{A.26}$$

Observe that this ${}_4F_3$ function of unit argument is balanced, i.e. the sum of the upper parameters equals the sum of the lower parameters minus one.

Taking into account Eqs. (A.25) and (A.26) and the relation

$$\hat{C}^{\lambda}_{n}(x) = \frac{1}{d^{\lambda}_{n}} C^{\lambda}_{n}(x); \qquad d^{\lambda}_{n} = \left[\frac{\pi 2^{1-2\lambda}\Gamma(n+2\lambda)}{n!(n+\lambda)\Gamma^2(\lambda)}\right]^{1/2}, \tag{A.27}$$

one has the following linearization formula for the orthonormal Gegenbauer polynomials:

$$\left[\hat{C}_n^{\alpha}(x)\right]^2 = \sum_{k=0}^{n} b(\alpha,\beta,n;k)\hat{C}_{2k}^{\beta}(x), \tag{A.28}$$

with

$$b(\alpha,\beta,n;k) = \frac{d_{2k}^{\beta}}{[d_n^{\alpha}]^2} a(\alpha,\beta,n;k). \tag{A.29}$$

Then, with $\alpha = \lambda$ and $\beta = \lambda + \mu_{j+1}$ we obtain the desidered transformation (A.24), namely

$$\left[\hat{C}_n^{\lambda}(x)\right]^2 = \sum_{k=0}^{n} b(\lambda,\lambda+\mu_{j+1},n;k)\hat{C}_{2k}^{\lambda+\mu_{j+1}}(x), \tag{A.30}$$

where

$$\begin{aligned} b(\lambda,\lambda+\mu_{j+1},n;k) = {} & \frac{(n+\lambda)\Gamma(k+1/2)\Gamma(k+\lambda)\Gamma(k+n+2\lambda)}{\pi^{1/2}\Gamma(1-k+n)\Gamma(k+\lambda+1/2)\Gamma(k+2\lambda)\Gamma(2k+\lambda+\mu_{j+1})} \\ & \times \left(\frac{2^{1-2\lambda-2\mu_{j+1}}\Gamma(2k+2\lambda+2\mu_{j+1})}{(2k+\lambda+\mu_{j+1})\Gamma(2k+1)}\right)^{1/2} \\ & \times {}_4F_3\left(\begin{matrix} k-n, & k+n+2\lambda, & k+\lambda, & k+\lambda+\mu_{j+1}+\frac{1}{2} \\ & 2k+\lambda+\mu_{j+1}+1, & k+2\lambda, & k+\lambda+\frac{1}{2} \end{matrix}\,\middle|\, 1\right). \end{aligned} \tag{A.31}$$

The use of this expression twice in the integral $I_n^{\lambda}(j)$ on the right hand side of Eq. (A.23) gives

$$\begin{aligned} I_n^{\lambda}(j) \equiv \int_{-1}^{+1} |\hat{C}_n^{\lambda}(x)|^4 \omega_{\lambda+\mu_{j+1}}(x)dx &= \sum_{k=0}^{n}\sum_{k'=0}^{n} b(\lambda,\lambda+\mu_{j+1},n;k)b(\lambda,\lambda+\mu_{j+1},n;k') \\ &\times \int_{-1}^{+1} |\hat{C}_{2k}^{\lambda+\mu_{j+1}}(x)||\hat{C}_{2k'}^{\lambda+\mu_{j+1}}(x)|\omega_{\lambda+\mu_{j+1}}(x)dx \\ &= \sum_{k=0}^{n} b^2(\lambda,\lambda+\mu_{j+1},n;k). \end{aligned} \tag{A.32}$$

Then, according to Eqs. (A.23) and (A.32), one has finally the following expression for the average density of hyperspherical harmonics:

$$\begin{aligned} W_{l,\{\mu\}}(d) &= \frac{1}{2\pi}\prod_{j=1}^{d-2}\sum_{k=0}^{n} b^2(\lambda,\lambda+\mu_{j+1},n;k) \\ &= \frac{1}{2\pi}\prod_{j=1}^{d-2}\sum_{k=0}^{\mu_j-\mu_{j+1}} b^2(\alpha_j+\mu_{j+1},\alpha_j+2\mu_{j+1},\mu_j-\mu_{j+1};k). \end{aligned} \tag{A.33}$$

In particular, the two- and three-dimensional values are

$$W_l(2) = \frac{1}{2\pi}, \tag{A.34}$$

and

$$W_{l,m}(3) = \sum_{k=0}^{l-|m|} C_k(l,|m|) \times \left[{}_3F_2 \left(\begin{matrix} -l+|m|+k, & |m|+k+1/2, & l+|m|+k+1 \\ |m|+k+1, & 2|m|+2k+3/2 \end{matrix} \middle| 1 \right) \right]^2, \tag{A.35}$$

respectively, where the coeficients $C_k(l,|m|)$ are given by

$$C_k(l,|m|) = \frac{(4|m|+4k+1)(2l+1)^2\Gamma(k+1/2)\Gamma(2|m|+k+1/2)}{16\pi^2 k!(2|m|+k)!} \times \left[\frac{(l+|m|+k)!\Gamma(|m|+k+1/2)}{(|m|+k)!(l-|m|-k)!\Gamma(2|m|+2k+3/2)} \right]^2. \tag{A.36}$$

Let us remark that these quantities depend only on the dimensionality d of the hyperspace and the multiindex $(l,\{\mu\}) \equiv (\mu_1 \equiv l, \mu_2, ..., \mu_{d-1})$ which labels the hyperspherical harmonics. Besides, the function ${}_3F_2$ is terminating since $-l+|m|+k \leq 0$; so, it has a finite number of terms what reduces its computation to a mere sum.

For the sake of completeness let us also mention that the evaluation of the integral of the product of four hyperspherical harmonics given by Eq. (A.11), and similarly for integrals with a higher number of hyperspherical harmonics, which naturally appear in classical and non-relativistic [126, 153, 319, 400, 404] and relativistic [401, 410] quantum-mechanical problems, can be done either by taking into account the theory of the Gegenbauer polynomials (as it has been illustrated here) or, alternatively, by use of the theory of the harmonic polynomials following the lines discussed by John Avery and co-workers [406, 411].

A.3 The Shannon entropy: lower bounds

The Shannon entropy, according to Eqs. (A.8) and (A.12), is given by

$$S_{l,\{\mu\}}(d) = -\int_{S_d} |\mathcal{Y}_{l,\{\mu\}}(\Omega_d)|^2 \ln |\mathcal{Y}_{l,\{\mu\}}(\Omega_d)|^2 d\Omega_d. \tag{A.37}$$

Here we find a lower bound to this quantity by means of the algebraic properties of the hyperspherical harmonics [153, 400, 402, 403] and the Jensen inequality [412]

$$\varphi\left(\frac{\int f d\mu}{\int d\mu}\right) \leq \frac{\int \varphi\left(f\right) d\mu}{\int d\mu}, \tag{A.38}$$

where $\varphi(x)$ is a convex function, $\int f(x)d\mu \leq \infty$ and $d\mu$ is a nonnegative measure.

The use of expression (A.3), normalized according to Eq. (A.6), leads to the expression [162]

$$\begin{aligned} S\left(\mathcal{Y}_{l,\{\mu\}}\right) = \ln 2\pi - \sum_{j=1}^{d-2} \int_0^{\pi} \left[\hat{C}^{\mu_j-\mu_{j+1}}_{\alpha_j+\mu_{j+1}}(\cos\theta_j)\right]^2 (\sin\theta_j)^{2\alpha_j+2\mu_{j+1}} \\ \times \ln\left[\left[\hat{C}^{\mu_j-\mu_{j+1}}_{\alpha_j+\mu_{j+1}}(\cos\theta_j)\right]^2 (\sin\theta_j)^{2\mu_{j+1}}\right] d\theta_j. \end{aligned} \tag{A.39}$$

Taking into account Eq. (A.38) with $\varphi(x) = -\ln x$, $f(\theta_j) = \left[\hat{C}^{\mu_j-\mu_{j+1}}_{\alpha_j+\mu_{j+1}}(\cos\theta_j)\right]^2 (\sin\theta_j)^{2\mu_{j+1}}$ and $d\mu = \left[\hat{C}^{\mu_j-\mu_{j+1}}_{\alpha_j+\mu_{j+1}}(\cos\theta_j)\right]^2 (\sin\theta_j)^{2\alpha_j+2\mu_{j+1}} d\theta_j$, we obtain the following expression:

$$\begin{aligned} S\left(\mathcal{Y}_{l,\{\mu\}}\right) \geq B(d) &\equiv \ln 2\pi - \sum_{j=1}^{d-2} \ln\left(\int_0^{\pi} \left[\hat{C}^{\mu_j-\mu_{j+1}}_{\alpha_j+\mu_{j+1}}(\cos\theta_j)\right]^4 (\sin\theta_j)^{2\alpha_j+4\mu_{j+1}}\right) \\ &= -\ln W_{l,\{\mu\}}(d), \end{aligned} \tag{A.40}$$

where $W_{l,\{\mu\}}(d)$ is the average density of hyperspherical harmonics that we have calculated in the previous section.

Let us point out that for $d = 2$ and 3 this expression gives the following lower bounds:

$$B(2) = \ln 2\pi \tag{A.41}$$

$$B(3) = -\ln\left(\sum_{k=0}^{l-|m|} C_k(l,|m|)\left[{}_3F_2\left(\left.\begin{matrix} -l+|m|+k, & |m|+k+1/2, & l+|m|+k+1 \\ |m|+k+1, & 2|m|+2k+3/2 \end{matrix}\right| 1\right)\right]^2\right),$$

where the coeficients $C_k(l,|m|)$ are given by Eq. (A.36), with the values of the l and m being $l = 0, 1, ...,$ and $-l \leq m \leq +l$.

For the sake of completeness we plot in Figure A.1 the values of the numerically exact Shannon entropy $S(Y_{l,m};3)$ and its lower bound $B(3)$ for various (l,m) cases. We observe that both quantities have the same qualitative behavior when l and m vary: (i) they globally decrease when l increases and m is fixed, and (ii) they have an inverted semicircular shape when l is fixed and m increases. Moreover, in order to be more transparent, we have shown in Figure A.2 the ratio $B(3)/S(Y_{l,m};3)$. Therein we notice that

the quality of the bound globally decreases with l, and it increases with $|m|$ for l fixed.

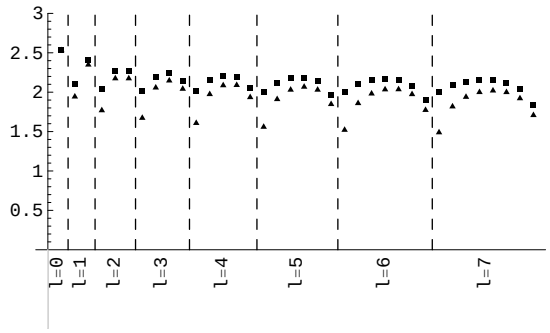

FIGURE A.1: Shannon entropy $S(Y_{l,m};3)$ (squared dots) and bound $B(3)$ (triangled dots) for the three-dimensional case.

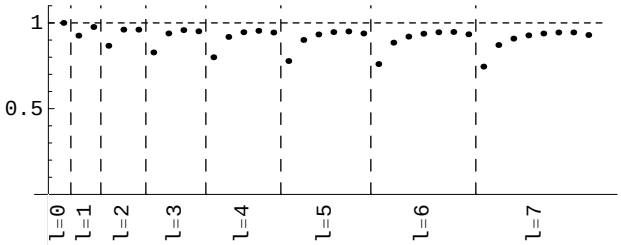

FIGURE A.2: Ratio of the three-dimensional bound $B(3)$ and the Shannon entropy $S(Y_{l,m};3)$

Appendix B

Chemical properties and information and complexity measures of selected molecules

Chemical properties of the molecules

Chemical formula	Name	Number of electrons	Energy (a.u.)	Dipole Moment (Debye)	Ionization Potential (a.u)	Hardness (a.u.)	Electrophilicy (a.u.)
NH_3	Ammonia	10	-56.420	1.7877	0.422	0.321	0.016
$LiOH$	Lithium hydroxide	12	-83.165	4.576	0.364	0.190	0.080
Li_2O	Dilithium oxide	14	-90.026	0.000	0.267	0.150	0.046
HBO	Boron hydride oxide	14	-100.468	2.840	0.510	0.339	0.043
HCO	Formyl radical	15	-113.565	1.587	0.387	0.260	0.031
NO	Nitric oxide	15	-129.534	2.003	0.421	0.259	0.050
H_2CO	Formaldehyde	16	-114.228	2.517	0.438	0.288	0.039
NHO	Nitrosyl hydride	16	-130.178	1.786	0.425	0.259	0.053
O_2	Oxygen diatomic	16	-149.948	0.000	0.552	0.491	0.004
CH_3O	Methoxy radical	17	-114.797	3.355	0.387	0.363	0.001
CH_3NH_2	Methyl amine	18	-95.589	1.4985	0.387	0.307	0.011
CH_3OH	Methyl alcohol	18	-115.435	1.945	0.444	0.334	0.018
NH_2OH	hydroxylamine	18	-131.410	0.901	0.424	0.326	0.015
H_2O_2	Hydrogen peroxide	18	-151.216	1.751	0.474	0.346	0.024
$NaOH$	Sodium hydroxide	20	-237.541	6.888	0.477	0.159	0.319
$HCCO$	Ketenyl radical	21	-113.859	1.762	0.411	0.312	0.016
C_3H_3	Radical propargyl	21	-115.643	0.181	0.351	0.282	0.009
BO_2	Boron dioxide	21	-174.884	0.000	0.533	0.361	0.041
$MgOH$	Magnesium hydroxide	21	-275.346	5.737	0.271	0.160	0.039
CH_2CCH_2	Allene	22	-116.289	0.000	0.371	0.275	0.017
CH_3CCH	Propyne	22	-116.292	0.733	0.346	0.300	0.004
C_3H_4	Cyclopropene	22	-116.292	0.733	0.346	0.264	0.013
CH_3CN	Acetonitrile	22	-132.221	4.629	0.457	0.331	0.024
CH_3NC	Methyl isocyanide	22	-132.340	3.808	0.464	0.334	0.025
CH_2NN	Diazomethane	22	-148.326	4.502	0.391	0.231	0.056
NH_2CN	Cyanamide	22	-148.388	4.502	0.391	0.305	0.012
$HCCOH$	Ethynol	22	-152.141	1.747	0.371	0.282	0.014
CH_2CO	Ketene	22	-152.197	1.461	0.361	0.249	0.025
HN_3	Hydrogen azide	22	-164.349	1.961	0.398	0.268	0.032
$HCNO$	Fulminic acid	22	-168.134	3.248	0.403	0.294	0.020
$HNCO$	Isocyanic acid	22	-168.261	2.238	0.447	0.308	0.031
N_2O	Nitrous oxide	22	-184.212	0.426	0.489	0.324	0.042
CO_2	Carbon dioxide	22	-188.150	0.000	0.539	0.377	0.035
FCN	Cyanogen fluoride	22	-192.205	2.147	0.498	0.360	0.026
HBS	Hydrogen boron sulfide	22	-423.039	1.397	0.401	0.250	0.046
C_3H_5	Allyl radical	23	-116.874	0.923	0.333	0.281	0.005
CH_3CO	Acetyl radical	23	-152.755	2.428	0.360	0.258	0.020
NO_2	Nitrogen dioxide	23	-204.636	0.078	0.499	0.290	0.075
PO	Phosphorus monoxide	23	-415.862	0.135	0.327	0.175	0.067

NS	Mononitrogen monosulfide	23	-452.183	1.971	0.354	0.186	0.077
C_3H_6	Cyclopropane	24	-117.518	0.000	0.417	0.331	0.011
C_2H_5N	Aziridine	24	-133.525	1.899	0.389	0.307	0.011
$NHCHNH_2$	Aminomethanimine	24	-149.592	2.745	0.365	0.284	0.012
C_2H_4O	Ethylene oxide	24	-153.372	2.200	0.446	0.347	0.014
CH_3CHO	Acetaldehyde	24	-153.416	2.628	0.422	0.289	0.031
$CHONH_2$	Formamide	24	-169.461	3.761	0.415	0.308	0.018
CH_2O_2	Dioxirane	24	-189.156	2.866	0.482	0.341	0.030
$HCOOH$	Formic acid	24	-189.304	1.299	0.468	0.324	0.032
HNO_2	Nitrous acid	24	-205.223	2.084	0.471	0.287	0.060
O_3	Ozone	24	-224.882	0.715	0.486	0.231	0.142
FNO	Nitrosyl fluoride	24	-229.213	1.893	0.511	0.290	0.085
CF_2	Difluoromethylene	24	-237.220	0.417	0.469	0.287	0.058
H_2CS	Thioformaldehyde	24	-436.815	1.678	0.349	0.202	0.054
SO	Sulfur monoxide	24	-472.622	1.815	0.424	0.290	0.031
CH_3CHCH_3	Isopropyl radical	25	-118.042	1.378	0.328	0.287	0.003
$CH_2CH_2CH_3$	n-Propyl radical	25	-118.050	4.976	0.349	0.272	0.011
CH_3CHOH	Ethoxy radical	25	-153.397	1.131	0.464	0.353	0.018
CH_3OO	Methylperoxy radical	25	-189.745	4.890	0.476	0.361	0.018
FO_2	Dioxygen monofluoride	25	-249.576	1.555	0.552	0.370	0.045
NF_2	Difluoroamino radical	25	-253.764	1.485	0.533	0.409	0.019
CH_3S	Thiomethoxy	25	-437.452	0.075	0.372	0.222	0.051
C_3H_8	Propane	26	-118.750	0.076	0.467	0.350	0.019
CH_3NHCH_3	Dimethylamine	26	-134.753	1.212	0.365	0.297	0.008
$CH_3CH_2NH_2$	Ethylamine	26	-134.766	1.503	0.384	0.303	0.011
CH_3OCH_3	Dimethyl ether	26	-154.594	1.539	0.419	0.327	0.013
CH_3CH_2OH	Ethanol	26	-154.612	1.886	0.436	0.330	0.017
CH_3OOH	Methyl peroxide	26	-190.380	1.521	0.444	0.333	0.018
F_2O	Difluorine monoxide	26	-274.101	0.405	0.569	0.363	0.059
SiO_2	Silicon dioxide	30	-439.124	0.000	0.500	0.255	0.118
OCS	Carbonyl sulfide	30	-510.726	0.774	0.418	0.270	0.041
$ClCN$	Chlorocyanogen	30	-551.636	5.950	0.465	0.315	0.036
PO_2	Phosphorus dioxide	31	-491.029	0.202	0.470	0.258	0.087
PS	Phosphorus sulfide	31	-738.487	0.978	0.311	0.153	0.083
SO_2	Sulfur dioxide	32	-547.716	2.114	0.489	0.253	0.111
$ClNO$	Nitrosyl chloride	32	-589.211	2.082	0.434	0.239	0.080
S_2	Sulfur diatomic	32	-795.264	0.000	0.384	0.257	0.032
$OClO$	Chlorine dioxide	33	-609.561	2.783	0.474	0.267	0.081
ClO_2	Chlorine dioxide	33	-609.586	1.016	0.474	0.267	0.081
CH_3SCH_3	Dimethyl sulfide	34	-477.214	1.635	0.334	0.265	0.009
CH_3CH_2SH	Ethanethiol	34	-477.218	1.682	0.353	0.264	0.015
SF_2	Sulfur difluoride	34	-596.892	1.658	0.396	0.247	0.045
H_2S_2	Hydrogen sufide	34	-796.507	1.410	0.387	0.243	0.043
CS_2	Carbon disulfide	38	-833.302	0.000	0.372	0.214	0.059

SSO	Disulfur monoxide	40	-870.246	1.431	0.404	0.186	0.128
CCl_2	Dichloromethylene	40	-957.158	1.186	0.401	0.219	0.075
$MgCl_2$	Magnesium dichloride	46	-1119.088	0.000	0.450	0.235	0.098
S_3	Sulfur trimer	48	-1192.913	0.871	0.361	0.146	0.158
$SiCl_2$	Dichlorosilylene	48	-1208.352	1.294	0.380	0.192	0.093
ClS_2	Sulfur chloride	49	-1254.976	0.960	0.343	0.175	0.080

TABLE B.1: Chemical properties of the molecules

Complexiy values

Chemical formula	$C_r(LMC)$	$C_p(LMC)$	$C_{rp}(LMC)$	$C_r(FS)$	$C_p(FS)$	$C_{rp}(FS)$
NH_3	18.329	4.890	89.633	22.098	6.275	138.665
$LiOH$	15.817	4.839	76.545	22.569	6.115	137.998
Li_2O	14.707	4.843	71.226	24.406	6.323	154.319
HBO	15.921	5.710	90.901	26.266	6.750	177.287
HCO	20.482	7.614	155.955	32.700	8.300	271.396
NO	18.222	7.168	130.609	30.542	7.988	243.978
H_2CO	16.159	5.408	87.391	28.659	6.678	191.377
NHO	15.386	5.329	81.996	28.056	6.753	189.456
O_2	14.269	5.018	71.601	26.625	6.596	175.606
CH_3O	21.197	6.553	138.900	35.209	7.551	265.849
CH_3NH_2	16.455	4.717	77.619	31.372	6.233	195.534
CH_3OH	17.196	5.058	86.977	31.282	6.470	202.402
NH_2OH	16.469	5.224	86.038	30.668	6.772	207.692
H_2O_2	15.692	5.298	83.140	29.600	6.966	206.195
$NaOH$	16.663	5.765	96.069	30.033	6.786	203.792
$HCCO$	18.736	5.848	109.576	32.104	7.482	240.193
C_3H_3	14.619	5.307	77.576	34.925	6.691	233.679
BO_2	14.240	5.258	74.872	32.142	6.613	212.558
$MgOH$	28.094	21.582	606.322	42.104	24.193	1018.634
CH_2CCH_2	14.887	5.254	78.209	36.060	6.722	242.410
CH_3CCH	14.859	5.204	77.322	36.012	6.642	239.193
C_3H_4	14.859	5.204	77.322	36.012	6.642	239.193
CH_3CN	15.147	5.375	81.417	35.842	6.795	243.557
CH_3NC	15.179	5.395	81.893	35.998	6.680	240.459
$CH2NN$	14.979	5.389	80.730	35.364	6.868	242.894
NH_2CN	14.621	5.352	78.256	34.778	6.787	236.049
$HCCOH$	15.133	5.259	79.577	34.778	6.618	230.157
CH_2CO	15.096	5.398	81.488	34.758	6.761	235.010
HN_3	14.139	5.206	73.603	33.966	6.807	231.193
$HCNO$	14.556	5.252	76.453	33.987	6.747	229.303
$HOCN$	14.422	5.264	75.922	33.817	6.673	225.656
$HNCO$	14.111	5.255	74.159	33.281	6.727	223.888
N_2O	13.642	4.935	67.319	32.764	6.542	214.329
CO_2	13.458	4.967	66.854	31.982	6.470	206.926
FCN	14.216	5.152	73.238	32.573	6.474	210.885
HBS	39.219	12.909	506.268	45.008	13.545	609.627
C_3H_5	18.363	5.750	105.581	42.281	7.095	299.994
CH_3CO	19.461	6.781	131.961	41.942	8.218	344.662
NO_2	15.622	6.023	94.086	36.221	7.105	257.364
PO	32.401	14.006	453.829	44.319	14.029	621.770
NS	37.529	13.892	521.334	46.670	13.788	643.470
C_3H_6	14.573	4.700	68.496	36.814	6.216	228.832

C_2H_5N	15.076	4.854	73.171	37.026	6.357	235.383
$NHCHNH_2$	15.284	5.025	76.799	37.056	6.458	239.322
C_2H_4O	15.564	5.031	78.296	36.753	6.448	236.990
CH_3CHO	15.986	5.219	83.430	37.453	6.557	245.587
$CHONH_2$	15.099	5.118	77.269	36.021	6.476	233.265
CH_2O_2	15.099	5.282	79.758	35.870	6.790	243.544
$HCOOH$	14.796	5.204	77.001	35.225	6.528	229.965
HNO_2	14.424	5.168	74.547	35.028	6.611	231.566
O_3	14.057	5.075	71.342	34.472	6.660	229.580
FNO	14.001	5.170	72.385	33.829	6.606	223.461
CF_2	14.085	5.253	73.983	33.166	6.476	214.793
H_2CS	38.934	11.926	464.325	47.354	12.728	602.734
SO	28.632	9.671	276.908	40.560	10.750	436.024
CH_3CHCH_3	18.342	5.215	95.647	43.754	6.616	289.479
$CH_2CH_2CH_3$	18.640	5.284	98.489	44.232	6.656	294.427
CH_3CHOH	15.947	5.118	81.609	37.328	6.479	241.853
CH_3OO	18.130	6.056	109.797	41.062	7.142	293.257
FO_2	15.576	5.928	92.339	36.994	7.197	266.258
NF_2	15.602	6.039	94.216	36.560	7.173	262.231
CH_3S	48.622	14.312	695.908	55.725	13.947	777.211
C_3H_8	15.184	4.475	67.955	39.247	6.051	237.486
CH_3NHCH_3	15.823	4.645	73.503	39.583	6.168	244.134
$CH_3CH_2NH_2$	15.794	4.632	73.166	39.522	6.169	243.825
CH_3OCH_3	16.602	4.888	81.144	39.681	6.289	249.561
CH_3CH_2OH	16.492	4.847	79.941	39.477	6.311	249.153
CH_3OOH	16.305	5.139	83.786	38.912	6.599	256.795
F_2O	13.780	5.021	69.189	34.504	6.686	230.701
SiO_2	21.279	7.197	153.135	42.587	8.418	358.485
OCS	29.439	8.637	254.249	47.959	9.847	472.247
$ClCN$	34.096	9.156	312.185	50.455	10.743	542.020
PO_2	26.608	9.562	254.412	48.502	10.036	486.758
PS	33.482	18.602	622.825	53.355	18.347	978.882
SO_2	25.582	8.033	205.489	46.479	9.105	423.187
$ClNO$	31.033	9.169	284.526	50.569	10.255	518.602
S_2	29.557	13.830	408.768	49.503	15.541	769.315
$OClO$	30.434	9.286	282.608	51.335	10.152	521.178
ClO_2	31.652	9.814	310.638	52.740	10.507	554.167
CH_3SCH_3	43.179	8.841	381.755	62.193	10.184	633.383
CH_3CH_2SH	43.193	9.148	395.128	62.192	10.349	643.612
SF_2	23.088	7.614	175.794	45.869	8.693	398.764
H_2S_2	33.365	14.977	499.718	54.844	15.983	876.593
CS_2	31.540	11.615	366.320	57.500	13.232	760.837
SSO	28.568	11.232	320.885	56.396	12.275	692.232
CCl_2	33.193	12.496	414.800	59.796	13.525	808.719
$MgCl_2$	27.977	11.443	320.138	60.209	12.364	744.450

S_3	29.189	13.970	407.786	64.165	15.508	995.053
$SiCl_2$	29.108	13.964	406.462	63.384	14.697	931.524
ClS_2	31.640	15.477	489.713	68.048	15.910	1082.619

TABLE B.2: Complexiy values

Information planes

Chemical formula	I_r	I_p	J_r	J_p	D_r	D_p	L_r	L_p
NH_3	35.359	3.951	0.625	1.588	0.526	0.035	34.873	141.252
$LiOH$	42.817	2.871	0.527	2.130	0.586	0.022	27.011	219.366
Li_2O	40.522	3.028	0.602	2.088	0.446	0.023	32.993	212.967
HBO	44.908	3.083	0.585	2.189	0.504	0.025	31.573	228.637
HCO	47.148	3.727	0.694	2.227	0.502	0.032	40.769	234.576
NO	53.282	3.066	0.573	2.605	0.595	0.024	30.633	296.801
H_2CO	44.410	3.103	0.645	2.152	0.442	0.024	36.591	222.885
NHO	50.288	2.734	0.558	2.470	0.523	0.019	29.415	273.967
O_2	57.172	2.309	0.466	2.856	0.636	0.015	22.433	340.759
CH_3O	41.945	3.951	0.839	1.911	0.390	0.035	54.285	186.471
CH_3NH_2	33.729	4.042	0.930	1.542	0.260	0.035	63.319	135.176
CH_3OH	39.736	3.451	0.787	1.875	0.349	0.028	49.302	181.200
NH_2OH	44.865	3.073	0.684	2.204	0.413	0.023	39.892	230.958
H_2O_2	50.972	2.671	0.581	2.608	0.502	0.018	31.235	297.351
$NaOH$	67.031	1.867	0.448	3.635	0.787	0.012	21.169	489.255
$HCCO$	45.164	3.759	0.711	1.990	0.443	0.030	42.302	198.209
C_3H_3	35.850	3.973	0.974	1.684	0.215	0.034	67.870	154.263
BO_2	51.429	2.501	0.625	2.644	0.408	0.017	34.874	303.534
$MgOH$	72.165	6.982	0.583	3.465	0.893	0.047	31.457	455.310
CH_2CCH_2	34.380	4.181	1.049	1.608	0.196	0.037	75.823	143.893
CH_3CCH	34.372	4.154	1.048	1.599	0.196	0.036	75.698	142.733
C_3H_4	34.372	4.154	1.048	1.599	0.196	0.036	75.698	142.733
CH_3CN	38.577	3.710	0.929	1.831	0.240	0.031	63.212	174.949
CH_3NC	38.665	3.655	0.931	1.828	0.239	0.031	63.408	174.421
CH_2NN	42.763	3.341	0.827	2.056	0.282	0.026	53.081	208.023
NH_2CN	42.721	3.243	0.814	2.093	0.282	0.025	51.843	213.709
$HCCOH$	43.351	3.159	0.802	2.095	0.298	0.025	50.718	214.029
CH_2CO	43.450	3.188	0.800	2.121	0.299	0.025	50.501	217.992
HN_3	46.920	2.946	0.724	2.311	0.325	0.021	43.476	247.947
$HCNO$	47.560	2.860	0.715	2.359	0.341	0.021	42.641	255.808
$HOCN$	47.639	2.807	0.710	2.377	0.342	0.020	42.216	258.724
$HNCO$	47.582	2.792	0.699	2.409	0.342	0.020	41.290	263.993
N_2O	51.862	2.551	0.632	2.565	0.385	0.017	35.444	289.908
CO_2	52.542	2.408	0.609	2.687	0.401	0.016	33.521	310.842
FCN	53.291	2.381	0.611	2.719	0.421	0.016	33.730	316.488
HBS	95.653	3.402	0.471	3.982	1.721	0.023	22.782	560.801
C_3H_5	33.000	4.950	1.281	1.433	0.179	0.047	102.365	121.145
CH_3CO	41.737	4.253	1.005	1.932	0.274	0.036	71.105	189.554
NO_2	54.331	2.580	0.667	2.754	0.407	0.019	38.422	322.651
PO	93.118	3.147	0.476	4.458	1.398	0.021	23.176	664.281
NS	98.935	3.131	0.472	4.403	1.641	0.021	22.869	652.189
C_3H_6	31.688	4.197	1.162	1.481	0.165	0.037	88.384	127.209

C_2H_5N	35.547	3.795	1.042	1.675	0.201	0.032	75.036	153.063
$NHCHNH_2$	39.358	3.440	0.942	1.877	0.237	0.028	64.484	181.539
C_2H_4O	40.077	3.343	0.917	1.929	0.251	0.027	61.989	189.055
CH_3CHO	40.139	3.418	0.933	1.919	0.251	0.028	63.621	187.575
$CHONH_2$	43.829	2.985	0.822	2.169	0.287	0.023	52.590	225.540
CH_2O_2	48.619	2.763	0.738	2.457	0.338	0.019	44.730	271.863
$HCOOH$	48.366	2.641	0.728	2.472	0.337	0.019	43.871	274.330
HNO_2	52.388	2.476	0.669	2.670	0.374	0.017	38.591	307.969
O_3	57.042	2.273	0.604	2.930	0.424	0.014	33.161	354.055
FNO	57.622	2.179	0.587	3.032	0.441	0.014	31.752	372.608
CF_2	58.849	2.027	0.564	3.196	0.472	0.013	29.864	403.204
H_2CS	91.074	3.216	0.520	3.958	1.471	0.021	26.464	555.725
SO	99.453	2.257	0.408	4.762	1.557	0.013	18.384	733.511
CH_3CHCH_3	30.608	4.986	1.430	1.327	0.152	0.048	120.639	107.892
$CH_2CH_2CH_3$	30.608	5.061	1.445	1.315	0.152	0.050	122.622	106.476
CH_3CHOH	40.048	3.403	0.932	1.904	0.251	0.028	63.517	185.402
CH_3OO	46.628	3.180	0.881	2.246	0.311	0.025	58.331	237.541
FO_2	59.692	2.315	0.620	3.109	0.452	0.015	34.438	386.854
NF_2	60.253	2.234	0.607	3.211	0.468	0.015	33.362	406.065
CH_3S	87.510	3.862	0.637	3.612	1.356	0.030	35.868	484.462
C_3H_8	29.589	4.508	1.326	1.342	0.141	0.041	107.825	109.781
CH_3NHCH_3	33.093	4.072	1.196	1.515	0.171	0.035	92.334	131.596
$CH_3CH_2NH_2$	33.089	4.080	1.194	1.512	0.171	0.035	92.142	131.252
CH_3OCH_3	37.259	3.626	1.065	1.734	0.214	0.030	77.576	161.232
CH_3CH_2OH	37.242	3.639	1.060	1.734	0.214	0.030	77.032	161.232
CH_3OOH	45.030	3.016	0.864	2.188	0.288	0.022	56.702	228.464
F_2O	62.458	1.983	0.552	3.372	0.475	0.011	28.982	437.147
SiO_2	78.996	2.080	0.539	4.048	0.762	0.013	27.939	574.802
OCS	87.733	2.483	0.547	3.966	1.032	0.015	28.528	557.507
$ClCN$	92.739	2.670	0.544	4.024	1.204	0.016	28.325	569.800
PO_2	83.663	2.406	0.580	4.172	0.854	0.016	31.157	601.416
PS	116.668	3.329	0.457	5.512	1.534	0.020	21.829	913.419
SO_2	88.687	2.040	0.524	4.464	0.955	0.012	26.780	665.719
$ClNO$	93.484	2.329	0.541	4.403	1.105	0.014	28.082	652.087
S_2	120.651	2.681	0.410	5.796	1.593	0.014	18.551	984.958
$OClO$	93.811	2.236	0.547	4.541	1.065	0.014	28.573	683.123
ClO_2	93.908	2.337	0.562	4.497	1.065	0.015	29.708	673.077
CH_3SCH_3	71.901	3.629	0.865	2.806	0.760	0.027	56.783	331.815
CH_3CH_2SH	71.886	3.604	0.865	2.872	0.760	0.027	56.799	343.484
SF_2	90.936	1.799	0.504	4.832	0.913	0.010	25.287	749.769
H_2S_2	113.715	2.896	0.482	5.519	1.411	0.016	23.642	915.087
CS_2	108.093	2.762	0.532	4.790	1.152	0.016	27.385	740.069
SSO	107.860	2.281	0.523	5.382	1.071	0.013	26.687	881.223
CCl_2	115.767	2.464	0.517	5.490	1.267	0.014	26.202	907.920
$MgCl_2$	118.212	2.129	0.509	5.808	1.090	0.012	25.658	987.999

S_3	120.348	2.613	0.533	5.935	1.062	0.014	27.479	1020.606
$SiCl_2$	121.417	2.349	0.522	6.257	1.093	0.013	26.623	1104.761
ClS_2	123.420	2.643	0.551	6.020	1.095	0.015	28.897	1042.597

TABLE B.3: Information planes

Bibliography

[1] R. V. Hartly. *Transmision of information.* Bell Sys. Tech. J., **7** 335 (1928).

[2] H. Nyquist. *Certain topics in telegraph transmission theory.* Bell Sys. Tech. J., **3** 324 (1924).

[3] R. A. Fisher. *Theory of statistical estimation.* Proc. Cambridge Phil. Soc., **22** 700 (1925). Reprinted in Collected Papers of R. A. Fisher, edited by J.H. Bennet (University of Adelaide Press, South Australia), 1972, pp. 15–40.

[4] E. T. Jaynes. *Information theory and statistical mechanics.* Phys. Rev., **106** 620 (1957).

[5] E. T. Jaynes. *Information theory and statistical mechanics. II.* Phys. Rev., **108** 171 (1957).

[6] A. Berger, V. D. Pietra and S. D. Pietra. *A maximum entropy approach to natural language processing.* Comp. Linguis., **22** 39 (1996).

[7] D. Bouwmeester, A. Ekert and A. Zeilinger. *The Physics of Quantum Information.* Springer, Berlin (2000).

[8] A. Ephremides and B. Hajek. *Information theory and comunication networks: an unconsummated union.* IEEE Trans. Inf. Theory, **44** 1 (1998).

[9] A. Borst and F. E. Theunissen. *Information theory and neural coding.* Nature Neurosci., **2** 947 (1999).

[10] F. Attneave. *Informationstheorie in der Psychologie: Grundbegriffe.* Velags Hans Huber, Wien (1974).

[11] J. A. F. Diniz-Filho, T. F. L. V. B. Rangel and L. M. Bini. *Model selection and information theory in geographical ecology.* Global Ecol. Biogeog., **17** 479 (2008).

[12] J. C. Angulo. *Information entropy and uncertainty in D-dimensional many-body systems.* Phys. Rev. A, **50** 311 (1994).

[13] J. S. Dehesa, A. Martínez-Finkelshtein and V. N. Sorokin. *Quantum-information entropies for highly excited states of single-particle systems with power-type potentials.* Phys. Rev. A, **66** 062109 (2002).

[14] M. Ho, R. P. Sagar, V. H. Smith Jr and R. O. Esquivel. *Atomic information entropies beyond the Hartree.* J. Phys. B: At. Mol. Opt., **27** 5149 (1994).

[15] M. A. Nielsen and I. L. Chuang. *Quantum Computation and Quantum Information.* Cambridge University Press, Cambridge (2000).

[16] C. E. Shannon and W. Weaver. *The Mathematical Theory of Communication*. University of Illinois Press, Urbana (1949).

[17] S. Kullback. *Information Theory and Statistics*. Dover, New York (1959).

[18] P. Adriaans and J. van Benthem. *Philosophy of Information*. Elsevier, Amsterdam (2007).

[19] Y. Bar-Hillel and R. Carnap. *Semantic information*. British J. Philos. Sci., **3** 147 (1958).

[20] H. Atmanspachera and G. Weidenmann. *Information Dynamics*. Plenum, New York (1991).

[21] U. Birchler and M. Bütler. *Information Economics*. Routledge, London (2007).

[22] C. G. Timpson. *Quantum Information Theory and the Foundations of Quantum Mechanics*. Ph.D. Thesis. Oxford University (2004).

[23] E. Jablonka. *Information: Its interpretations, its inheritance and its sharing*. Phil. Soc., **69** 578 (2002).

[24] V. Majernik and S. Shpyrko. *Battacharyye statistical divergence of quantum observables*. Rep. Math. Phys., **61** 319 (2008).

[25] V. Majernik. *A dissimilarity measure for an arbitrary number of probability distributions*. Int. J. Gen. Sys., **33** 673 (2004).

[26] V. Majernik, E. Majernikova and S. Sphyrko. *Uncertainty relation expression by the Shannon-like entropies*. Central Europ. J. Phys., **3** 393 (2003).

[27] V. Majernik and E. Majernikova. *Uncertainty relations expressed by means of information energies*. Acta Physica, **17** 19 (2003).

[28] M. Ohya and D. Petz. *Quantum Entropy and Its Use*. Springer Verlag, Heidelberg (2004).

[29] D. Petz. *From f-divergence to quantum quasi-entropies and their use* (2009). ArXiv: 0909.3647v1.

[30] D. Petz. *Quantum Information Theory and Quantum Statistics*. Springer, Berlin (2008).

[31] C. Arndt. *Information Measures*. Springer, Berlin (2001).

[32] C. E. Shannon. *A mathematical theory of communication*. Bell Syst. Tech. J., **27** 379 (1948).

[33] A. Renyi. *On measures of information and entropy*. In *Proceedings of the 4th Berkley Symposium on Mathematics, Statistics and Probability*, 547 (1961).

[34] C. Tsallis. *Possible generalization of Boltzmann-Gibbs statistics*. J. Stat. Phys., **52** 479 (1988).

[35] E. T. Jaynes. *On the rationale of maximum entropy methods*. Proc. IEEE, **70** 939 (1982).

[36] C. Tsallis. *Introduction to Nonextensive Statistical Mechanics. Approaching a Complex World*. Springer, Berlin (2009).

[37] B. R. Frieden. *Science from Fisher Information*. Cambridge University Press, Cambridge (2004).

[38] R. F. Nalewajski. *Information Theory of Molecular Systems*. Elsevier, Amsterdam (2006).

[39] R. F. Nalewajski. *Information principles in the theory of electronic structure*. Chem. Phys. Lett., **372** 28 (2003).

[40] R. Daudel. *The Fundamentals of Theoretical Chemistry*. Pergamon, Oxford (1969).

[41] C. Aslangul, R. Constanciel, R. Daudel and P. Kottis. Adv. Quan. Chem., **6** 94 (1972).

[42] R. F. Nalewajski. *Information principles in the loge theory*. Chem. Phys. Lett., **375** 196 (2003).

[43] D. C. Dowson and A. Wragg. *Maximum-entropy distributions having first and second moments*. IEEE Trans. Inf. Theory, **19** 689 (1973).

[44] I. Bialynicki-Birula and J. Mycielski. *Uncertainty relations for information entropy in wave mechanics*. Commun. Math. Phys., **44** 129 (1975).

[45] S. B. Sears, R. G. Parr and U. Dinur. *On the quantum-mechanical kinetic-energy as a measure of the information in a distribution*. Israel J. Chem., **19** 165 (1980).

[46] S. R. Gadre and S. B. Sears. *An application of information theory to Compton profiles*. J. Chem. Phys., **71** 4321 (1979).

[47] S. R. Gadre. *Information entropy and Thomas-Fermi theory*. Phys. Rev. A, **30** 620 (1984).

[48] S. R. Gadre and R. D. Bendale. *Information entropies in quantum chemistry*. Current Sci., **5** 970 (1985).

[49] R. S. Gadre and R. D. Bendale. *Rigorous relationships among quantum-mechanical kinetic energy and atomic information entropies: Upper and lower bounds*. Phys. Rev. A, **36** 1932 (1987).

[50] Y. Alhassid and R. D. Levine. *Entropy and chemical change. Maximal entropy (subject to constraints) procedure as a dynamical theory*. J. Chem. Phys., **67** 432 (1977).

[51] J. C. Angulo and J. S. Dehesa. *Tight rigorous bounds to atomic information entropies*. J. Chem. Phys., **97** 6485 (1992). Erratum: J. Chem. Phys. **98** 9223 (1993).

[52] E. Romera and J. S. Dehesa. *Weiszacker energy of many-electron systems*. Phys. Rev. A, **59** 256 (1994).

[53] R. J. Yáñez, W. van Assche and J. S. Dehesa. *Position and momentum information entropies of the D-dimensional harmonic oscillator and hydrogen atom*. Phys. Rev. A, **50** 3065 (1994).

[54] M. Ho, R. P. Sagar, J. M. Pérez-Jordá, V. H. Smith Jr and R. O. Esquivel. *A numerical study of molecular information entropies*. Chem. Phys. Lett., **219** 15 (1994).

[55] R. O. Esquivel, A. L. Rodriguez, R. P. Sagar, M. Ho and V. H. S. Jr. *Physical interpretation of information entropy: Numerical evidence of the Collins conjecture*. Phys. Rev. A, **54** 259 (1996).

[56] E. T. Jaynes. *The Maximum Entropy Problem.* MIT Press, Cambridge (1978).

[57] A. Katz. *Principles of Statistical Mechanics.* Freeman, San Francisco (1967).

[58] A. Rényi. *Probability Theory.* North Holland, Amsterdam (1970).

[59] A. Stam. *Some inequalities satisfied by the quantities of information of Fisher and Shannon.* Inform. Control, **2** 101 (1959).

[60] A. N. Kolmogorov. *Three approaches to the quantitative definition of information.* Probl. Inf. Transm., **1** 3 (1965).

[61] E. H. Kennard. *Zur Quntenmechanik einfacher bewegungstypen.* Z. Phys., **44** 326 (1927).

[62] J. Hilgevoord and J. Uffink. *The Mathematical Expression of the Uncertainty Principle.* Kluwer, Dordrecht (1988).

[63] H. Landau and H. Pollak. *Prolate spheroidal wavefunctions, Fourier analysis and uncertainty-II.* Bell Syst. Tech. J., **40** 65 (1961).

[64] T. M. Cover and J. A. Thomas. *Elements of Information Theory.* Wiley, New York (1991).

[65] H. Hatori. *A note on the entropy of a continuous distribution,.* Kodai Math. Sem. Rep., **10** 172 (1958).

[66] J. B. M. Uffink. *Measures of Uncertainty and the Uncertainty Principle.* Ph.D. Thesis. University of Amsterdam (1990).

[67] K. Zyczkowski. *Rényi extrapolation of Shannon entropy.* Open Syst. Inf. Dyn., **10** 297 (2003).

[68] J. Pipek and I. Varga. *Universal classification scheme for the spatial-localization properties of one-particle states in finite, d-dimensional systems.* Phys. Rev. A, **46** 3148 (1992).

[69] I. Varga and J. Pipek. *Rényi entropies characterizing the shape and the extension of the phase space representation of quantum wave functions in disordered systems.* Phys. Rev. E, **68** 026202 (2003).

[70] O. Gühne and M. Lewenstein. *Entropic uncertainty relations and entanglement.* Phys. Rev. A, **70** 022316 (2004).

[71] F. Franchini, A. R. Its and V. E. Korepin. *Rényi entropy of the xy spin chain.* J. Phys. A, **41** 025302 (2008).

[72] V. Giovannetti and S. Lloyd. *Additivity properties of a gaussian channel.* Phys. Rev. A, **69** 062307 (2004).

[73] E. Romera and A. Nagy. *Rényi information of atoms.* Phys. Lett. A, **372** 4918 (2008).

[74] E. Romera and F. de los Santos. *Fractional revivals through Rényi uncertainty relations.* Phys. Rev. A, **78** 013837 (2008).

[75] D. G. Arbó, C. O. Reinhold, J. Burgdörfer, A. K. Pattanayak, C. L. Stokely, W. Zhao, J. C. Lancaster and F. B. Dunning. *Pulse-induced focusing of Rydberg wave packets.* Phys. Rev. A, **67** 063401 (2003).

[76] J. N. Kapur. *Measures of Information and Their Applications*. John Wiley and Sons, New York (1994).

[77] J. Havrda and F. Charvat. *Quantification method of classification processes: concept of structural α-entropy*. Kybernetika, **3** 1 (1967).

[78] M. Gell-Mann and C. Tsallis. *Nonextensive Entropy; Interdisciplinary Applications*. Oxford University Press, New York (2004).

[79] C. Vignat, A. Her and J. Costa. *About closedness by convolution of the Tsallis maximizers*. Physica A, **340** 147 (2004).

[80] C. Brukner and A. Zeilinger. *Operationally invariant information in quantum measurements*. Phys. Rev. Lett., **83** 3354 (1999).

[81] W. H. Zurek, S. Habid and J. P. Paz. *Coherent states via decoherence*. Phys. Rev. Lett., **70** 1187 (1993).

[82] H. Maassen and J. B. M. Uffink. *Generalized entropic uncertainty relations*. Phys. Rev. Lett., **60** 1103 (1988).

[83] M. J. W. Hall. *Universal geometric approach to uncertainty, entropy and information*. Phys. Rev. A, **59** 2602 (1999).

[84] A. Zygmund. *Trigonometric Series*. Cambridge University Press, Cambridge (1959).

[85] G. H. Hardy, J. E. Littlewood and G. Polya. *Inequalities*. Cambridge University Press, Cambridge (1934).

[86] G. U. Yule. *On some properties of the normal distribution, univariate and bivariate, based on the sum of squares of frequencies*. Biometrika, **30** 1 (1938).

[87] H. S. Sichel. *Fitting growth and frequency curves by the method of frequency moments*. J. Roy. Sta. Soc. Ser. A, **110** 337 (1947).

[88] S. Liu and R. G. Parr. *Expansions of the correlation-energy density functional $E_c[\rho]$ and its kinetic-energy component $T_c[\rho]$ in terms of homogeneous functionals*. Phys. Rev. A, **53** 2211 (1996).

[89] S. Liu and R. G. Parr. *Expansions of density functionals in terms of homogeneous functionals: Justification and nonlocal representation of the kinetic energy, exchange energy,and classical Coulomb repulsion energy for atoms*. Phys. Rev. A, **55** 1792 (1997).

[90] J. S. Dehesa, S. López-Rosa and D. Manzano. *Entropy and complexity analyses of d-dimensional quantum systems*. In K. D. Sen, ed., *Statistical Complexities: Applications in electronic structures*. Springer, Berlin (2010).

[91] R. López-Ruiz, H. L. Mancini and X. Calbet. *A statistical measure of complexity*. Phys. Lett. A, **209** 321 (1995).

[92] M. T. Martin, J. Pérez and A. Plastino. *Fisher information and nonlinear dynamics*. Physica A, **291** 523 (2001).

[93] S. R. Gadre. *Reviews of Modern Quantum Chemistry: A Celebration in the Contributions of Robert G. Parr.* vol. 1. World Scientific, Singapore (2003).

[94] S. E. Massen and C. P. Panos. *A link of information entropy and kinetic energy for quantum many-body systems.* Phys. Lett. A, **280** 65 (2001).

[95] A. Nagy. *Fisher information in density functional theory.* J. Chem. Phys., **119** 9401 (2003).

[96] R. González-Férez and J. S. Dehesa. *Shannon entropy as an indicator of atomic avoided crossings in strong parallel magnetic and electric fields.* Phys. Rev. Lett., **91** 113001 (2003).

[97] R. González-Férez and J. S. Dehesa. *Characterization of atomic avoided crossings by means of Fisher's information.* Eur. Phys. J. D., **32** 39 (2005).

[98] B. R. Frieden and A. Plastino. *A critical comparison of the three information-based approaches to physics.* Found. Phys. Lett., **13** 89 (2000).

[99] N. H. March and S. Kais. *Kinetic energy functional derivative for the Thomas-Fermi atom in D dimensions.* Int. J. Quant. Chem., **65** 411 (1998).

[100] S. Luo. *Fisher information, kinetic energy and uncertainty relation inequalities.* J. Phys. A, **35** 5181 (2002).

[101] R. G. Parr and W. Yang. *Density-Functional Theory of Atoms and Molecules.* Oxford University Press, New York (1989).

[102] A. Dembo, T. M. Cover and J. A. Thomas. *Information theoretic inequalities.* IEEE Trans. Inf. Theory, **37** 1501 (1991).

[103] S. López-Rosa, J. C. Angulo and J. Antolín. *Rigorous properties and uncertainty-like relationships on product-complexity measures: Applications to atomic systems.* Physica A, **388** 2081 (2009).

[104] E. Romera. *Stam's principle, D-dimensional uncertainty-like relationships and some atomic properties.* Mol. Phys., **100** 3325 (2002).

[105] S. López-Rosa, R. O. Esquivel, J. C. Angulo, J. Antolín, J. S. Dehesa and N. Flores-Gallegos. *Fisher Information study in position and momentum spaces for elementary chemical reactions.* J. Chem. Theory Comput., **6** 145 (2010).

[106] A. Plastino, A. R. Plastino and B. H. Soffer. *Fisher information and thermodynamics first law.* Physica A, **369** 432 (2006).

[107] B. R. Frieden. *Fisher information as a measure of time.* Astrophys. Space Sci, **244** 387 (1996).

[108] C. Vignat and J. Bercher. *Analysis in the Fisher-Shannon information plane.* Phys. Lett. A, **312** 27 (2003).

[109] M. T. Martin, F. Pennini and A. Plastino. *Fisher's information and the analysis of complex signals.* Phys. Lett. A, **256** 173 (1999).

[110] L. Telesca, V. Lapenna and M. Lovallo. *Fisher information analysis of earthquake-related geoelectrical signals*. Natural Hazards Earth Sys. Sci., **5** 561 (2005).

[111] J. C. Angulo. *Uncertainty relationships in many-body systems*. J. Phys. A, **26** 6493 (1993).

[112] G. B. Folland and A. Sitaram. *The uncertainty principle: A mathematical survey*. Fourier Anal. Appl., **3** 207 (1997).

[113] A. K. Rajagopal. *The Sobolev inequality and the Tsallis entropic uncertainty relation*. Phys. Lett. A, **205** 32 (1995).

[114] D. D. Dodonov and V. I. Man'ko. *Invariants and the Evolution of Non-stationary Quantum States*. Nova Publishers, New York (1989).

[115] M. Zakai. *A class of definitions of duration (or uncertainty) and the associated uncertainty relations*. Inform. Control., **3** 101 (1960).

[116] I. I. Hirschman. *New bounds for the uncertainly principle*. Amer. J. Math., **79** 152 (1957).

[117] W. Beckner. *Inequalities in the Fourier analysis*. Ann. Math. Soc., **102** 159 (1975).

[118] N. L. Guevara, R. P. Sagar and R. O. Esquivel. *Shannon-information entropy sum as a correlation measure in atomic systems*. Phys. Rev. A, **67** 012507 (2003).

[119] S. R. Gadre, S. B. Sears, S. J. Chakravorty and R. D. Bendale. *Some novel characteristics of atomic information entropies*. Phys. Rev. A, **32** 2602 (1985).

[120] I. Bialynicki-Birula. *Formulations of uncertainty relations in terms of Rényi entropies*. Phys. Rev. A, **74** 052101 (2006).

[121] S. Zozor and C. Vignat. *On classes of non-Gaussian asymptotic minimizers in entropic uncertainty principles*. Physica A, **375** 499 (2007).

[122] S. Zozor, M. Portesi and C. Vignat. *Some extensions of the uncertainty principle*. Physica A, **387** 4800 (2008).

[123] J. S. Dehesa, A. R. Plastino and P. Sánchez-Moreno. *The Fisher-information-based uncertainty relation for quantum systems* (2010). Preprint.

[124] J. S. Dehesa, A. Martínez-Finkelshtein and V. N. Sorokin. *Information-theoretic measures for Morse and Pöschl-Teller potentials*. Mol. Phys., **104** 613 (2006).

[125] J. S. Dehesa, R. González-Férez and P. Sánchez-Moreno. *The Fisher-information-based uncertainty relation, Cramér-Rao inequality and kinetic energy for the D-dimensional central problem*. J. Phys. A, **40** 1845 (2007).

[126] D. R. Herschbach, J. Avery and O. Goscinski. *Dimensional Scaling in Chemical Physics*. Kluwer, Dordrecht (1993).

[127] P. Harrison. *Quantum Wells, Wires and Dots: Theoretical and Computational Physics of Semiconductor Nanoestructures*. Wiley-Interscience, New York (2005).

[128] S. S. Li and J. B. Xia. *Electronic states of a hydrogenic donor impurity in semiconductor nanostructures*. Phys. Lett. A, **366** 120 (207).

[129] M. M. Nieto. *Hydrogen atom and relativistic pi-mesic atom in N-space dimensions.* Amer. J. Phys, **47** 1067 (1979).

[130] M. I. Dykman, P. M. Platzman and P. Seddigard. *Qubits with electrons on liquid helium.* Phys. Rev. B, **67** 155402 (2003).

[131] G. Amelino-Camelia and J. Kowaslki-Glikman. *Planck Scale Effects in Astrophysics and Cosmology.* Springer, Berlin (2005).

[132] M. M. Nieto. *Electrons above a Helium surface and the one-dimensional Rydberg atom.* Phys. Rev. A, **61** 034901 (2000).

[133] F. Burgbacher, C. Lämmerzahl and A. Macias. *Is there a stable hydrogenic atom in higher dimendions?* J. Math. Phys., **40** 625 (1999).

[134] V. Aquilanti, S. Cavalli and C. Coletti. *The d-dimensional hydrogen atom: hyperspherical harmonics as momentum space orbitals and alternative Sturmian basis sets.* Chemical Physics, **214** 1 (1997).

[135] V. Aquilanti, S. Cavalli, C. Colleti, D. de Fazio and G. Grossi. *New Methods in Quantum Theory.* Kluwer, Dordrecht (1996).

[136] K. Andrew and J. Supplee. Am. J. Phys., **58** 1177 (1990).

[137] E. Witten. *Quarks, atoms and the 1/N expansions.* Phys. Today, **33** 38 (1980).

[138] L. Sälen, R. Nepstad, J. R. Hansen and L. B. Madsen. *The N-dimensional Coulomb problem: Stark effect in hyperparabolic and hyperspherical coordinates.* J. Phys. A, **40** 1845 (2007).

[139] S. H. Dong and Z. Q. Ma. *Nonrelativistic Levinson's theorem in d dimensions.* Phys. Rev. A, **65** 042717 (2002).

[140] G. Chen. *The recursion relations for the n-dimensional harmonic oscillator.* Phys. Lett. A, **328** 123 (2004).

[141] C. Itsikson and J. B. Zuber. *Quantum Field Theory.* Dover, New York (2006).

[142] V. Aquilanti and J. Avery. *Sturmian expansions for quantum mechanical many-body problems, and hyperspherical harmonics.* Adv. Quantum Chem., **71** 39 (2001).

[143] V. Aquilanti, S. Cavalli, C. Coletti, D. D. Domenico and G. Grossi. *Hyperspherical harmonics as Sturmian orbitals in momentum space: a systematic approach to the few-body Coulomb problem.* Int. Rev. Phys. Chem., **20** 673 (2001).

[144] V. F. Tarasov. *Exact numerical values of diagonal matrix elements* $< r^k >_{nl}$*, as* $n \leq 8$ *and* $-7 \leq k \leq 4$*, and the symmetry of Appel's function* $f_2(1,1)$. Int. J. Modern Phys., **18** 3177 (2004).

[145] J. D. Hey. *On the momentum representation of hydrogenic wave functions: Some properties and an application.* Am. J. Phys., **61** 28 (1993).

[146] W. van Assche, R. J. Yáñez, R. González-Férez and J. S. Dehesa. *Functionals of Gegenbauer polynomials and D-dimensional hydrogenic momentum expectation values.* J. Math. Phys., **41** 6600 (2000).

[147] R. F. Stebbings and F. B. Dunning. *Rydberg States of Atoms and Molecules.* Cambridge University Press, Cambridge (1983).

[148] T. F. Gallagher. *Rydberg Atoms.* Cambridge University Press, Cambridge (1994).

[149] S. Lundee. *Fine structure in high-L Rydberg states: A path to properties of positive ions.* Ad. At. Mol. Opt. Phys., **52** 161 (2005).

[150] S. G. Karshenboim and V. B. Smirnov. *Precision Physics of Simple Atomic Systems.* Springer, Berlin (2003).

[151] J. S. Dehesa, S. López-Rosa, B. Olmos and R. J. Yáñez. *Fisher information of D-dimensional hydrogenic systems in position and momentum spaces.* J. Math. Phys., **47** 052104 (2006).

[152] E. Romera, P. Sánchez-Moreno and J. S. Dehesa. *Uncertainty relation for Fisher information of D-dimensional single-particle systems with central potentials.* J. Math. Phys., **47** 103504 (2006).

[153] J. Avery. *Hyperspherical Harmonics and Generalized Sturmians.* Kluver, Dordrecht (2000).

[154] V. Fock. *Zur Theorie des Wasserstoffatoms.* Z. Phys., **98** 145 (1935).

[155] J. R. Lombardi. *Hydrogen atom in the momentum representation.* Phys. Rev. A, **22** 797 (1980).

[156] H. A. Bethe and E. E. Salpeter. *Quantum Mechanics of One- and Two-electron Atoms.* Springer, Berlin (1957).

[157] J. D. Hey. *Further properties of hydrogenic wave functions.* Am. J. Phys., **61** 741 (1993).

[158] A. Ray, K. Mahata and P. P. Ray. *Moments of probability distribution, wavefunctions, and their derivatives at the origin of N-dimensional central potentials.* Am. J. Phys., **56** 462 (1988).

[159] A. Aptekarev, J. Dehesa, A. Martínez-Finkelshtein and R. Yáñez. *Quantum expectation values of D-dimensional rydberg hydrogenic states y use of Laguerre and Gegenbauer asymptotics.* J. Phys. A, **43** 145204 (2010).

[160] J. Sánchez-Ruiz and J. S. Dehesa. *Entropic integrals of orthogonal hypergeometric polynomials with general supports.* J. Comput. Appl. Math., **118** 311 (2000).

[161] J. S. Dehesa, A. Martínez-Finkelshtein and J. Sánchez-Ruiz. *Quantum information entropies and orthogonal polynomials.* J. Comput. Appl. Math., **133** 23 (2001).

[162] R. J. Yáñez, W. van Assche, R. González-Férez and J. S. Dehesa. *Entropic integrals of hyperspherical harmonics and spatial entropy of D-dimensional central potentials.* J. Math. Phys., **40** 5675 (1999).

[163] V. S. Buyarov, J. S. Dehesa, A. Martínez-Finkelshtein and J. Sánchez-Lara. *Computation of the entropy of polynomials orthogonal on an interval.* SIAM J. Sci. Comput., **26** 488 (2004).

[164] P. Sánchez-Moreno, R. González-Férez and J. S. Dehesa. *Improvement of the Heisenberg and Fisher-information-based uncertainty relations for d-dimensional central potentials.* New J. Phys., **8** 330 (2006).

[165] W. P. Schleich and J. P. Dahl. *Dimensional enhancement of kinetic energies.* Phys. Rev. A, **65** 052109 (2002).

[166] G. Szëgo. *Orthogonal Polynomials.* AMS, Providence (1975).

[167] T. A. Heim. *The WKB approximation applied to expectation values of r^ν.* J. Phys. B: At. Mol. Opt., **27** 225 (1994).

[168] A. I. Aptekarev, V. S. Buyarov and J. S. Dehesa. *Asymptotic behavior of the L^p-norms and the entropy for general orthogonal polynomials.* Russian Acad. Sci. Sb. Math., **82** 373 (1995).

[169] J. S. Dehesa, R. J. Yáñez, A. I. Aptekarev and V. S. Buyarov. *Strong asymptotics of Laguerre polynomials and information entropies of two-dimensional harmonic oscillator and one-dimensional Coulomb potentials.* J. Math. Phys., **39** 3050 (1998).

[170] A. I. Aptekarev, J. S. Dehesa and R. J. Yáñez. *Spatial entropy of central potentials and strong asymptotics of orthogonal polynomials.* J. Math. Phys., **35** 4423 (1994).

[171] A. I. Aptekarev, V. S. Buyarov, W. van Assche and J. S. Dehesa. *Asymptotics of entropy integrals for orthogonal polynomials.* Doklady Math., **53** 47 (1996).

[172] H. B. Schlegel. *Optimization of equilibrium geometries and transition structures.* Adv. Chem. Phys., **67** 249 (1987).

[173] H. Eyring. *The activated complex in chemical reactions.* J. Chem. Phys., **3** 107 (1935).

[174] E. Wigner. *The transition state method.* Trans. Faraday Soc., **34** 29 (1938).

[175] K. Fukui. *The path of chemical-reactions the IRC approach.* Acc. Chem. Res., **14** 363 (1981).

[176] C. González and H. Schlegel. *Reaction-path following in mass-weighted internal coordinates.* J. Phys. Chem., **94** 5523 (1990).

[177] C. Y. Peng and H. B. Schlegel. *Combinig synchronous transit and quasi-Newton methods to find transition-states.* Isr. J. Chem., **33** 449 (1993).

[178] C. Y. Peng, P. Y. Ayala, H. B. Schlegel and M. J. Frisch. *Using redundant internal coordinates to optimize equilibrium geometries and transition states.* J. Comput. Chem., **17** 49 (1996).

[179] L. Fan and T. Ziegler. *Nonlocal density functional theory as a practical tool in calculations on transition-states and activation-energies-applications to elementary reaction steps in organic-chemistry.* J. Am. Chem. Soc., **114** 10890 (1992).

[180] B. Safi, B. Chocho and P. Geerlings. *Quantum chemical study of the thermodynamics and kinetic aspects of the S(N)2 reaction in gas phase and solution using DFT interpretation.* J. Phys. Chem. A, **105** 591 (2001).

[181] J. A. Pople, A. R. Krishnan, H. B. Schlegel and J. S. Binkley. *Electron correlation theories and their application to study of simple reaction potential surfaces.* Int. J. Quant. Chem., **14** 545 (1978).

[182] N. González-García, J. Pu, A. González-Lafont, J. M. Lluch and D. G. Truhlar. *Searching for saddle points by using the nudge elastic band method: An implementation for gas-phase systems.* J. Chem. Theory Comput., **2** 895 (2006).

[183] K. Ishida, K. Morokuma and A. Komornicki. *Intrinsic reaction coordinate: An abinition calculation for HNC-]HCN and H-+CH4-]CH4+H-.* J. Chem. Phys., **66** 2153 (1977).

[184] M. W. Scmidt, M. S. Gordon and M. Dupuis. *The intrinsic reaction coordinate and the rotational barrier in silaethylene.* J. Am. Chem. Soc., **107** 2585 (1985).

[185] C. P. Baskin, C. F. B. adn C. W. Bauschlicher Jr. and H. F. Schaefer III. *Reaction pathways for triplet methylene abstraction CH2(B-3(1)+H2-]CH3+H).* J. Am. Chem. Soc., **96** 2709 (1974).

[186] S. Shaik, A. Ioffe, A. C. Reddy and A. Pross. *Is the avoided crossing state a good approximation for the transition-state of a chemcial-reaction-an analysis of menschutkin and ionic S(N)2 reactions.* J. Am. Chem. Soc., **116** 262 (1994).

[187] D. G. Hammond. *A correlation of reaction rate.* J. Am. Chem. Soc, **77** 334 (1955).

[188] J. E. Leffler. *Parameters for the description of transition states.* Science, **117** 340 (1953).

[189] Z. Shi and R. Boyd. *Transition-state electronic-structures in SN2 reactions.* J. Am. Chem. Soc., **103** 1072 (1991).

[190] R. F. W. Bader and P. MacDougall. *Toward a theory of chemical-reactivity based on the charge-density.* J. Am. Chem. Soc., **107** 6788 (1985).

[191] N. Balakrishnan and N. Sathyamurthy. *Maximization of entropy during a chemical-reaction.* Chem. Phys. Lett., **164** 267 (1989).

[192] M. Ho, H. Schmider, D. F. Weaver, V. H. Smith, R. P. Sagar and R. O. Esquivel. *Shannon entropy of chemical changes: S(N)2 displacement reactions.* Int. J. Quant. Chem., **77** 376 (200).

[193] E. H. Knoerr and M. E. Eberhart. *Toward a density-based representation of reactivity: S(N)2 reaction.* J. Phys. Chem. A, **105** 880 (2001).

[194] S. S. Shaik, H. B. Schlegel and S. Wolfe. *Theoretical Aspects of Physical Organic Chemistry: The S_N2 reaction.* Wiley, New York (1992).

[195] A. Tashibana. *Electronic energy density in chemical reaction systems.* J. Chem. Phys., **115** 3497 (2001).

[196] A. Toro-Labbé, S. Guitierrez-Oliva, J. S. Murray and P. J. Politzer. *The reaction force and the transition region of a reaction.* J. Mol. Model, **15** 707 (2009).

[197] A. Toro-Labbé, S. Guitierrez-Oliva, J. S. Murray and P. J. Politzer. *A new perspective on chemical and physical processed: the reaction force.* Mol. Phys., **105** 2619 (2007).

[198] J. S. Murray, A. Toro-Labbé, T. Clark and P. Politzer. *Analysis of diatomic bond dissociation and formation in terms of the reaction force and the position-dependetn raction force constant.* Mol. Model, **15** 701 (2009).

[199] P. Jaque, A. Toro-Labbé, P. Geerlings and F. de Proft. *Theoretical study of the Regiolesectivity of* $[2+2]$ *Photocycloaddition reactions of Acrolein with Olefins.* J. Phys. Chem. A, **113** 332 (2009).

[200] T. Koga and M. Morita. *Maximum-entropy inference and momentum density approach.* J. Chem. Phys., **79** 1933 (1983).

[201] S. E. Massen and C. P. Panos. *Universal property of the information entropy in atoms, nuclei and atomic clusters.* Phys. Lett. A, **246** 530 (1998).

[202] R. Nalewajski and R. Parr. *Information theory thermodynamics of molecules and their Hirshfeld fragments.* J. Phys. Chem. A, **105** 7391 (2001).

[203] E. Romera and J. S. Dehesa. *The Fisher-Shannon information plane, an electron correlation tool.* J. Chem. Phys., **120** 8906 (2004).

[204] K. D. Sen. *Characteristic features of Shannon information entropy of confined atoms.* J. Chem. Phys., **123** 074110 (2005).

[205] A. Nagy. *Fisher information in a two-electron entangled artificial atom.* Chem. Phys. Lett., **425** 154 (2006).

[206] S. Liu. *On the realtionship between densities of Shannon entropy and Fisher information for atoms and molecules.* J. Chem. Phys., **126** 191107 (2007).

[207] A. Borgoo, P. Jaque, A. Toro-Labbé, C. Van Alsenoy and P. Geerlings. *Analyzing Kullback-Leibler information profiles: an indication of their chemical relevance.* Phys. Chem. Chem. Phys., **11** 476 (2009).

[208] K. C. Chatzisavvas, C. C. Moustakidis and C. P. Panos. *Information entropy, information distances, and complexity in atoms.* J. Chem. Phys., **123** 174111 (2005).

[209] N. L. Guevara, R. P. Sagar and R. O. Esquivel. *Local correlation measures in atomic systems.* J. Chem. Phys., **122** 084101 (2005).

[210] R. G. Parr, R. F. Nalewajski and P. W. Ayers. *What is an atom in a molecule.* J. Phys. Chem. A, **109** 3957 (2005).

[211] R. O. Esquivel, N. Flores-Gallegos, C. Iuga, E. Carrera, J. C. Angulo and J. Antolín. *Phenomenological description of the transition state, and the bond/breaking and cond/forming processes of selected elementary chemical reactions:an information-theoretic study.* Theor. Chem. Acc., **124** 445 (2009).

[212] R. O. Esquivel, N. Flores-Gallegos, C. Iuga, E. Carrera, J. C. Angulo and J. Antolín. *Phenomenological description of selected elementary chemical reactions mechanisms: An information-theoretic study.* Phys. Lett. A (2009).

[213] D. G. Rawlings and E. R. Davidson. *Molecular electron density distributions in position and momentum space.* J. Phys. Chem., **89** 969 (1958).

[214] P. Kaijser and V. H. Smith Jr. Adv. Quant. Chem., **10** 37 (1997).

[215] M. Kohut (2007). Program DGRID, version 4.2.

[216] P. Politzer and D. G. Truhlar. *Chemical Applications of Atomic and Molecular Electrostatic Potentials.* Academic Press, New York (1981).

[217] P. Geerlings, F. de Proft and W. Langenaeker. *Conceptual density functional theory.* Chem. Rev., **103** 1793 (2003).

[218] T. A. Koopmans. *ber die Zuordnung von Wellenfunktionen und Eigenwerten zu den Einzelnen Elektronen eines Atoms.* Physica, **1** 104 (1933).

[219] J. F. Janak. *Proff that $\partial E/\partial n_i = \epsilon$ in density-functional theory.* Phys. Rev. B, **18** 7165 (1978).

[220] T. K. Ghanty and S. K. Ghosh. *Correlation between hardness, polarizability, and size of atoms, molecules, and clusters.* J. Chem. Phys., **97** 4951 (1993).

[221] R. Roy, A. K. Chandra and S. Pal. *Correlation of Polarizability, Hardness, and Electronegativity: Polyatomic Molecules.* J. Phys. Chem., **98** 10447 (1994).

[222] S. Hati and D. Datta. *Hardness and Electric Dipole Polarizability. Atoms and Clusters.* J. Phys. Chem., **98** 10451 (1994).

[223] Y. Simon-Manso and P. Fuenteaelba. *On the Density Functional relationship between static dipole polarizability and global Softness.* J. Phys. Chem. A, **102** 2029 (1998).

[224] P. K. Chattaraj, U. Sakar and D. R. Roy. *Electrophilicity index.* Chem. Rev., **106** 2065 (2006).

[225] R. G. Pearson. *Hard and soft acids and bases.* J. Am. Chem. Soc., **85** 3533 (1963).

[226] R. G. Pearson. *Hard and soft acids and bases.* Dowen, Hutchinson and Ross, Stroudsberg (1973).

[227] R. G. Pearson. *Chemical Hardness.* Wiley, New York (1997).

[228] P. W. Ayers. *The physical basis of the hard/soft acid/base principle.* Farady Discuss., **135** 161 (2007).

[229] M. J. Frisch, G. W. Trucks, H. B. Schlegel, G. E. Scuseria, M. A. Robb, J. R. Cheeseman, J. A. Montgomery Jr., T. Vreven, K. N. Kudin, J. C. Burant, J. M. Millam, S. S. Iyengar, J. Tomasi, V. Barone, B. Mennucci, M. Cossi, G. Scalmani, N. Rega, G. A. Petersson, H. Nakatsuji, M. Hada, M. Ehara, K. Toyota, R. Fukuda, J. Hasegawa, M. Ishida, T. Nakajima, Y. Honda, O. Kitao, H. Nakai, M. Klene, X. Li, J. E. Knox, H. P. Hratchian, J. B. Cross, V. Bakken, C. Adamo, J. Jaramillo, R. Gomperts, R. E. Stratmann, O. Yazyev, A. J. Austin, R. Cammi, C. Pomelli, J. W. Ochterski, P. Y. Ayala, K. Morokuma, G. A. Voth, P. Salvador, J. J. Dannenberg, V. G. Zakrzewski, S. Dapprich, A. D. Daniels, M. C. Strain, O. Farkas, D. K. Malick, A. Rabuck, K. Raghavachari, J. B. Foresman, J. V. Ortiz,

Q. Cui, A. G. Baboul, S. Clifford, J. Cioslowski, B. B. Stefanov, G. Liu, A. Liashenko, P. Piskorz, I. Komaromi, R. L. Martin, D. J. Fox, T. Keith, M. A. Al-Laham, C. Y. Peng, A. Nanayakkara, M. Challacombe, P. M. W. Gill, B. Johnson, W. Chen, M. W. Wong, C. González and J. A. Pople. *Gaussian 03 Revision D.01* (2004).

[230] J. M. Pérez-Jordá and E. San-Fabián. *A simple, efficient and more reliable scheme for automatic numerical integration.* Comput. Phys. Commun, **77** 46 (1993).

[231] J. M. Pérez-Jordá, A. D. Becke and E. San-Fabián. *Automatic numerical integration techniques for polyatomic molecules.* J. Chem. Phys., **100** 6520 (1994).

[232] G. Schaftenaar and J. H. Noordik. *Molden: a pre- and post-processing program for molecular and electronic structures.* J. Comp.-Aided Mol. Des., **14** 123 (2000).

[233] J. C. Polanyi and A. H. Zewail. *Direct observation of the transition-state.* Acc. Chem. Res., **28** 119 (1995).

[234] C. Tsallis, R. S. Mendes and A. R. Plastino. *The role of constraints within generalized non-extensive statistics.* Physica A, **261** 534 (1998).

[235] S. Martínez, F. Nicolas, F. Pennini and A. Plastino. *Tsallis entropy maximization procedure revisited.* Physica A, **286** 489 (2000).

[236] J. P. Boon and C. Tsallis. *Nonextensive statistical mechanics.* Europhys. News, **36** (2005).

[237] R. F. Nalewajski and R. Parr. *Information theory, atoms in molecules, and molecular similarity.* Proc. Natl. Acad. Sci. U.S.A., **97** 8879 (2000).

[238] A. Kociszewski. *The existence conditions for maximum entropy distributions having prescribed the first three moments.* J. Phys. A, **19** L823 (1989).

[239] J. M. Einbu. *On the existence of a class of maximum-entropy probability distributions.* IEEE Trans. Inf. Theory, **23** 772 (1977).

[240] M. Junk. *Maximum entropy for reduced moment problems.* Math. Models and Meth. Appl. Sci, **10** 1001 (2000).

[241] J. C. Cuchí. *Sobre el Método de Mínima Entropía Relativa y sus Aplicaciones en Física Atómica y Molecular.* Ph.D. Thesis. Universidad de Zaragoza (2005).

[242] M. Reginatto. *Derivation of the equations of nonrelativistic quantum mechanics using the principle of minimum fisher information.* Phys. Rev. A, **58** 1775 (1998).

[243] M. Frontini and A. Tagliani. *Maximum entropy and lacunary Stieltjes moment problem.* Appl. Math. Comput., **97** 183 (1998).

[244] J. N. Kapur. *Maximum Entropy Models in Science and Engineering.* Wiley, New York (1993).

[245] L. Rebollo-Neira, A. Plastino and J. Fernández-Rubio. *On the $q = \frac{1}{2}$ non-extensive maximum entropy distribution.* Physica A, **258** 458 (1998).

[246] K. Bandyopadhyay, . A. Bhattacharyya and A. K. Battacharya. *On some problems of the maximum entropy.* Pramana, **54** 365 (2000).

[247] M. Grendar Jr. and M. Grendar. *Maximum entropy method with non-linear constraints: challenges.* In G. Erickson and Y. Zhai, eds., *Bayesian inference and Maximum Entropy methods in Science and Engineering*, 97–109. AIP, Melville (2004).

[248] A. Plastino and A. R. Plastino. *Tsallis entropy and Jaynes' information theory formalism.* Brazilian J. Phys., **29** 50 (1999).

[249] P. Ishwar and P. Moulin. *On the existence and characterization of the maxent distribution under general moment inequality constraints.* IEEE Trans. Inf. Theory, **51** 3322 (2005).

[250] Karmeshu. *Entropy Measures, Maximum Entropy Principle and Emerging Applications.* Springer, New York (2003).

[251] A. G. Bashkirov. *Maximum Rényi entropy principle for systems with Power-law hamiltonians.* Phys. Rev. Lett., **93** 130601 (2004).

[252] P. S. Wesson. *Five-dimensional Physics. Classical and Quantum Consequences of Kaluza-Kleins Cosmology.* World Scientific, New York (2006).

[253] B. R. Frieden, A. Plastino, A. R. Plastino and B. H. Soffer. *Schrödinger link between nonequilibrium thermodynamics and Fisher information.* Phys. Rev. E, **66** 046128 (2002).

[254] F. E. Udwadia. *Some results on maximum entropy distributions for parameters known to lie in finite intervals.* SIAM Rev., **31** 103 (1989).

[255] H. Landau. *Maximum entropy and the moment problem.* AMS, **16** 47 (1987).

[256] S. Abe and A. K. Rajagopal. *Quantum entanglement inferred by the principle of maximum nonaditive entropy.* Phys. Rev. A, **60** 3461 (1999).

[257] B. R. Frieden, A. Plastino, A. R. Plastino and B. H. Soffer. *Fisher-based thermodynamics: Its Legendre transform and concavity properties.* Phys. Rev. E, **60** 48 (1999).

[258] B. R. Frieden. *Estimation of distribution laws and physical laws by a principle of extremized physical information.* Physica A, **198** 262 (1993).

[259] B. R. Frieden. *Applications to optics and wave mechanics of the criterion of maximum Cramér-Rao bound.* J. Modern Opt., **35** 1297 (1988).

[260] B. R. Frieden and B. H. Soffer. *Lagrangians of physics and the game of Fisher-information transfer.* Phys. Rev. E, **52** 2274 (1995).

[261] B. R. Frieden and B. H. Soffer. *A critical comparison of the three information-based approaches to physics.* Found. Phys. Lett., **13** 89 (2000).

[262] S. Luo. *Maximum Shannon entropy, minimum Fisher information and an elementary game.* Found. Phys. Lett., **32** 1757 (2002).

[263] J. A. Shohat and J. D. Tamarkin. *The Problem of Moments.* AMS, Providence (1943).

[264] A. Tagliani. *Maximum entropy solutions and moment problem in unbounded domains.* Appl. Math. Lett., **16** 519 (2003). See references herein.

[265] H. Gzyl, P. L. N. Inverardi, A. Tagliani and M. Villasana. *Maxentropic solution of fractional moment problems.* Appl. Math. Comput., **173** 109 (2006).

[266] P. L. N. Inverardi, A. Petri, G. Pontuale and A. Tagliani. *Stieltjes moment problem via fractional moments*. Appl. Math. Comput., **166** 664 (2005).

[267] D. C. Brody, I. R. C. Buckley and I. C. Constantinou. *Option price calibration from Rényi entropy*. Phys. Lett. A, **366** 289 (2007).

[268] D. C. Brody, I. R. C. Buckley, I. C. Constantinou and B. K. Meister. *Entropy calibration revisited*. Phys. Lett., **337** 257 (2007).

[269] T. Koga, K. Kanayama, S. Watanabe and A. J. Thakkar. *Analytical Hartree-Fock wave functions subject to cusp and asymptotic constraints: He to Xe, Li+ to Cs+, H- to I-*. Int. J. Quant. Chem., **71** 491 (1999).

[270] R. Benesch and V. H. Smith Jr. *Wave Mechanics: The First Fifty Years*. Butterworths, London (1973).

[271] Merriam-Webster. *Webster's Ninth New Collegiate Dictionary*. Merriam-Webster Inc. Springfield, MA (1985).

[272] C. F. Gershenson and F. Heylighen. *How can we think the complex?* Institutes Study of Coherence and Emergence/Information Age Publishing (2005).

[273] N. Pippenger. *Complexity theory*. Sci. Am., **36** 114 (1978).

[274] F. E. Yates. *Complexity and limits to knowledge*. Am. J. Phylos., **235** (1978).

[275] G. J. Klir. *The emergence of two-dimensional sciece in the information-society*. Sys. Res., **2** 131 (1985).

[276] P. Grassberger. *Toward a quantitative theory of self-generated complexity*. Int. J. Theory Phys., **25** 907 (1986).

[277] N. Rescher. *Complexity: A Philosophical Overview*. Transaction Publishers, New York (1998).

[278] N. Goldenfeld and L. Kadanoff. *Simple lessons from complexity*. Science, **284** 87 (1999).

[279] O. Goldreich. *Computational Complexity: A Conceptual Perspective*. Cambridge University Press, Cambridge (2008).

[280] J. T. Bonner. *Perspective: The size-complexity rule*. Evolution, **58** 1883 (2004).

[281] J. C. Angulo and J. Antolín. *Atomic complexity measures in position and momentum spaces*. J. Chem. Phys., **128** 164109 (2008).

[282] D. Bonchev and D. H. Rouvray. *Complexity in Chemistry*. Taylor and Francis, London (2003).

[283] A. Borgoo, F. De Proft, P. Geerlings and K. D. Sen. *Complexity of Dirac-Fock atom increases with atomic number*. Chemical Physics Letters, **444** 186 (2007).

[284] D. W. McShea. *Metazoan complexity and evolution: is there a trend?* Evolution, **50** 477 (1996).

[285] D. W. McShea. *Functional complexity en organisms: Parts as proxies.* Biolog. Philos., **15** 641 (2000).

[286] K. Krohn and J. Rhodes. *Complexity of finite semigroups.* Ann. Math., **88** 128 (1968).

[287] W. B. Arthur. *Complexity and economy.* Science, **284** 107 (1999).

[288] B. Castellani and F. Hafferty. *Sociology and Complexity Science.* Springer, Berlin (2009).

[289] C. R. Shalizi, K. L. Shalizi and R. Haslinger. *Quantifying self-organization with optimal predictors.* Phys. Rev. Lett., **93** 118701 (2004).

[290] O. A. Rosso, M. T. Martin and A. Plastino. *Brain electrical activity analysis using wavelet-based informational tools (II): Tsallis non-extensivity and complexity measures.* Physica A, **320** 497 (2003).

[291] M. Gell-Mann. *The Quark and the Jaguar.* W.H. Freeman, New York (1994).

[292] D. P. Feldman and C. J. P. *Measures of statistical complexity: Why ?.* Phys. Lett. A, **238** 244 (1998).

[293] P. W. Lamberti, M. P. Martin, A. Plastino and O. A. Rosso. *Intensive entropic non-triviality measure.* Physica A, **334** 119 (2004).

[294] P. W. Anderson. *Is complexity physics - is it science - what is it.* Phys. Today (1991).

[295] G. Parisi. *Statistical physics and biology.* Phys. World, **6** (1993).

[296] J. S. Shiner, M. Davison and P. T. Landsberg. *Simple measure for complexity.* Phys. Rev. E, **59** 1459 (1999).

[297] C. Anteneodo and A. R. Plastino. *Some features of the López-Ruiz-Mancini-Calbet (LMC) statistical measure of complexity.* Phys. Lett. A, **223** 348 (1996).

[298] R. G. Catalan, J. Garay and R. López-Ruiz. *Features of the extension of a statistical measure of complexity to continuous systems.* Phys. Rev. E, **66** 011102 (2002).

[299] M. T. Martin, A. Plastino and O. A. Rosso. *Statistical complexity and disequilibrium.* Physics Letters A, **311**(2-3) 126 (2003).

[300] R. López-Ruiz. *Shannon information, LMC complexity and Rényi entropies: a straightforward approach.* Biophys. Chem., **115** 215 (2005).

[301] T. Yamano. *A statistical measure of complexity with nonextensive entropy.* Physica A, **340** 131 (2004).

[302] T. Yamano. *A statistical complexity measure with nonextensive entropy and quasi-multiplicativity.* J. Math. Phys., **45** 1974 (2004).

[303] R. Carbó, L. Lleyda and M. Arnau. *How similar is a molecule to another? An electron density measure of similarity between two molecular structures.* Int. J. Quant. Chem., **17** 1185 (1980).

[304] O. Onicescu. *Theorie de l'information. Energie informationelle.* C.R. Acad. Sci. Paris A, **263** 25 (1966).

[305] J. C. Angulo, J. Antolín and K. D. Sen. *Fisher-Shannon plane and statistical complexity of atoms.* Physics Letters A, **372** 670 (2008).

[306] K. D. Sen, J. Antolín and J. C. Angulo. *Fisher-Shannon analysis of ionization processes and isoelectronic series.* Phys. Rev. A, **76** 032502 (2007).

[307] A. Dembo, T. Cover and J. Thomas. *Information theoretic inequalities.* IEEE Trans. Infom. Theory, **37** 1501 (1991).

[308] J. Antolín and J. C. Angulo. *Complexity analysis of ionization processes and isoelectronic series.* Int. J. Quant. Chem., **109** 586 (2009).

[309] J. S. Dehesa, P. Sánchez-Moreno and R. J. Yáñez. *Cramér-Rao information plane of orthogonal hypergeometric polynomials.* J. Comput. Appl. Math., **186** 523 (2006).

[310] X. Calbet and R. López-Ruíz. *Tendency towards maximum complexity in a nonequilibrium isolated system.* Phys. Rev. E, **63** 066116 (2001).

[311] M. T. Martin, A. Plastino and O. A. Rosso. *Generalized statistical complexity measures: Geometrical and analytical properties.* Physica A, **369** 439 (2006).

[312] E. Romera and A. Nagy. *Fisher-Rényi entropy product and information plane.* Phys. Lett. A, **372** 6823 (2008).

[313] J. S. Dehesa, F. J. Gálvez and I. Porras. *Bounds to density-dependent quantities of D-dimensional many-particle systems in position and momentum spaces: Applications to atomic systems.* Phys. Rev. A, **40** 35 (1989).

[314] S. Fraga and G. Malli. *Many Electron Systems: Properties and Interactions.* Saunders, Philadelphia (1968).

[315] I. R. Epstein. *Calculation of atomic and molecular momentum expectation values and total energies from compton-scattering data.* Phys. Rev. A, **8** 160 (1973).

[316] M. Hoffmann-Ostenhof and T. Hoffmann-Ostenhof. *"Schrödinger inequalities" and asymptotic behavior of the electron density of atoms and molecules.* Phys. Rev. A, **16** 17782 (1977).

[317] J. S. Dehesa, S. López-Rosa, A. Martínez-Finkelshtein and R. J. Yáñez. *Information theory of d-dimensional hydrogenic systems: Application to circular and Rydberg states.* Int. J. Quantum Chem., **110** 1529 (2009).

[318] J. Sañudo and R. López-Ruiz. *Statistical complexity and Fisher-Shannon information in the h-atom.* Phys. Lett. A, **372** 5283 (2008).

[319] J. Avery. *Selected applications of hyperspherical harmonics in quantum theory.* J. Phys. Chem., **97** 2406 (1993).

[320] L. C. Biedenharn and J. D. Louck. *Angular Momentum in Quantum Physics. Theory and Application.* In *Encyclopedia of Mathematics and its Applications*, vol. 8. Addison-Wesley, Reading, Massachusetts (1981).

[321] W. Greiner. *Relativistic Quantum Mechanics: Wave Equations.* Springer, Berlin (2000). 3rd edn.

[322] A. Borgoo, P. Geerlings and K. D. Sen. *Electron density and Fisher information of Dirac-Fock atoms.* Phys. Lett. A, **372**(31) 5106 (2008).

[323] J. Sañudo and R. López-Ruiz. *Complexity invariance by replication in the quantum square well.* In. Rev. Phys., **2** 223 (2008).

[324] J. Sañudo and R. López-Ruiz. *Alternative evaluation of statistical indicators in atoms: The non-relativistic and relativistic cases.* Phys. Lett. A, **37(3)**(30) 2549 (2009).

[325] J. Katriel and K. D. Sen. *Relativistic effects on information measures for hydrogen-like atoms.* Journal of Computational and Applied Mathematics, **233** 1399 (2010). Proceedings of Special Functions, Information Theory, and Mathematical Physics, dedicated to Professor Jesus Sanchez Dehesa on the occasion of his 60th birthday.

[326] E. Schrödinger. *Quantisierung als Eigenwertproblem I.* Ann. Physik, **79** 361 (1926).

[327] O. Klein. *Quantentheorie und fünfdimensionale Relativistätstheorie.* Z. Phys., **37** 895 (1926).

[328] V. Fock. *Zur schrödingerschen Wellenmechanik.* Z. Phys., **38** 242 (1926).

[329] V. Fock. *über die invariante Form der Wellen-und der Bewegungsgleichungen für einen geladenen.* Z. Phys., **39** 226 (1926).

[330] C. Y. Chen and S. H. Dong. *Evaluation of matrix elements of r^k and recurrence relations for the Klein-Gordon equation with a Coulomb field.* Phys. Scr., **73** 511 (2006).

[331] S. Dong, X. Gu, Z. Ma and J. Yu. *The Klein-Gordon equation with a Coulomb potential in D dimensions.* Int. J. Modern Phys. E, **12** 555 (2003).

[332] R. C. Barret and D. F. Jackson. *Nuclear Size and Structure.* Clayendon Press, Oxford (1979).

[333] D. Manzano, R. J. Yáñez and J. S. Dehesa. *Relativistic Klein-Gordon charge effects by information-theoretic measures.* New J. Phys., **12** 023014 (2010).

[334] R. G. Parr and R. G. Pearson. *Absolute hardness: companion parameter to absolute electronegativity.* J. Am. Chem. Soc., **105** 7512 (1983).

[335] P. W. Ayers, R. G. Parr and R. G. Pearson. *Elucidating the hard/soft acid/base principle: A perspective based on half-reactions.* J. Chem. Phys., **124** 196107 (2006).

[336] R. G. Pearson. *The HSAB principle - More quantitative aspects.* Inorg. Chim. Acta, **240** 93 (1995).

[337] R. G. Parr, L. V. Szentpály and S. liu. *Electrophilicity index.* J. Am. Chem. Soc., **122** 1922 (1999).

[338] N. I. of Standars and Technology. *Computational Chemistry Comparison and Benchmark DataBase.* Http://cccbdb.nist.gov/.

[339] F. Kuzer. *Fulminic acid in the history of organic chemistry.* J. Chem. Ed., **77** 851 (2000).

[340] K. Pearson. *On the criterion that a given system of deviations from the probable in the case of a correlated system of variables is such that it can be reasonably supposed to have arised from random sampling.* Phils. Mag., **50** 157 (1900).

[341] S. Kullback and A. Leibler. *On information and sufficient.* Ann. Math. Stat., **22** 79 (1951).

[342] H. Jeffreys. *An invariant form for the prior probability in estimation problems.* Proc. R. Soc. London, Ser A, **186** 453 (1946).

[343] A. Bhattacharyya. *On some analaogue of the amount of information and their use in statistical estimation.* Sankhya, **8** 1 (1946).

[344] I. Csiszár. *Information-type measures of difference of probability distributions and indirect observation.* Stud. Sci. Math. Hung., **2** 299 (1967).

[345] J. H. Lin. *Divergence measures based on the Shannon entropy.* IEEE Trans. Inf. Theory, **37** 145 (1991).

[346] I. J. Taneja, P. L. Pardo, D. Morales and M. L. Menéndez. *On generalized information and divergence measures and their applications: a brief review.* Questiio, **13** 47 (1989).

[347] I. J. Taneja. *On Generalized Information MEasures and Thermalir Applications.* Academic, New York (1989).

[348] I. J. Taneja and P. Kumar. *Relative information of type s, csiszar's f-divergence, and information inequalities.* Inf. Sci., **166** 105 (2004).

[349] P. Bernaola-Galván, I. Grosse, P. Carpena, J. L. Oliver, R. Román-Roldán and H. E. Stanley. *Finding borders between coding and noncoding DNA regions by an entropic segmentation method.* Phys. Rev. Lett., **85** 1342 (2000).

[350] X. Huang, S. Li and Y. Wang. In *Proceedings of IEEE Computer Society Conference on Computer Vision and Pattern Recognition*, 144–149 (2005).

[351] S. Pavoine, S. Ollier and D. Pontier. *Measuring diversity from dissimilarities with Rao's quadratic entropy: Are any dissimilarities suitable?* Theor. Popul. Biol., **67** 231 (2005).

[352] R. O. Duda, P. E. Hart and D. G. Stork. *Patterns Classification.* John Wiley and Sons, New York (2001).

[353] S. Y. Chung and S. Subbiah. *A structural explanation for the twilight zone of protein sequence homology.* Struct., **4** 1123 (1996).

[354] K. Suzuki, H. Yamada and S. Hasimoto. *A similarity-based neural network for facial expression analysis.* Patter Recognition Lett., **28** 1104 (2007).

[355] P. Resnik. *Semantic similarity in a taxonomy: An information-based measure and its application to problems of ambiguity in natural language.* J. Artificial Intell. Research, **11** 95 (1999).

[356] A. P. Majtey, P. W. Lamberti, M. T. Martin and A. Plastino. *Wootters' distance revisited: a new distinguishability criterium.* Eur. Phys. J. D., **32** 413 (2005).

[357] R. Carbó-Dorca, L. Amat, E. Besalu, X. Girones and D. Robert. *Quantum mechanical origin of QSAR: theory and applications.* J. Mol. Struct., **504** 181 (2000).

[358] A. P. Majtey, A. Borrás, M. Casas, P. W. Lamberti and A. Plastino. *JensenShannon divergence as a measure of the degree of entanglement.* Int. J. Quant. Inform., **6** 715 (2008).

[359] R. Carbó-Dorca, X. Girones and P. G. Mezey. *Fundamentals of Molecular Similarity.* Kluwer Academic, New York/Plenum, New York (2001).

[360] J. Burbea and C. R. Rao. *On the convexity of some divergence measures based on entropy functions.* IEEE Trans. Inf. Theory, **28** 489 (1982).

[361] J. C. Angulo and J. Antolín. *Atomic quantum similarity indices in position and momentum spaces.* J. Chem. Phys., **126** 044106 (2007).

[362] A. Borgoo, M. Godefroid, K. D. Sen, F. De Proft and P.Geerlings. *Quantum similarity of atoms: a numerical hartree-fock and information theory approach.* Chem. Phys. Lett., **399** 186 (2004).

[363] A. Borgoo, M. Torrent-Sucarrat, F. De Proft and P.Geerlings. *Quantum similarity study of atoms: A bridge between hardness and similarity indices.* J. Chem. Phys., **126** 234104 (2007).

[364] J. Antolín and J. C. Angulo. *Quantum similarity indices for atomic ionization processes.* Eur. Phys. J. D., **46** 21 (2008).

[365] P. Hammad. *Measure d'ordre α de l'information au sens de Fisher.* Revue de Statistique Appliquée, **26** 73 (1978).

[366] J. C. C. J. Antolín and J. C. Angulo. *Minimum-cross-entropy estimation of atomic charge densities from scattering factors.* J. Phys. B: At. Mol. Opt., **32** 577 (1999).

[367] M. N. Do and M. Vetterli. *Wavelet-based texture retrieval using generalized Gaussian density and Kullback-Leibler distance.* IEEE Trans. Image Proc., **11** 146 (2002).

[368] A. P. Majtey, P. W. Lamberti and D. P. Prato. *Jensen-Shannon divergence as a measure of distinguishability between mixed quantum states.* Phys. Rev. A, **72** 052310 (2005).

[369] A. K. C. Wong and M. You. *Entropy and distance of random graphs with application to structural pattern-recognition.* IEEE Trans. Pattern. Anal. Mach. Intell., **7** 599 (1985).

[370] C. R. Rao and T. Nayak. *Cross entropy, dissimilarity measures, and characterizations of quadratic entropy.* IEEE Trans. Inf. Theory, **31** 589 (1985).

[371] I. Grosse, P. Bernaola-Galván, P. Carpena, R. Román-Roldán, J. L. Oliver and H. E. Stanley. *Analysis of symbolic sequences using the Jensen-Shannon divergence.* Phys. Rev. E, **65** 041905 (2002).

[372] P. W. Lamberti, A. P. Majtey, A. Borras, M. Casas and A. Plastino. *Metric character of the quantum jensen-shannon divergence.* Phys. Rev. A, **77** 052311 (2008).

[373] J. Antolín, J. C. Angulo and S. López-Rosa. *Fisher and Jensen-Shannon divergences: quantitative comparisons among distributions. Application to position and momentum atomic densities.* J. Chem. Phys., **130** 074110 (2009).

[374] S. López-Rosa, J. Antolín, J. C. Angulo and R. O. Esquivel. *Divergence analysis of atomic ionization processes and isoelectronic series.* Phys. Rev. A, **80** 012505 (2009).

[375] J. Lin and S. K. M. Wong. *A new directed divergence measures and its characterization.* Int. J. Gen. Syst., **17** 73 (1990).

[376] B. Fuglede and F. Topsoe. *Jensen-Shannon divergence and Hilbert space embedding.* IEEE Int. Sym. Inform. Theo., **31** (2004).

[377] P. Lamberti and A. Majtey. *Non-logarithmic Jensen-Shannon divergence.* Physica A, **329** 81 (2003).

[378] A. B. Hamza and H. Krim. *Image registration and segmentation by maximizing the Jensen-Rényi divergence.* Lect. Notes Comput. Sci., **2683** 247 (2003).

[379] Y. He, A. B. Hamza and H. Krim. *A generalized divergence measure for robust image registration.* IEEE Trans. Signal Proc., **51** 1211 (2003).

[380] D. Karakos, S. Khudanpur, J. Eisner and C. Priebe. *Iterative denoising using Jensen-Rényi divergences with an application to unsupervised document categorization.* In *IEEE International Conference on Acoustics, Speech and Signal Processing, Vol. II*, 509–512 (2007).

[381] A. B. Hamza. *Nonextensive information-theoretic measure for image edge detection.* J. Electron. Imaging, **15** 013011 (2006).

[382] A. F. T. Martins, N. A. Smith, E. P. Xing, P. M. Q. Aguiar and M. A. T. Figueiredo. *Nonextensive information theoretic kernels on measures.* J. Machine Learn. Research, **10** 935 (2009).

[383] P. Biane and R. Speicher. *Free diffusions, free entropy and free Fisher information.* ANN. I.H.P. Probab. Stat., **37** 581 (2001).

[384] D. Robert and R. Carbó-Dorca. *General trends in atomic and nuclear quantum similarity measures.* Int. J. Quant. Chem., **77** 685 (2000).

[385] M. Ho, R. P. Sagar, H. Schmider, D. F. Weaver and V. H. Smith. *Measures of distance for atomic charge and momentum densities and their relationship to physical-properties.* Int. J. Quant. Chem., **108** 5469 (1998).

[386] Y. Tal. *Asymptotic-behavior of ground-state charge-density in atoms.* Phys. Rev. A, **18** 1781 (1978).

[387] K. D. Sen, C. P. Panos, K. C. Chatzisavvas and C. C. Moustakidis. *Net Fisher information measure versus ionization potential and dipole polarizability in atoms.* Phys. Lett. A, **364** 286 (2007).

[388] T. Kato. *On the eigenfunctions of many-particle systems in quantum mechanics.* Commun. Pure Appl. Math., **10** 151 (1957).

[389] N. H. March. *Spatially dependent generalization of Katos theorem for atomic closed shells in a bare Coulomb field.* Phys. Rev. A, **33** 88 (1986).

[390] V. H. Smith Jr, D. D. Robertson and A. N. Tripathi. *Monotonicity of the electron momentum density for atomic closed shells in a bare Coulomb field.* Phys. Rev. A, **42** 61 (1990).

[391] N. H. March and R. Santamaría. *Electron and kinetic energy densities for an arbitrarily closed shell in a bare Coulomb field from s-state densities.* Phys. Rev. A, **39** 2835 (1989).

[392] I. A. Howard and N. H. March. *Total kinetic energy density for closed shells in a bare Coulomb field solely in terms of s-state information.* J. Phys. A, **35** L635 (2002).

[393] N. H. March and J. Cizek. *Dimensionality dependence of total energy of closed shells in a bare Coulomb field for large atomic number.* Int. J. Quant. Chem., **33** 301 (1986).

[394] J. C. Angulo and E. Romera. *Bare Coulomb field and atomic reciprocal form factor.* Int. J. Quant. Chem., **106** 485 (2006).

[395] C. Lin and M. Lin. *Series solution of the differential equation determining the nth-shell one-electron density of a bare Coulomb problem in quantum physics.* Comm. Nonlinear Sci. and Num. Sim., **13** 667 (2008).

[396] T. Koga, K. Kanayama, S. Watanabe, T. Imai and A. J. Thakkar. *Analytical Hartree-Fock wave functions for the atoms Cs to Lr.* Theor. Chem. Acc., **104** 411 (2000).

[397] A. J. Takkar and V. H. Smith Jr. *Accurate charge densities and twoelectron intracule functions for the heliumlike ions.* J. Chem. Phys., **67** 1191 (1977).

[398] G. Green. *On the determination of the exterior and interior attractions of ellipsoids of variable densities.* Trans. Cambridge Philos. Soc., **5** 395 (1835).

[399] M. J. M. Hill. *On functions of more than two varibles analogous to tesseral harmonics.* Trans. Cambridge Philos. Soc., **13** 273 (1883).

[400] J. Avery. *Hyperspherical Harmonics: Applications in Quantum Theory.* Kluver, Dordrecht (1989).

[401] E. Kyriakopoulos. *Dinamical groups and the Bethe-Salpether equations.* Phys. Rev., **174** 1846 (1968).

[402] A. F. Nikiforov, V. B. Uvarov and S. K. Suslov. *Classical Orthogonal Polynomials of a Discrete Variables.* Springer, Berlin (1991).

[403] N. K. Vilenkin. *Special Functions and the Theory of Group Representation.* AMS, Providence (1968).

[404] V. Aquilanti, S. Cavalli and G. Grossi. *Hiperspherical coordinates for molecular dynamics by the method of trees and the mapping of potential energy surfaces for triatomic systems.* J. Chem. Phys., **8** 1362 (1986).

[405] J. D. Louck. *Generalized orbital angular momentum and the n-fold degenerate quantum-mechanical oscillator: Part II The n-fold degenerate oscillator.* J. Mol. Spectrosc., **4** 298 (1960).

[406] J. Avery. *A formula for angular and hyperangular integration.* J. Math. Chem., **24** 169 (1998).

[407] E. Heller. *Quantum localization and the rate of exploration of phase space.* Phys. Rev. A, **35** 1360 (1987).

[408] A. Chatterjerr. *Large-N expansions in quantum mechanics, atomic physics and some O(N) invariant systems.* Phys. Rev., **186** 249 (1990).

[409] J. Sánchez-Ruiz. *Linearization and connection formulae involving squate of Gegenbauer polynomials.* Appl. Math. Lett., **14** 3162 (2001).

[410] J. L. A. Coelho and R. L. P. G. Amaral. *Coulomb and quantum oscillator problems in conical spaces with arbitrary dimensions.* J. Phys. A, **35** 5255 (2002).

[411] Z. Y. Wen and J. Avery. *Some properties of hyperspherical harmonics.* J. Math. Phys., **26** 396 (1985).

[412] D. S. Mitrinovic, J. E. Pecaric and A. M. Fink. *Classical and New Inequalities in Analysis.* Kluwer, Dordrecht (1993).

List of Figures

List of Tables